UNIVERSITÄT HOHENHEIM

ATP4 and Wnt-signaling are required for ciliogenesis and left-right axis development of *Xenopus*

Dissertation zur Erlangung des Doktorgrades
der Naturwissenschaften (Dr. rer. nat.)

Fakultät Naturwissenschaften

Universität Hohenheim
Institut für Zoologie

vorgelegt von

Peter Walentek

aus Königshütte/Polen

2012

Erklärung gemäß §8 Absatz 2 Aufzählungspunkt 2 der Promotionsordnung zum Dr. rer. nat. der Universität Hohenheim

Hiermit erkläre ich, dass ich die vorgelegte Dissertation selbständig angefertigt und nur die angegebenen Quellen und Hilfsmittel verwendet habe. Wörtlich oder inhaltlich übernommene Stellen sind als solche gekennzeichnet.

Stuttgart, den 04.Juni 2012

Peter Walentek

"I am too much of a sceptic to deny the possibility of anything."

Thomas Henry Huxley

Letter to Herbert Spencer (1886). In L. Huxley, The Life and Letters of Thomas Henry Huxley (1903).

Abstract

The vertebrate body plan displays left-right (LR) asymmetries of organ placement superimposed on an overt bilaterally symmetrical organization. Symmetry is broken during embryogenesis, and asymmetric gene expression precedes asymmetric organ morphogenesis. The proton/potassium pump ATP4 was shown to play a role in LR-development of the frog *Xenopus laevis* as well as in other deuterostomes. Two opposing models of symmetry-breakage were proposed, the "ion-flux" and the "leftward flow" model. The former proposed that symmetry was broken by LR-asymmetric expression of the α-subunit of ATP4 during cleavage stages. The latter claimed a cilia-based leftward flow at the gastrocoel roof plate (GRP) to take center stage during neurulation, i.e. a day later in development.

In the present thesis work, the role of ATP4a in symmetry-breakage was re-addressed and evidence for symmetrical expression and function of ATP4a was gathered. ATP4a was shown to be required for two Wnt-signaling dependent steps during the setup of cilia-driven leftward flow at the GRP: (1) Wnt/β-catenin (β-cat) dependent expression of *Foxj1* during gastrulation, and (2) Wnt/planar cell polarity (PCP) dependent posterior localization of motile cilia during neurulation. These data challenge the "ion-flux" hypothesis and argue for a conserved ATP4- and cilia-dependent symmetry-breakage mechanism throughout the vertebrates. Furthermore, the function of Wnt-signaling components was analyzed in the context of GRP-formation: The receptor Frizzled 8 (Fz8) and β-cat were required for *Foxj1* expression during gastrulation. Morphogenesis of the GRP, posterior polarization of motile cilia and expression of *Xnr1* and *Coco* in somitic cells were all required for LR-development. Loss of non-canonical Xwnt11b-signaling perturbed these process, suggesting that non-canonical Wnt-signaling branches, in addition to Wnt/PCP, were relevant for LR-development.

ATP4-mediated Wnt-signaling was also required for *Foxj1* expression and motile cilia in other epithelia during *Xenopus* development, i.e. the skin, floor plate and the ependymal cell layer. In the floor plate β-cat was required for *Foxj1* expression downstream of Hedgehog-signaling. In the skin mucociliary epithelium ATP4a and Wnt/β-cat were required downstream of Notch/Delta-mediated cell-type specification of multiciliated cells. This was also true for a new cell type of serotonergic cells described here, which was

I

characterized morphologically, by analysis of gene expression and response to manipulations of Wnt- and Notch/Delta-signaling.

In summary, the data presented in this thesis suggest a conserved function of ATP4a and Wnt-signaling in vertebrate symmetry-breakage and Foxj1-dependent ciliogenesis in *Xenopus*.

Zusammenfassung

Wirbeltiere weisen Links-Rechts-(LR-)Asymmetrien in der Positionierung ihrer inneren Organe auf, welche von dem im Allgemeinen bilateral-symmetrischen Körperbauplan überlagert werden. Die bilaterale Symmetrie wird während der Embryonalentwicklung gebrochen, dabei geht die asymmetrische Aktivität von Genen der asymmetrischen Organmorphogenese voraus. Der Protonen/Kalium-Pumpe ATP4 wurde eine Rolle während der LR-Entwicklung von *Xenopus laevis* und weiteren Deuterostomiern zugesprochen. Zum Ablauf des Symmetriebruchs wurden jedoch zwei gegensätzliche Modelle vorgeschlagen: das „Ionen-Fluss"- und das „Flüssigkeitsstrom"-Modell. Während das erste Modell impliziert, dass eine LR-asymmetrische Verteilung der α-Untereinheit von ATP4 in Furchungsstadien zum Symmetriebruch führt, schlägt das zweite Modell vor, dass ein cilienabhängiger, linksgerichteter Flüssigkeitsstrom über Zellen der Archenteron-Dachplatte (GRP) zum Symmetriebruch während Neurulastadien führt. Dies wäre ein Tag später in der Entwicklung als vom „Ionen-Fluss" Modell vorgeschlagen.

In dieser Arbeit wurde die Funktion von ATP4a während des Symmetriebruchs nochmals näher untersucht. Die erhaltenen Ergebnisse legten eine symmetrische Verteilung und Funktion von ATP4 während der LR-Entwicklung nahe. Es konnte gezeigt werden, dass die Funktion von ATP4a in zwei Wnt-abhängigen Signalprozessen für die Entstehung des linksgerichteten Flüssigkeitsstroms benötigt wurde: (1.) Für die Wnt/β-Catenin-abhängige Expression von *Foxj1* während der Gastrulation, und (2.) für die Wnt/PCP-abhängige (planare Zellpolarität) posteriore Positionierung von motilen Cilien während der Neurulation. Diese Daten stellten die „Ionen-Fluss"-Hypothese in Frage und unterstützten die Idee eines konservierten Symmetriebruch-Mechanismus in Wirbeltieren, welcher ATP4- und Cilien-abhängig ist. Zudem wurden die Funktionen von weiteren Komponenten des Wnt-Signalwegs währen der Entstehung der GRP untersucht: Der Rezeptor Frizzled 8 (Fz8) und β-Catenin wurden für die Expression von *Foxj1* während der Gastrulation benötigt. Funktionsverlust des non-kanonischen Liganden Xwnt11b hingegen störte die Morphogenese der GRP, die posteriore Ausrichtung von motilen Cilien, sowie die Expression von *Coco* und *Xnr1* in somitischen Zellen der GRP. Dies legte nahe, dass neben Wnt/PCP die Aktivität weiterer non-kanonischer Signalzweige des Wnt-Signalweges für die LR-Entwicklung notwendig waren.

ATP4-abhängige Wnt-Signalaktivität war auch für die Expression von *Foxj1* und die Entstehung motiler Cilien in anderen ciliierten Epithelien während der Entwicklung von *Xenopus* notwendig: z.B. in der Haut, der neuralen Bodenplatte und im Ependym. In der Bodenplatte des Neuralrohrs wurde β-Catenin dem Hedgehog-Signalweg nachgeschaltet für die *Foxj1* Expression benötigt. Im mucociliären Epithel der Haut wurden ATP4a und Wnt/β-Catenin gebraucht, nachdem die Zellen über den Notch/Delta-Signalweg spezifiziert wurden. Diese Art der Regulation wurde auch in einem neuen Zelltyp serotonerger Zellen beobachtet, welcher hier mittels morphologischer Analyse, Analyse der Genexpression und anhand der Reaktion auf Manipulation des Notch/Delta-Signalwegs charakterisiert wurde.

Zusammenfassend kann gesagt werden, dass die in dieser Dissertation vorgelegten Daten für eine evolutionäre Konservierung der Funktionen von ATP4a und des Wnt-Signalweges beim Symmetriebruch der Wirbeltiere sprechen, sowie eine Verbindung zwischen ATP4a und Wnt bei der Foxj1-abhängigen Entstehung von Cilien in *Xenopus* herstellen.

TABLE OF CONTENTS

TABLE OF FIGURES

INTRODUCTION

RESULTS

DISCUSSION

Introduction

Developmental Biology – On The Emergence Of Pattern And Structure

The fascinating field of developmental biology approaches one of the most fundamental questions in biology: How can a whole organism be formed from a single egg cell, fertilized by a tiny sperm cell? This question, with all its philosophical as well as biological implications, has challenged minds throughout human history. During the long time of theoretical and experimental attempts towards understanding the processes that eventually lead to the emergence of a viable hatchling or new-born, insights into the mechanisms that shape the embryo were dramatically expanded. Although the sheer complexity of the process is still overwhelming and the endless list of unresolved mysteries is becoming rather longer than shorter with time, some fundamental principles in the development of multicellular structures could be extrapolated: The key to understanding development is the knowledge of how patterns emerge and how distinct structures are shaped. Therefore, it is necessary to break down development into separable processes, which can be tested experimentally, and add one piece after the other to the greater puzzle.

This study tries to elucidate the influence of the ion-pump ATP4 (also called the gastric H^+/K^+-ATPase) on the early development of the frog *Xenopus laevis*, with a special focus on symmetry-breakage of the left-right (LR) axis. Therefore, the following sections will introduce the model organism *Xenopus laevis*, give an overview of mechanisms of LR-development and will describe the structure and function of ATP4. Relevant aspects of developmental mechanisms will be described using examples from *Xenopus*. Furthermore, a brief introduction on general mechanisms of cell-cell communication will be given, including an overview on cilia. Selected signaling pathways, which are of special interest in order to understand the results, will be briefly described.

The African Clawed Frog – *Xenopus laevis*

Historical Background Of *Xenopus* Research

The African clawed frog, *Xenopus laevis*, belongs to the class of amphibians and taxonomic family of Pipidae or "tongueless frogs". This fully aquatic species lives in muddy ponds in central Africa, which often tend to vary in water levels, and is therefore adapted to a broad rage of salt-concentrations and temperatures. Moreover, females of *Xenopus* species are able to respond to human pregnancy hormones (gonadotropins), which stimulate egg maturation and deposition throughout the whole year. Injection of (first morning) urine of potentially pregnant women into the dorsal lymph-sac, also called "Hogben test", was used until the 1960s for pregnancy tests (Gurdon et al. 2000), hence the German common name *Apothekerfrosch*, "pharmacy-frog".

Xenopus As A Model Organism For The Study Of Developmental Events

The ability to deliver batches of several hundreds of eggs in a predictive manner and the ease of animal husbandry have made *Xenopus* an optimal model organism for modern biomedical research, especially in developmental biology. Scientists can get hundreds of eggs from one female, which can be kept in culture. These eggs are often used either in electrophysiology, or after *in vitro* fertilization as model organism in developmental biology. The size of eggs and early embryos is relatively large (1mm in diameter), due to the high amount of maternally deposited yolk in the egg. Size and robustness of eggs and embryos, as well as the possibility to keep them in water-filled petri dishes, facilitates various forms of manipulation ranging from injections (mRNA/DNA, proteins and drugs) to incubation (differential media, protein solutions and pharmacological agents) to physical manipulations (ex-/transplantation, ablation and disruption) (Sive et al. 2000).

Many of these features are not exclusive to *Xenopus*, but shared within the class of Amphibia: e.g. the famous German embryologists Hans Spemann and Hilde Mangold performed their Nobel Prize-winning experiments on axis induction in *Triturus* species (Spemann and Mangold 1924). Therefore, it is rather the ease of animal husbandry alongside historical reasons that made *Xenopus laevis* become one of the most important

organisms in modern developmental biology. Experiments in *Xenopus* contributed fundamental findings to various fields, e.g. genomic equivalence of the nuclei, cell cycle control, existence of mitochondrial DNA and its maternal inheritance, as well as discovery of the first eukaryotic transcription factor, to name just a few (Harland et al. 2011).

The Normal Development Of *Xenopus laevis*

The normal early development of *Xenopus* can be separated into multiple phases, namely: fertilization, cleavage, blastulation, gastrulation and neurulation, followed by a phase of organogenesis and growth. At the end of early development the amphibian larva, called tadpole, emerges as a free swimming aquatic creature. The larval stage is terminated by hormone-induced metamorphosis, during which the organism is remodeled in order to generate the adult frog (e.g. retraction of gills and formation of functional lungs).

The focus of this study is on the early development, after fertilization and up to tadpole stages. Therefore I present an introduction into some of the main processes, which take place during this time-frame of development:

Cleavage And Blastula Stages

After fertilization, the maternal and paternal pro-nuclei fuse and the new genome of the embryo is assembled. During cleavage, hundreds of cells are generated from the fertilized egg by mitotic cell divisions. These cell divisions only take about 40 minutes to one hour each and are some of the fastest in the animal kingdom. This speed is possible only because all necessary proteins and factors for genome duplication and cell division are maternally deposited in the egg cytoplasm and yolk. The G-phases (1 and 2) are skipped, and the cell(s) only cycle from S- to M-phase and back. The absence of G-phases, during which protein synthesis takes place, has several consequences which make the very early embryo special in comparison to later stages: (a) There is no growth during this phase of development, rather the size of the embryo decreases; (b) only cell number increases; (c) there is barely any zygotic transcription (although some examples are known; Skirkanich et al. 2011; Gilbert 2003a).

After the first cleavages, the blastocoel cavity starts to be formed at the animal hemisphere of the blastula. This fluid-filled cavity is required for gastrulation to occur (Gilbert 2003a): It generates free space into which cells can enter, and spatially separates the most animal ("upper") cells from the vegetal ("bottom") ones. The latter secrete inductive signals that influence adjacent cells to form mesoderm (Heasman 2006). At mid-blastulation stages transcription is activated (mid-blastula transition; Newport et al. 1982), thereby facilitating differential gene-expression.

In summary, the rapid generation of many cells and the activation of transcription are crucial to "set the stage" for morphogenetic signaling events and concomitant changes in subsets of cells – hence, for the generation of diversity among cells.

Gastrulation

Gastrulation can be seen as a consequence of functional diversity among the cells generated by rapid cleavage and signaling events. During this phase of development, the embryo starts to get organized into groups of cells committed to a specific germ layer, ecto-, meso- and endoderm (Heasman 1997). The three germ layers not only get organized functionally to form prospective neural tissue and skin (ectoderm), muscles, blood and inner organs (mesoderm), and the future gut (endoderm) including derivatives (e.g. swim bladder/lungs), they also get organized by gastrulation movements (migration, involution and epiboly) in a topological sense: Meso- and endodermal cells get inside of the embryo and are covered by ectoderm, placing the endoderm inner-most, the ectoderm outer-most and the mesoderm lying in between (Gilbert 2003a).

Functional diversity among cells of the early gastrula can be best observed in the context of classical transplantation experiments of Mangold and Spemann (1924), which were originally carried out in order to understand how cell-fate specification takes place in different parts of the early embryo. They cut out a piece of tissue, just above the dorsal lip (area of dense pigmentation and first "entrance" for cells into the blastocoel cavity), and transplanted it into the ventral side of a host blastula. This small piece was able to evoke dramatic changes in the host by organizing itself and surrounding cells into a secondary anterior-posterior (AP) and dorso-ventral (DV) axis, resulting in Siamese twins. This

experiment demonstrates that cells of the gastrula are not all the same, as cells from other parts of the gastrula did not have this ability, but rather developed according to their new surrounding. Dorsal most cells communicate with surrounding cells during gastrulation in order to generate patterns and structures.

This group of cells, which was later named Spemann's organizer, is crucial for gastrulation. Both edges of the dorsal lip expand towards the ventral marginal-zone (VMZ), eventually forming a ring of cells which enter the inside of the embryo, i.e. the blastopore (Keller et al. 2003). Signal gradients of molecules secreted by the organizer induce differential gene expression along the dorso-ventral (DV) and animal-vegetal axes (Niehrs 2001). This differential gene expression results in formation of different tissues from formally non-distinguishable cells (Heasman 2006). Taking the mesoderm as an example, it forms from dorsal-most to ventral: prechordal plate/notochord, somites, heart, pronephros and blood cells (Gilbert 2003a).

As more and more cells get inside and the blastopore is progressively closed, the blastocoel is reduced and replaced by another fluid-filled cavity of importance during development - the archenteron or gastrocoel (Shook et al. 2004). This cavity will remain the inner lumen of the developing gut, and the surrounding cells will differentiate along the AP-axis to form the gastrointestinal tract, from mouth to anus.

Neurulation

During neurulation, which overlaps with late stages of gastrulation, the embryo develops most prominently the neural tube on the dorsal side. Again, the orchestrated combination of diverse signaling events, cell movements and cell-shape changes facilitates the successive emergence of patterns and distinct structures (Gilbert 2003b).

The notochord is formed during late gastrulation/early neurulation. It is derived from dorsal most mesoderm and consists of compacted cells, which are in a tight association with each other. Therefore, they form a stable rod-like structure at the dorsal midline, underneath the neuroectoderm (Gilbert 2003b). The notochord stabilizes the larva and is required for "fish-like" swimming, as it functionally antagonizes the forces generated by muscle fibers.

Paraxial (left and right adjacent to the notochord), the presomitic mesoderm is transformed in bilateral-symmetric aggregates of cells, called the somites (Brent et al. 2002). The somites are precursors of dermis, bones, muscles and tendons. The segmented arrangement of somite pairs along the AP-axis illustrates a principal scheme of developmental events: metamerism. During segmentation of the presomitic mesoderm into somites along the AP-axis, differential gene expression in distinct somites establishes groups of cells which acquire distinct fates (Couso 2009). This is demonstrated best by comparison of vertebrae along the AP-axis: Differently shaped cervical vertebrae (e.g. atlas, axis, etc.), thoracic vertebrae connected to differently shaped ribs, lumbar and the (mostly fused) sacral vertebrae are all formed from different somites along the AP-axis (Gilbert 2003c).

Ectoderm overlying the dorsal mesodermal structures forms the neural plate, which gives rise to the neural tube. The neural tube is formed by extensive cell-shape changes within groups of cells of the neural plate. Lateral cells start to form the neural folds – a thickening of the tissue – including the dorsal-lateral hinge points (DLHPs), which fold towards the ventral side. The medial-most cells connect to the notochord and change their shape by apical constriction, eventually forming the medial hinge point (MHP) and folding paraxial neural plate cells upwards. Therefore, the neural folds get into close proximity and can fuse with each other, eventually covering the prospective lumen of the neural tube (Gilbert 2003b).The neural tube gives rise to the central nervous system, but also peripheral neural cells and non-neural cells are generated. In *Xenopus*, neural tube closure starts at the caudal end and extends progressively anterior-wards (Ueno et al. 2003). The largest diameter of the neural tube is found at the anterior end, which will form the brain. Failure of neural tube closure has dramatic consequences for the developing organism, including lack of anterior brain structures (anencephaly) (Wallingford 2006; Copp et al. 2010).

Organogenesis And Growth

The generation of organs and general growth of the embryo is accomplished during subsequent tailbud and tadpole stages. Although the various organs of a vertebrate differ in size, placement, form and function, the generation of this diversity follows similar principles: Groups of cells get more and more subdivided into different parts, which start to

express different genes. This way, organs get shaped step by step, and each step modulates the reaction potential or competence of cell groups to react to developmental signals – the cells get progressively restricted in their developmental potential (or further determined) (e.g. Asashima et al. 2009).

A common variation of this theme is that a group of cells splits into several independent populations, which migrate into different locations and acquire different fate. This way the differentiation of cell populations is due to the unique "cocktail" of signaling molecules which they were exposed to while migrating to their final location. An example for this type of development is the neural crest (NC) (Epperlein et al. 1996). The NC develops from the lateral-most cells of the neural plate and is induced during gastrulation/neurulation. These cells do not integrate into the roof of the neural tube, but undergo epithelial to mesenchymal transition and migrate in streams to different locations, where they form such diverse tissues as pigment cells, cartilage, connective tissue and neurons (Mayor et al. 2001). While their fate is eventually determined at their final location, the cells composing the NC are already restricted in their potential even before they start to migrate. Cranial (anterior most) NC cells (NCC) migrate properly and contribute to the facial cartilage even when transplanted from one embryo into the corresponding location of a host embryo. This is not the case when they are transplanted into a more posterior location of the NC (trunk NC), which e.g. can differentiate into pigment cells, in contrast to the cranial population. The cranial NCCs fail to migrate and differentiate (neither cartilage, nor pigment) in the wrong environment, demonstrating their already restricted developmental potential at that stage (Borchers et al. 2000).

Beside the formation of individual organs, the embryo starts to change its shape from neurulation onwards (Lecuit et al. 2007). Two major modes can be observed during embryogenesis, i.e. increase in volume and elongation of the AP-axis. While increase in volume is mainly a result of active water transport into the increasing number of cells and embryonic cavities, elongation of the AP-axis requires complex cell-cell interactions and signaling events. The process which contributes most to AP-axis elongation is convergent extension (CE) (Wallingford et al. 2002). CE movements are performed by cells of the dorsal meso- and ectoderm, i.e. notochord and neural plate, respectively. While cells converge from lateral towards the midline, the cells in the midline extend along the AP-axis. Therefore, the embryo gains in length at the expense of a decrease in width. Similar to NCC migration, this process also demonstrates that individual cells and cell groups can

interpret signals from their environment, leading to coordinated behavior that shapes tissues, which in turn shape the embryo (Keller et al. 2008).

This holds also true for the morphogenesis of organs, as the shape of organs is generated by coordinated behavior in terms of cell shape change and migration as well. Taking the developing heart as an example, organogenesis starts with the definition of the heart field within the mesoderm. During gastrulation/neurulation, the heart field is induced as two bilateral symmetric groups of cells next to the somitogenic mesoderm. During neurulation, these cell groups start to migrate towards the anterior ventral midline, where they fuse and form a tube, lying in AP-direction (Abu-Issa et al. 2007). The different parts of the heart, like sinus venosus, atrium or ventricle, are patterned along the AP-axis. Then, the heart tube is bent by coordinated cell shape changes, e.g. apical constriction, and hinge points are formed (Linask et al. 2007), like during neural tube closure. In this way different parts of the organ are spatially rearranged in respect to each other to form the functional heart (Gilbert 2003d).

How Cells Communicate – Signals That Shape The Embryo

General Mechanisms Of Cell-Cell Communication

The ability of cells to communicate with each other is crucial for all coordinated developmental events, and common features of cell-cell communication can be found in all signaling pathways. In most cases the first step of communication is represented by a signaling molecule. This can be a wide range of proteins, peptides and chemicals – even ions can serve this function. The signaling molecule is either released by one cell and can diffuse, or gets transported away from the source, represented on the outer surface of the cell´s membrane, or can cross from cell to cell via cytoplasmatic contacts, e.g. gap junctions (GJs) (Alberts et al. 2008).

The production, shuttling and modification of signaling molecules (also called ligands) represents an important level of regulation and complexity in cell signaling. Diffusible molecules often interact with other molecules which modulate the signaling potential. Binding to different partners can be required for signaling to occur, or it can inhibit signaling by negatively influencing binding affinity to the receptor, to name just one example. It can also modulate the diffusion behavior, i.e. facilitating or restricting long-range signaling across several cell diameters away from the source (Xu et al. 1998; Mii et al. 2009; Ruel et al. 2009; Bayramov et al. 2011).

After the ligand is released from the signaling cell, it travels to another cell and is able to evoke a response when this cell is competent to receive the signal. Prerequisite for signal detection is the presence of a receptor, to which the ligand can bind. In most cases, receptors are located in the cell membrane, as most ligands cannot cross the lipid bilayer and need to be detected outside of the cell. Binding of the ligand to the receptor leads to biochemical reactions, often accompanied by conformational changes and modification (e.g. phosphorylation) of the intracellular part of the protein. Therefore, the task of most receptors is the interpretation of an extracellular signal and the translation of this signal into an intracellular reaction (Alberts et al. 2008).

In the majority of cases, the signal is amplified within the cell´s cytoplasm by activation of second messengers, e.g. cAMP, calcium ions (Ca^{2+}) or proteins. Amplification is often

achieved by enzymatic function of the receptor, of a co-receptor or other proteins, which were activated by the receptor. Therefore, one activated receptor can activate many second messenger molecules (Chen et al. 2007; Ilagan et al. 2007; MacDonald et al. 2007; Semenov et al. 2007; Delmas 2008; Harder et al. 2008; Dutko et al. 2011). The diversity of cellular mechanisms of communication is the core of the developmental signaling events, which give rise to differential form and function in cells and tissues.

Structure Of Motile And Non-Motile Cilia

The cilium is a membrane-covered organelle, extending to the outside. The core of a cilium is composed of microtubuli, i.e. filaments of acetylated α- and β-tubulin (Figure Int-1). They are organized in nine outer doublets and can contain either non, two or four inner tubules (Feistel et al. 2006). The outer doublets are interconnected by nexins, and radial spokes project from each doublet towards the center of the cilium/inner tubules (Satir et al. 2007). The cilium can be either non-motile (primary cilium) and serves as cellular sensor, or motile and able to fulfill coordinated beating. This motion is accomplished by molecular motor proteins, namely dyneins, which connect to the tubulin doublets and exert force (Satir 1980). The force slides one doublet against the other, and the sum of sliding results in bending of the cilium (Riedel-Kruse et al. 2007) (inset in Figure Int-1).

Ciliogenesis starts at the basal body, which also serves as centriole after duplication (Avasthi et al. 2011). Therefore, cells which undergo mitosis have to retract their cilium, and the daughter cells have to form new ones (Jackson 2011). For ciliogenesis to occur, the ninefold symmetric basal body is translocated to the apical membrane where it docks to the subapical actin-filament meshwork (Gomperts et al. 2004; Satir et al. 2007; Vladar et al. 2008). This is thought to stabilize the basal body, promote ciliogenesis and regulate ciliary length (Avasthi et al. 2011) (Figure Int-1). At the same time, a ciliary vesicle is detached from the Golgi apparatus and connects to the basal body. Shuttling of proteins to the basal body is highly regulated and can also occur in vesicles. This holds also true for proteins located in the ciliary membrane, which facilitates the specific localization of (e.g.) receptors to the cilium (Molla-Herman et al. 2010) (Figure Int-1). As the cilium grows, it pushes the ciliary vesicle towards the membrane, which fuses with the cell membrane (Avasthi et al. 2011). Growth of the cilium takes place at the tip (plus-end), and cargo that is aimed to be attached at the tip needs to be actively transported along the tubulin

filaments. All transport along the cilium is dependent on the intraflagellar transport (IFT) machinery, which is composed from an A- and B-complex (Cole et al. 2009; Taschner et al. 2011) (Figure Int-1).

From base to tip, the cilium is subdivided into functional parts: The basal body is responsible for organized shuttling of factors from and to the ciliary compartment (Satir et al. 2007). Transition fibers at the base of the cilium delimit the ciliary compartment and mark the transition between cell and ciliary membrane. They attach to the transition zone of the ciliary membrane, which forms the ciliary pocket at the base (Molla-Herman et al. 2010) (Figure Int-1). This is also the place where cilia-related endocytosis happens, as well as the area where vesicles from the Golgi apparatus fuse. The longest part of the cilium is the shaft, which covers the nine tubulin doublets (Eggenschwiler et al. 2007). The length of the shaft varies considerably in motile as well as non-motile cilia and is of functional relevance (Riedel-Kruse et al. 2007). The tip of the cilium is the most active place, as it is the site of polymerization and depolymerization (Marshall et al. 2001).

Signaling Properties Of The Cilium

The ciliary membrane contains a specific subset of cellular proteins, among which various signaling receptors can be found (Eggenschwiler et al. 2007). Another level of signaling regulation is added when cell-cell signaling depends on receptors or processing at the cilium (Jackson 2011). Signaling pathways, which are strictly dependent on a cilium (e.g. vertebrate Hedgehog-signaling), can only be activated when the cell is not dividing, because the receptor-containing cilium is retracted during mitosis (Rohatgi et al. 2007). Cilia are also able to sense mechanical stress exerted by solid and fluid matter. When specialized mechanosensory cilia are deflected, a cellular response is triggered (Davenport et al. 2005; Berbari et al. 2009).

Moreover, cilia play a role in sensory cells: Both types of vertebrate photoreceptors contain highly specialized cilia, which harbor light sensitive pigments. In vertebrate cone- and rod-cells, the opsin-containing outer segment is connected to the inner segment by ciliary structures (Fliegauf et al. 2007; Oh et al. 2012). Therefore, the whole outer segment of the photoreceptor can be imagined as specialized cilium with highly enlarged membrane surface and inner volume. Smell is also a cilia-dependent sensation in vertebrates, and

odorant receptors are located on cilia, which project in bundles from olfactory primary sensory neurons into the mucosa of the nasal epithelium (Krieger et al. 1999).
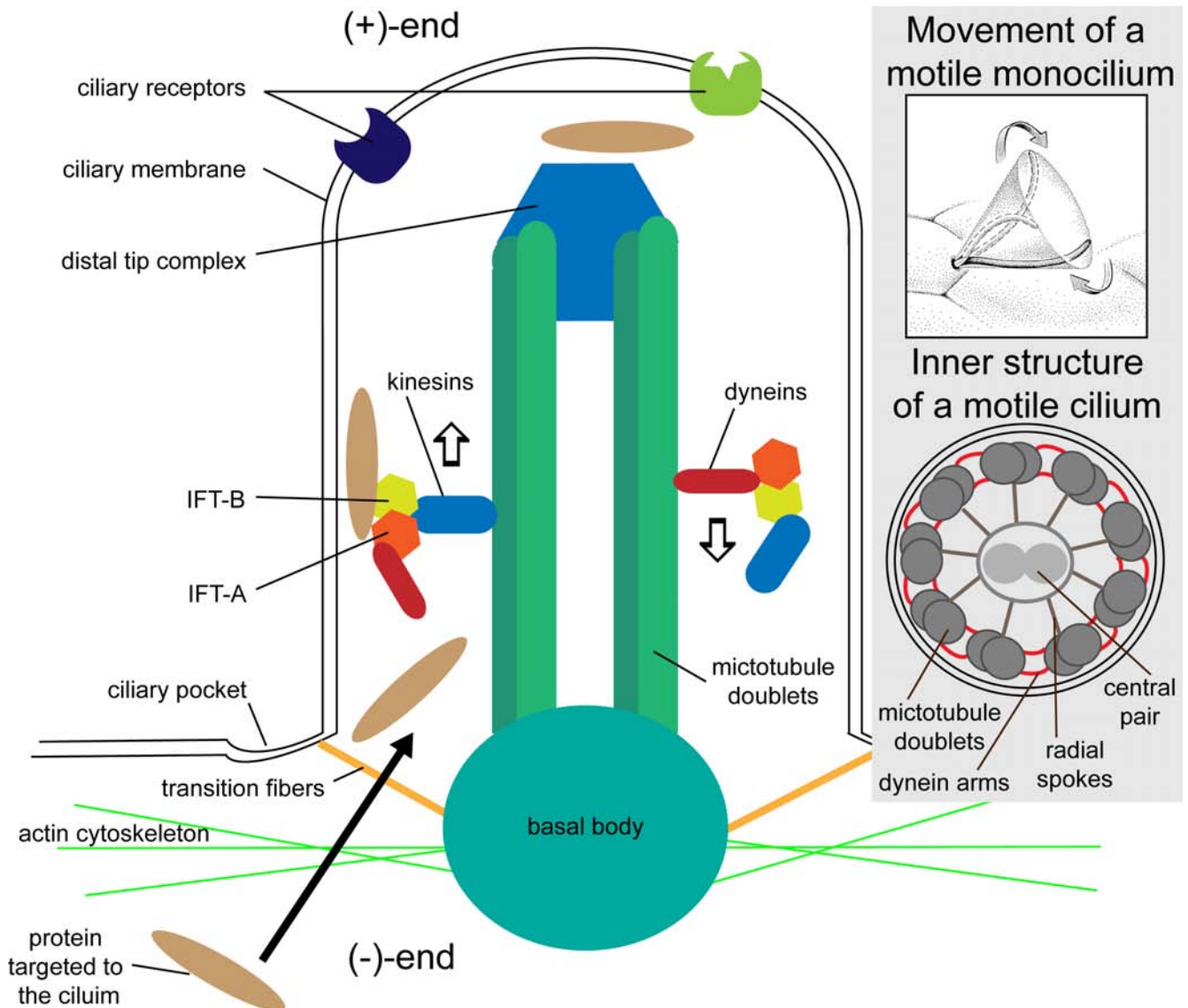
Figure Introduction-1: The Cilium – Structure And Function

Ciliogenesis starts at the basal body where microtubule doublets polymerize. The basal body is anchored at the membrane by transition fibers, which connect to the ciliary pocket (place of endocytosis and vesicle fusion). The basal body is also stabilized at the apical membrane by the actin cytoskeleton meshwork. Proteins, which are targeted to the ciliary compartment, enter the cilium at the base via the basal body (and associated proteins). Transport along the microtubules is accomplished by intraflagellar transport (IFT) complexes. IFT-B, together with kinesins (KIFs), are responsible for transport towards the (+)-end, while IFT-A, together with dyneins, are responsible for transport towards the (-)-end. The microtubules are stabilized at the (+)-end by the distal tip complex of proteins, which also mediate assembly/disassembly of microtubule doublets. Moreover, the cilium is involved in signaling events, e.g. the ciliary membrane contains specific receptors. Reviewed in: *Eggenschwieler et al. 2007*.
Gray inset: (Upper panel) Movement of a motile monocilium at the PNC/GRP.
Taken from: *Blum et al. 2009**.
(Lower panel) Cross section of a motile cilium, containing dynein arms, radial spokes and a central pain complex. Reviewed in: *Basu et al. 2008*.

Developmental Signaling Pathways

In the following sections three major developmental signaling pathways, i.e. Wnt, Hedgehog and Notch/Delta, will be introduced. In contrast to other signaling pathways, which were implicated in LR-development (e.g. BMP and FGF) as well, basic understanding of these three pathways is essential for understanding this work:

(1) Wnt-Signaling

Wnts are secreted glycolipoproteins, discovered during the 1970s in *Drosophila melanogaster* and later in mammals (Sharma et al. 1976; Nusse et al. 1982). Over time, the Wnt-signaling pathway turned out to be a highly branched pathway, causing developmental defects, cancer and other diseases when dysregulated (Lucero et al. 2010; Wend et al. 2010).

Activation of the pathway requires a member of the Wnt-ligand family to bind to a transmembrane receptor of the Frizzled (Fz) family, which in turn recruits other membrane-bound and cytoplasmatic factors. In most cases the cytoplasmatic phosphoprotein Dishevelled (Dsh) is recruited to the complex, but this step is not required for all pathway branches (Macdonald et al. 2007; Semenov et al. 2007). The (combinations of) players are specific to the different branches, and are a prerequisite for the diversity of this ancient pathway, conserved throughout the animal kingdom – from jellyfish to man (Watanabe et al. 2009). Different branches can be separated into the canonical (β-catenin ;β-cat dependent) and several non-canonical branches, including the planar cell polarity (PCP) pathway, the Wnt/Ca^{2+} pathway, Wnt/Ror2 pathway and the protein kinase A (PKA) and protein kinase C (aPKC) dependent pathways (Macdonald et al. 2007; Semenov et al. 2007). An in depth introduction covering all pathway branches would exceed the aim and scope of this thesis. Therefore, I will focus on the two branches which are most relevant for this work, i.e. the canonical Wnt/β-cat and the non-canonical Wnt/PCP pathways (Figure Int-2):

The Wnt-signalosome and signaling pathway activation
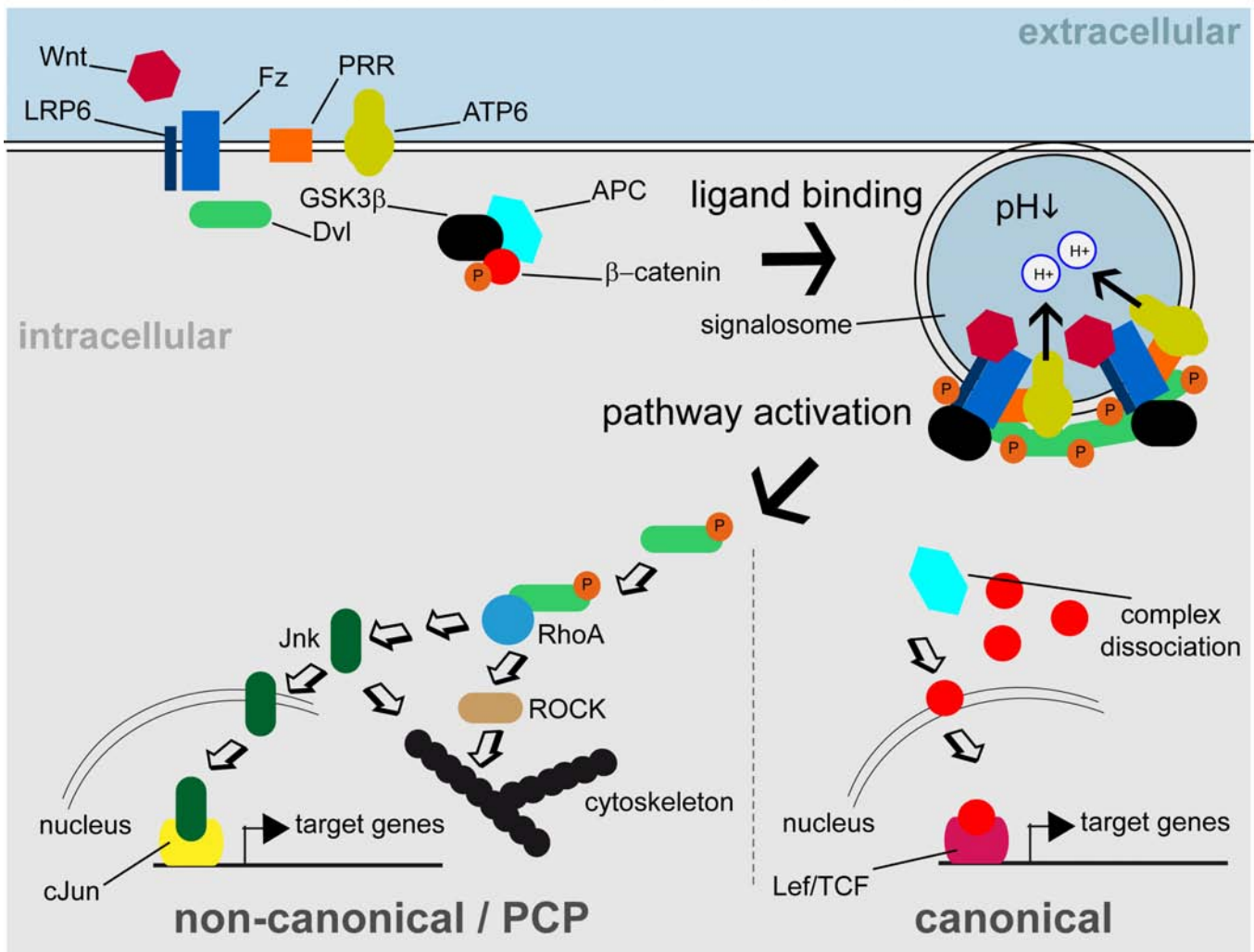
Figure Introduction-2: The Wnt-Signalosome And Signaling Pathway Activation

Upon binding of a Wnt-ligand to a Frizzled (Fz) receptor at the outer surface of the plasma membrane, Dishevelled (Dvl) is recruited to the complex and phosphorylated (P) by Fz. Dvl polymerizes with other Dvl molecules, therefore recruiting more receptors/co-receptors to the complex, and probably inducing signalosome formation/internalization. The vacuolar H^+-ATPase (ATP6) is bound to Fz via prorenin receptor (PRR) and acidifies the signalosome. Decrease in signalosome pH facilitates activation of the canonical Wnt/β-catenin (β-cat) or Wnt/planar cell polarity (PCP) branch of signaling.

Within the **canonical branch**, the glycogen synthase kinase 3 β (GSK3β) is ultimately recruited to the intracellular tail of low-density lipoprotein receptor-related protein 6 (LRP6), which inhibits complexation with adenomatous polyposis coli (APC), β-cat binding and degradation. Stabilized β-cat can enter the nucleus and activate gene expression with Lef/TCF transcription factors.

Within the **PCP branch** phosphorylated Dvl activates small Rho A GTPase (RhoA), which in turn activates the Rho-associated protein kinase (ROCK) and the c-Jun N-terminal kinase (Jnk). ROCK and Jnk both act on the actin cytoskeleton, and Jnk can also enter the nucleus and stimulate gene expression via the cJun transcription factor.

Reviewed in: *Macdonald et al. 2007; Semenov et al. 2007 and Niehrs et al. 2010*.

The molecular mechanism of the canonical pathway is best understood, and activation of this branch results in transcriptional regulation of context-dependent target genes. Some Wnt ligands can activate this pathway branch, e.g. Wnt3a and Wnt8a, while other Wnts seem to have minor, context-dependent or no influence, e.g. Wnt11 and Wnt5a (Wallingford et al. 2001; Kofron et al. 2007; Yamamoto et al. 2008; Bourhis et al. 2010; In der Rieden et al. 2010; Nishita et al. 2010; Uysal-Onganer et al. 2012). Essentially, the same is true for the Fz receptors (Djiane et al. 2000; Wallingford et al. 2001; Hendrickx et al. 2008). Activation requires the recruitment and activation of Dvl proteins. Dvl binds directly to the activated intracellular part of Fz via its central PDZ domain, which is pivotal for activation. Furthermore, Dvl has the ability to polymerize by binding to other Dvl molecules to the DIX-domain (Gao et al. 2010). The polymerization of Dvl is necessary for signalosome formation, an endocytotic process, involving clathrins (Bilic et al. 2007; Ohkawara et al. 2011) (Figure Int-2). The internalization of the Wnt-signalosome is necessary for activation of the low-density lipoprotein related proteins LRP5 or 6, that serve as co-receptors (Niehrs et al. 2010). Upon internalization of the signalosome, a closed compartment is established, and the lumen is acidified by the proton pump vacuolar H^+-ATPase (ATP6) (Cruciat et al. 2010). The low pH is a prerequisite for the activation of LRP5/6 by two kinases: casein kinase 1γ (CK1γ) and the glycogen synthase kinase 3 β (GSK3β), which phosphorylate the intracellular tail of LRPs (Niehrs et al. 2010). Why this process requires low pH in the signalosome has remained enigmatic. The phosphorylated intracellular part of LRP5/6 is able to recruit axin to the complex, which in turn is associated with GSK3β and likely promotes further LRP5/6 phosphorylation on the five PPPSPxS motives (P, proline; S, serine or threonine; x, variable) of LRPs (Niehrs et al. 2010). When the pathway is not activated, axin forms a complex with the adenomatous polyposis coli (APC) and GSK3β, which are both responsible for binding, phosphorylation and subsequent degradation of β-cat (Chen et al. 2000; Aoki et al. 2007). β-cat is involved in many cellular processes, e.g. cell-cell adhesion, but within the canonical Wnt-branch it serves as transcriptional co-activator in the nucleus. Upon pathway activation the degradation of β-cat is inhibited, it can enter the nucleus and form transcriptional activator complexes together with factors from the transcription-factor/lymphoid enhancer-binding factor (TCF/LEF) family, which directly bind to regulatory DNA-sequences of target genes and promote transcription (MacDonald et al. 2009) (Figure Int-2).

For activation of the Wnt/PCP pathway in vertebrates (but not necessarily in *Drosophila*) Wnt ligands, e.g. Wnt11r or Wnt5b, have to activate Fz. Fz recruits Dvl, like in the canonical pathway (Cha et al. 2008; Hardy et al. 2008; Vladar et al. 2008; Gao et al. 2011; Wallingford et al. 2011). Signalosome formation and ATP6-components are also required, implicating that pH-shift in the signalosome is necessary for activation of the PCP-branch as well (Buechling et al. 2010; Hermle et al. 2010). The role of LRPs in Wnt/PCP is not quite clear, because CK1γ- and GSK3β-dependent phosphorylation does not take place. Nevertheless, gain- and loss-of LRP6 function dysregulates Wnt/PCP (Tahinci et al. 2007). Upon activation of Dvl, the cytoplasmatic factor Dvl-associated activator of morphogenesis (Daam) is bound by the PDZ- as well as by the DEP-domains of Dvl (Cadigan et al. 2006; Gao et al. 2010). Binding of Daam to Dvl releases inhibition of Daam, which then can associate with the small GTPase Rho A (RhoA). The Dvl/Daam/RhoA-complex is able to activate the ROCK kinase and other effectors (Semenov et al. 2007), which modify the actin cytoskeleton (Skoglund et al. 2008) (Figure Int-2). Actin remodeling is crucial for directed migration, CE movements and ciliogenesis (Wallingford 2006).

Planar polarity is established by asymmetric distribution of Dvl and Van Gogh like (Vangl) to the posterior- and anterior-apical membrane, respectively (Vladar et al. 2009). The initial asymmetric cue in vertebrates seems to be provided by Wnt-gradients (Gao et al. 2011). In *Drosophila* and within some vertebrate tissues, polarity is also mediated by direct cell-cell interactions, e.g. via Fat/Dachsous, which can act in parallel to Wnt/PCP in *Drosophila* and mouse (Ishiuchi et al. 2009; Donoughe et al. 2011). Another aspect of Wnt/PCP is transcriptional regulation of target genes. This is mediated by Dvl and the small GTPase Rac 1 (Rac1). The Dvl/Rac1-complex activates the c-jun-N-terminal kinase (Jnk). In consequence, this enables the transcriptional co-activator c-Jun to bind to c-Fos and act as transcription factor, like β-cat in the canonical Wnt pathway (Semenov et al. 2007; Ohkawara 2011) (Figure Int-2).

(2) Hedgehog-Signaling

Hedgehog (HH) is another example for a secreted signaling molecule with many roles in development and disease (Jiang et al. 2008). It was originally discovered in *Drosophila*, but HH signaling defects are also correlated with cancer and embryonic mispatterning in vertebrates (Perrimon et al. 1987; Chang et al. 1994). HH (like Wnt) is a morphogen,

which acts dose-dependently. An example for HH defects during development is cyclopia: DV- and proximal-distal (or medio-lateral) patterning of the neural tube and brain is under control of HH. Disruption of the pathway in sensitive stages affects separation of the eye-fields, causing development of one single eye and holoprosencephaly (fusion of anterior brain lobes), the most common structural malformation of the forebrain in humans (Chiang et al. 1996; Wallis et al. 1999). Sonic hedgehog (Shh), one of three vertebrate HH homologs (Shh, Indian and Desert hh), is released at the midline of the developing brain, generating a gradient from medial to lateral. Thereby, it controls the expression of two paired-box genes (Pax), namely *Pax2* and *Pax6* (Amato et al. 2004). Because *Pax2* transcription is activated by high levels of Shh, it induces optic stalk development near the midline, while the more distal parts of the eye, e.g. the retina, develop under the control of *Pax6* (which is inhibited by *Pax2* expression). Lack of Shh leads to a lack of *Pax2* expression and shifting of the *Pax6* expression domain towards the midline, hence inducing formation of one single eye.

The HH ligands need to undergo profound post-translational modification during maturation in the Golgi apparatus, i.e. the C-terminal (membrane-bound) part of the protein is cleaved off to release the diffusible ligand (Gallet 2011). Cholesterol modification of ligands enables interaction with the lipophilic membrane, which might be the reason for the requirement of the transmembrane protein Dispatched (Disp; a sterol sensing domain-containing protein) for long-range signaling, but not for juxtacrine signaling (Cohen 2003; Chen et al. 2007). The cholesterol is also required for the formation of micelle-like aggregations of HH ligands and long-range signaling. When released, the ligand can bind to Patched (Ptc) and releases repression of Smoothened (Smo) within the membrane. In absence of ligand, the Ptc/Smo-complex is located at the cell membrane, but when Smo is released from Ptc, it is translocated to the primary cilium in vertebrates, where it becomes enriched in the ciliary tip (Bisgrove et al. 2006). The intracellular mediators of the pathway are the zinc finger proteins of the glioma-associated oncogene (Gli) family. Glis are bound by suppressor of fused (Sufu), targeted to the primary cilium and phosphorylated by PKA, presumably after exit from the ciliary compartment (Wang et al. 2007; Tuson et al. 2011). Gli1 and 2 are degraded or recycled when the pathway is not activated. In contrast, unactivated, phosphorylated and Sufu-bound Gli3 is cleaved at the proteasome, which turns it into a strong transcriptional repressor of HH target genes (Chen et al. 2007; Wang et al. 2007). Interestingly, shuttling to the cilium is not necessary for Sufu to act as inhibitor of the pathway, which might explain inhibition of the pathway in absence of primary cilia.

Upon pathway activation, Smo associates with Sufu and Gli. This releases Gli from Sufu inhibition, prevents phosphorylation by PKA at the basal body and thereby stabilizing Gli and activating HH target genes (Chen et al. 2009; Ruel et al. 2009).

(3) Notch/Delta-Signaling

While Wnt- and HH-signaling act via diffusible ligands (Chen et al. 2007; Macdonald et al. 2007; Semenov et al. 2007), this is not the case in Notch-signaling (Ilagan et al. 2007). Here, not only the receptor is a transmembrane protein, but also the (canonical) Delta-like (Dll) and Jagged ligands. This mode of signaling limits the Notch-signaling range to direct cell-cell interactions, and therefore contributes a new mode of developmental cell signaling to the highly conserved tool-box of metazoan signaling pathways (Wnt-, HH-, Notch-, JAK/STAT-, BMP/TGFβ- and PI3K/AKT-signaling pathways) (Alberts et al. 2008). The core pathway is rather simple in comparison to the Wnt- and HH-pathways: In contrast to other pathways, it does not rely on second messengers (Ilagan et al. 2007).

The receptor Notch is a single pass type 1 transmembrane protein, and four family members (Notch1-4) are found in mammals (Kopan et al. 2009). During receptor maturation, the protein is glycosylated in the endoplasmic reticulum (ER) (Andersson et al. 2011). In Fringe-containing cells, further sugars are added to the ligand-binding part of Notch while the protein passes the trans-Golgi network (Andersson et al. 2011). These modifications affect the binding affinity to different ligands, i.e. Furin glycosylated Notch-receptors less likely bind to Jagged, but are very affine to Dll ligands. Moreover, the Notch receptor is cleaved by Furins at an extracellular domain, near the membrane, which yields a heterodimeric receptor protein (only held together by non-covalent binding). The receptor is then exposed to the outer membrane of the cell, where it can interact with Dll or Serrate ligands, which activate the pathway. Upon ligand binding, the N-terminal part of the receptor is endocytosed and degraded (Denef 2010; Niehrs et al. 2010). The dissociation of the N-terminal part may release repression via binding to other Notch-receptor proteins in the membrane (thereby preventing cis-activation), but this is still under debate (Andersson et al. 2011).

In consequence, the Notch extracellular truncated (NEXT) domain in the signal receiving cell is processed by ADAM metalloprotease and subsequently by γ-secretase. These

cleavage events may happen, context-dependent, directly at the cell membrane or in endocytosed vesicles, eventually leading to the release of Notch-intracellular domain (NICD) into the cytoplasm (Kopan et al. 2009). NICD is the active transducer of signaling and translocates to the nucleus, where it regulates gene expression. NICD binds to CSL (CBF1/suppressor of hairless/LAG-1) / RBP-J (recombination signal binding protein for immunoglobulin kappa J), which is stabilized by mastermind-like (Maml) proteins, and binds to target regions of the DNA (Kopan et al. 2009).

While morphogens induce a graded response along a diffusion gradient, resulting in dose-dependent differential gene regulation (i.e. high amounts = activation of gene A, low amounts = activation of gene B), Notch-signaling intensity seems to correlate with the amount of gene activation (i.e. high amounts = strong activation of gene A, low amounts = weak activation of gene A). The Notch/Delta-pathway is often utilized to define sharp borders between two adjacent cell fields (like in the *Drosophila* wing), for lateral-inhibition of differential cells within one tissue (like in *Drosophila* sensory neurons of the eye) and for cell-cycle exit control in differentiating daughter cells within stem cell niches. Dysregulation of the pathway is implicated in cancer initiation and progression and other human syndromes as well as developmental defects (Ja et al. 2003; Talora et al. 2008).

Patterning The Early Embryo: Anterior-Posterior And Dorso-Ventral Axis Development

In *Xenopus*, patterning of the embryo starts already in the oocyte. The oocyte is composed in an asymmetric manner with differences between the animal and vegetal halves of the cell. The animal part is pigmented, while the vegetal part is unpigmented. Within the cell, the cytoplasm is situated animally, because dense yolk droplets are accumulated vegetally. During fertilization, the sperm can only interact with the oocyte at the animal surface, as species-specific sperm receptors are only located within the pigmented area. This restriction is of functional relevance for primary axis induction, i.e. the proper generation of the anterior-posterior (AP) and dorso-ventral (DV) axes (Klein 1987; Tian et al. 1997b, 1997a; Heasman 2006a, 2006b; Nagai et al. 2009): The DV-axis is initiated by sperm entry, and at the opposite of the sperm entry point, the dorsal-most part of the embryo will emerge.

After entering the oocyte, the sperm not only contributes the genetic material, but also a centriole. The centriole is used as microtubuli organizing center, and tubulin filaments form in coordinated patterns upon fertilization (Elinson et al. 1989; Gilbert 2003a). Polymerized tubulin connects the centriole with the cell cortex, and after attachment, it is retracted towards the centriole. This process pulls the cortex of the zygote, which shifts about 30° towards the sperm entry point, relative to the cytoplasm and yolk (Scharf et al. 1980; Heasman 1997). The vegetal pole contains factors which are bound to the cortex and get transported more animally by cortical rotation. The point where these factors accumulate defines the dorsal-most point of the embryo, i.e. the tissue which will form the organizer and induce gastrulation. These factors belong to the Wnt-signaling pathway and include mRNAs encoding the ligand Wnt11 (*Xwnt11b*), the intracellular component Dvl and β-cat stabilizing factor Gbp (or Frat1) (Elinson et al. 1989; Heasman 1997; Tao et al. 2005; Heasman 2006b; Kofron et al. 2007; Tadjuidje et al. 2011). The germ vesicle gets translocated in the very same way and may also play a role in axis induction (discussed in Cuykendall et al. 2009). As a consequence of cortical rotation, β-cat is stabilized preferentially on the dorsal and not the ventral side, accumulates in the nuclei of dorsal cells and activates gene expression after the mid-blastula transition (MBT) (Newport et al. 1982).

The animal-vegetal axis correlates roughly with the AP-axis, but – more importantly – localized mRNAs of vegetal factors define the three germ layers (endo-, meso- and ectoderm). On the one hand, the vegetally localized T-box transcription factor Veg T initiates expression of endodermal genes. On the other hand it activates transcription of transforming growth factor β (TGFβ) genes from the nodal family (*Xenopus* nodal related proteins; Xnrs) (Heasman 2006a, 2006b). Moreover, *Xnr* expression is synergistically enhanced by β-cat. This leads to the generation of a concentration gradient of Xnr proteins along the endodermal DV-axis, which pattern the overlying prospective mesoderm. The area with the highest Xnr concentration (dorsal-most) is the Nieuwkoop center which induces the organizer in adjacent mesodermal cells (Niehrs 2001, 2010).

The molecular nature of the organizer is defined by a specific set of transcription factors, e.g. goosecoid (Gsc), as well as secreted inhibitors (e.g. noggin and chordin) of another group of TGFβ signaling molecules from the bone morphogenetic protein (BMP) family. The inhibition of BMP signaling in the organizer and the creation of a DV-gradient by secreted antagonists set up the DV-coordinate system, which influences patterning in all three germ layers, e.g. notochord formation and induction of neural fate (Blum et al. 1992; Steinbeisser et al. 1995; Knecht et al. 1997; Sasai et al. 1997; Niehrs 2010).

As mentioned above, the animal-vegetal polarity correlates with the AP-axis. This is accomplished by secreted and membrane-bound Wnt-signaling inhibitors, e.g. frizbee (Frzb; also called *Xenopus* secreted Frizzled related protein 3; Xsfrp3) and dickkopf (Dkk), respectively. The level of Wnt-signaling inhibition is highest in prospective anterior regions, and the release of Wnt inhibition abolishes head induction (Niehrs 2001).

Taken together, a "Cartesian coordinate system" for the DV- and AP-axes is established by signaling activity gradients of BMP- and Wnt-signaling, respectively. This two-gradient system is probably conserved and could also apply to non-vertebrate deuterostomes, as well as to protostomes (de Robertis et al. 1996; Niehrs 2010).

Left-Right Axis Development

Generating *De Novo* Asymmetries

The third axis is the left-right (LR) axis, along which asymmetric organs (e.g. the heart and the gastrointestinal tract) are formed. LR-axis asymmetry is a consistent feature of the vertebrate body-plan (Basu et al. 2008; Fakhro et al. 2011). The vertebrate embryo starts developing as a bilateral-symmetrical structure in respect to the dorsal midline (Schweickert et al. 2011). This symmetry needs to be broken as development proceeds and before asymmetric organs are formed. Asymmetry has to be established *de novo* by a process that is biased towards one direction: Within the vast majority of species, only one of two possible arrangements of visceral organ placement is dominant (referred to as *situs solitus*), and the "mirror-image" (called *situs inversus*) is only very rarely seen (Hirokawa et al. 2012).

In the early 1990s the existence of a chiral "F-molecule" was postulated by Wolpert and Brown to be the basis for the generation of LR-asymmetry and for the bias towards *situs solitus* (Brown et al. 1990). The hypothesis proposed that intrinsic molecular chirality results in asymmetric function of larger-scale cellular structures, e.g. cytoskeletal components. If this kind of molecular asymmetry is of instructive nature in regard to LR-axis development, then this would explain the bias to *situs solitus* (as chirality is an important feature of biomolecules, e.g. only the L-form of amino acids is used for proteins). This hypothesis was supported by earlier findings, which revealed the cause of Kartagener's triad: This human condition is correlated with LR-axis defects and *situs* inversion, which was linked to immotility of primary cilia (primary cilia dyskinesia) (Afzelius 1976, 1999; Berdon et al. 2004). Cilia are composed of microtubules, which fit the postulated "F-molecule" prediction: cytoskeletal components, which are able to conduct asymmetric movements (Bisgrove et al. 2006) .

Direct evidence that cilia and the generation of fluid flow were responsible for the establishment of LR-asymmetry was provided by the group of Hirokawa, who demonstrated the existence of a directed, leftward flow of extra-cellular fluid at the mouse posterior notochord (PNC; also referred to as the "node") (Nonaka et al. 1998). This fluid flow was generated by the movement of motile monocilia (Nonaka et al. 1998; Takeda et

al. 1999). Furthermore, superimposing artificial flow towards the right side of the PNC activated the nodal cascade at the right side, demonstrating the instructive potential of this event regarding the LR-axis (Nonaka et al. 2002).

The directionality of flow requires Wnt/PCP mediated planar-polarity cues (Antic et al. 2010; Borovina et al. 2010; Hashimoto et al. 2010; Song et al. 2010). Initially, motile monocilia grow at a central position of the cell´s apical surface, but get posteriorly localized by cytoskeletal rearrangements, which require the core-PCP component Vangl2. In combination with the posterior tilt of the cilia, their clockwise beating results in an effective stroke towards the left side (while the cilium reaches into the fluid), and an ineffective stroke towards the right side (while the cilium is sliding over the cell membrane) (Hilfinger et al. 2008; Hashimoto et al. 2010). Therefore, AP- and DV-axis information (which mediate generation of the ciliated epithelium and cilia polarization) are translated into an LR symmetry-breaking cue: the leftward flow.

The initial symmetry-breaking event needs to be translated and "imprinted" on the tissues, which will form asymmetric organs. Thus far, the exact mechanism of flow perception is still not understood, but two models were proposed (McGrath et al. 2003; Karcher et al. 2005; Hirokawa et al. 2006, 2009; Hamada 2008; Vick et al. 2009; Field et al. 2011; Kamura et al. 2011; Hirokawa et al. 2012):

Morphogen model
In this model a morphogen, released by the ciliated epithelium at the midline, travels with the fluid flow and accumulates on the left side. This morphogen then triggers laterality. Shh as well as retinoic acid (RA) were proposed to serve as LR-morphogens in the mouse (Norris 2005, Tanaka et al. 2005).

Two cilia model
The two cilia model distinguishes between motile cilia at the center of the ciliated structure and non-motile cilia at the edges of the structure. The non-motile cilia sense fluid, which in turn triggers Ca^{2+}-influx and downstream events (Pennekamp et al. 2002; McGrath et al. 2003).

In any case, the results of leftward flow are a left-asymmetric down-regulation of the cerberus/dan family member Coco (in *Xenopus*; Cerl2/Dand5 in mouse and charon in fish)

and activation of the nodal cascade in the left lateral plate mesoderm (LPM) (Lohr et al. 1998; Pearce et al. 1999; Zhu et al. 1999; Shiratori et al. 2001; Hashimoto et al. 2004; Marques et al. 2004; Toyoizumi et al. 2005; Ohi et al. 2007; Vonica et al. 2007; Belo et al. 2009; Blum et al. 2009; Schweickert et al. 2010 and 2011) (Figure Int-5 D and E).

In the LPM, nodal acts in a positive feedback-loop on its own expression, but it also activates the transcription of its inhibitor *Lefty,* and the homeodomain transcription-factor *Pitx2* (paired-like homeodomain 2), which is required for asymmetric organogenesis (Lohr et al. 1998; Shiratori et al. 2001; Toyoizumi et al. 2005; Ohi et al. 2007; Blum et al. 2009; Schweickert et al. 2011).
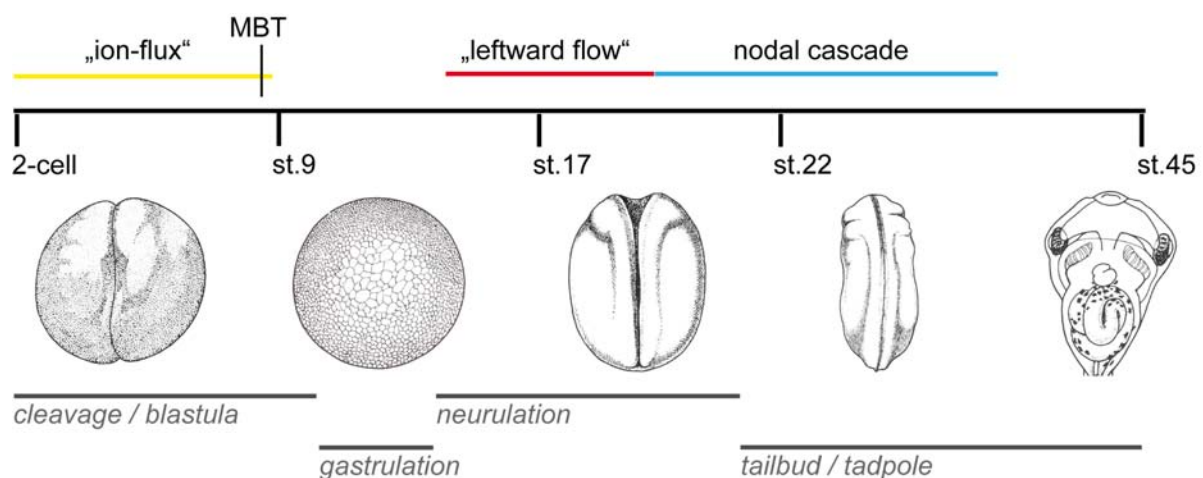
Figure Introduction-3: Developmental Timing Of Left-Right Relevant Events

Two opposing hypotheses propose different timing of symmetry-breakage in *Xenopus* left-right axis development. The **"ion-flux"** (yellow) model proposes symmetry-breakage during cleavage and blastulation, while the **"leftward flow"** (red) model proposes symmetry-breakage to happen during neurulation. In both models, the highly conserved **nodal cascade** (blue) is activated from late neurula stages onwards, and before asymmetric organogenesis takes place in late tadpole stages.
Embryo drawings are taken from: *www.xenbase.org; after Nieuwkoop and Faber 1994***.

Symmetry-Breakage: Different Species, Different Modes?

In *Xenopus laevis,* an alternative mechanism was proposed: the "ion-flux" hypothesis (Levin 2003). It is based on asymmetric expression, localization and function of ion transporters during cleavage stages (2- to 64-cell), mainly the gastric $H^+/K^+ATPase\ \alpha$ (ATP4a) and functionally associated potassium and proton channels/pumps (Levin et al. 2002; Rutenberg et al. 2002) (Figure Int-3). The asymmetric localization was hypothesized to generate an asymmetric distribution of ions on the left and the right side of the future midline, which eventually drives accumulation of a charged component, i.e. Serotonin (5-

hydroxytryptamine; 5-HT) (Fukumoto et al. 2005a; Fukumoto et al. 2005b). This process was further proposed to take place via gap junctions (GJs) (Levin et al. 1998). The localization of 5-HT on the right side mediates epigenetic modification (Carneiro et al. 2011) (Figure Int-3 and Int-4). Although the mechanism and timing presented by this model differed radically compared to other species, it was tempting and justifiable, because the frog embryo also establishes DV- and AP-axis very early in development (Klein 1987; Heasman 2006). Furthermore, a flow event comparable to the one observed in the mouse embryo was not yet detected in *Xenopus* when this model was put forward.

	st.1	st.3	st.6/7	st.9-12	st.14-16	st.17-19	st.20++	st.40++
ion-flux	asymmetric mRNA & protein localization	5-HT transport via GJC	asymmetric 5-HT accumulation	asymmetric activation of HDAC via 5-HT	right asymmetric inactivation nodal-promoter		asymmetric nodal cascade LPM	asymmetric organ placement
leftward flow	normal development of primary axes		SM specification *Foxj1* expression	GRP morpho-genesis & ciliogenesis	leftward flow & asymmetric Coco inhibition	transport of cue(s) to LPM via GCJ		

Figure Introduction-4: Comparison Of Timing And Sequence Of Events, Between The "Ion-Flux" And "Leftward Flow" Models

"ion-flux": After fertilization, during early cleavage stages, mRNAs and proteins are asymmetrically distributed, which generates asymmetric membrane potentials and pH. Along electrochemical gradients, generated by asymmetric ion channels and pumps, serotonin (5-HT) is transported via gap junction communication (GJC), and accumulates on the right side of the embryo. Asymmetric 5-HT activates the histon deacetylase (HDAC), which inhibits *nodal / Xnr1* expression on the right side of the embryo.
"leftward flow": During early development, the primary axes (anterior-posterior and dorso-ventral) are formed. When gastrulation starts, the superficial mesoderm (SM) is patterned and *Foxj1* expression is induced. After involution of the SM into the archenteron, the gastrocoel roof plate (GRP) starts to grow motile cilia, which are posteriorly localized and produce a leftward flow. Leftward flow down-regulates *Coco* on in the left somitic GRP, which releases repression of nodal, and laterality cues can be transported via GJC to the left lateral plate mesoderm (LPM).
Asymmetric **nodal cascade** induction and **asymmetric organogenesis** are common to both models.

This situation has changed when leftward flow was found to occur in the archenteron at the beginning of neurulation in the frog (Schweickert et al. 2007). Relevance for LR-patterning was demonstrated by physical inhibition of flow through application of highly viscose methyl-cellulose at the gastrocoel roof plate (GRP), i.e. the cilia-bearing epithelium generating leftward flow in amphibians (Shook et al. 2004; Schweickert et al. 2007; Saenz-Ponce et al. 2012) (Figure Int-5). When gastrulation starts (st. 10.5), cells of the superficial mesoderm (SM) are located just above the dorsal-lip as the outer epithelium of the

organizer (Shook et al. 2004). During gastrulation (st. 11-12), the cells invaginate into the dorsal roof of the archenteron and form an triangle-shaped epithelium (st. 13) (Figure Int-5 A and B). The epithelium starts to grow motile monocilia, which are initially localized at the apical center of the cells, but get localized to posterior parts of the cells during maturation of the GRP (st.13-16/17). A weak flow can be first detected by st. 15, which gets increasingly robust until st. 17. From st. 18 on, flow decreases and is completely lost by st. 20 (the same stage when *Xnr1* starts being expressed in the left LPM) (Blum et al. 2007; Schweickert et al. 2007). Moreover, molecular loss of cilia or motility in GRP cells caused absence of leftward flow and LR-defects, thus confirming the findings of Schweickert et al. (2007) at the molecular level (Stubbs et al. 2008; Vick et al. 2009). Taken together, two mechanisms seem to break symmetry in *Xenopus* (Figure Int-3 and Int-4).
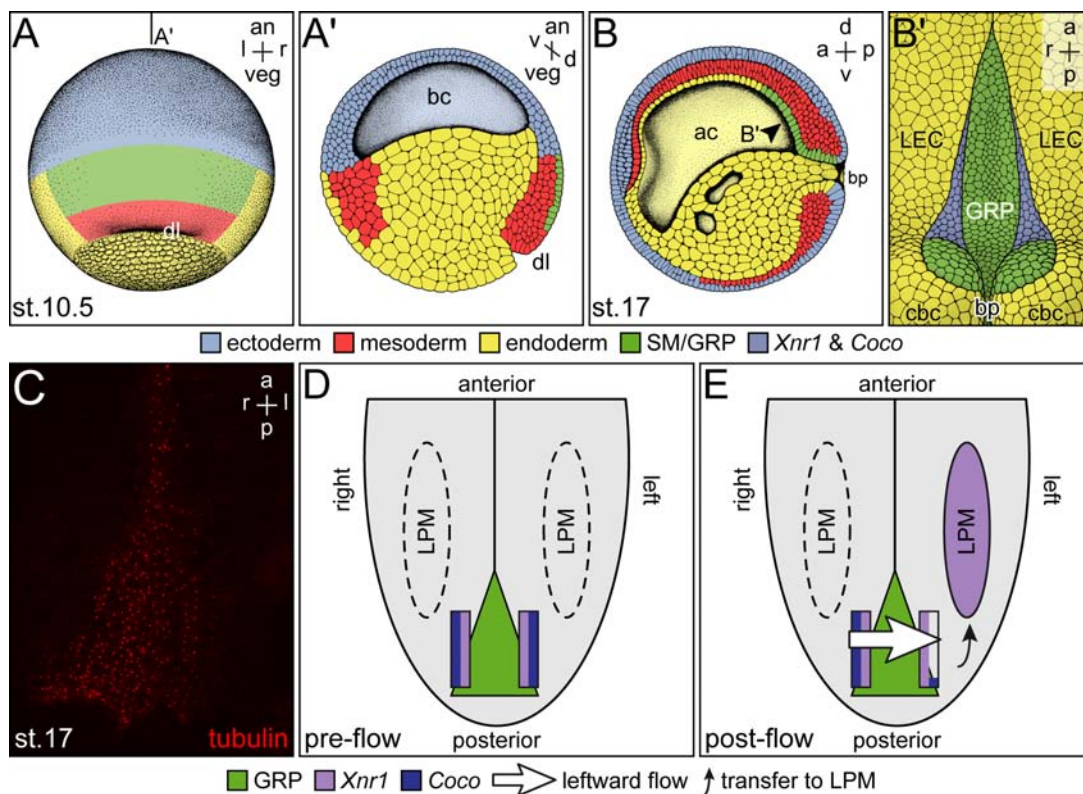
Figure Introduction-5: The Superficial Mesoderm, The Gastrocoel Roof Plate And LR-Development In *Xenopus laevis*

LR development in *Xenopus laevis*. **(A, A`)** The superficial mesoderm (SM; green) constitutes the outer cell layer of Spemann's organizer and is located animally to the dorsal lip (dl). Mesodermal cells in the deep marginal zone are colored red. (A) dorsal view of early gastrula, **(A`)** sagittal section. **(B, B`)** Following SM invagination, the ciliated gastrocoel roof plate (GRP) differentiates at the posterior archenteron (ac) in neurula embryos. Note that the GRP is not covered with endoderm (yellow) and flanked by lateral endodermal cells (LEC). Ciliated GRP cells cover dorsal aspects of the circumblastoporal collar (cbc) and blastoporus (bp) as well. Note also that lateral somitic GRP cells (blue) are unique for co-expressing the secreted growth factors *Xnr1* and *Coco* and project cilia centrally. **(B)** st. 17 neurula mid-sagittal section, **(B`)** ventral view on GRP. **(C)** GRP cilia. Immuno-histochemistry using anti-acetylated tubulin antibody; ventral view. **(D, E)** The Nodal inhibitor Coco is the target of leftward flow. Schematic dorsal explants of early **(D; pre-flow)** and late **(E; post-flow)** neurulae in ventral view. **(D)** GRP (green) is flanked by a bilateral symmetric expression of *Xnr1* (purple) and *Coco* (blue) in somitic GRP cells. Lateral plate mesoderm (LPM) is devoid of asymmetric gene activity. →

(E) Flow dependent left asymmetric down-regulation of Coco mRNA releases Xnr1 from Coco repression. Transfer of left positional information by the relieved Xnr1 protein, induces *Xnr1* transcription in the left LPM.
Taken from: *Schweickert et al. 2011***.*

The chicken is a vertebrate which does not seem to rely on cilia-driven fluid flow, whereas components of the "ion-flux" model are required for LR-development, e.g. ATP4a, 5-HT and GJ (Vandenberg et al. 2009). In contrast to *Xenopus*, the chicken does not display asymmetries at the mRNA level for ATP4a, but ATP4a-dependent asymmetric voltage-gradients left and right of the primitive streak were reported during gastrulation (Levin et al. 2002). The first sign of asymmetry is the morphology of Hensen's node, accompanied by asymmetric expression of Shh around the node. The morphological asymmetry is generated by movements of cells towards the left side of the node, and because these cells express *Shh*, HH-signaling is activated only on the left side (Levin et al. 1995; Gros et al. 2009).

The postulation of three very different mechanisms to initiate LR-asymmetry during development in vertebrates raised questions which became the subject of controversial debates (Tabin 2006; Blum et al. 2009):

(1) Do the "ion-flux" and "leftward flow" mechanisms cooperate in symmetry-breakage of *Xenopus*? This would suggest that *Xenopus* represents an evolutionary bridge between early mechanisms (also found in lower deuterostomes) (Shimeld et al. 2006; Hibino et al. 2006; Hibino, et al. 2006) and leftward flow (also reported for fish and mammals) (Nonaka et al. 1998; Essner et al. 2002, 2005; Okeda et al. 2005; Feistel et al. 2006).

(2) Is the vertebrate symmetry-breakage mechanism evolutionary conserved, or do different animal species break symmetry in different ways, indicating multiple evolutionary origins of asymmetry (Tabin 2006)?

(3) What is the initial evolutionary base of LR-asymmetry, especially in the light of nodal-dependent shell asymmetry in snails, which is induced by asymmetric spiral cleavage (Grande et al. 2009; Kuroda et al. 2009)?

Gastric H⁺/K⁺ATPase (ATP4) – Functions In Digestion And Development

Structure And Function Of ATP4

The gastric H^+/K^+ATPase (ATP4) is a member of the P-type ATPase superfamily of membrane-spanning ion pumps (Chan et al. 2010). This family of proteins can be found in all kingdoms of life and is subdivided into five classes (I-V). The gastric and non-gastric H^+/K^+ATPases, ATP4 and ATP12, respectively, are classified as type IIC ATPases (P-IIC), which display high structural similarities with the best characterized Na^+/K^+ATPase (ATP1) (Axelsen et al. 1998). ATP4 transports protons (H^+) across membranes in exchange for potassium (K^+) ions against the electro-chemical gradient (~ 1:1.000.000) by utilizing ATP as energy-donor in an electro-neutral manner ($2H^+:2K^+$) (Rabon et al. 1990) (Figure Int-6). It acts as a tetrameric complex consisting of two catalytic α subunits and two accessory β subunits (Shin et al. 2009). The catalytic α subunits (1033 or 1034 amino acids in length) contain the ATP-binding pocket and are mainly responsible for selectivity and transport of ions. ATP4a consists of ten transmembrane domains (TM1-10), and ATP4b (290 to 299 amino acids in length) binds to TM7 and TM10. The β–subunits are necessary for the correct folding of the protein (chaperon-like function) and stable insertion into the plasma-membrane (Beggah et al. 1999; Geering 2001) (Figure Int-6).

Mechanism Of Ion Transport And The Role Of Accessory Potassium-Channels

Ion exchange in P-IICs follows the E1-E2-mechanism, described here for ATP4 (Rabon et al. 1990) (Figure Int-6): The first step takes place on the intracellular side, where a hydronium ion ($H3O^+$) binds to the catalytic subunit´s ion-binding pocket. Furthermore, ATP is bound to the cytoplasmatic surface of the protein and phosphorylates it. This phosphorylation induces a conformational change from the E1 to the E2 form, in which the ion-binding site is exposed to the extracellular side. $H3O^+$ is released from the protein, and extracellular K^+ binds to the ion-binding pocket. The binding of K^+ to the protein triggers dephosphorylation and conformational change, back to the E1 configuration. Upon new ATP-binding, the K^+ is released into the cytoplasm, and the cycle starts again.

K$^+$-binding to the binding pocket is the rate-limiting step of H$^+$-secretion (DuBose et al. 1999; Munson et al. 2007; Morth et al. 2011). Therefore, extracellular K$^+$-concentration needs to be high for ATP4 function. This task is fulfilled by K$^+$-channels, which release K$^+$ from the cell into the extracellular lumen, and which are found co-expressed with ATP4, e.g. KNCQs and multimeric Kir channels (Heitzmann et al. 2008).
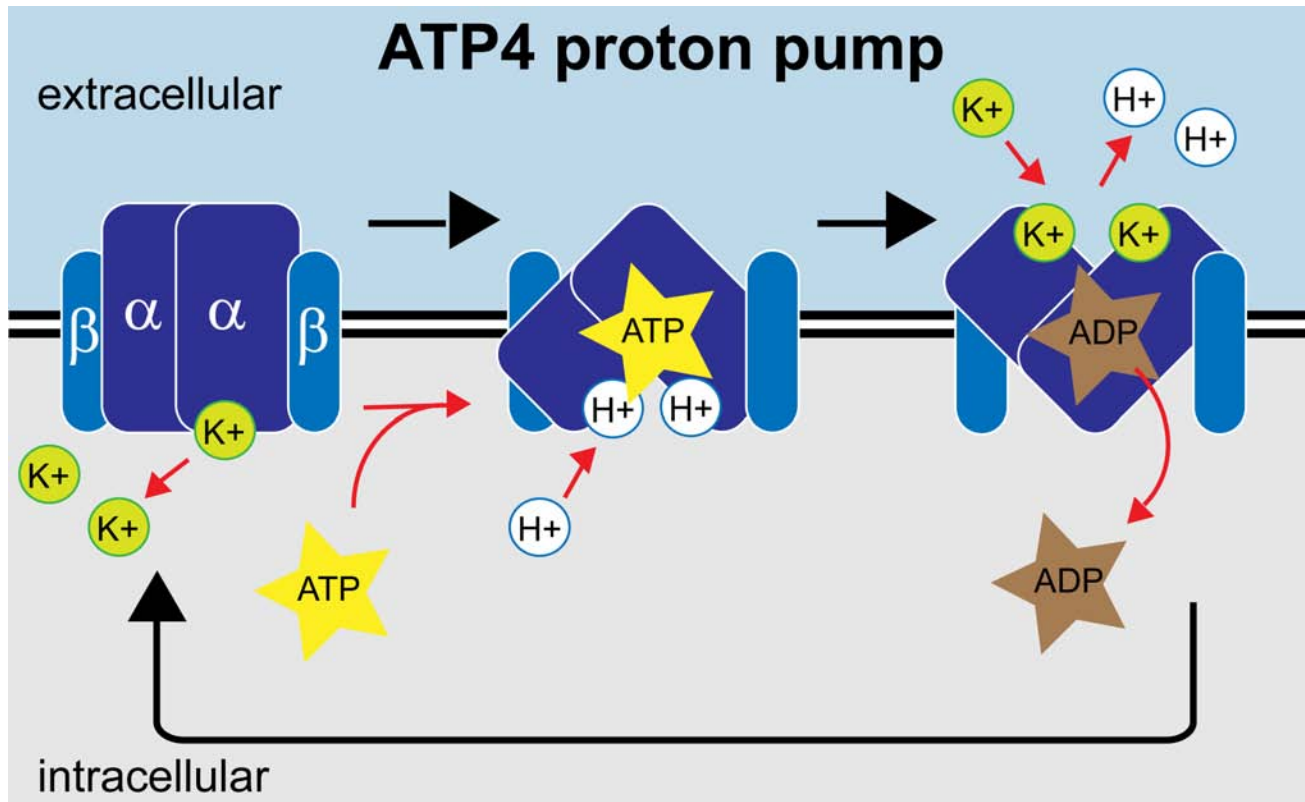
Figure Introduction-6: Schematic Function Of The Gastric H$^+$/K$^+$-ATPase (ATP4)

The transmembrane ATP4 consists of two catalytic α-subunits and two accessory β-subunits. Protons (H$^+$) and ATP can interact with the intracellular part of ATP4. ATP-dependent phosphorylation alters the conformation of the protein, which releases H$^+$ into the extracellular space. Potassium (K$^+$) ions bind to the extracellular part of the protein, and ADP can dissociate from ATP4. This again changes the protein conformation, and K$^+$ is released into the intracellular space. This cycle is then repeated.
Mechanism reviewed in: Rabon et al. 1990.

Pharmacological Inhibition Of ATP4

In general there are two strategies for ATP4 inhibition (Shin et al. 2006, 2009). The first one is the "classic" inhibition by proton-pump inhibitors (PPIs), which are pyridyl methylsulfinyl benzimidazoles that represent weak bases. PPIs like Omeprazole or Lansoprazole need to be activated by low pH, which prevents inhibition of inactive ATP4 molecules. When ATP4 is active and pH is low, the pro-drug is converted into the active form and binds covalently via disulfid-bridges to cysteins 813 and 822. Covalent binding of

PPIs to ATP4 inhibits further function of the protein in a non-reversible way.

The second strategy of ATP4 inhibition is by application of acid-pump antagonists (APAs), i.e. imidazole pyridine compounds (e.g. SCH28080), which compete with K^+-ions for binding. This form of inhibition is faster, because pH-dependent activation of the compound does not take place. Moreover, the inhibition is reversible in contrast to PPIs (Munson et al. 2007).

ATP4 Function In Vertebrates

The most prominent function of ATP4 in the vertebrate organism is gastric proton release and acid-induced digestion of food in the stomach. More recently, ATP4 has also been implicated in epithelial cell differentiation and HH-signaling in gastric tissue (Zavros et al. 2008). Moreover, reports of ATP4 expression in various tissues, e.g. brain and kidney, indicate a broader function than HCl production in the stomach (Herrmann et al. 2007; Rotte et al. 2009; Fohl et al. 2011). In the frog *Xenopus*, ATP4 was also found in the stomach, but in addition, early development relied on ATP4-function (Levin et al. 2002; Ikuzawa et al. 2004).

Aim Of Study

ATP4-function was linked to LR-development in *Xenopus*, where asymmetric expression was observed during cleavage stages (Levin et al. 2002). The "ion-flux" hypothesis suggested that asymmetric function generates voltage-gradients, which break symmetry during early stages, and that the role of cilia-driven leftward flow is limited to reinforcing these early cues (Levin et al. 2002; Levin 2003; Aw et al. 2009). This view was challenged when experiments demonstrated that asymmetric gene expression in the LPM was lost after inhibition of leftward flow (Schweickert et al. 2007; Vick et al. 2009). These findings raised the question as to a possible role of ATP4 in the context of leftward flow.

The general aim of this thesis work therefore was to elucidate the mechanism of ATP4-dependent developmental signaling events during symmetry-breakage, LR-axis patterning and ciliogenesis in *Xenopus laevis*.

(1) Specifically this work aimed at uncovering the exact timing and function of ATP4 during the early development of *Xenopus* and its impact on symmetry-breakage. For this aim, distribution of ATP4a mRNA and protein was re-investigated. Molecular gain- and loss-of-function experiments were performed, and their impact on LR-development was analyzed.

(2) Further, Wnt-signaling was addressed as an important factor for early animal development. Regulated Wnt-pathway activity during primary-axes induction and gastrulation were reported to be required for correct LR-axis development in *Xenopus*. Therefore, the role(s) of Wnt-signaling components in *Xenopus* LR-development were analyzed, with a special focus on ligand-driven pathway activation by Xwnt11b during gastrulation and neurulation.

(3) Finally, ATP4-function was studied in other ciliated epithelia during *Xenopus* development to gain insight into general mechanisms of ciliogenesis. Experiments were performed in monociliated cells of (a) the GRP, (b) the floor plate of the neural tube, and multiciliated cells of (c) mucociliary epithelia, e.g. in the *Xenopus* larval skin. In addition, the floor plate- and the skin-system were used to investigate interaction of ATP4 and Wnt-signaling, with other signaling pathways, which are known to influence ciliation and function of these tissues, i.e. the Notch/Delta- and the Hedgehog-signaling pathways.

Results

Sequence And Expression Analysis Of ATP4a

Cloning Of *Xenopus laevis ATP4a*

A full length sequence of *ATP4a* from *Xenopus laevis* was cloned from gastric cDNA using primers matching NM_001090874. The sequence was verified by analysis of conserved regions and cross-species comparison of ATP4a protein sequences (Figure 1). ATP4a protein sequences confirmed the high degree of conservation within the vertebrate group and supported divergence of ATP4a and ATP12a at the base of the vertebrate lineage (Figure 1C) (Axelsen et al. 1998; Okamura et al. 2003).

ATP4a mRNA Is Expressed Symmetrically During Cleavage Stages

In order to re-investigate the role of *ATP4a* in left-right (LR) axis specification (Levin et al. 2002), mRNA expression analysis by whole mount *in situ* hybridization (WMISH) and semi-quantitative reverse-transcriptase polymerase chain reaction (RT-PCR) were performed on specimens throughout early development.

RT-PCR revealed high levels of maternal *ATP4a* mRNA during early cleavage stages which continuously declined during blastula (st. 8), gastrula (st. 10-12) and neurula (st. 13/14-17) stages (Figure 2) (*Xenopus* stages according to Nieuwkoop and Faber 1994). In addition, strong PCR signals from stage 43 onwards were detected (not shown).

WMISH for *ATP4a* was performed on embryos ranging from 2-cell stage up to tadpole stages (st. 45), with a large number (n=320) of cleavage stage embryos (from 2- to 64-cell stage) (Figure 3 A-D). As signals in different batches may vary considerably (Aw et al. 2008), embryos were derived from eight different females from our colony at Hohenheim and two females from a colony in Heidelberg (courtesy of the Steinbeisser laboratory). Equal amounts of maternal mRNA were detected in all blastomeres and no asymmetric distribution along the LR-axis was observed (Figure 3 A-C). Maternal mRNA was

33

deposited throughout the animal hemisphere (Figure 3 B`, B``). In thin sections the WMISH signals appeared dotted throughout the animal hemisphere (Figure 4).
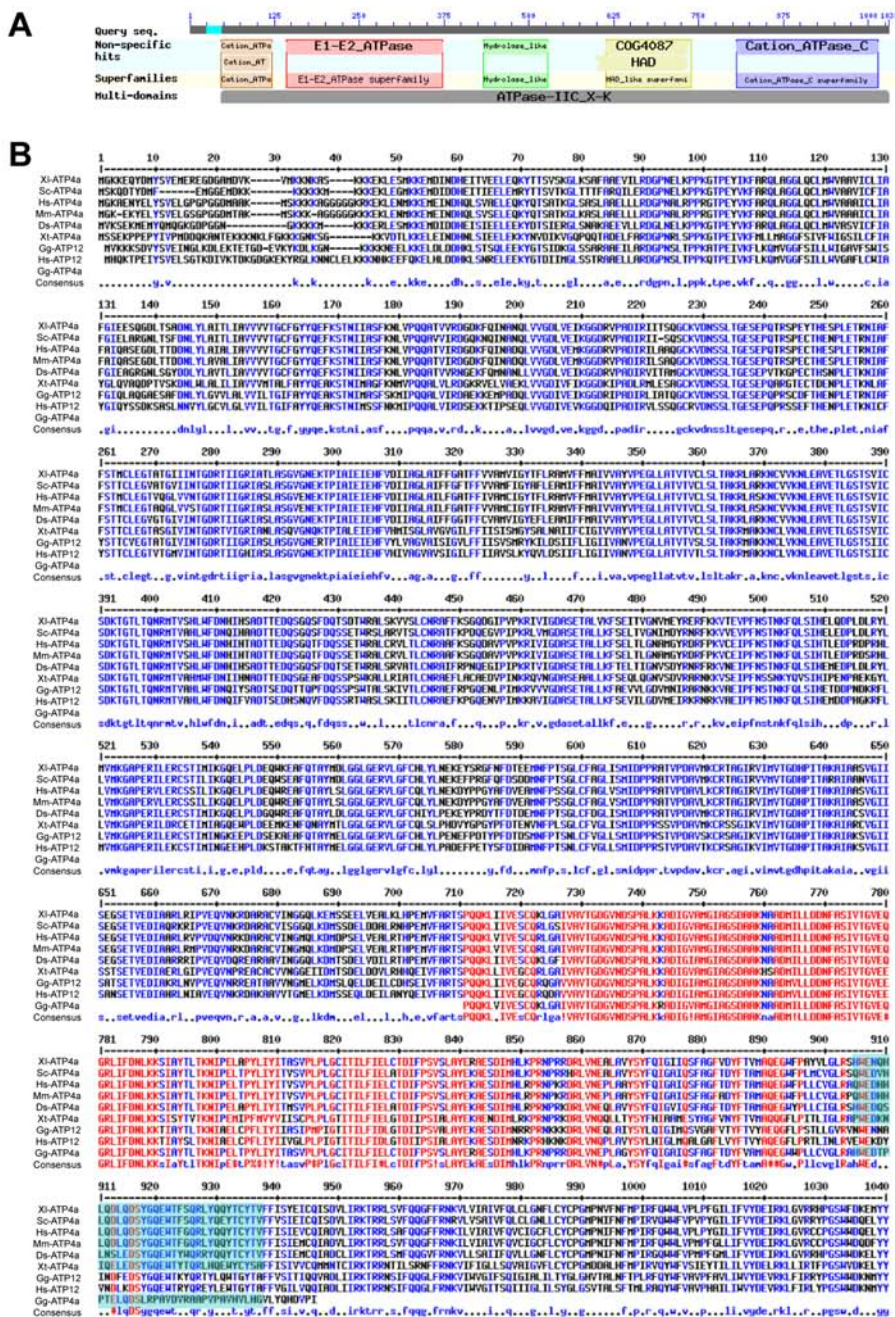
Figure 1: Sequence Analysis Of The *Xenopus laevis* Gastric H⁺/K⁺-ATPase (ATP4)

Sequence analysis of NM_001090874: **(A)** Conserved region analysis via BLAST (http://blast.ncbi.nlm.nih.gov/) revealed a cation binding site (orange), E1-E2 ATPase motives (red), a hydrolase-like motive (green), a HAD-like hydrolase motive (yellow) and a cation ATPase C-type motive (blue).
(B) Amino acid (AA) sequence alignment (using Multalign, multalin.toulouse.inra.fr/multalin) of NM_001090874 with annotated ATP4a and ATP12a sequences from *Homo sapiens sapiens* (Hs), *Mus musculus* (Mm), *Gallus gallus* (Gg) *Xenopus laevis* (Xl) and *X. tropicalis* (Xt), *Sinciperca chutasi* (Sc), and *Dasyatis sabina* (Ds). Presence of SCH28080-binding site in ATP4a-sequences is indicated by blue box.
(C) Phylogenetic analysis of ATP4a and ATP12a sequences revealed clustering of NM_001090874 with other ATP4a sequences, while ATP12a sequences formed a separate cluster, indicating divergence of both molecules at the base of the vertebrate lineage. Please note that clustering of the *X. tropicalis* (Xt) sequence for ATP12a (NM_00103037) clustered with ATP4a sequences, while the non-annotated sequence CR926442 clustered with other ATP12a sequences. Phylogenetic analysis was performed with www.phylogeny.fr, *Dereeper et al. 2008, 2010*.
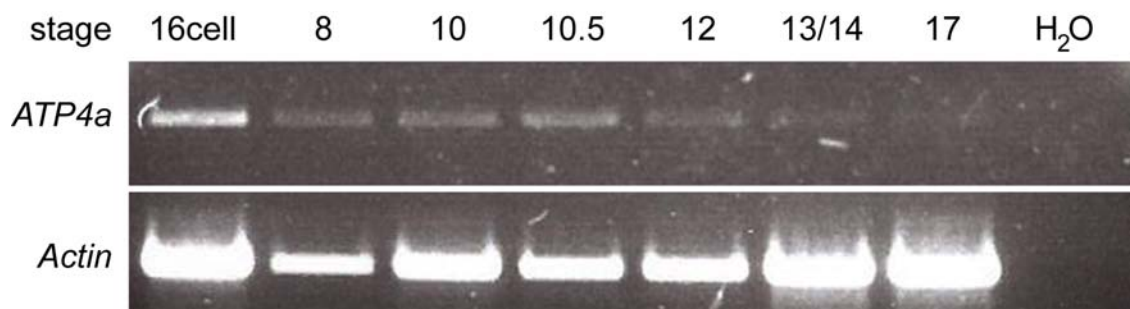
Figure 2: *ATP4a* mRNA Is Present During *Xenopus* LR-Development

Reverse transcriptase (RT)-PCR analysis of *ATP4a* transcript levels during early development of *Xenopus laevis*. RT-PCR for *actin* served as loading control. Note that mRNA levels decreased, but expression persisted through stage 17. Water served as negative control (H₂O). Reprinted from *Walentek et al. 2012*[#].

At the onset of gastrulation (st. 9), weaker signals were detected in tissues from all prospective germ layers, which appeared strongest in prospective mesodermal cells (Figure 3 E). At stage 10.5, when the dorsal lip is present, WMISH signals decreased in comparison to earlier stages, and were strongest in deep dorsal mesoderm (Figure 3 F). During late gastrulation and throughout neurulation no signals were detected (not shown). Weak signals reappeared by early tailbud stages (st. 28) in the anterior notochord (Figure 3 G). Strong signals were detected from stage 43 onwards in the larval stomach and weaker signals in the oesophagus/small intestine (Figure 3 H, I and Figure 43 A). Specificity of the *in situ* probe was confirmed by signals in stomach epithelial cells (Figure 3 H) and lack of signal in sense-probe controls (Figure 3 C).

In summary, the asymmetrical expression pattern of *ATP4a* transcripts (Levin et. Al 2002; Aw et al. 2008) could not be reproduced and, therefore, protein localization was analyzed as well.
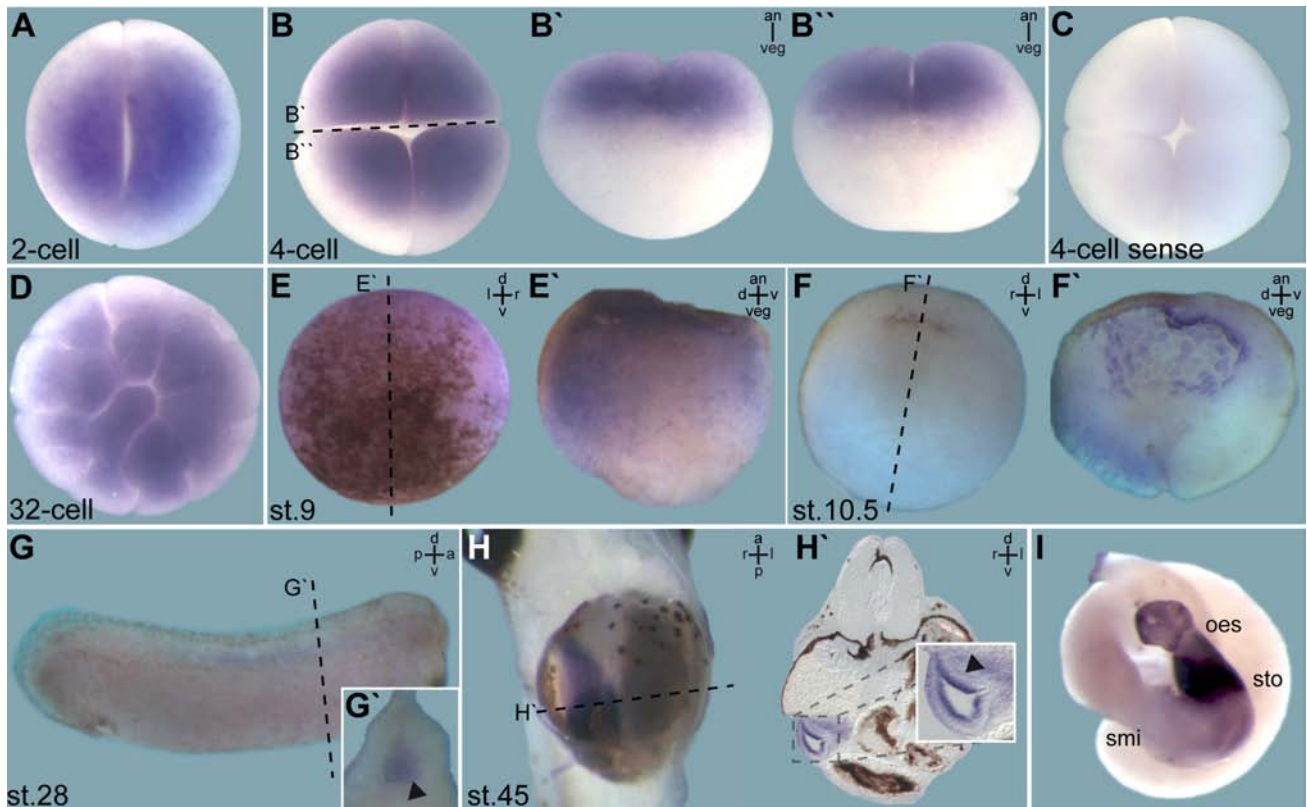
Figure 3: Whole-Mount In Situ Hybridization (WMISH) Analysis Of *ATP4a* mRNA Expression

WMISH for *ATP4a* transcripts was performed from early cleavage (2-cell), up to tadpole stage (st. 45).
(A, B and D) *ATP4a* was symmetrically localized in cleavage stages. **(B`, B``)** In bi-sected 4-cell embryos, *ATP4a* mRNA was restricted to the animal cytoplasm. **(C)** A sense-probe control did not reveal any staining. **(E, F)** During late blastulation/early gastrulation (st. 9 – 10.5), staining intensity decreased and staining was enriched in dorsal mesodermal tissues, as observed in bi-sections **(E`, F`)**. **(G)** In tailbud stages (st. 28), staining was found exclusively within the anterior notochord (black arrowhead in **G`**). **(H, I)** In late tadpole stages (st. 45) strong staining was found in the endoderm, specifically enriched within the gastric epithelium (black arrowhead in **H`**). **(I)** In prepared gastrointestinal tract specimens, staining was found in the stomach (sto), but weaker staining was also evident in the oesophagus (oes) and the proximal part of the small intestine (smi).
Planes of section are indicated by dashed lines in (B), (E) and (F-H). a = anterior, an = animal, d = dorsal, l = left, p = posterior, r = right, st. = stage, v = ventral and veg = vegetal.
Reprinted and modified from: *Walentek et al. 2012*[#].
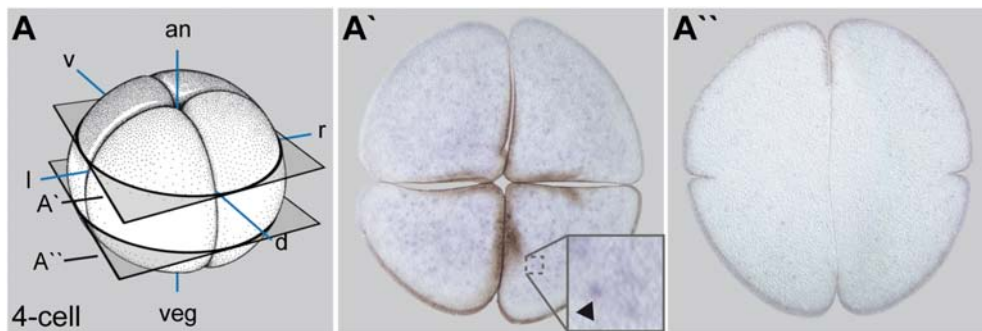
Figure 4: *ATP4a* mRNA Is Located In A Dotted Pattern Within The Animal Cytoplasm

After WMISH for *ATP4a* transcripts, a 4-cell stage embryo was sectioned along the animal-vegetal axis (schematically depicted in **A**). *ATP4a* mRNA was present in a dotted pattern (black arrowhead in inset of **A`**), and absent from the vegetal halve **(A``)**.

an = animal, d = dorsal, l = left, r = right, v = ventral and veg = vegetal.
Embryo drawing used in (A) reprinted and modified after: *Blum et al. 2009b*[##].

Protein Expression Analysis Of ATP4a Indicates Presence Of Protein Throughout Development

Protein analysis of ATP4a by immuno-histochemistry (IHC) using a specific antibody (Chen et al. 1998; Levin et al. 2002; Aw et al. 2008) detected low-level symmetric protein localization in 4-cell stage embryos (Figure 5 A). Elevated levels of ATP4a protein could be detected from blastula stages onwards (Figure 5 C-K). In particular, protein was found in the superficial mesoderm (SM) (Figure 5 D) and the GRP (Figure 5 K, L), i.e. tissues which are relevant for leftward flow (Schweickert et al. 2011). Specificity of the antibody was shown by absence of signals in specimens treated without primary antibody (-ATP4a/+Cy3 in Figure 4 B, M and N). Moreover, strong signals in st. 45 gastric tissue (Figure 6 H) were found.

In tailbud (st. 25) and tadpole (st. 40) stages, protein was found in most cells of the embryonic skin (Figure 6 A-D). Moreover, a bi-sected specimen at stage 40 revealed an increased presence of ATP4a protein in ecto- and mesodermal structures, e.g. skin, neural tube, muscles and notochord (Figure 6 E-G), in comparison to the endoderm (Figure 6 E).

In addition, the subcellular distribution of ATP4a (Figure 7) was analyzed in confocal sections. Strong signals were detected from blastula stages (st. 8) onwards in animal cells, in which the protein was found at the apical membrane (Figure 7 A). In a subset of animal cells, the protein accumulated during cytokinesis at the center of the apical membrane (Figure 7 A````). In contrast to animal cells (Figure 7 A), vegetal cells (Figure 7 B) were

filled with yolk droplets (blue auto-fluorescence in Figure 7 B``- also described in Beyer et al. 2011) and were much bigger in size than animal cells at the same stage (Figure 7 A). In vegetal cells, protein was found in the cytoplasm, but excluded from lipid droplets (Figure 7 B```). Extensive localization to the apical membrane was not observed (Figure 7 B````).

During gastrulation (st. 10.5), the signal intensity was slightly elevated in dorsal and animal regions (Figure 4 E), thereby recapitulating mRNA localization at this stage (Figure 3 F). In some cells of the animal cap, the superficial mesoderm (SM) and the dorsal lip, ATP4a protein was not only found at the membrane, but co-localized with the nucleus as well (Figure 5 E-H).

During later stages, e.g. during neurulation (st. 17), the protein was localized to the apical membrane in ectodermal cells (Figure 7 C````, D````) in much the same way as seen in stage 25 skin tissue (Figure 6 A``, A```). In cells displaying high and low signal levels respectively (Figure 7 C and D), protein was found in vesicle-like structures at or beneath the apical membrane of cells (Figure 7 C````, D```). In addition, cells displaying high signal levels harbored high amounts of protein in the apical membrane (Figure 7 D````).

Although signal strength varied between GRP cells, protein was found throughout (Figure 7 E). Frame-by-frame analysis of confocal stacks taken from the boundary between GRP and the lateral endodermal crest (LEC) confirmed presence of protein in both lineages (Figure 7 F). In terms of localization, the distribution of ATP4a protein was similar to the one observed (Figure 6 H) and described for gastric cells (Sawaguchi et al. 2004; Zavros et al. 2008; Forte et al. 2010), i.e. at the apical membrane and in vesicle-like structures within the cell.

Summary

In conflict with previous reports, symmetric expression of *ATP4a* mRNA and protein was found during *Xenopus* development. Nevertheless, the presence of ATP4a mRNA and protein in tissues and stages relevant for flow-dependent symmetry-breakage in the frog did not argue against a role in LR-axis specification in general.
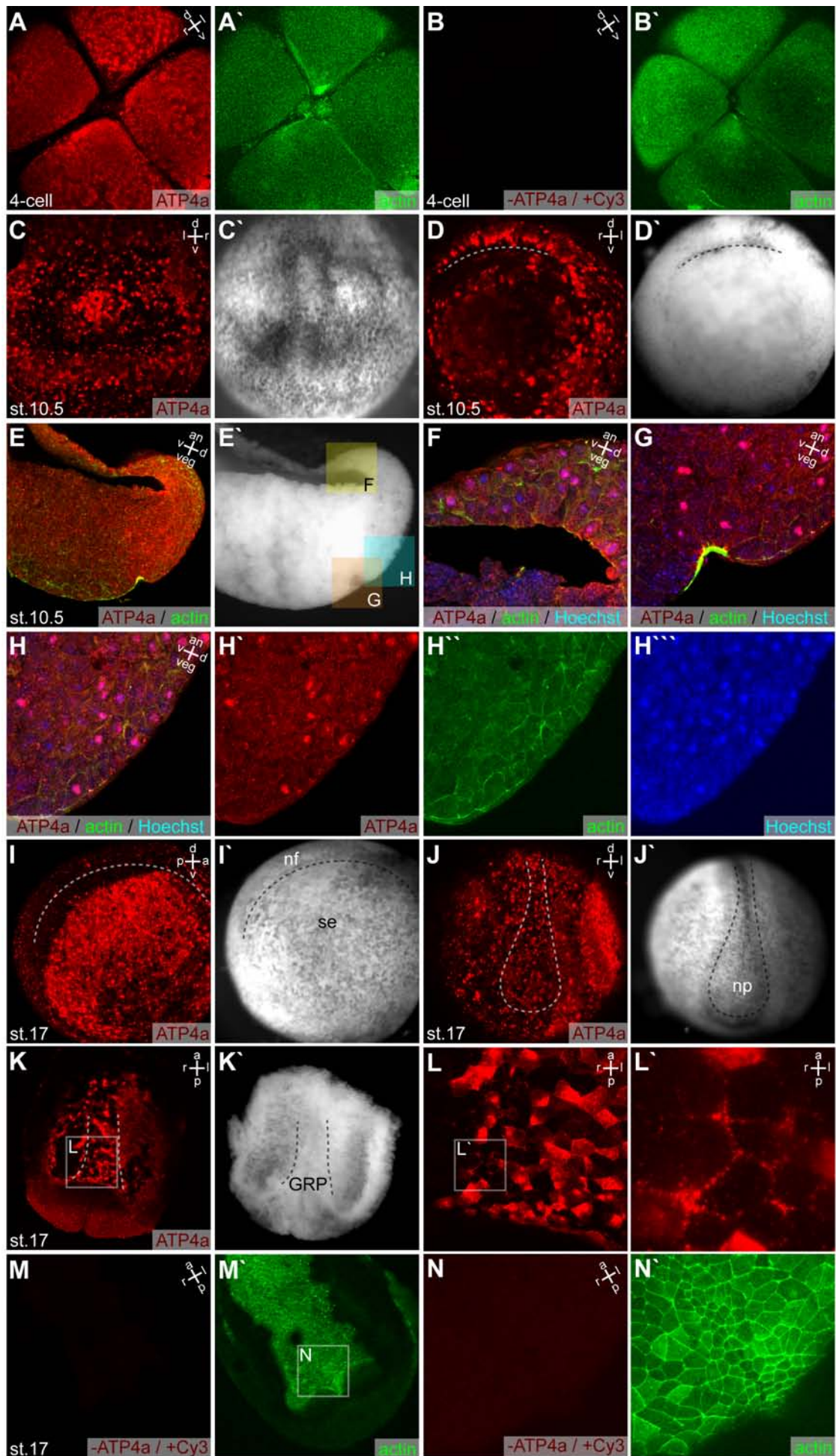
Figure 5: ATP4a Protein Localization During LR-relevant Stages

Immuno-histochemistry (IHC) with an antibody previously used for ATP4a localization in *Xenopus* (*Aw et al., 2008*). **(A, B)** ATP4a protein (red) was specifically localized to the plasma membrane in 4-cell stage embryos **(A)**, as negative control without ATP4a (-ATP4a/+Cy3) antibody did not reveal any fluorescent signal **(B)**. The level of the plasma membrane was visualized by actin staining, using phalloidin-Alexa488 (actin, green in **A`, A``, H``, M** and **N**).
(C-H) During gastrulation (st. 10.5), ATP4a was enriched in animal cells **(C)**, and in mesodermal cells, e.g. at the dorsal lip (**D**, dorsal lip is indicated by dashed line). **(E)** Bi-section revealed presence of ATP4a protein throughout the embryo, but slightly enriched on the dorsal halve. ATP4a protein was present in the animal cap **(F)**, at the dorsal lip **(G)** and within the superficial mesoderm **(H)**, where it co-localized with the plasma membrane (actin staining, green, **H``**) and in some cells with the nucleus (Hoechst staining, blue, **H```**). **(I-J)** During neurula stages (st. 17), ATP4a was enriched in the skin ectoderm (se), as compared to the neural folds (nf) **(I, I`)**, or the neural plate (np, indicated by dashed outline in **J, J`**). **(K-L)** In dorsal explants ATP4a was found at the GRP and in LECs (indicated by dashed lines in **(K, K`)**. **(L, L`)** Higher magnification revealed ATP4a localization to the plasma membrane and within vesicle-like structures beneath the apical membrane. **(M, N)** Negative controls in dorsal explants did not reveal staining in the red channel.

Pictures in (C`), (D`), (E`), (I`), (J`) and (K`) are bright field pictures. a = anterior, an = animal, d = dorsal, GRP = gastrocoel roof plate, l = left, nf = neural folds, np = neural plate, p = posterior, r = right, se = skin ectoderm, st. = stage, v = ventral and veg = vegetal.

Figure 6: ATP4a Protein Localization During Later *Xenopus* Development

IHC with an antibody previously used for ATP4a localization in *Xenopus* (*Aw et al., 2008*).
(A-D) ATP4a protein (red) was localized to the plasma membrane (3D lateral projections in **A``, A```**) of skin ectodermal cells in early (st. 25, **A**) and late (st. 40, **B, C and D**) tadpole stages. The level of the plasma membrane was visualized by actin staining, using phalloidin-Alexa488 (green), and the nucleus was stained by Hoechst (blue) in (**A`-A```, B`, C`, D`, E`, F`, G`, and H` and H``**, respectively). **(E-G)** ATP4a was enriched in mesodermal and ectodermal tissues, i.e. skin ectoderm (se), neural tube (nt), the notochord (no) and the muscles (m), indicated in **(F`)**. **(H)** Gastric tissue from a st. 45 tadpole served as positive control and revealed presence of ATP4a protein as previously described by others (please see references in the text).

a = anterior, an = animal, d = dorsal, l = left, m = muscles, no = notochord, nt = neural tube, p = posterior, r = right, se = skin ectoderm, st. = stage, v = ventral and veg = vegetal.
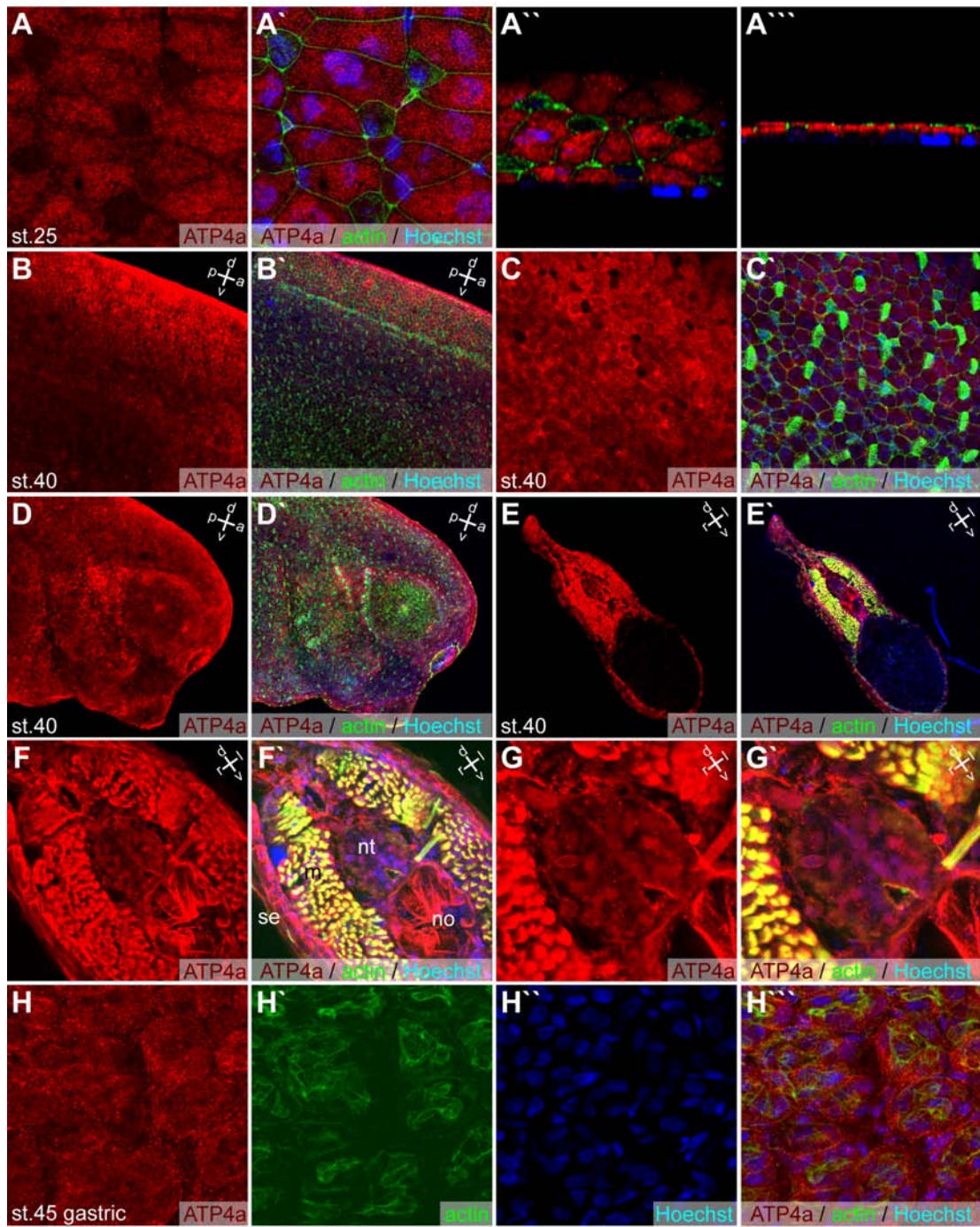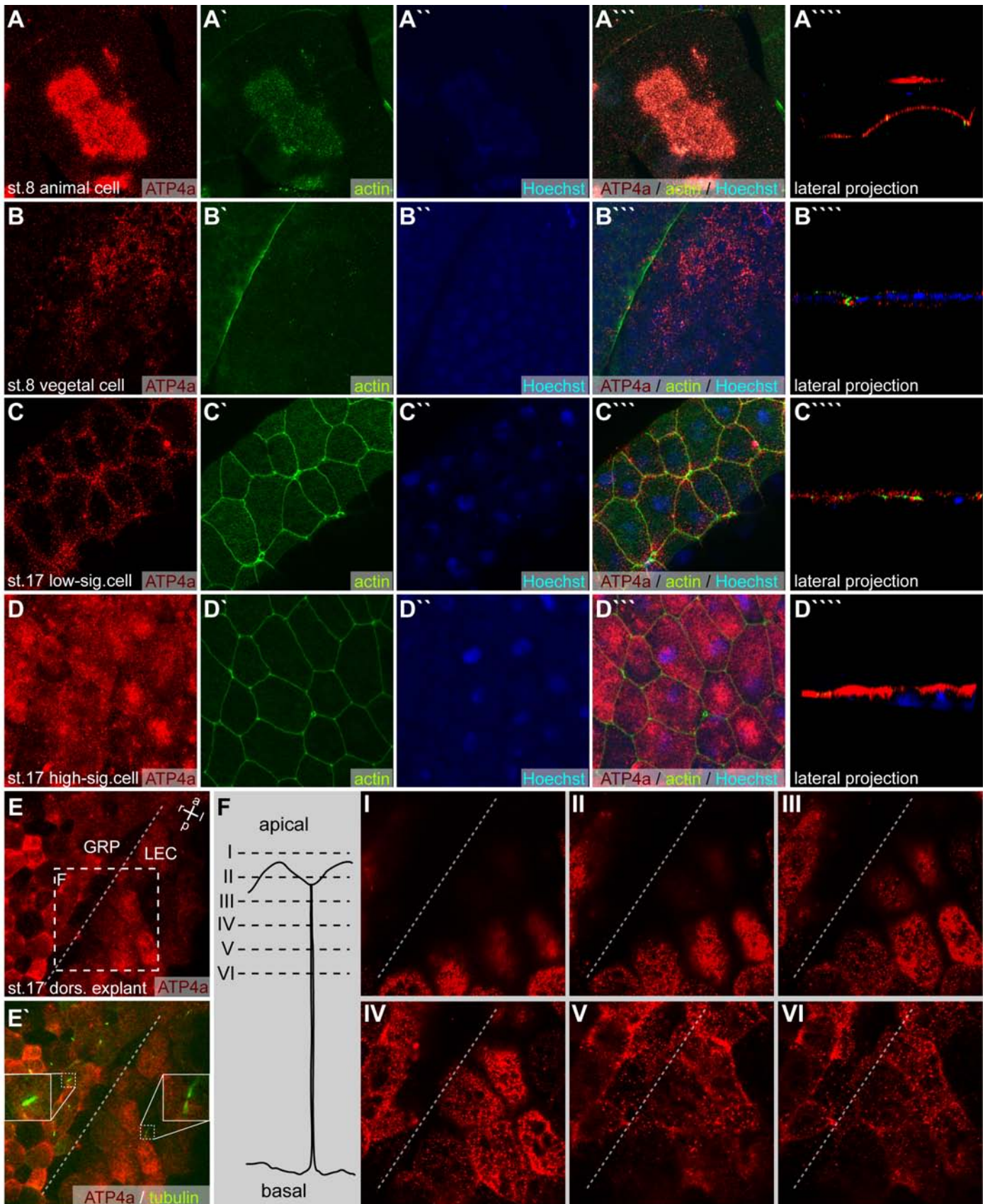
Figure 7: Subcellular ATP4a Protein Localization

IHC with an antibody previously used for ATP4a localization in *Xenopus* (*Aw et al., 2008*).
(A) During cytokinesis, ATP4a protein (red) was localized to the center of the plasma membrane in animal cells of the blastula (st. 8) (merged picture in **A```**, 3D lateral projections in **A````**). **(B)** In vegetal cells of the blastula (st. 8), weaker signals were detected in the cytoplasm, but excluded from yolk droplets (blue auto-fluorescent signal in the blue/Hoechst channel, merged picture in **B```**, 3D lateral projections in **B````**). **(C)** ATP4a protein in low-signal cells (low-sig. cell) during neurula stages (st. 17) was localized to vesicle-like structures at the apical/lateral plasma membrane (merged picture in **C```**, 3D lateral projections in **C````**). **(D)** In high-signal cells (high-sig. cell) during neurula stages (st. 17), high amounts of ATP4a protein were localized to the apical membrane and vesicle-like structures at the apical/lateral plasma membrane (merged picture in **D```**, 3D lateral projections in **D````**). **(E)** In dorsal explants during neurula stages (st. 17), ATP4a protein was present in GRP cells and lateral endodermal crest cells (LECs), which are marked by presence of cilia and mid-bodies, respectively (as revealed by staining of acetylated tubulin; green channel in **E`**), and depicted in left and right inset in **(E`)**.
(F) Schematic representation of confocal sections: **(F-I - -VI)** Series of confocal (optical) single sections revealed presence of ATP4a at the apical membrane and within the animal cytoplasm in vesicle-like structures.

ATP4a - red channel, actin cytoskeleton – green channel in **(A`-D`)**, auto-fluorescence – blue channel in **(A``-B``)**, nucleus – blue channel in **(C``-D``)** and acetylated α-tubulin – green channel in **(E`)**. a = anterior, l = left, p = posterior, r = right and st. = stage.
Reprinted and modified from: *Walentek et al. 2012*[#].

Functional Analysis Of *ATP4a* In Left-Right Axis Formation

Selection Of Loss-Of-Function Approach

In order to analyze the functional relationship between *ATP4a* and LR-axis specification two independent loss-of-function approaches were chosen: (1) Inhibition of mRNA translation by injection of anti-sense morpholino oligonucleotides (MOs) (Eisen et al. 2008; Mimoto et al. 2011). These were designed to specifically target the translational start site of *ATP4a* mRNA (*ATP4a*MO). (2) The second approach made use of commercially available inhibitors of ATP4 protein function, i.e. the acid pump antagonist (APA) SCH28080 (Munson et al. 2007). The compound was chosen for incubation experiments, because APAs are acting fast, very specific, and their inhibition is reversible.

Both approaches complement each other, as MO injections can be used for lineage specific knock-down (Figure 8), while incubation experiments act systemically and have the added benefit that they can be applied or terminated at specific time points during development.
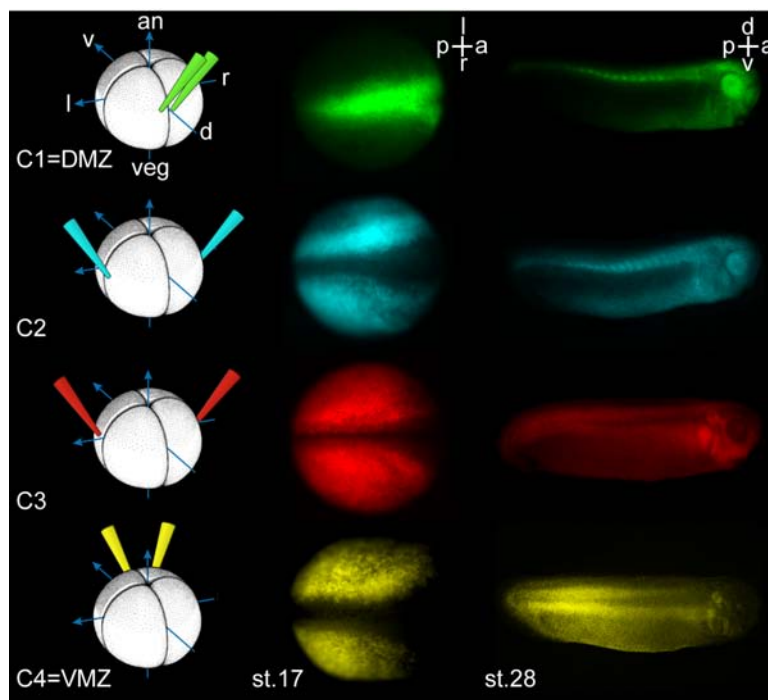
Figure 8: Differential Targeting Of Tissues And Lineage Analysis

Injection of lineage tracer rhodamine-B dextran into the marginal region (prospective C-tier of 32-cell embryo) of 4-cell embryos revealed specific targeting of GRP tissue only when dorsal blastomeres were injected close to the dorsal pole (dorsal marginal zone, DMZ, top). More lateral injections of dorsal blastomeres (C2 lineage) or injection of ventral blastomeres (C3 and C4) targeted the intermediate mesoderm (C2/C3), lateral plate mesoderm (C2/C3) and ventral mesoderm (VMZ), respectively.

a = anterior, an = animal, d = dorsal, l = left, p = posterior, r = right, st. = stage, v = ventral and veg = vegetal.
Reprinted from: *Walentek et al. 2012*[#]. Injection scheme modified after: *Blum et al. 2009b*[##].

ATP4a Is Required In Dorsal-Medial Cells And Post-MBT For LR-Axis Specification

MO-mediated knock-down of *ATP4a* was performed in different cell lineages (Figure 8): (1) The dorsal marginal-zone (DMZ), from which the organizer and the GRP are derived (Blum et al. 2009b). (2) The C2-lineage, which contributes to lateral GRP cells, the lateral plate mesoderm (LPM) and the intermediate mesoderm. (3) The C3-lineage which contributes to the lateral and intermediate mesoderm. (4) The ventral marginal-zone (VMZ), which will form blood cells, among others.

After injection at the 4-cell stage, morphants were grown to tailbud stages (~ st. 30) and analyzed for asymmetric gene expression of *Pitx2c* in the LPM by WMISH (Figure 9 A). In contrast to uninjected controls (uninj.) or injections of control MO (CoMO), 1pmol/embryo *ATP4a*MO injections into the DMZ induced *Pitx2c* misexpression in up to 80% of

specimens. In 60% of *ATP4a* morphants bilateral expression was found (Figure 9 A, B). LR-defects decreased significantly (p<0.001) when *ATP4a*MO was targeted to the C2-lineage (~30%), and only 10% of LR-defects were detected upon *ATP4a*MO injections to C3- or VMZ-lineages (Figure 9 B). Taken together, *ATP4a* was required in the dorsal-medial lineage for correct LR-development and not in ventral cells as previously proposed (Levin et al. 2002).

Specificity of MO-induced effects was tested in rescue experiments: 1pmol/embryo *ATP4a*MO was injected into the DMZ together with *ATP4a* mRNA or 0.2pmol/embryo *ATP4a*MO together with an *ATP4a* DNA expression construct. In both cases, co-injection of *ATP4a* together with *ATP4a*MO significantly (p<0.01 and <0.001, respectively) rescued *Pitx2c* expression patterns in morphants (Figure 9 B). These results argued for specificity of MO-effects and indicated that *ATP4a* function was required post MBT in LR-development, as DNA constructs are transcribed only after stage 8/9 (Newport et al. 1982).

Asymmetric organ placement was also analyzed in stage 45 tadpoles in uninjected, CoMO-injected embryos and *ATP4a* morphants (Figure 9 C). Assessment of organ placement was prevented in a high fraction of embryos by cyst formation (Figure 9 C and Figure 10) (Wessely et al. 2011), which indicated malfunction of the pronephros in *ATP4a* morphants. High lethality in morphants was observed as well (not shown). Non-cystic survivors revealed ~30% of LR-defects when *ATP4a*MO was targeted to the DMZ, but not when it was delivered to the VMZ (Figure 9 D). Thus, laterality defects indicated by aberrant marker gene expression were confirmed by analysis of organ *situs*. Furthermore, bilateral expression of asymmetric genes was linked to heterotaxia in *ATP4a* morphants (Figure 9 B, D).

Asymmetric gene expression, asymmetric organ placement and cyst formation were analyzed following pharmacological inhibition of ATP4 by SCH28080 as well (Figure 9 and 10). Control incubation using the vehicle dimethyl sulfoxide (0.4% DMSO) did not affect LR-development (Figure 9 B, D). In contrast, incubation of embryos in 100-200µM SCH28080 did alter *Pitx2c* expression in 50% of specimens (Figure 9 B, D). Bilateral expression was found in 30% of SCH28080-treated embryos. Moreover, asymmetric organ placement was altered in a dose-dependent manner (Figure 9 D): Increase in SCH28080 concentration from 100µM to 200µM increased effects on organ placement, from 30 to 50%, respectively. Dose-dependency was also observed for cyst formation (Figure 10).
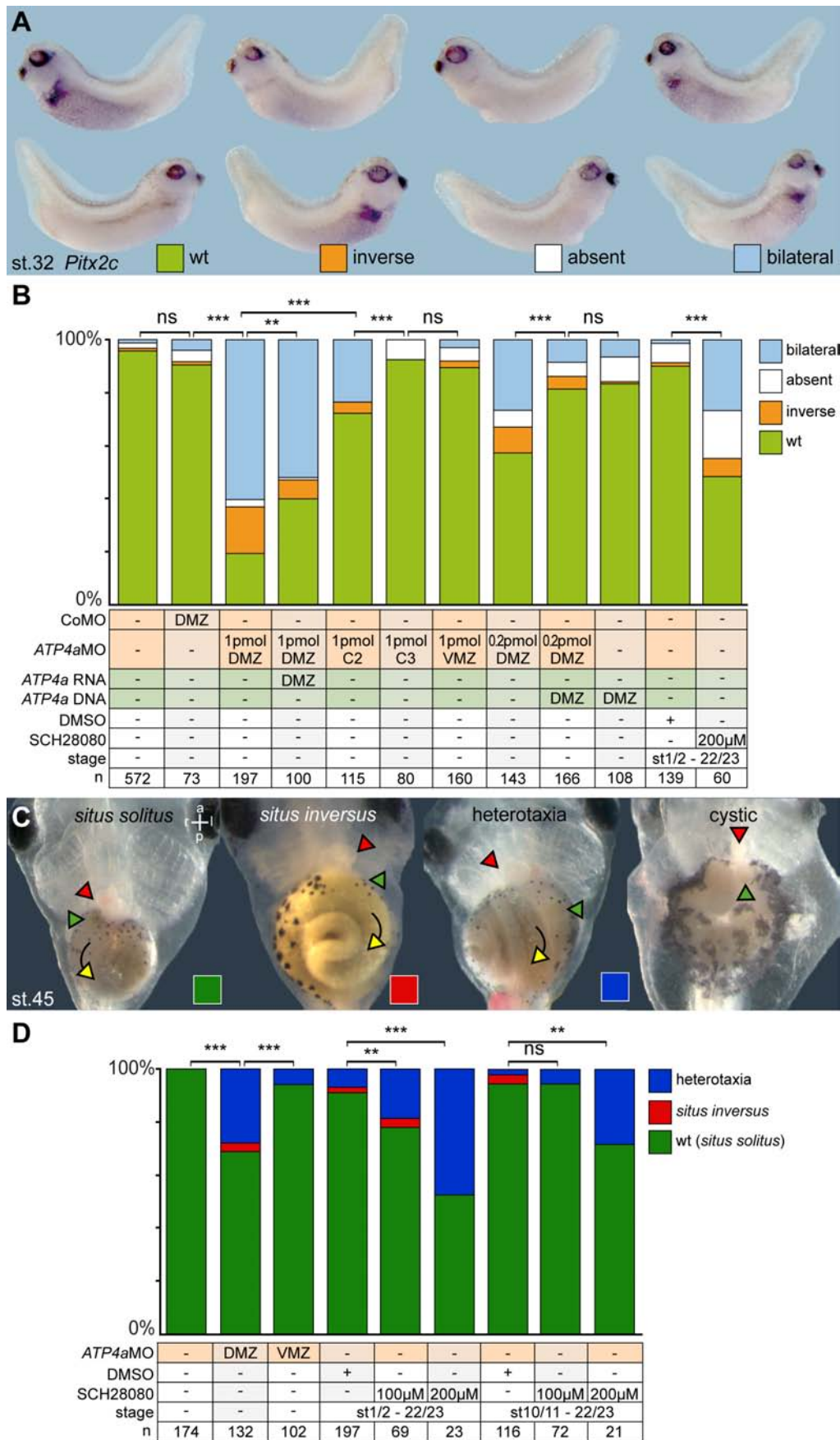
Figure 9: ATP4a Is Required In The Dorsal-Medial Lineage Post-MBT For LR-Development

(A-B) *Pitx2c* expression patterns encountered in *ATP4a* morphants and SCH28080 treated specimens **(A)**. **(B)** Quantification of *Pitx2c* expression patterns, treatment as indicated. →

(C-D) *Situs* defects encountered in *ATP4a* morphants and SCH28080 treated specimens: The outflow tract of the heart and the position of the gall bladder are indicated by green and red arrowheads, respectively, and the direction of gut looping is marked by yellow arrows. Note that morphants occasionally (and dose-dependently) developed cysts, and therefore organ *situs* could not be determined **(C)**. **(D)** Quantification of *situs* defects, treatment as indicated.

a = anterior, l = left, p = posterior, r = right and st. = stage. Statistical analysis: Chi²-test; ns = not significant, * = p<0.05, ** = p<0.01 and *** = p<0.001. Reprinted from: *Walentek et al. 2012*[#].

*ATP4a*MO	-	DMZ	VMZ	-	-	-	-	-	-
DMSO	-	-	-	+	-	-	+	-	-
SCH28080	-	-	-	-	100µM	200µM	-	100µM	200µM
stage	-	-	-	st1/2 - 22/23			st10/11 - 22/23		
n	174	196	109	220	76	56	125	107	63
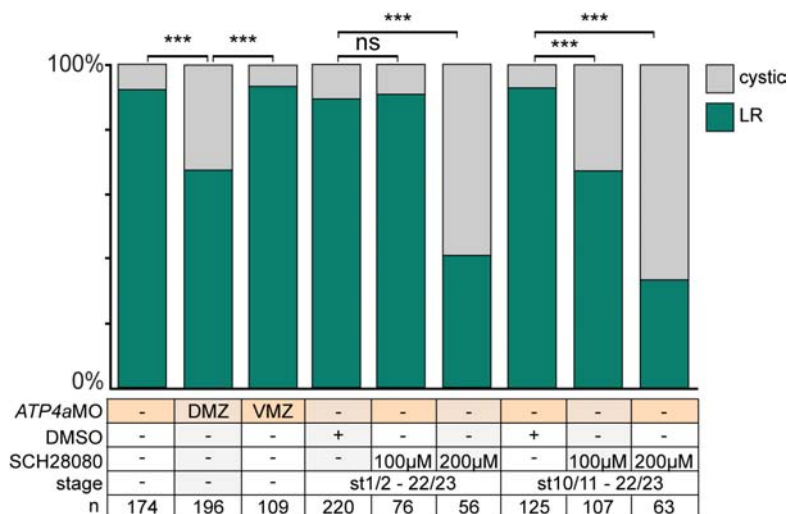
Figure 10: Rates Of Cystic Phenotype After Loss Of ATP4-function

Frequency of cystic phenotype (cystic – please compare with **Figure 9 C**) after *ATP4a*MO injection or SCH28080 treatment.

Statistical analysis: Chi²-test; ns = not significant, * = p<0.05, ** = p<0.01 and *** = p<0.001.

The previous study implicated that only early exposure to SCH28080 induced LR-defects, but not treatment from gastrulation onwards (Levin et al. 2002), thus these experiments were recapitulated and extended: Incubation in 100µM SCH28080, indeed, did not alter LR-development significantly (p>0.05) when applied from stage 10 onwards (Figure 9 D). Nevertheless, effects on LR-development could be evoked by application of higher concentrations (200µM) from stage 10 onwards (Figure 9 D). These experiments provided the proof that loss of ATP4 function from gastrulation onwards can be sufficient to alter LR-development.

In summary, molecular and pharmacological loss-of-function and rescue experiments revealed a requirement for ATP4 in LR-development only on the dorsal side of the embryo. These effects were restricted to post-MBT stages. Loss of ATP4 function induced bilateral expression of asymmetric genes (i.e. *Pitx2c*), which could be correlated with heterotaxic organ placement. In addition, loss of ATP4-function induced cyst formation, indicating defects in pronephros development.

Maternal But Not Zygotic *ATP4a* Is Required For LR-Axis Patterning

In order to discriminate between maternal and zygotic contribution of *ATP4a* transcripts in LR-development, an *ATP4a* splice-site-MO (*ATP4a*-Spl-MO) was designed (Aartsma-Rus 2012). Injections of up to 2pmol/embryo of *ATP4a*-Spl-MO into the DMZ at 4-cell stage did not have an impact on LR-development (Figure 11 B). This was a dose ten times higher than the smallest dose of *ATP4a*MO (0.2pmol/embryo) that was able to induce LR-defects in a highly significant (p<0.001; not shown) manner (Figure 9 B). These results argued against the requirement for zygotically expressed *ATP4a* mRNA in LR-development.
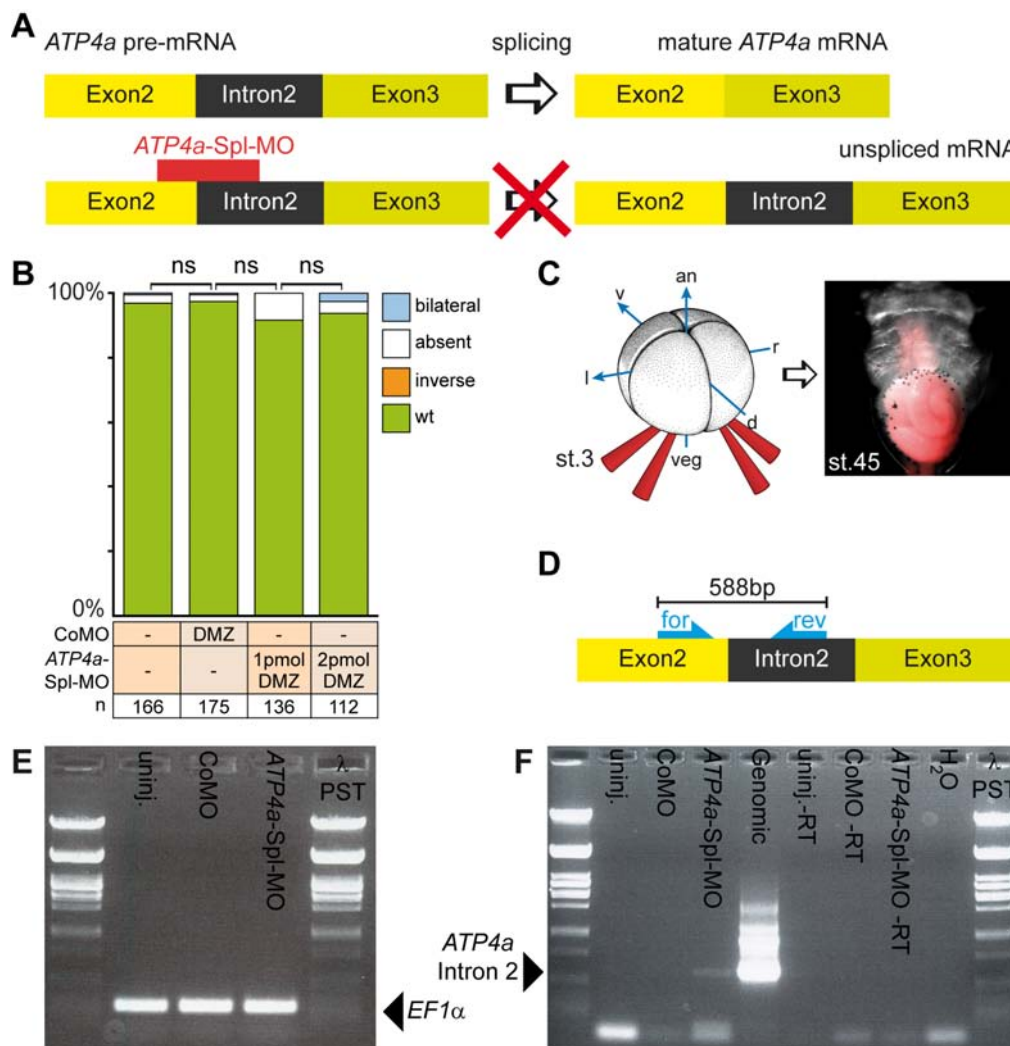
Figure 11: Loss Of Zygotic *ATP4* Expression Does Not Affect LR-Development

(A) Schematic representation of *ATP4a* pre-mRNA and splicing of Intron2 (upper line).
Schematic representation of *ATP4a*-Spl-MO mediated inhibition of pre-mRNA splicing (lower line).
(B) Quantification of *Pitx2c* expression patterns in *ATP4a*-Spl morphants. Please note that even high amounts (2pmol) of *ATP4a*-Spl-MO did not interfere significantly with LR-development. **(C)** Targeting of lineage tracer to the larval gut (st. 45) by vegetal injections at 4-cell stage. **(D)** Schematic representation of primer positions used in **(F)**, relative to the intron/exon boundary of Exon3/Intron2. **(E, F)** RT-PCR on st. 45 cDNAs from uninjected controls (uninj.), CoMO and *ATP4a*-Spl-MO injected specimens - Pst1-digested λ-DNA was used for size control. →

(E) Elongation factor 1α (EF1α) served as loading control. **(F)** Intron2-containing sequences were present in *ATP4a*-Spl-MO injected specimens and when genomic DNA was used, confirming functionality of *ATP4a*-Spl-MO. Negative controls for genomic DNA-content were performed on -RT extracts and a water sample (H_2O).

an = animal, bp = base pairs, d = dorsal, l = left, r = right, st. = stage, v = ventral and veg = vegetal. Statistical analysis: Chi²-test; ns = not significant, * = $p<0.05$, ** = $p<0.01$ and *** = $p<0.001$.

Functionality of the *ATP4a*-Spl-MO was tested by vegetal injections, which targeted the prospective gut (Figure 11 C), i.e. where zygotic *ATP4a* expression was found (Figure 3 H, I). Embryos were cultured until stage 45, when the tadpole stomach has formed and *ATP4a* expression was strong. cDNAs from uninjected, CoMO-injected and *ATP4a*-Spl-MO injected embryos were generated. Utilization of an *ATP4a* intron 2 specific reverse primer (Figure 11 D) confirmed presence of unspliced mRNA only in *ATP4a*-Spl-MO injected morphants (Figure 11 F). The specificity of primers was tested on genomic DNA and without DNA/cDNA (Figure 11 F), which served as positive and negative controls, respectively. RT-PCR for the house-keeping gene *elongation factor 1α* (*EF1α*) was used as loading control in these experiments (Figure 11 E) (Beyer et al. 2011).

In conclusion, this set of experiments suggested that *ATP4a*-Spl-MO was functional, and the lack of impact on LR-development implicated that maternally deposited, but not zygotically transcribed mRNA was required post-MBT for symmetry breakage and correct asymmetric gene expression.

ATP4 Gain-Of-Function Alters LR-Axis Development

Loss of *ATP4a* or *ATP4b* affected LR-development. In contrast to *ATP4a*MO (1pmol/embryo, ~80% *Pitx2c* expression), *ATP4b*MO was less effective (2pmol/embryo, ~20%) (Figure 12). Moreover, *Pitx2c* expression was lost in *ATP4b* morphants (Figure 12). Cyst formation was also observed (not shown). Gain-of-function experiments for *ATP4a* and *ATP4b* were performed. Injections of *ATP4a* DNA resulted in absent *Pitx2c* expression, in contrast to bilateral expression upon knock-down (Figure 12). Gain-of-function by means of *ATP4b* DNA injection also prevented *Pitx2c* expression. Interestingly, in gain-of-function experiments, *ATP4b* DNA was more effective (~50% of manipulated embryos had LR-defects) than *ATP4a* DNA (~25% LR-defects) (Figure 12), although the

same concentrations were used (1ng/µl). Furthermore, specificity was confirmed by co-injection of DNAs and MOs, which significantly rescued LR-development in *ATP4a* morphants and embryos over-expressing *ATP4b*, respectively. Taken together, gain and loss of either ATP4-subunit altered LR-development.
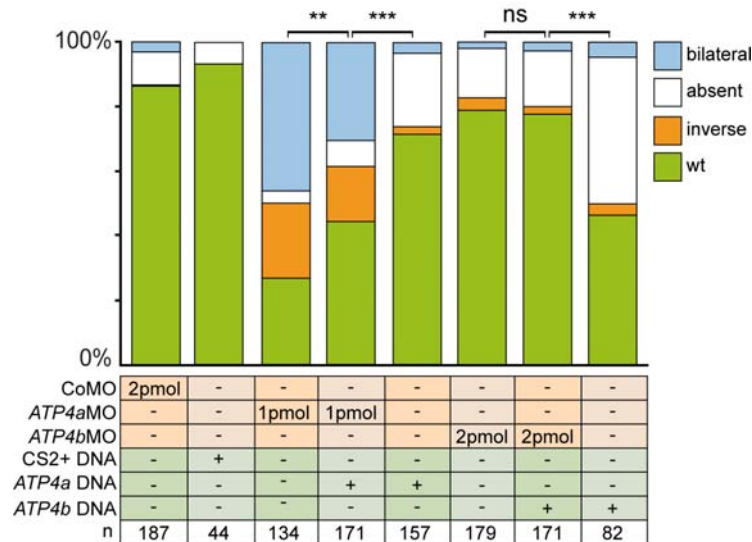
Figure 12: Gain And Loss Of ATP4a Or ATP4b Affects Laterality in *Xenopus*

Quantification of *Pitx2c* expression patterns after loss or gain of ATP4a/ATP4b function. Please note that specifically loss of ATP4a and gain of ATP4b function severely impaired LR-development. These conditions could be in part rescued by co-injection of *ATP4a* DNA or *ATP4b*MO, respectively. Please note further that all specific gain- and loss-of-function treatments were significantly different from control injections (not indicated).

Statistical analysis: Chi²-test; ns = not significant, * = p<0.05, ** = p<0.01 and *** = p<0.001.

ATP4a Is Required For Cilia-Driven Leftward Flow

Loss of *ATP4a* in the dorsal-medial cell-lineage was correlated with the highest rates of LR-defects (Figure 9 B). This lineage gives rise to the organizer and the superficial mesoderm, which in turn generates the GRP following involution over the dorsal lip (Blum et al. 2009b). Therefore, cilia-driven leftward flow was analyzed in control embryos and upon interference with ATP4 function by *ATP4a*MO injection or SCH28080 incubation. Flow parameters were determined in dorsal explants which were placed in buffer containing FITC-labeled latex beads (diameter 0.5µm) at stage 17, when leftward-flow was most robust. Fluid flow dependent movement of beads was recorded and processed for further analysis as described in Schweickert et al. (2007). Targeting was confirmed by co-injection of fluorescent lineage tracer. Three key parameters of flow were analyzed:

(1) Directionality, which is represented by the dimensionless parameter ρ (rho). A value of ρ=1 indicated that all trails pointed to the same direction. Conversely, when ρ=0, all trails were moving in random directions. (2) Number of directed trails. All individual trails, which show a ρ–value below 0.6 were excluded from further analysis, because they cannot be distinguished from particles moved by Brownian motion. Therefore, the number of particles reflected the directionality of single particle movement. (3) In addition to parameters reported in most studies, velocity was also used as a readout, because insufficient strength of flow might potentially affect LR-development as well (Schweickert et al. 2007; Tran et al. 2007; Vick et al. 2009; Schweickert et al. 2010; Beyer et al. 2011).
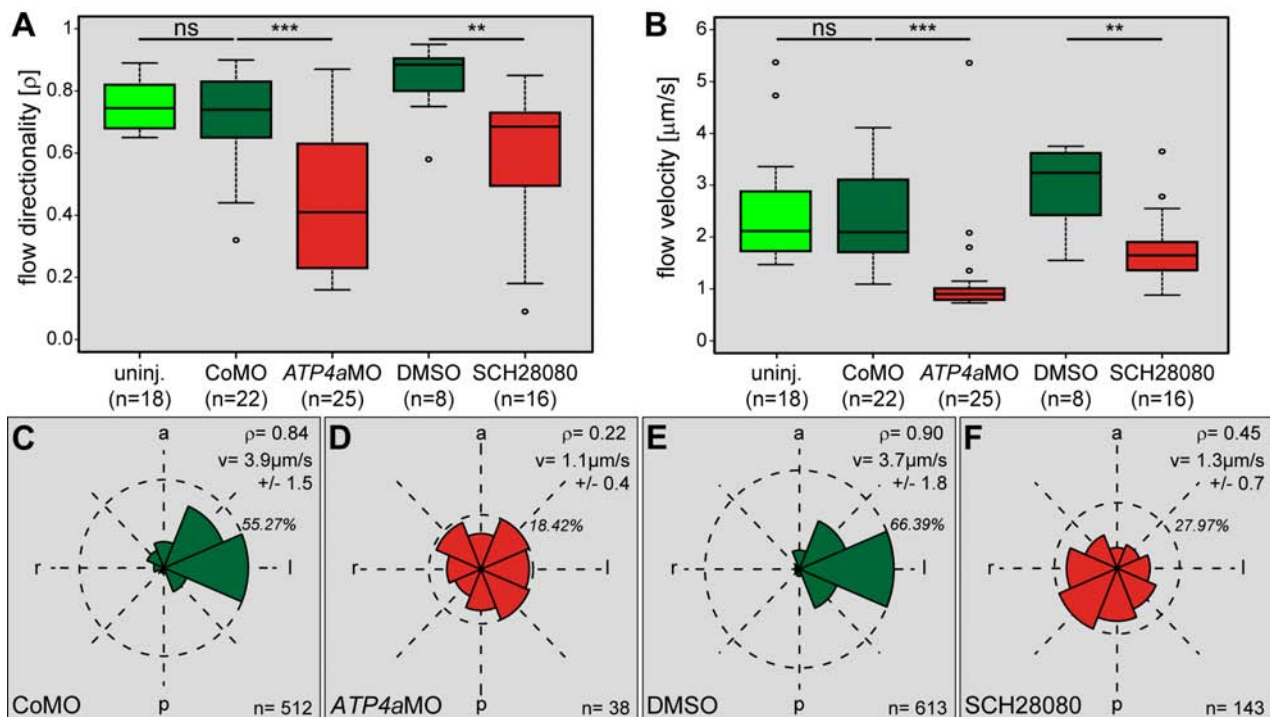
Figure 13: Loss Of ATP4 Function Impairs Cilia-Driven Leftward Flow

(A–F) Quantification of flow analysis in dorsal explants. **(A)** Directionality and **(B)** velocity of fluorescent beads added to GRP explants at st. 17 were drastically reduced in *ATP4a* morphants or SCH28080-treated specimens, as compared to wildtype, CoMO-injected, or DMSO-treated embryos. n represents the number of explants analyzed.
(C–F) Frequency distribution of trajectory angles in representative explants injected/incubated with **(C)** CoMO, **(D)** *ATP4a*MO, **(E)** DMSO, and **(F)** SCH28080. Dashed circles indicate maximum frequency in histogram specified in percent.

a = anterior, l = left, n = number of particles above threshold, p = posterior, r = right, v = average velocity of particles, ρ = quality of flow. Statistical analysis: Wilcoxon sum of ranks (Mann-Whitney) test; ns = not significant, * = p<0.05, ** = p<0.01 and *** = p<0.001.
Reprinted from: *Walentek et al. 2012*[#].
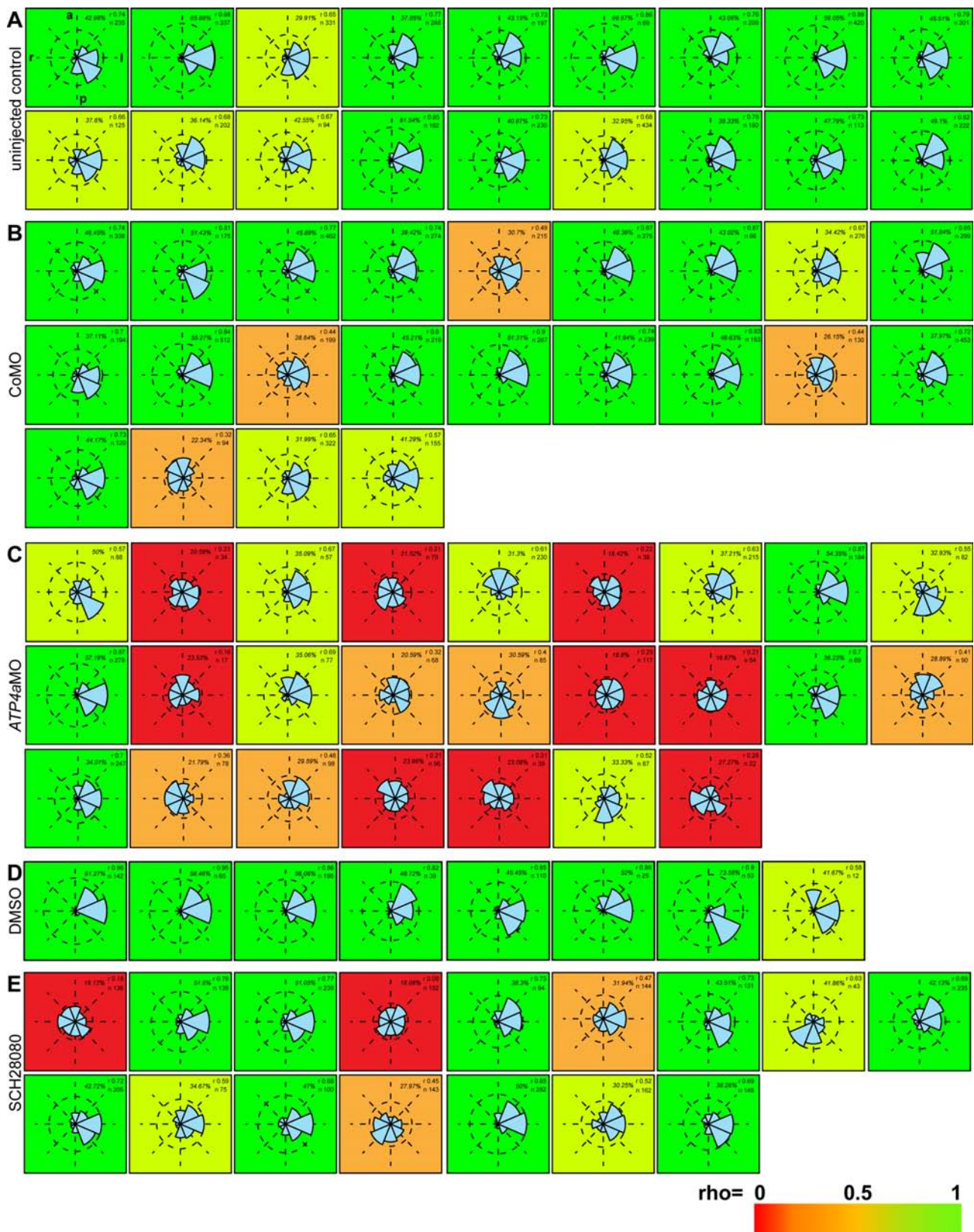
Figure 14: Single Representation Of Flow Diagrams After Loss Of ATP4 Function

(A) Uninjected controls. **(B)** CoMO-injected controls. **(C)** *ATP4a*MO-injected specimens. **(D)** DMSO- and **(E)** SCH28080-treated embryos.

Color code: red = strongly impaired flow, orange = significantly affected flow, yellow = moderately affected flow and green = wildtype-flow. Reprinted from: *Walentek et al. 2012*[#].

Analysis revealed that control flow reached ρ-values of 0.76±0.08, 0.7±0.16 and 0.84±0.12 in untreated, CoMO-injected and DMSO-treated specimens (Figure 13 A, C, E and Figure 14), respectively. In contrast, flow was disturbed in *ATP4a* morphants and upon SCH28080 incubation (200µM) with ρ-values of 0.45±0.22 and 0.6±0.21, respectively (Figure 13 A, D, F and Figure 14). The number of particle trails with ρ>0.6 was also decreased (Figure 14). In wildtype, CoMO injected and DMSO-treated explants flow velocities of 2.5±1.09 µm/s, 2.43±0.95 µm/s and 2.98±0.78 µm/s were observed, respectively (Figure 13 B, C, E). Average velocity of moving particles was reduced to 1.16±0.93 µm/s in *ATP4a* morphants and to 1.78±0.69 µm/s in SCH28080-treated specimens (Figure 13 B, D, E). In summary, flow was attenuated in strength, and directionality was randomized after loss of ATP4 function (Figure 13 A, B and Movie 1). These results were in agreement with the data obtained from differential targeting and post-MBT rescues (Figure 9 B).
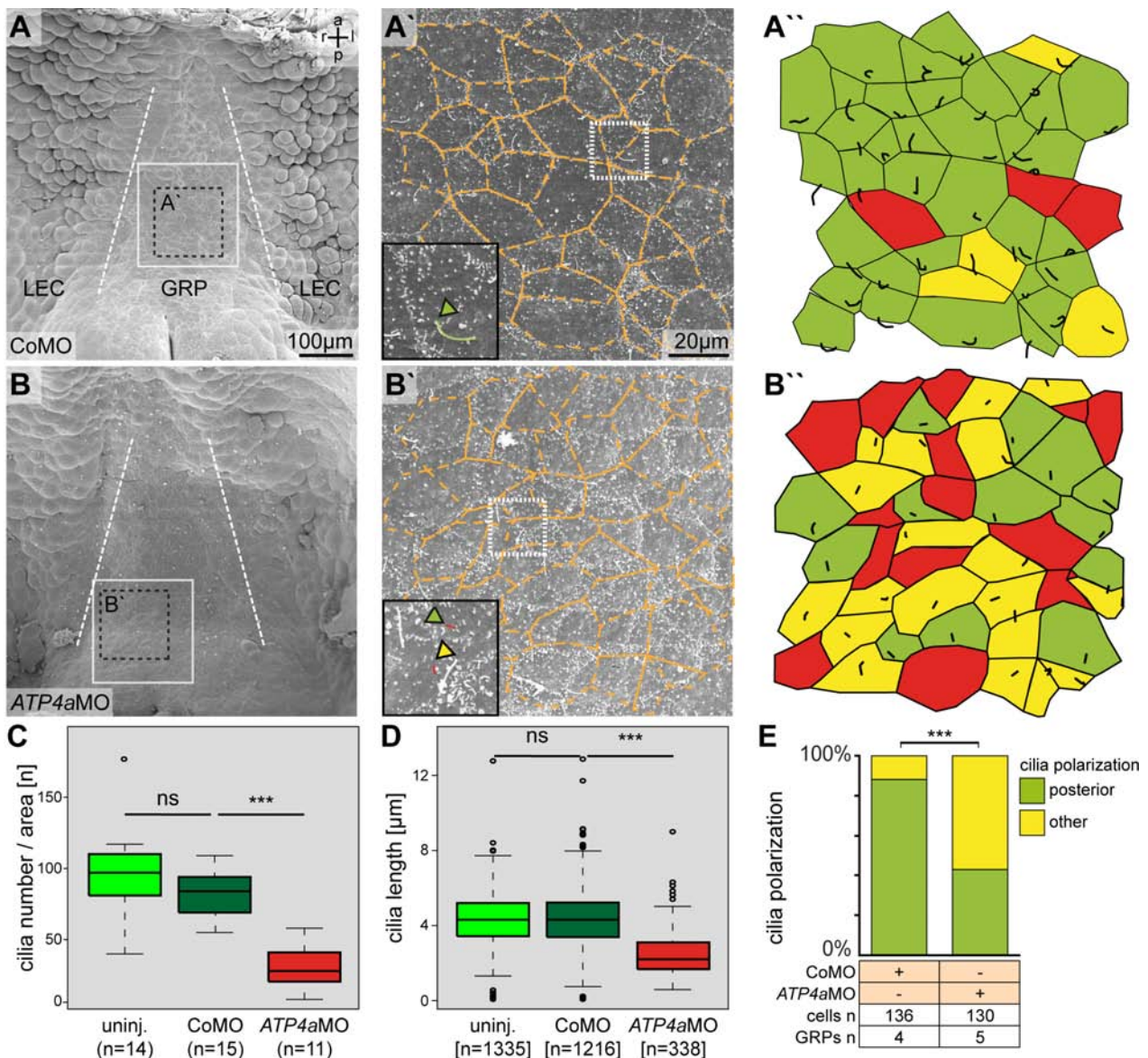
Figure 15: Analysis Of Ciliation Defects At The GRP After Loss Of ATP4 Function

(A–E) SEM analysis of GRP ciliation and morphology. **(A, B)** Representative dorsal explants reveal shorter cilia, fewer ciliated cells, and polarization defects in *ATP4a* morphant **(B)** as compared to CoMO-injected specimen **(A)**. Cell boundaries are indicated by dashed orange lines in higher magnification of SEM pictures in **(A`)** and **(B`)**. Blow-ups in **(A`)** and **(B`)** illustrate a long and posteriorly polarized cilium in **(A`)**, indicated by a green arrowhead, and two short cilia in **(B`)**, of which one emerges from a central position, indicated by a yellow arrowhead. **(A``, B``)** Evaluation of cilia polarization: Green = posterior, yellow = other, red = no cilium. **(C-E)** Quantification of ciliation rate **(C)** and cilia length **(D)** of GRP cilia in defined areas, as indicated by white squares in **(A)** and **(B)**. Cilia polarization **(E)** was assessed in areas of defined size, as indicated by dashed boxes in **(A)** and **(B)**.

Number of dorsal explants (in parentheses) or cilia [in brackets] analyzed. a = anterior, l = left, p = posterior, r = right. Statistical analysis: Box-plots - Wilcoxon sum of ranks (Mann-Whitney) test, Bar-graphs - Chi²-test; ns = not significant, * = p<0.05, ** = p<0.01 and *** = p<0.001. Reprinted from: *Walentek et al. 2012*[#].

Ciliogenesis Defects Of GRP Cilia In *ATP4a* Morphants Cause Aberrant Flow

Aberrant flow can either be attributed to loss of the flow-generating structure, lack of ciliary motility or to ciliogenesis defects, namely impaired cilia growth and polarization on the cell surface (Tran et al. 2007; Vick et al. 2009; Beyer et al. 2011). Flow analysis revealed residual flow (Figure 13), therefore loss of the GRP structure and complete loss of ciliary motility was ruled out. Next, ciliation of the GRP was analyzed by scanning electron microscopy (SEM – as described in Schweickert et al. 2007). The overall structure of the GRP was not altered in *ATP4a* morphants (Figure 15 A, B) and the cell size was normal (not shown). However, ciliation was greatly reduced in comparison to control specimens (Figure 15 A`, A`` and B`, B``). For quantification, SEM micrographs were analyzed using ImageJ and Cell-Gridder (Thumberger 2011). Ciliation rate and cilia length were significantly reduced in *ATP4a*MO injected embryos (Figure 15 C, D). Furthermore, over 50% of the remaining cilia were not correctly polarized to the posterior pole of GRP cells (Figure 15 E). In summary, the cause of flow defects was the impaired ciliogenesis of GRP cilia in *ATP4a* morphants.

Turbulent And Weak Flow In Morphants Is Sufficient For Bilateral Down-Regulation Of *Coco* And Activation Of The Nodal Cascade

In general, LR-defects in *ATP4a* morphants could be attributed to defects in ciliogenesis of GRP cilia and turbulent flow. In over 50% of morphants, bilateral expression of asymmetric marker genes was observed (Figure 9 B). The midline barrier (i.e. *Lefty* expressing dorsal

tissue) prevents the diffusion of asymmetric signals from the left to the right side (Cha et al. 2006; Cheng et al. 2000). Therefore, bilateral expression of *Pitx2c* suggested defects in the establishment of the midline barrier, in addition to turbulent flow. Expression of midline genes, i.e. *Xbra* and *Lefty* (also called *Antivin* in *Xenopus*), was analyzed after *ATP4a*MO injection into the DMZ (Figure 16). Surprisingly, *Xbra* and *Lefty* expression was not affected (Figure 16 A-C).

Next, the presence and correct expression of genes in flow sensing lateral (somitic) GRP cells were investigated. WMISH for *Xnr1* and *Coco* revealed normal expression before flow (not shown) and argued against defects related to the flow sensing mechanism (Schweickert et al. 2010). When *Xnr1* and *Coco* expression was analyzed following flow stages (st. 20), flow-dependent down-regulation of left *Coco* expression was lost in morphants, as compared to controls (Figure 17 A, B). Loss of left-sided *Coco* repression and lack of Xnr1 de-repression was thus far only reported when flow was lost (Schweickert et al. 2007, Vick et al. 2009). This was accompanied by loss of asymmetric gene expression in the LPM. As *ATP4a* morphants displayed bilateral induction of the nodal cascade (Figure 9 B), loss of *Coco* asymmetry implicated bilateral down-regulation of *Coco*. This hypothesis was tested in epistatic loss-of-function experiments. *Coco*, as well as *Pitx2c* expressions, were used as readouts.
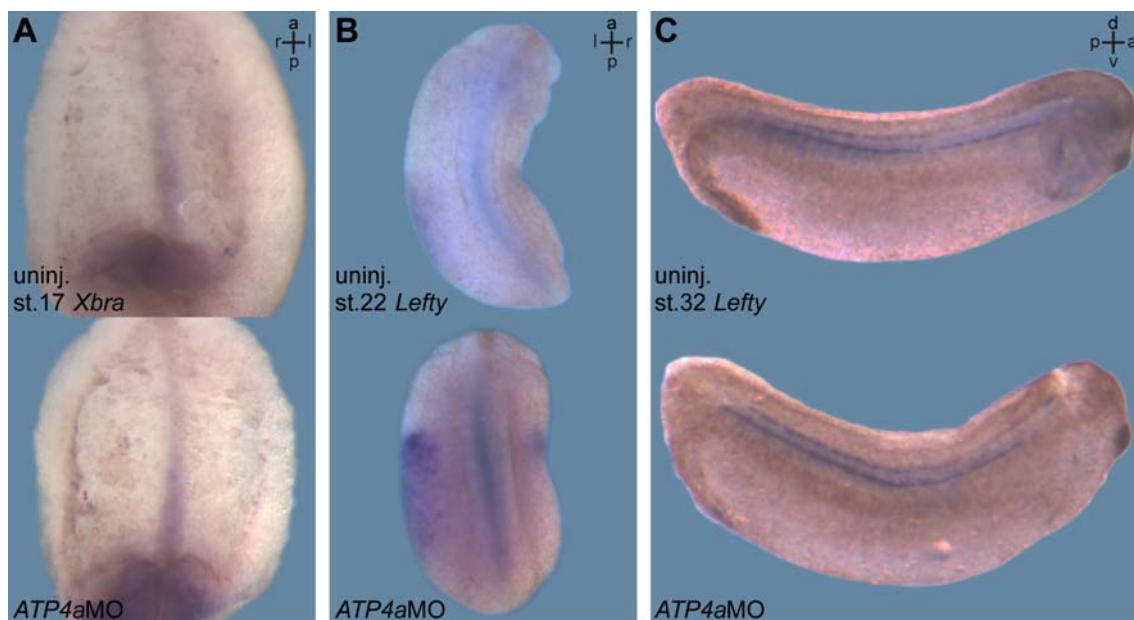
Figure 16: Midline Formation Is Unaffected After Loss Of ATP4 Function

(A-C) Analysis of midline marker gene expression by WMISH revealed normal midline formation in *ATP4a* morphants. **(A)** *Xbra* expression (st. 17) in the circumblastular collar and notochord. **(B)** Early *Lefty* expression (st. 22) at the midline was not affected in *ATP4a* morphants. Please note bilateral *Lefty* expression in the LPMs of *ATP4a* morphant. **(C)** Late *Lefty* expression in the notochord, floor plate and dorsal endoderm in cleared tailbud stage embryos (st. 32).

a = anterior, d = dorsal, l = left, p = posterior, r = right, st. = stage and v = ventral.

Bilateral knock-down of *Xnr1* by injection of *Xnr1*MO prevented induction of the nodal cascade in the LPM as previously reported (Figure 17 C-1) (Schweickert et al. 2010). Parallel loss of *ATP4a* did not induce bilateral expression in absence of *Xnr1* (Figure 17 C-2), placing *ATP4a* function upstream of *Xnr1* de-repression. When *Xnr1*MO was injected to the left side only, *Pitx2c* expression was prevented as well (Figure 17 C-3). When *ATP4a* was knocked-down bilaterally, loss of left *Xnr1* function resulted in right-sided induction of the nodal cascade (Figure 17 C-4). Conversely, when *Xnr1*MO was injected to the right side only, normal left-sided induction of the nodal cascade was not prevented (Figure 17 C-5). Loss of *Xnr1* function on the right side in *ATP4a* morphants inhibited right-sided induction and restored asymmetric expression of *Pitx2c* in the left LPM (Figure 17 C-6). Taken together, these experiments indicated that *ATP4a*MO-induced bilateral expression of *Pitx2c* was *Xnr1*-dependent and might represent a direct result of a weak and turbulent flow.

This hypothesis would require that effects of *ATP4a*MO rely on ciliary motility. Therefore, ciliary motility was inhibited by injection of *Dnah9*MO (*Dnah9*-Spl-MO in Vick et al. 2009). Indeed, parallel loss of ciliary motility and *ATP4a* led to a loss of nodal cascade induction as reported previously for loss of ciliary motion alone (Figure 17 C-7). Moreover, when bilateral loss of *ATP4a* was combined with unilateral knock-down of *Dnah9*, induction of the nodal cascade was prevented on the side where ciliary motion was inhibited (Figure 17 C-8, -9).

Next, a triple knock-down was performed: (1) *ATP4a*MO was injected bilaterally (resulting in bilateral *Pitx2c* expression), (2) *Xnr1*MO was injected to the left side (resulting in inverse expression of *Pitx2c*; Figure 17 C-4) and (3) *Dnah9*MO to the right side (resulting in left-sided *Pitx2c* expression; Figure 17 C-9). In specimens treated this way, *Pitx2c* expression was absent on either side in the LPM. Therefore, effects of *ATP4a*MO on LR-axis specification relied on *Xnr1*-mediated detection of flow and *Dnah9*-dependent ciliary motion.

In conclusion, bilateral symmetric *Coco* expression post flow (Figure 17 A, B) represented bilateral down-regulation. This was tested in *ATP4a*MO injected specimens, in which ciliary motility was inhibited on the left side: Inverted right-only repression of *Coco* was observed (Figure 17 A, B), demonstrating that flow-dependent down-regulation on the right side took place.
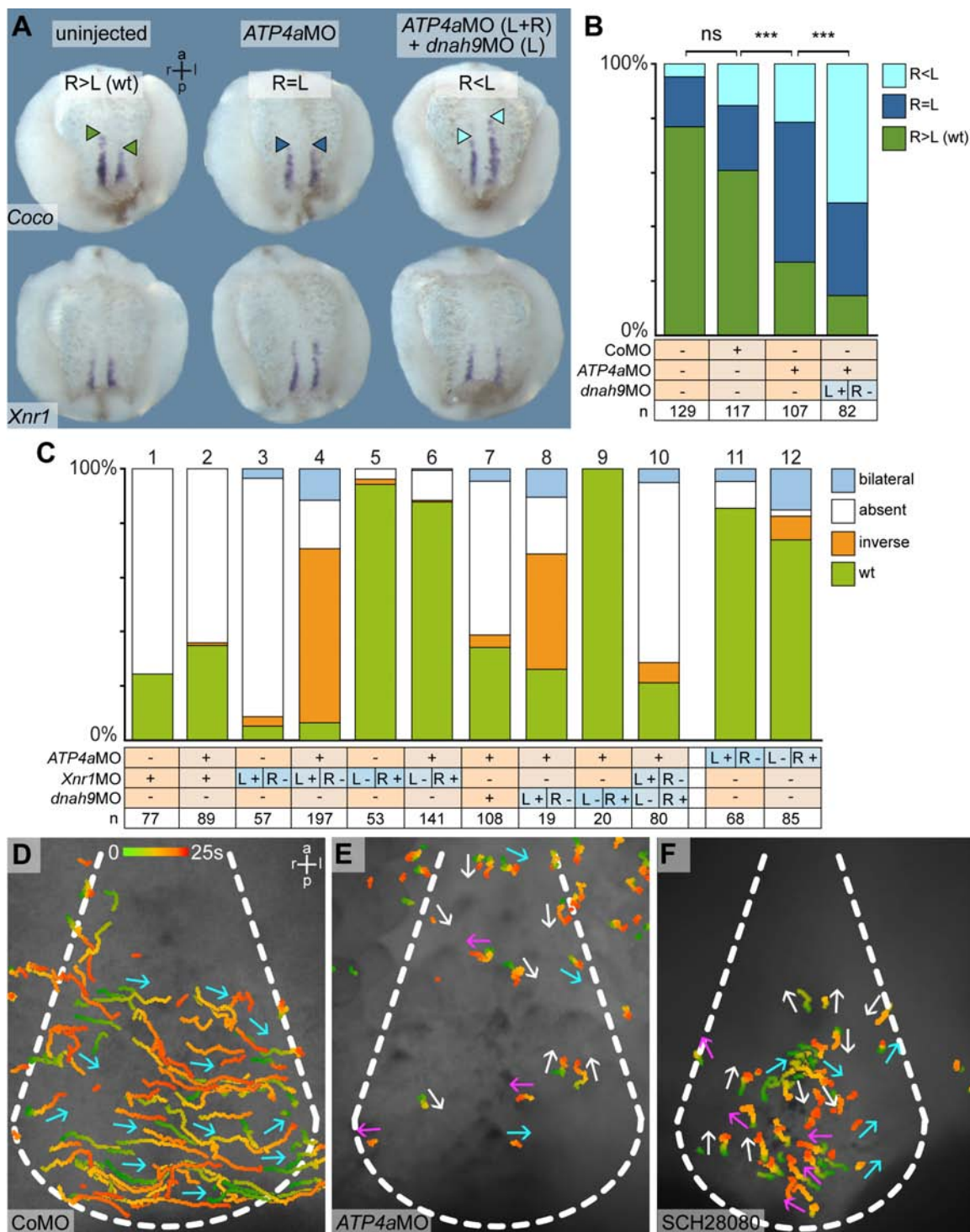
Figure 17: Turbulent Flow In *ATP4a* Morphants Causes Bilateral Nodal Cascade Induction

(A-B) WMISH of st. 20 dorsal explants with probes specific for (top) *Coco* and (bottom) *Xnr1* **(A)**. Left-sided *Coco* repression was lost in (middle) *ATP4a* morphants and inverted upon (right) parallel left-sided knock-down of flow. *Xnr1* expression was unaffected. **(B)** Quantification of *Coco* expression patterns. **(C)** Quantification of *Pitx2c* expression patterns in st. 26–32 tadpoles following MO injections into the C1 lineage (dorsal midline-GRP) of 4-cell stage embryos as indicated. Note that the bilateral induction (please compare **Figure 9 B**) in *ATP4a* morphants was dependent on both the presence of GRP-Xnr1 and ciliary motility. Please further note that unilateral knock-down of *ATP4a* was less efficient in inducing bilateral *Pitx2c* expression than bilateral injections. **(D–F)** Analysis of bead trajectories in time-lapse movies of dorsal explants from representative **(D)** CoMO-injected or **(E)** *ATP4a*MO-injected embryos and **(F)** specimen treated with SCH28080. Flow is displayed as GTTs of 25 s length (color bar in **D**). →

Note that trajectories in **(E)** and **(F)** project to the left side (indicated with blue arrows) and right side (indicated with pink arrows) of the GRP, whereas GTTs in **(D)** point uniformly to the left. White arrows represent trajectories running anteriorly or posteriorly.

a = anterior, GTT = gradient time-trail, l = left, p = posterior, r = right and st. = stage. Statistical analysis: Chi²-test; ns = not significant, * = $p<0.05$, ** = $p<0.01$ and *** = $p<0.001$.
Reprinted and modified from: *Walentek et al. 2012*[#].

Analysis of flow patterns in *ATP4a* morphants and SCH28080 treated specimens revealed particle movements towards the left and right margins of the GRP (Figure 17 D-F and Movie 1). In 9 (of 25) severely affected *ATP4a*MO morphant explants ρ-values were below 0.3, the number of directed particles was below 120/movie and no more than 28% of particle trails projected towards the same direction. Therefore, flow strength/directionality equivalent to only ~15 directed particles was sufficient to induce bilateral down-regulation of *Coco* and concomitant bilateral induction of the nodal cascade. This finding was unexpected and possibly the first case where bilateral induction was clearly correlated with flow patterns and not with midline-barrier defects.

Turbulent And Weak Flow On The Left Side Of The GRP Enhances Right-Sided Induction Of The Nodal Cascade In *ATP4a* Morphants

Vick et al. (2009) reported that flow on the left side of the GRP was necessary and sufficient for left-sided induction of the nodal cascade, and flow on the right side was dispensable. Flow directionality and strength were diminished in *ATP4a* morphants (Figure 13), but the residual flow was sufficient to induce the nodal cascade bilaterally (Figure 17). Therefore, unilateral knock-down of *ATP4a* was tested and compared with effects of bilateral loss-of-function (Figure 9 B).

When *ATP4a*MO was injected only to the left side at 4-cell stage (Figure 17 C-11), over 80% of embryos developed normally in terms of *Pitx2c* expression. In ~10% of morphants *Pitx2c* expression was lost, indicating that ciliation and flow were reduced to a level, which was not able to induce *Coco* down-regulation. In these specimens the wildtype flow on the right side did not compensate for loss of flow on the left side. Vick et al. (2009) suggested that flow on the contra-lateral side is not relevant for sensing of flow. Therefore, it was astonishing that *ATP4a*MO injections to the right side only (Figure 17 C-12) were a lot less effective than bilateral knock-down (Figure 9 B), when *Pitx2c* expression was analyzed. Therefore, loss of *ATP4a* on the left side enhanced effects on the right side of the GRP.

ATP4a Is Required For Canonical And Non-Canonical Wnt Signaling

When high amounts (1pmol/injection) of *ATP4a*MO were applied, morphant phenotypes developed features known from Wnt signaling defects (Figure 18 A): *ATP4a* morphants showed loss of anterior most head structures, reduced pigmentation, shortening of the AP-axis and cyst formation (Figure 18 A and Figure 9 C) (Borchers et al. 2000; Wallingford et al. 2001; Tao et al. 2005; Tran et al. 2007; Cruciat et al. 2010). In a recent report, ATP6 (also called vacuolar H$^+$ATPase) was found to be necessary for canonical and non-canonical Wnt signaling (Cruciat et al. 2010). Moreover, ciliogenesis defects in Kupffer's vesicle of zebrafish embryos were observed upon loss of ATP6 function. For this reason, a possible interaction of ATP4 with Wnt signaling was tested.

First, engrailed *2* (*En2*) expression, a direct target of canonical Wnt/β-catenin (β-cat) in the mid-/hindbrain barrier, was assessed after *ATP4a* knock-down (McGrew et al. 1999). A significant reduction in *En2* expression levels was observed after *ATP4a*MO injections, which was rescued by co-injection of 1ng/µl *β-cat* DNA (Figure 18 B).

Next, the level of interaction was experimentally tested by induction of secondary axes. In *Xenopus*, this can be achieved by misexpression of Wnt-pathway components on the ventral side of the embryo (Figure 18 C-F) (Sokol et al. 1991). Secondary axis formation was observed when *Xwnt8a* (80%), *Dvl2* (90%), *β-cat* (>90%) or *Sia* (~40%) mRNAs were injected to the ventral side at 4-cell stage (Figure 18 G). Co-injections of *ATP4a*MO significantly reduced induction of secondary axes by *Xwnt8a* (~20% reduction) and *Dvl2* (~40% reduction), but not by *β-cat* or *Sia* (Figure 18 G). This implicated that the functional interaction of *ATP4a* and Wnt signaling took place at the level of membrane-bound signalosome components, including *Dvl2* (Cruciat et al. 2010).

Effects on non-canonical Wnt signaling of the planar cell polarity (PCP) branch were tested as well. Neural tube closure requires PCP-dependent convergent extension (CE) movements within the neuroectoderm (Wallingford et al. 2001). The width of the neural plate, which directly correlates with neural tube closure, was analyzed in control and morphant embryos. Embryos were unilaterally injected into the right side and stained for the neural plate marker *Sox3* by WMISH (Rogers et al. 2008). While the neural tube of stage 18 control embryos was nearly completely closed, a significant widening of the neural plate on the injected side was observed in *ATP4a* morphants (Figure 19 A).

Figure 18: ATP4a Is Required For Canonical Wnt-Signaling
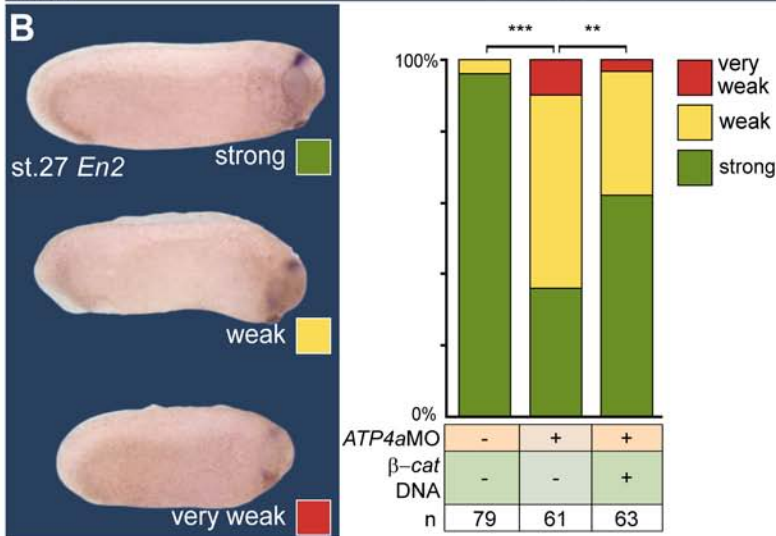
(A) Phenotypes of *ATP4a* morphant tadpoles (st. 45), which were less pigmented, displayed shortened AP-axes, small heads and reduced eyes.
(B) Reduced *En2* expression at the mid-hindbrain boundary of morphant st. 27 tadpoles could be rescued by co-injection of *β-cat* DNA.
(C-G) *Xwnt8-* and *Dvl2*-mediated, but not *β-cat* or *Xsia*-induced, twinning requires ATP4a.
(C-F) Representative examples of embryonic twinning after ventral gain of indicated Wnt-component.
(G) Quantification of embryonic twinning.
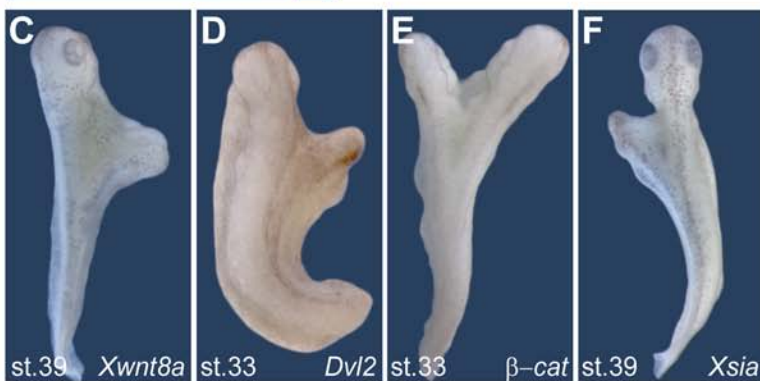
Statistical analysis: Chi²-test; ns = not significant, * = p<0.05, ** = p<0.01 and *** = p<0.001.

Reprinted and modified from: *Walentek et al. 2012[#]*.
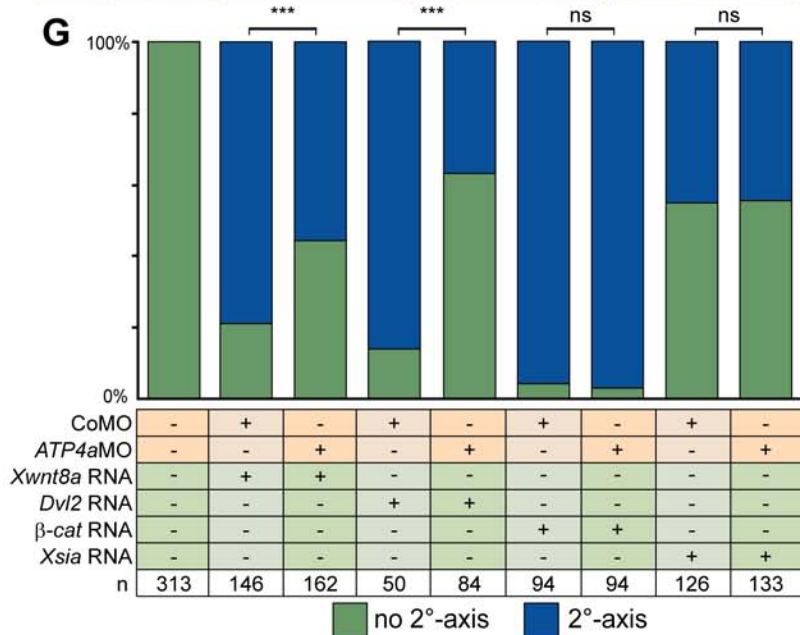
Specificity of the effect was confirmed by partial rescue upon co-injection of 60ng/µl *ATP4a* mRNA (Figure 19 A). CE movements also significantly contribute to the lengthening of the embryo during development (Keller et al. 2008). Shortening of the AP-axis was

analyzed in tailbud stages (st. 32). *ATP4a*MO injected specimens were significantly shorter than control specimens, and this effect was also partially rescued by co-injection of 80ng/µl of *ATP4a* mRNA (Figure 19 B).

The level of interaction in PCP-signaling was tested using a standard CE assay in *Xenopus* (Green et al. 1990): Embryos were injected at 4-cell stage into the animal hemisphere and grown until late blastula stages (st. 8/9). Then, the animal cap was explanted and cultured in presence of activin until early tailbud stages (st. 25-30). Activin treatment induces notochord formation within uncommitted animal cells. The notochord exerts CE movements during development. Therefore, the activin-treated explant elongates, which can be used as a readout for CE/PCP (Figure 19 C). Uninjected and CoMO injected explants elongated when activin was added (Figure 19 D), and elongation was reduced in ~30% of *ATP4a*MO injected animal caps (Figure 19 D). Moreover, when a constitutive active form of the Wnt/PCP-pathway component *RhoA GTPase* (*RhoA CA*) was co-injected with *ATP4a*MO, elongation of explants was restored in ~20% of specimens (Figure 19 D) (Paterson et al. 1990). In contrast, this was not the case when a dominant negative form of *RhoA* (*RhoA DN*) was co-injected (Figure 19 D) (Paterson et al. 1990).

Taken together, *ATP4a* was required for canonical as well as non-canonical Wnt signaling during *Xenopus laevis* development, and the level of interaction was upstream of intracellular effector molecules *β-cat* and *RhoA* in canonical and non-canonical signaling, respectively.

The *ATP4a* morphant phenotype was also characterized by reduced pigmentation and cyst formation (Figure 18 A and Figure 9 C). Both phenotypes were previously correlated with loss of *Wnt11*-mediated non-canonical Wnt-signaling defects (Matthews et al. 2008; Tételin et al. 2010). Both systems were analyzed, and loss of *ATP4a* was compared to the effects described upon *Wnt11* loss-of-function in the literature. When *ATP4a*MO was targeted to the NC, analysis of the NC marker *Twist1* revealed that loss of *ATP4a* was able to phenocopy these effects. *Twist1* expression intensity was decreased and migration of cells was inhibited (Figure 19 E) (Mayor et al. 2001). This was the case for pronephric development as well: Loss of *Wnt11* was reported to inhibit the formation and branching of the pronephric tubules in morphants (Tételin et al. 2010). The same effect was observed in *ATP4a* morphants (Figure 19 F). In conclusion, the phenotype in *ATP4a* morphants (Figure 18 A) could be explained by a decrease in canonical and non-canonical Wnt-signaling.
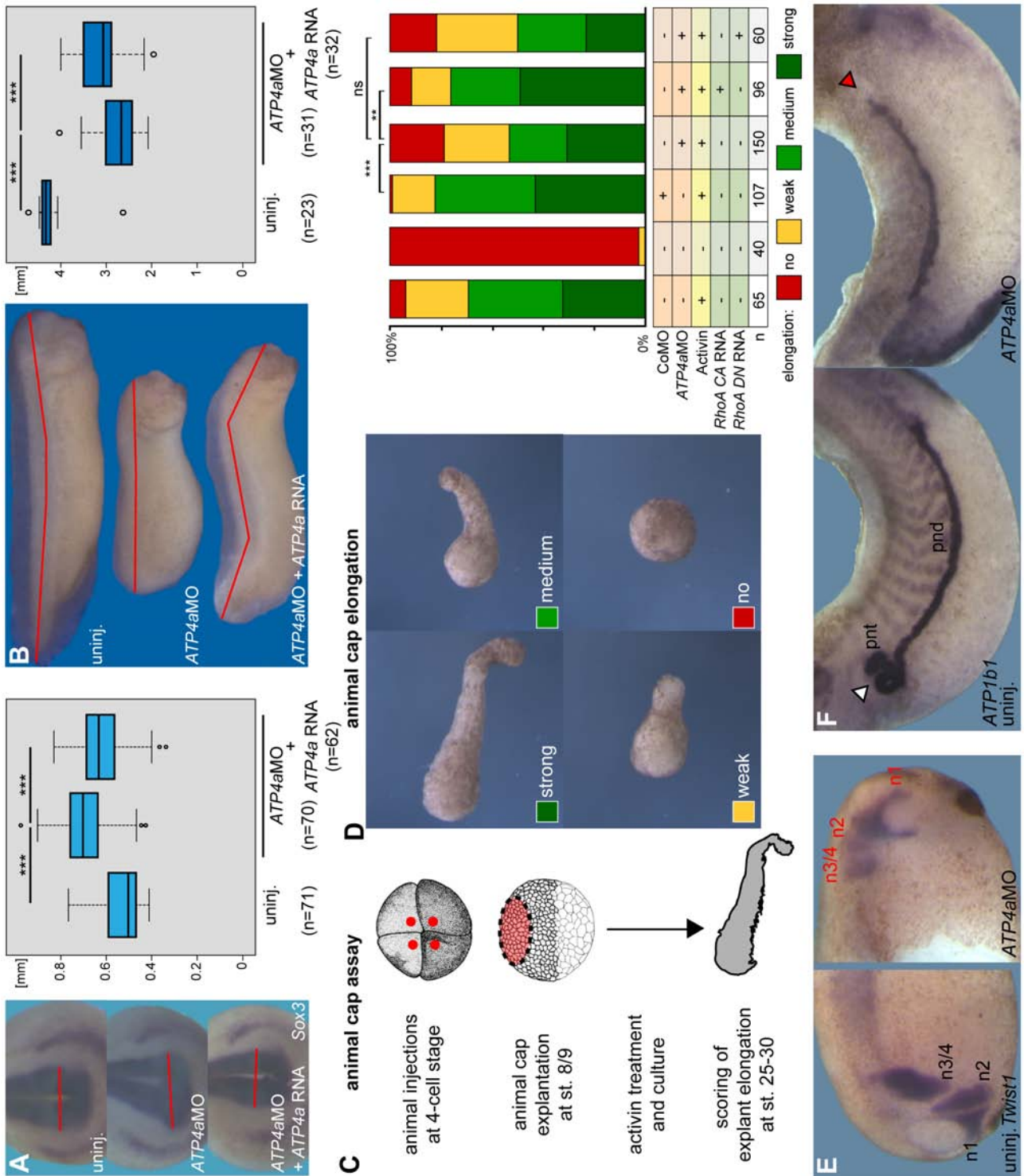
Figure 19: ATP4a Is Required For Non-Canonical Wnt-Signaling

(A - D) Analysis of convergent extension. **(A)** Neural tube closure: widening of the neural tube in *ATP4a* morphants. Embryos were injected unilaterally into the animal right blastomeres at the 4-cell stage, fixed and processed for *Sox3* expression to visualize the neural plate by WMISH at st. 18. Staging was according to the progress of neural tube closure on the uninjected (left) side. Note that the widening of the neural plate was partially rescued upon *ATP4a* mRNA co-injection. **(B)** Shortening of the anterior-posterior (AP) axis. Embryos were bilaterally injected into the DMZ at the 4-cell stage, and the AP extension was determined at st. 32. Note that MO-induced shortening was partially rescued by *ATP4a* mRNA co-injection. The width of the neural plate **(A)** and the length of embryos **(B)** were measured (as indicated by red lines). Results are depicted as box plots. →

(C-D) Convergent-extension movements of activin-induced animal cap explants: **(C)** Schematically depicted animal cap experiment. **(D)** Reduced elongation in *ATP4a*MO-injected explants was rescued by co-injection of *constitutively active (CA) RhoA* mRNA, but not after co-injection of *dominant negative (DN) RhoA* mRNA. **(E)** Neural crest cell specification and migration: Right-sided *ATP4a*MO-injection resulted in reduced and altered *Twist1* mRNA expression at st. 26 (n1-n3/4; neural crest migratory streams). **(F)** Right-sided pronephric tubule (pnt) defects upon unilaterally *ATP4a*MO-injection, as demonstrated by WMISH using the pronephros marker gene *ATP1b1*.

Statistical analysis: Box-plots - Wilcoxon sum of ranks (Mann-Whitney) test, Bar-graphs - Chi²-test; ns = not significant, * = p<0.05, ** = p<0.01 and *** = p<0.001.
Reprinted and modified from: *Walentek et al. 2012[#]*.

LR-Axis Defects Are Independent Of Primary Axis Development In *ATP4a* Morphants

Wnt-dependent development of the primary axes is thought to be a prerequisite for the correct setup of the LR-axis (Danos et al. 1995; Lohr et al. 1997). Therefore, a possible correlation of LR-defects with AP-axis defects was investigated. *ATP4a* morphant embryos were analyzed for *Pitx2c* expression (Figure 9 B) and AP-axis development (Figure 20, left panel). Quantification of *Pitx2c* expression patterns in wildtype-like embryos, embryos with a shorter AP-axis and/or defects in head patterning, revealed that LR-defects were not over-represented in any of these phenotypes (Figure 20). Therefore, there was no need to exclude specimens from analysis of specific effects on the LR-axis.
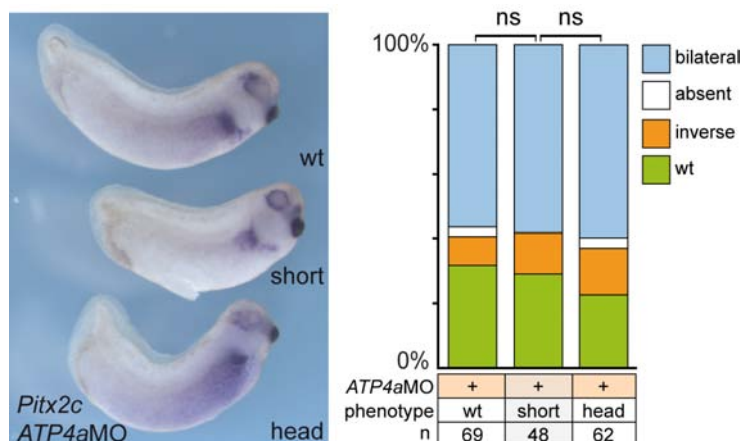
Figure 20: LR-Defects In *ATP4a* Morphants Are Not Coupled To Primary Axis Defects

Quantification of *Pitx2c* expression patterns in *ATP4a* morphants, which either displayed normal primary axes development (wt) or defects in AP-axis elongation (short) or defects in head patterning (head). Quantity and type of *Pitx2c* expression defects were not significantly lower in wt-like morphants.

Statistical analysis: Chi²-test; ns = not significant, * = p<0.05, ** = p<0.01 and *** = p<0.001.

***ATP4a* Mediated Wnt/β-cat Signaling Is Necessary And Sufficient For *Foxj1* Expression During Gastrulation**

LR- and ciliogenesis defects in *ATP4a* morphants (Figure 9, 16) and the requirement for ATP4 in Wnt-signaling (Figure 18, 20) suggested that ciliogenesis was under Wnt control. The forkhead-box transcription factor *Foxj1* (a master regulator of motile ciliogenesis) was expressed in the superficial mesoderm (SM) (Figure 21 A) (Stubbs et al. 2008). *Foxj1* expression during gastrulation was decreased in *ATP4a* morphants and in SCH28080 treated embryos (Figure 21 A, D-F). Co-injection of *β-cat* DNA rescued *Foxj1* expression in *ATP4a*MO injected specimens (Figure 21 B, D). *Foxj1* expression in the SM was also rescued by *β-cat* DNA injections in SCH28080 experiments (Figure 21 E-G). Drug treatment was less efficient, and batch dependency was observed, which prevented quantification. Therefore, only one experiment is shown for a proof of principal that pharmacological inhibition was comparable to MO injections (Figure 21 B, G). Next, the gain-of-function effects of canonical Wnt-signaling components, i.e. *β-cat* and a constitutive active version of the canonical co-receptor *LRP6* (*LRP6ΔE1-4*), were tested (Niehrs et al. 2010). Injection of *β-cat* DNA to the ventral side at the 4-cell stage induced *Foxj1* expression in more ventral aspects of the mesodermal ring (Figure 21 C). This was also the case when *LRP6ΔE1-4* DNA was used (not shown). It is noteworthy that, DNA injections of these Wnt components did not induce secondary axis formation (not shown).

In order to confirm the relevance of *ATP4a*MO-induced *Foxj1* down-regulation for LR-development, *Pitx2c* expression was analyzed. Co-injection of 0.5ng/μl *Foxj1* DNA partially rescued LR-defects in *ATP4a*MO injected specimens (Figure 21 H). Significantly, when *Foxj1* was knocked-down by *Foxj1*MO, loss of *Pitx2c* expression was observed (Figure 21 H). Dose-dependency was observed in the rate of *Pitx2c* misexpression, ranging from ~10%, to ~30% and 50% in 0.2, 1 and 2pmol/embryo injected *Foxj1* morphants, respectively (Figure 21 H). Taken together, *ATP4a* mediated Wnt/β-cat signaling was necessary and sufficient for mesodermal *Foxj1* expression during gastrulation. Loss of *ATP4a* only partially inhibited *Foxj1* expression, and bilateral *Pitx2c* expression was observed (Figure 21 A, H). In contrast, more pronounced loss of *Foxj1* by *Foxj1*MO caused absence of nodal cascade induction (Figure 21 H).
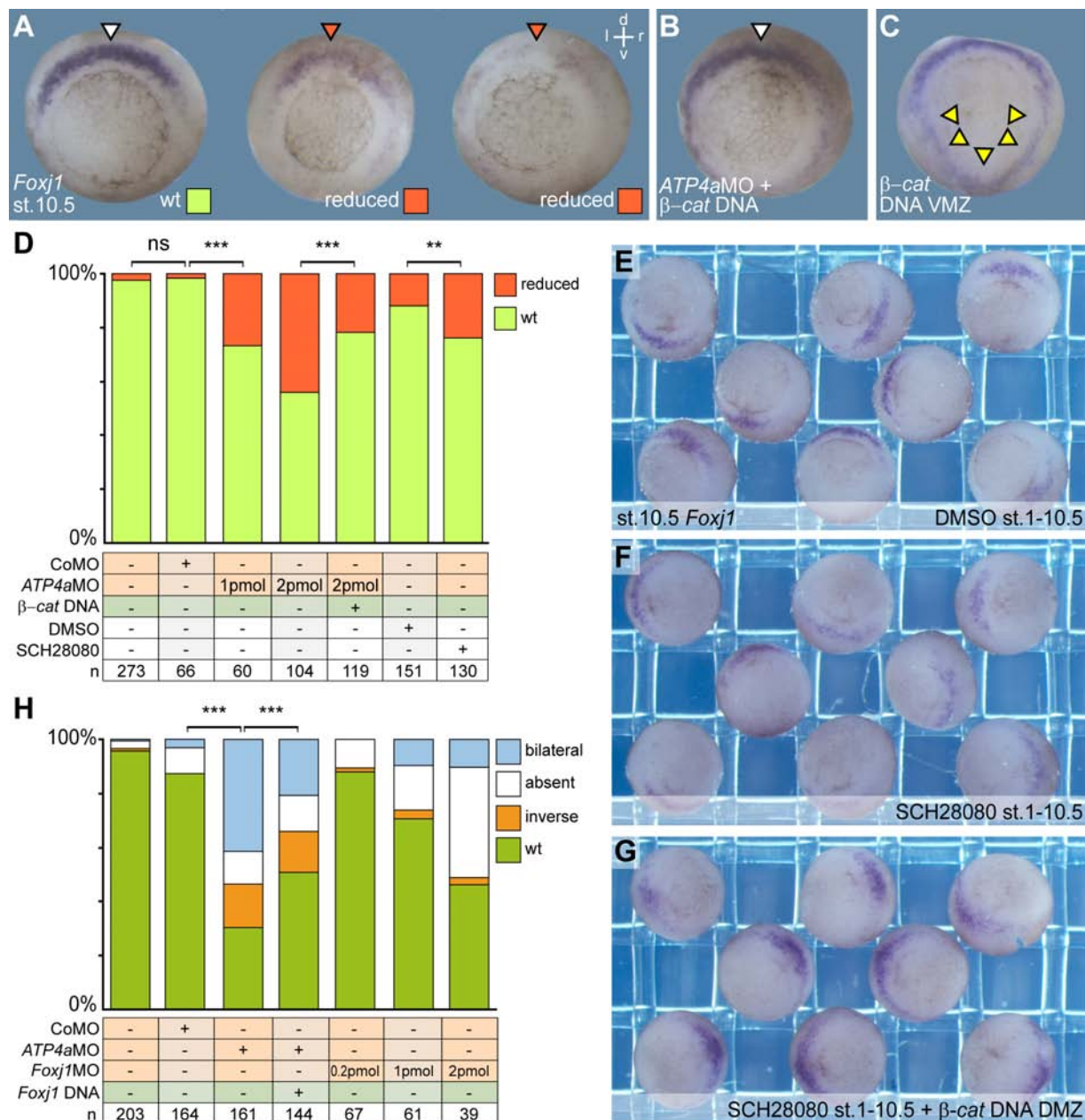
Figure 21: ATP4a Is Required For Wnt/β-cat Mediated Induction Of *Foxj1* During Gastrulation

(A–C) Reduced mRNA expression of *Foxj1* in the SM of *ATP4a* morphant or SCH28080-treated embryos **(A)** was rescued upon co-injection of a *β-cat* DNA expression construct **(B)**. **(C)** Ectopic expression of *Foxj1* on the ventral lip following injection of a *β-cat* DNA expression construct into ventral blastomeres at the 4-cell stage (VMZ lineage). **(D)** Quantification of *Foxj1* expression results. **(E-G)** Batches of control **(E)**, SCH28080 treated **(F)** and SCH28080 treated embryos, which were injected with *β-cat* DNA into the DMZ at 4-cell stage **(G)**. *Foxj1* expression was rescued in this experiment by co-injection of *β-cat* DNA. **(H)** Partial rescue of *Pitx2c* expression in *ATP4a* morphants upon co-injection of a *Foxj1* DNA expression construct. Please note that knock-down of *Foxj1* by *Foxj1*MO resulted predominantly in absent *Pitx2c* expression, while loss of ATP4a displayed bilateral expression patterns of *Pitx2c*.

d = dorsal, l = left, r = right, st. = stage and v = ventral. Statistical analysis: Chi²-test; ns = not significant, * = $p<0.05$, ** = $p<0.01$ and *** = $p<0.001$.
Reprinted and modified from: *Walentek et al. 2012*[#].

ATP4a Regulates Wnt/PCP-Dependent Cilia Polarization At The GRP

Although *Foxj1* DNA co-injection rescued LR-defects in ~25% of *ATP4a* morphants, the relatively low efficiency of rescue indicated that re-gaining *Foxj1* function was not sufficient to completely compensate for loss of ATP4 function (Figure 21 H). Decrease in *Foxj1* expression, reduced ciliation rates and a decrease in cilia length (Figure 15 C, D) were observed in *ATP4a* morphants. In addition, defects in cilia polarization were found as well (Figure 15 E). The posterior localization of the motile monocilium on the cell surface is a central requirement for the generation of a directional laminar flow to the left side. Polarization of GRP cilia was reported to be under control of Wnt/PCP signaling (Antic et al. 2010). Because *ATP4a* was also necessary for non-canonical Wnt signaling during *Xenopus* development, a role of *ATP4a* in cilia polarization was experimentally tested.
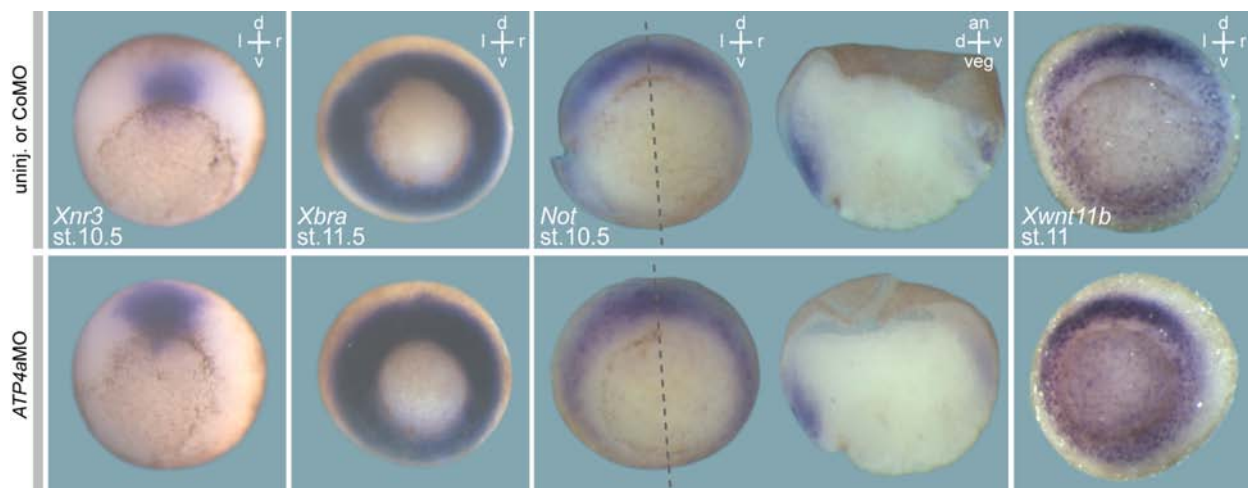
Figure 22: ATP4a Is Not Required For Organizer Induction, Mesoderm Formation And Expression of *Xwnt11b* During Gastrulation

(Upper row) Control specimens. (Bottom row) *ATP4a* morphants. Please note that organizer induction (*Xnr3* expression), mesoderm induction (*Xbra* expression), dorsal mesoderm formation (*Not* expression; plane of bi-section indicated by dashed line) and expression of *Xwnt11b* were not affected in *ATP4a* morphants.

d = dorsal, l = left, r = right, st. = stage and v = ventral.

Reduction of *Foxj1* expression levels in the SM during gastrulation (Figure 21 A, D) suggested that genes, which were required for dorsal CE-movements and -processes might have been affected in addition to the effect on *Foxj1*. Therefore, organizer function, dorsal mesoderm induction and Wnt-ligand expression were analyzed after *ATP4a* knock-down (Figure 22). The expression of direct targets of maternal Wnt/β-cat signaling and markers of the organizer, i.e. *goosecoid* (*Gsc*; not shown) and *Xnr3*, were not down-regulated, indicating normal organizer induction (Blum et al. 1992; Glinka et al. 1996).

Moreover, *Xnr3* was necessary for CE in dorsal mesoderm (Yokota 2003). Therefore, *ATP4a*MO inhibited PCP downstream of or in parallel to *Xnr3* function. Induction of mesoderm and in particular of dorsal mesoderm was not disturbed, as implicated by unaffected expression of *Xbra* and *Not* (Figure 22), which were both reported to be necessary for CE/PCP (von Dassow et al. 1993; Yamada et al. 1998; Tada et al. 2000). In addition, the expression of *Xwnt11b* was analyzed, a Wnt-ligand required for CE/PCP during gastrulation (Smith et al. 2000). The expression of this factor was unaffected after *ATP4a* loss-of-function as well (Figure 22).

Taken together, defects in posterior localization of motile cilia were a result of interference with Wnt/PCP-signaling perception during formation of the GRP in *ATP4a* morphants. In order to confirm this hypothesis, ciliogenesis was rescued in *ATP4a* morphants either with *Foxj1* DNA or by co-injection of *ATP4a* DNA, and GRP ciliation was analyzed by IHC and SEM (Figure 23). Ciliation rate, cilia length and posterior localization of cilia were affected in *ATP4a*MO morphants (Figure 23 B and E-G). When *Foxj1* DNA was co-injected, increased ciliation rate and ciliary length were observed (Figure 23 C, E, F). In contrast, posterior polarization was not established (Figure 23 G). The rate of posterior polarization was even decreased in these specimens. Rescue of *ATP4a*MO-induced defects by co-injection of *ATP4a* DNA was more efficient on all levels (Figure 23 D): Ciliation rate and ciliary length were improved (Figure 23 E, F), and a positive effect on cilia polarization was observed (Figure 23 G).

In IHC samples, cilia could not be distinguished from basal bodies, which were also stained by the antibody. Therefore, in IHC experiments cilia numbers were likely over-represented. The basic findings were confirmed by SEM analysis for discrimination of ciliation and basal bodies. In SEM micrographs an increase in cilia number was confirmed after co-injection of *Foxj1* DNA (Figure 23 H), but cilia polarization was not rescued (Figure 23 I).

In summary, loss of *ATP4a* did not affect organizer formation and dorsal mesoderm induction (Figure 22), but was specifically required for Wnt/PCP mediated posterior polarization of cilia, even in the presence of *Foxj1* (Figure 23).
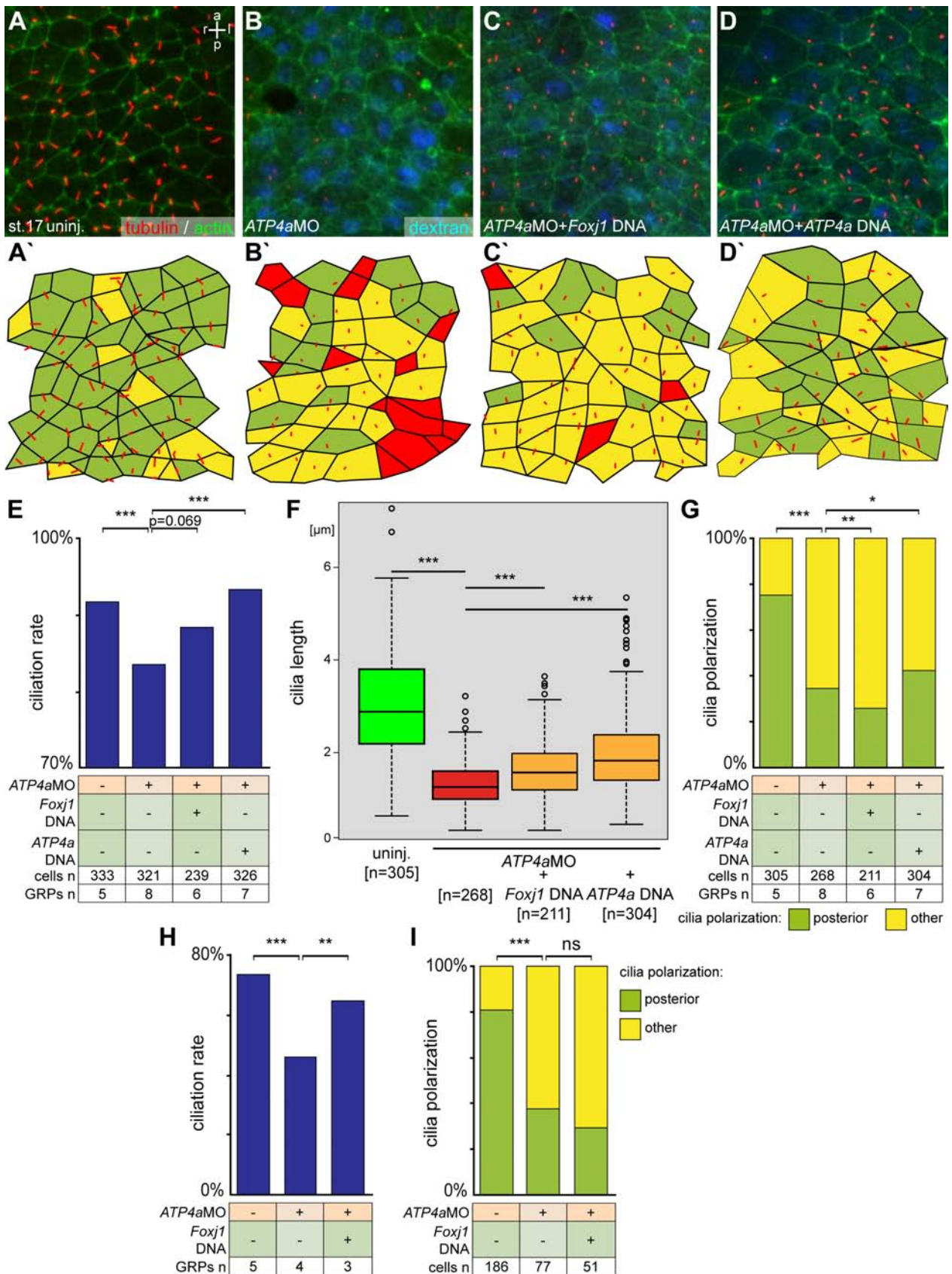
Figure 23: ATP4a Is Required For Posterior Polarization Of GRP Cilia, Downstream Of *Foxj1*

Embryos were injected at the 4-cell stage into the DMZ and dorsal explants were prepared at st. 17. Specimens were processed for IHC **(A-G)**, or for SEM analysis **(H, I)** to determine cilia polarization, ciliation rate and cilia length of GRP cilia. →

(A–G) IHC using antibodies against acetylated α-tubulin to visualize cilia (red) and actin (green) to outline cell boundaries. Cascade blue dextran was used as lineage tracer in **(B-D)**. **(A)** Control uninjected (uninj.) specimen. **(B)** *ATP4a* morphant. **(C)** Co-injection of *ATP4a*MO and *Foxj1* DNA. **(D)** Co-injection of *ATP4a*MO and *ATP4a* DNA. **(A`-C`)** Evaluation of results. **(E)** Quantification of ciliation rate – note that *Foxj1* or *ATP4a* co-injection partially rescued ciliation rates in *ATP4a* morphants. **(F)** Quantification of cilia length – note that *Foxj1* or *ATP4a* co-injection significantly rescued cilia length in *ATP4a* morphants. **(G)** Quantification of cilia polarization – note that *ATP4a* DNA co-injection, but not *Foxj1* DNA co-injection partially rescued cilia polarization in *ATP4a* morphants. Also note that co-injection of *Foxj1* aggravated polarization defects. **(H-I)** Ciliation rate **(H)** and cilia polarization **(I)** was also quantified in SEM specimens and confirmed findings obtained by IHC analysis. Note that ciliation rate was slightly over-represented in IHC samples.

Color code **(A`-D`)**: red = no cilium, yellow = mispolarized cilium and green = cilium posteriorly localized. a = anterior, l = left, p = posterior, r = right and st. = stage. Statistical analysis: Box-plots - Wilcoxon sum of ranks (Mann-Whitney) test, Bar-graphs - Chi²-test; ns = not significant, * = $p < 0.05$, ** = $p < 0.01$ and *** = $p < 0.001$. Reprinted and modified from: *Walentek et al. 2012*[#].

Summary

ATP4a was required for LR-axis development post MBT. The role of *ATP4a* was to mediate Wnt-signaling (Figure 24): (1) During gastrulation, *ATP4a*-dependent Wnt/β-cat signaling was necessary and sufficient for expression of *Foxj1*, the master regulatory gene of motile cilia. (2) During neurulation, *ATP4a* was necessary for Wnt/PCP-signaling, which was responsible for posterior localization of GRP cilia. Loss of ATP4 function impaired leftward flow. Residual and directionally randomized flow induced bilateral *Coco* down-regulation and caused bilateral nodal cascade induction in the LPM. Therefore, *ATP4a* was required for the generation of leftward flow and symmetry-breakage in *Xenopus* (Walentek et al. 2012).

Figure 24: Graphical Summary Of ATP4a Function In *Xenopus laevis* LR-Development

The gastric H⁺/K⁺ATPase α (ATP4a) is required for Wnt/β-cat dependent *Foxj1* expression during gastrulation, and Wnt/PCP dependent cilia polarization of GRP cilia during neurulation. Both processes are required for generation of directional leftward flow and symmetry-breakage in *Xenopus laevis*.

Reprinted from: *Walentek et al. 2012*[#].
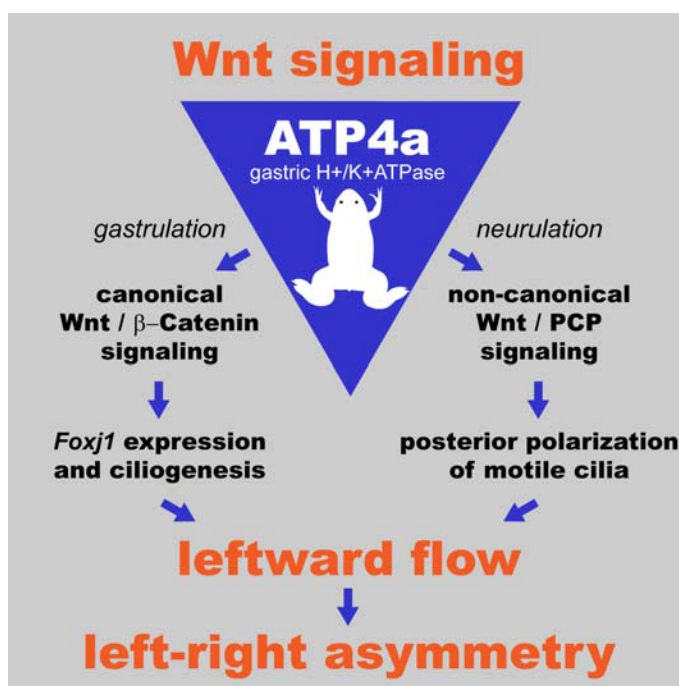
Wnt-Signaling During Gastrulation and GRP Formation

The Canonical Wnt-Receptor Frizzled 8 Mediates β-cat Dependent *Foxj1* Expression

Previous experiments on *ATP4a* and *Frizzeled8* (*Fz8*) implicated a specific role for the canonical Wnt-receptor *Fz8* in *Foxj1* expression and LR-axis development (Beyer 2011; Walentek et al. 2012). *Fz8* was expressed in the dorsal mesoderm during gastrulation, and loss of *Fz8* function perturbed GRP ciliation, leftward flow and *Pitx2c* expression (Beyer 2011). In order to test if *Fz8* regulated *Foxj1* expression in the SM via β–cat, rescue experiments were performed (Figure 25). *Fz8*MO injection to the DMZ at 4-cell stage reduced *Foxj1* expression in the SM (Figure 25 B, D). *Foxj1* expression was not only down-regulated, but also lost in about 50% of *Fz8* morphants (Figure 25 B, D). Co-injection of *β–cat* DNA partially rescued *Foxj1* expression in *Fz8* morphants (Figure 25 C, D). This data suggested that Fz8-mediated canonical Wnt/β-cat signaling post-MBT was required for *Foxj1* expression during gastrulation.
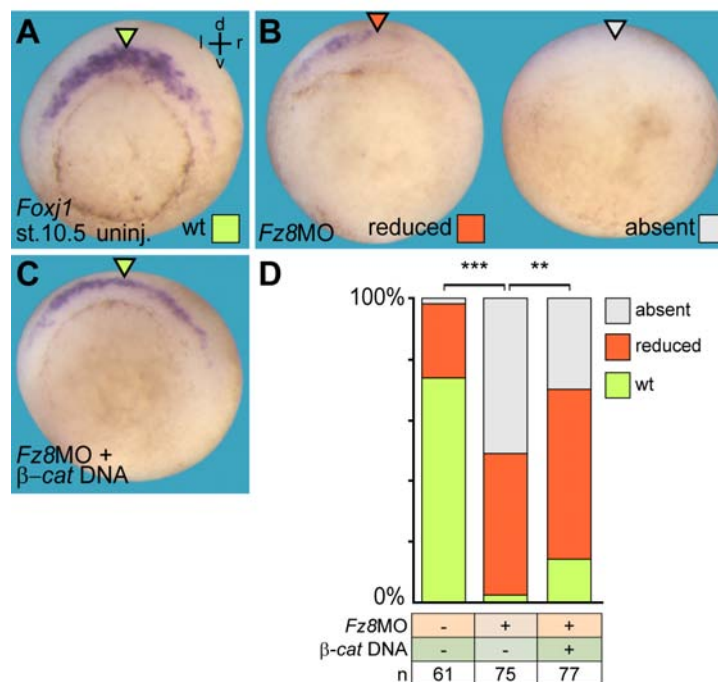
Figure 25: Frizzled8 Is Required For Wnt/β-cat Mediated Induction Of *Foxj1* In The Superficial Mesoderm

(A–B) Reduced mRNA expression of *Foxj1* (assessed by WMISH) in the SM of *Fz8* morphants injected to the DMZ lineage at the 4-cell stage **(B)** was rescued upon co-injection of a *β-cat* DNA expression construct **(C)**. **(D)** Quantification of results.

d = dorsal, l = left, r = right, st. = stage and v = ventral. Statistical analysis: Chi²-test; ns = not significant, * = p<0.05, ** = p<0.01 and *** = p<0.001.
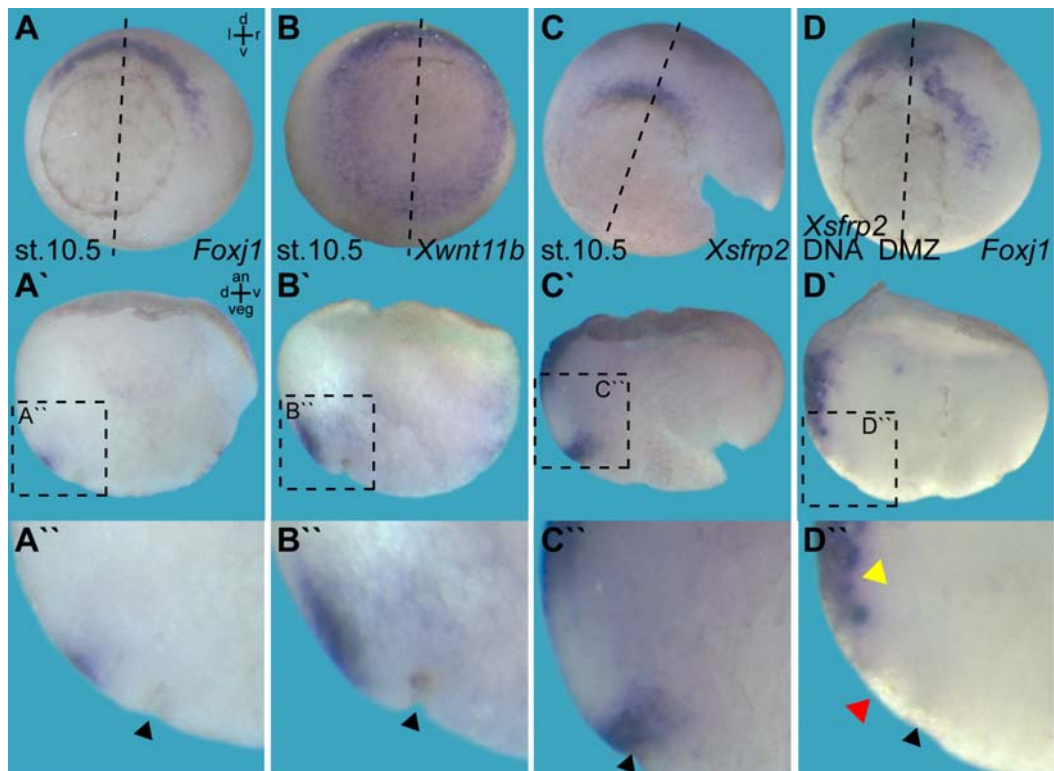
Figure 26: Ligand-Driven Wnt/β-cat Signaling Is Required For Expression Of *Foxj1* In The Superficial Mesoderm

(A) Expression of *Foxj1* in the SM after WMISH and in bi-sections **(A`, A``)**. Note that *Foxj1* is specifically expressed in the superficial layer with some distance to the dorsal lip (indicated by black arrowhead in **A``**). **(B)** Expression of *Xwnt11b* in the SM in whole-mounts and bi-sections **(B`, B``)**. Note that *Xwnt11b* is specifically expressed in the superficial layer with some distance to the dorsal lip (indicated by black arrowhead in **B``**). **(C)** Expression of *Xsfrp2* around the SM in whole-mounts and bi-sections **(C`, C``)**. Note that *Xsfrp2* is not expressed in the superficial mesoderm (dorsal lip is indicated by black arrowhead in **C``**). **(D, D`** and **D``)** Post-MBT gain of *Xsfrp2* in the DMZ lineage by injection of *Xsfrp2* DNA at the 4-cell stage inhibited *Foxj1* expression in the SM (red arrowhead in **D``**), but induced ectopic expression of *Foxj1* in the neuroectoderm, including deep tissues (indicated by yellow arrowhead in **D``**).

Planes of section are indicated by dashed lines. an = animal, d = dorsal, l = left, r = right, st. = stage, v = ventral and veg = vegetal.

Ligand-Dependent Wnt-Signaling Regulates *Foxj1* Expression In The Superficial Mesoderm Post-MBT

Published data indicated that *Xwnt11b* and *Xsfrp2* (*Xenopus secreted frizzled-related protein 2*) were expressed during gastrulation, hence qualifying for *Foxj1* regulation in the SM (Pera et al. 2000; Smith et al. 2000; Cha et al. 2009). WMISH for these genes during stages when *Foxj1* is expressed revealed co-expression of *Xwnt11b* and *Foxj1* (Figure 26 A, B). *Xsfrp2* was expressed at the edge of the involuting mesoderm and within a second domain in the prospective neuroectoderm (Figure 26 C), i.e. *Xsfrp2* was expressed adjacent to the expression domains of *Foxj1* and *Xwnt11b*. Xsfrps have a dual role in Wnt-

signaling: They are known as mediators of long-range Wnt-signaling (Mii et al. 2009), but can also prevent ligand/receptor interaction and pathway activation (Kawano et al. 2003). Expression of *Xsfrp2* (Figure 26 C) thus suggested a potential role as negative regulator of *Foxj1* expression (Figure 26 A).

A *Xsfrp2* DNA construct was injected into the DMZ at the 4-cell stage, and *Foxj1* expression was analyzed during gastrulation. Following *Xsfrp2* gain-of-function *Foxj1* expression in the SM was lost (Figure 26 D). This result thus confirmed the notion that Xsfrp2 was a negative regulator of *Foxj1* expression. Unexpectedly, *Foxj1* expression was observed more animally, extending into the neuroectoderm (Figure 26 D). *Foxj1* expression in these specimens was not restricted to the superficial layer within its new domain, but was found in deep cells as well (Figure 26 D``).

Two conclusions emerge from these results: (1) *Foxj1* expression in the SM required a Wnt-ligand, which could be inhibited by *Xsfrp2;* (2) *Xsfrp2* gain-of-function in the DMZ was able to induce ectopic *Foxj1* expression.

Xwnt11b Expression Suggests Multiple Roles In LR-Development

It was shown that *Xwnt11b* can activate the canonical and non-canonical signaling branches (Tada et al. 2000; Tao et al. 2005; Kofron et al. 2007). In zebrafish, the silberblick mutant carries a loss-of-function mutation for *Wnt11* and displays defects in the morphogenesis of Kupffer's vesicle (Oteiza et al. 2010). *ATP4a*MO injection phenocopied loss of Wnt11-signaling in the neural crest (NC) (Figure 19 E) and during pronephros development (Figure 19 F) (Matthews et al. 2008; Tételin et al. 2010), indicating that loss of *ATP4a* could affect Xwnt11b signaling in the SM.

First, expression analysis of *Xwnt11b* was performed (Figure 27). During gastrulation (st. 10 – 11.5), *Xwnt11b* was expressed around the blastopore and within the SM, which was progressively moving towards the dorsal lip (Figure 27 A-C). During early neurula stages (st. 13) the expression domain was restricted to the involuting cells around the blastopore (Figure 27 D). During late neurulation (st. 20) and early tailbud stages (st. 27) *Xwnt11b* was expressed in the somites and the neural crest (NC) (Figure 27 E, F). In tailbud stages, *Xwnt11b* was also found in the tailbud tip (Figure 27 F). Expression of *Xwnt11b* thus

indicated two distinct roles in LR-development: (1) During gastrulation, *Xwnt11b* potentially regulated *Foxj1* expression in the SM (Figure 27 A-C) via the canonical branch of Wnt-signaling. (2) During neurulation, *Xwnt11b* expression in the circum-blastular collar (CBC) (Figure 27 D``), i.e. a tissue adjacent to the posterior-most part of the GRP, suggested that *Xwnt11b* regulated cilia alignment via the PCP-pathway (Antic et al. 2010; Gao et al. 2011).
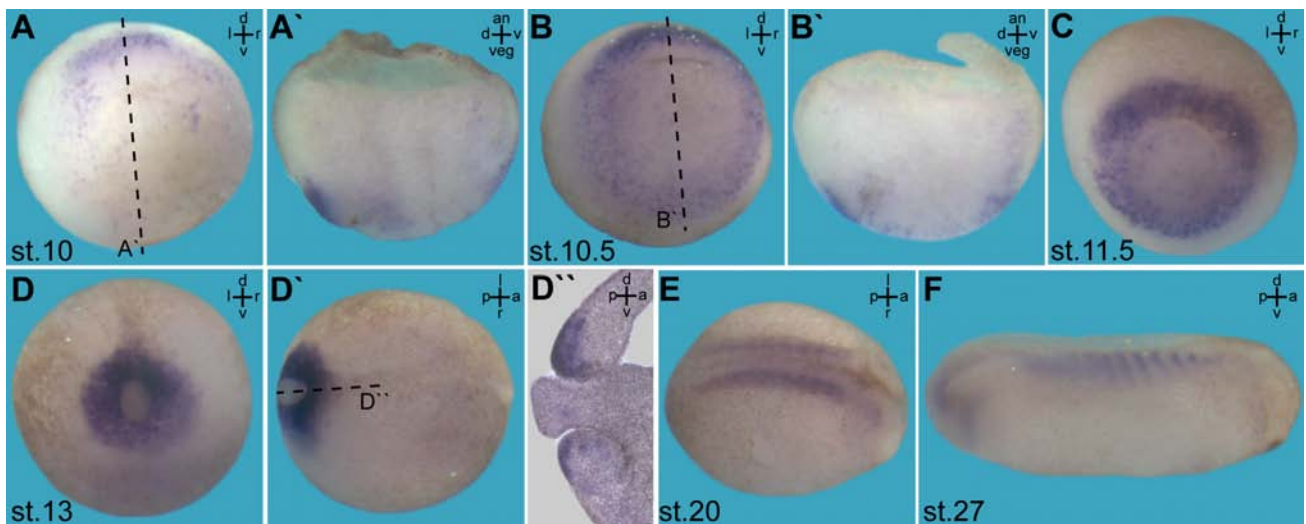
Figure 27: *Xwnt11b* Expression During LR-Relevant Developmental Stages Of *Xenopus*

WMISH expression analysis of *Xwnt11b* expression. **(A, A`)** Zygotic expression of *Xwnt11b* starts during early gastrulation (e.g. st.10) in the dorsal-most SM. **(A`)** Bi-section. **(B-D)** During subsequent gastrulation st. 10.5 **(B)**, st. 11.5 **(C)** and st. 13 **(D)**, *Xwnt11b* expression extends ventrally, where it is expressed in the deep ventral mesoderm **(B`)**. Please note that during late gastrulation/early neurulation (st.13, **D**), *Xwnt11b* is strongly expressed at the dorsal circumblastular collar **(D``)**, i.e. the tissue, which is situated posterior to the GRP during following stages. **(E-F)** During late neurulation (st. 20, **E**) and tailbud stages (st. 27, **F**), expression was found in somitic tissues **(E, F)** and at the tailbud **(F)**.

a = anterior, an = animal, d = dorsal, l = left, p = posterior, r = right, st. = stage, v = ventral and veg = vegetal.

Xwnt11b Is Required For Leftward Flow And LR-Development In *Xenopus*

The function of Xwnt11b was investigated in loss-of-function experiments. A *Xwnt11b*MO was designed and injected to the DMZ at 4-cell stage. In order to analyze a possible effect on organizer induction and dorsal mesoderm formation, markers were analyzed by WMISH: *Xnr3*, a direct target of early Wnt/β-cat signaling (Figure 28 A), and *Not* (Figure 28 B), a gene required for notochord formation, were not decreased in intensity. These results indicated normal organizer induction and dorsal mesoderm formation. Next, *Xwnt11b* morphant embryos were analyzed for *Foxj1* expression in the SM: An animal shift of the

Foxj1 expression domain was observed (Figure 28 C), probably indicating defects in CE movements. Down-regulation in *Foxj1* expression was found as well (Figure 28 C, D), but only in ~10% of specimens.

Next, the effect of *Xwnt11b*MO on LR-development was tested by *Pitx2c* expression analysis. In contrast to the minor effects on *Foxj1* expression in the SM (Figure 28 D), *Pitx2c* expression was lost (~55%) or altered (~15%) in a majority of *Xwnt11b* morphants (Figure 28 E). This indicated a requirement for *Xwnt11b* in a *Foxj1*-independent mechanism. In order to elucidate the level of interaction between *Xwnt11b* and LR-development, flow was analyzed in dorsal explants of uninjected and *Xwnt11b* morphant embryos. Cilia-driven leftward flow was disturbed upon *Xwnt11b* loss-of-function, i.e. directionality was lost (ρ=0.51±0.16) and velocity was significantly reduced (1.37±0.32 µm/s) as compared to control specimens, with values of ρ=0.84±0.07 and 3.01±0.93 µm/s, respectively (Figure 28 F-I).
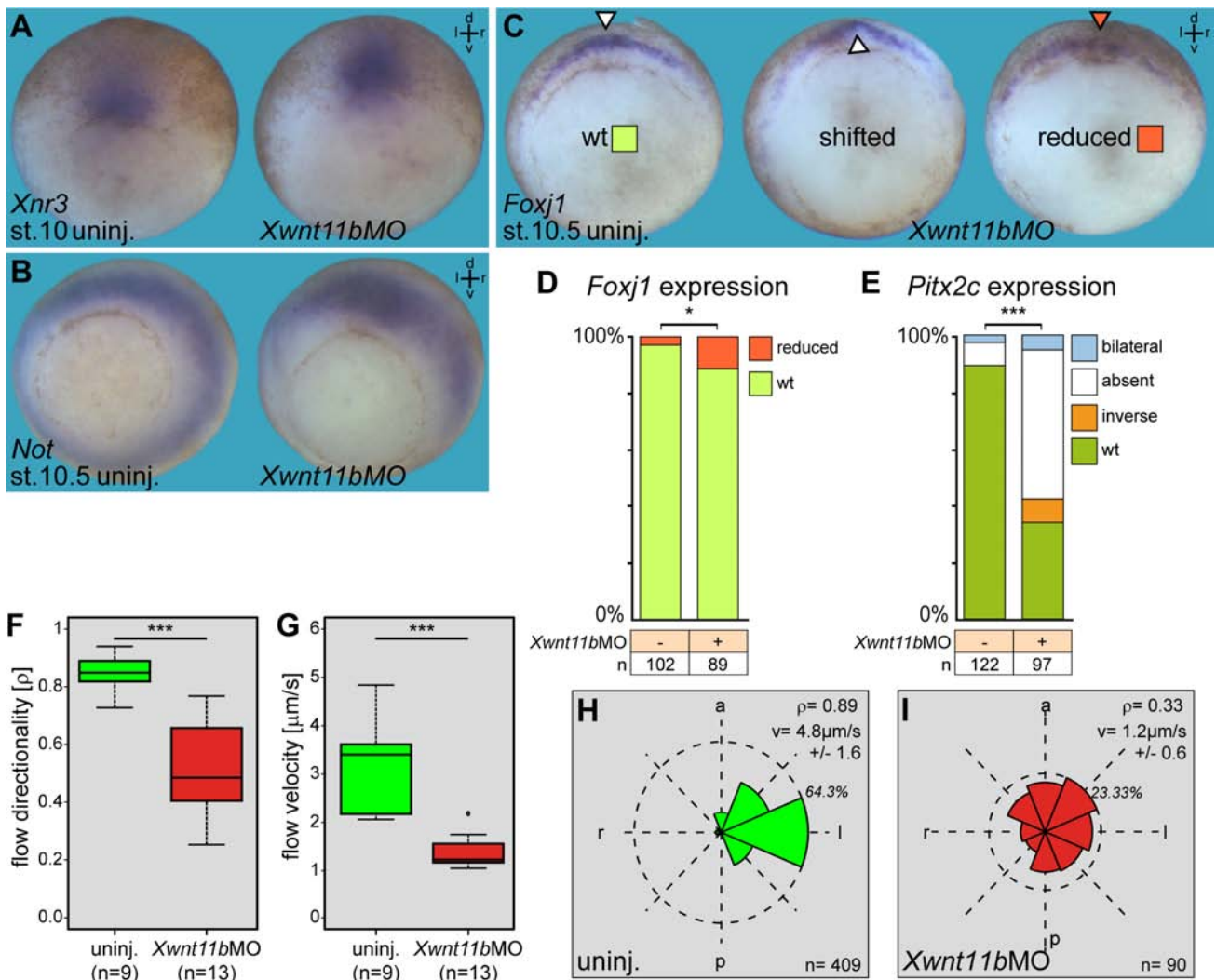
Figure 28: *Xwnt11b* Is Required For LR-Axis Formation And Leftward Flow

(A-E) WMISH expression analysis of *Xnr3* **(A)**, *Not* **(B)** and *Foxj1* **(C)** expression during gastrulation (st. 10.5), and of *Pitx2c* expression patterns in tailbud stage embryos (st. 27 – 32, not shown). Please note that organizer induction and dorsal mesoderm formation was not affected in *Xwnt11b* morphants, as judged by *Xnr3* **(A)** and *Not* **(B)** expression, respectively. **(D)** Quantification of *Foxj1* expression in *Xwnt11b* morphants revealed a minor but significant effect of *Foxj1* expression in the SM (indicated by red arrowhead in **C**). In most morphants, the *Foxj1* expression domain was only shifted towards the animal pole, probably indicating delay in SM involution. **(E)** A highly significant loss of *Pitx2c* expression was found in *Xwnt11b* morphants, indicating a Foxj1-independent function of Xwnt11b during LR-development. **(F-G)** Quantification of flow analysis in dorsal explants. **(F)** Directionality and **(G)** velocity of fluorescent beads added to GRP explants at st. 17 were drastically reduced in *Xwnt11b* morphants, as compared to uninjected (uninj.) embryos. n represents number of explants analyzed. **(H–I)** Frequency distribution of trajectory angles in representative explants injected with *Xwnt11b*MO **(I)** and uninj. specimens **(H)**. Dashed circles indicate maximum frequency in histogram specified in percent.

a = anterior, d = dorsal, l = left, n = number of particles above threshold, p = posterior, r = right, v = ventral in (A-C) or v = average velocity of particles in (H, I), ρ = quality of flow. Statistical analysis: Wilcoxon sum of ranks (Mann-Whitney) test; ns = not significant, * = $p<0.05$, ** = $p<0.01$ and *** = $p<0.001$.

Hence, *Xwnt11b* was required for LR-development, but not for *Foxj1* expression *per se* in the SM (Figure 28 D, E). Residual flow in morphants was observed, accompanied by loss of nodal cascade induction (Figure 28 E-I). These results indicated that *Xwnt11b* was required for LR-development beyond generation of leftward flow, because turbulent flow alone (in *ATP4a* morphants) was sufficient for bilateral nodal cascade induction.

Loss Of *Xwnt11b* Affects GRP Morphology, Ciliogenesis And Cilia Polarization

In order to investigate why knock-down of *Xwnt11b* prevented nodal cascade induction, GRP morphology, ciliogenesis and polarization of cilia were analyzed in dorsal explants of *Xwnt11b*MO injected embryos by IHC (Figure 23). In explants from uninjected specimens over 60% of GRP cells were ciliated (Figure 29 A, E and F). 60% of cilia were localized to the posterior pole of GRP cells (Figure 29 A`, D), and cell size was ~100µm² (Figure 29 G). In explants from *Xwnt11b*MO injected embryos, analysis of dorsal explants revealed: (1) decrease in cilia number (by ~10%) and (2) polarization rate (by ~30%) (Figure 29 B`, D and E); (3) shorter cilia (Figure 29 F) and (4) an (up to 10-fold) increase in GRP cell size (Figure 29 G). These results were confirmed in post-MBT loss-of-function experiments using DNA encoding a dominant negative *Xwnt11b* C-terminal deletion construct (*dnXwnt11b*) (Tada et al. 2000): Dorsal explants revealed (1) decreased cilia polarization by ~30% (Figure 29 C`, D); (2) cilia length was reduced (Figure 29 F) and (3) an increase

in average GRP cell size was observed (Figure 29 G). In contrast to *Xwnt11b*MO injection, over-expression of *dnXwnt11b* did not cause a reduction in ciliation rate (Figure 29 E), possibly indicating less pronounced inhibition.

In conclusion, *Xwnt11b* was necessary post-MBT for correct morphology of the GRP (increased cell size) and blastopore closure (not shown), as well as ciliation (cilia polarization and length) (Figure 29).

GRP-Expression Of *Xnr1* And *Coco* Is Under *Xwnt11b* Control

Induction of the nodal cascade was lost in *Xwnt11b*MO injected specimens (Figure 28 E) and a turbulent flow was observed (Figure 28 F-I). Because turbulent flow in *ATP4a* morphants was sufficient for nodal cascade induction (Walentek et al. 2012), loss of *Pitx2c* expression in the LPM in *Xwnt11b*-experiments indicated defects downstream of leftward flow. *Xnr1* and *Coco* were expressed in lateral (somitic) parts of the GRP and required for nodal cascade induction. Therefore, expression of these genes was analyzed by WMISH in manipulated specimens. Injection of *Xwnt11b*MO to the DMZ at the 4-cell stage and analysis of *Xnr1* revealed down-regulation (45%) or complete loss (55%) of *Xnr1* expression (Figure 30 A). *dnXwnt11b* DNA injections interfered with *Xnr1* expression as well (Figure 30 A). *Coco*-expression analysis after inhibition of *Xwnt11b* function revealed the same finding: *Coco* expression was down-regulated in 90% of *Xwnt11b*MO, as well as 50% of *dnXwnt11b* DNA injected specimens (Figure 30 B). Taken together, these results indicated that *Xwnt11b* was required for *Xnr1* and *Coco* expression, which were a prerequisite for induction of the nodal cascade in the LPM.

Summary

Taken together, post-MBT Wnt signaling was an important regulator of LR-axis development in three ways (Figure 31): (1) *Fz8*-dependent Wnt/β-cat signaling regulated *Foxj1* expression in the SM. (2) Non-canonical Wnt signaling was required for gastrulation movements (a prerequisite for GRP formation) and cilia polarization during GRP morphogenesis. (3) *Xwnt11b*-dependent Wnt-signaling of a yet unknown branch was required for correct setup of the *Xnr1*/*Coco*-mediated flow-sensing mechanism.
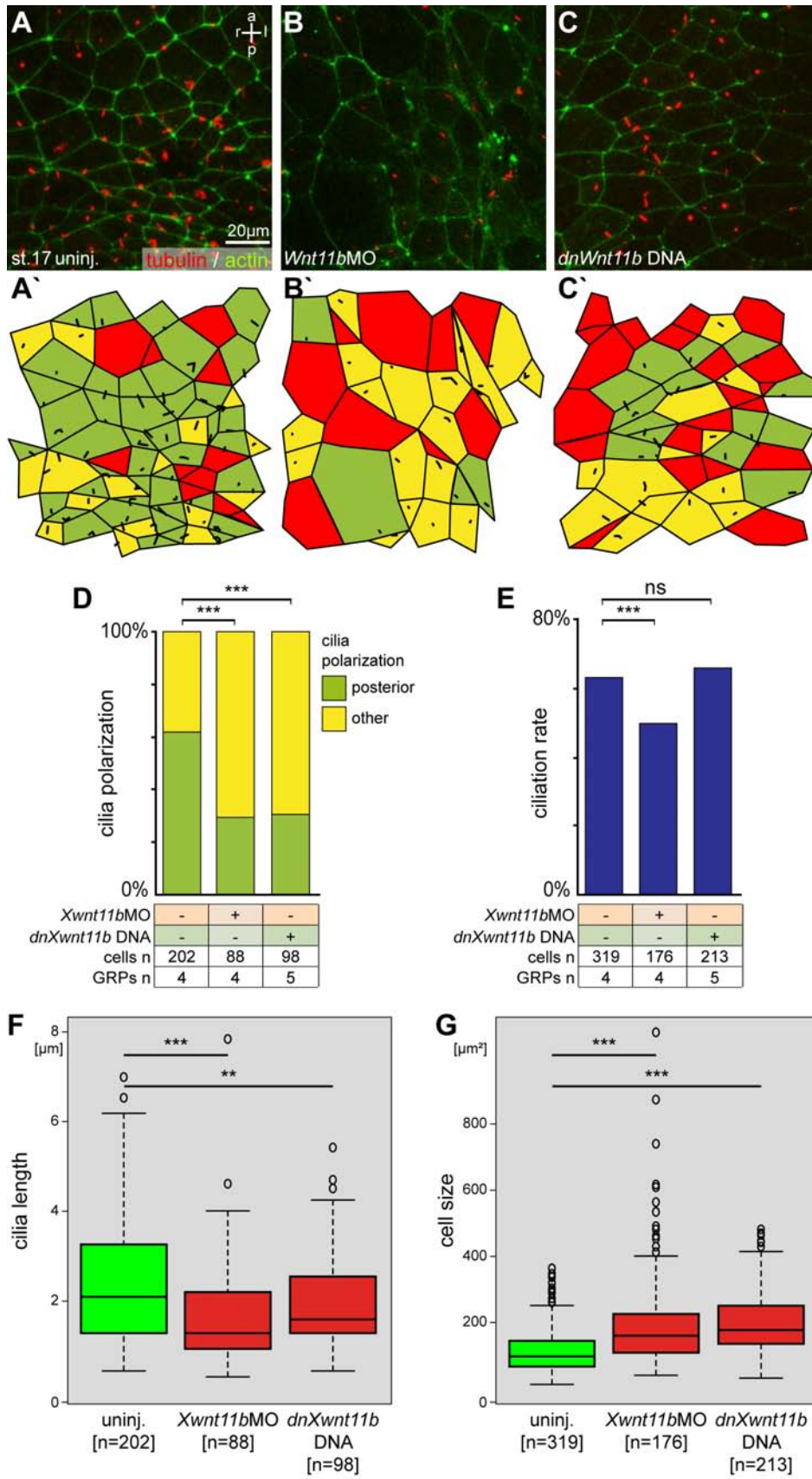
Figure 29: Post-MBT Xwnt11b Is Required For Posterior Polarization Of GRP Cilia And GRP Morphology

(A–G) Embryos were injected at the 4-cell stage into the DMZ and dorsal explants were prepared at st. 17. Specimens were processed for IHC **(A-C)** to determine cilia polarization **(D)**, ciliation rate **(E)**, cilia length **(F)** and GRP cell size **(G)**. **(A–C)** IHC using antibodies against acetylated α-tubulin to visualize cilia (red) and actin (green) to outline cell boundaries. **(A)** Control uninjected (uninj.) specimen. **(B)** *Xwnt11b* morphant. **(C)** Embryo after injection of *dominant negative (dn) Xwnt11b* DNA. **(A`-C`)** Determination of results. **(D)** Quantification of cilia polarization revealed loss of polarization after loss of Xwnt11b function post-MBT. **(E)** Quantification of ciliation rate – note that only MO-mediated loss of Xwnt11b significantly decreased ciliation rate, indicating a minor effect of Xwnt11b on ciliation. **(F)** Quantification of cilia length revealed a significant decrease after loss of Xwnt11b function. **(G)** Quantification of GRP cell size revealed a highly significant increase in cell size after manipulation of Xwnt11b, indicating severe defects in non-canonical Wnt-signaling.

Color code **(A`-C`)**: red = no cilium, yellow = mispolarized cilium and green = cilium posteriorly localized. a = anterior, l = left, p = posterior, r = right and st. = stage. Statistical analysis: Box-plots - Wilcoxon sum of ranks (Mann-Whitney) test, Bar-graphs - Chi²-test; ns = not significant, * = p<0.05, ** = p<0.01 and *** = p<0.001.
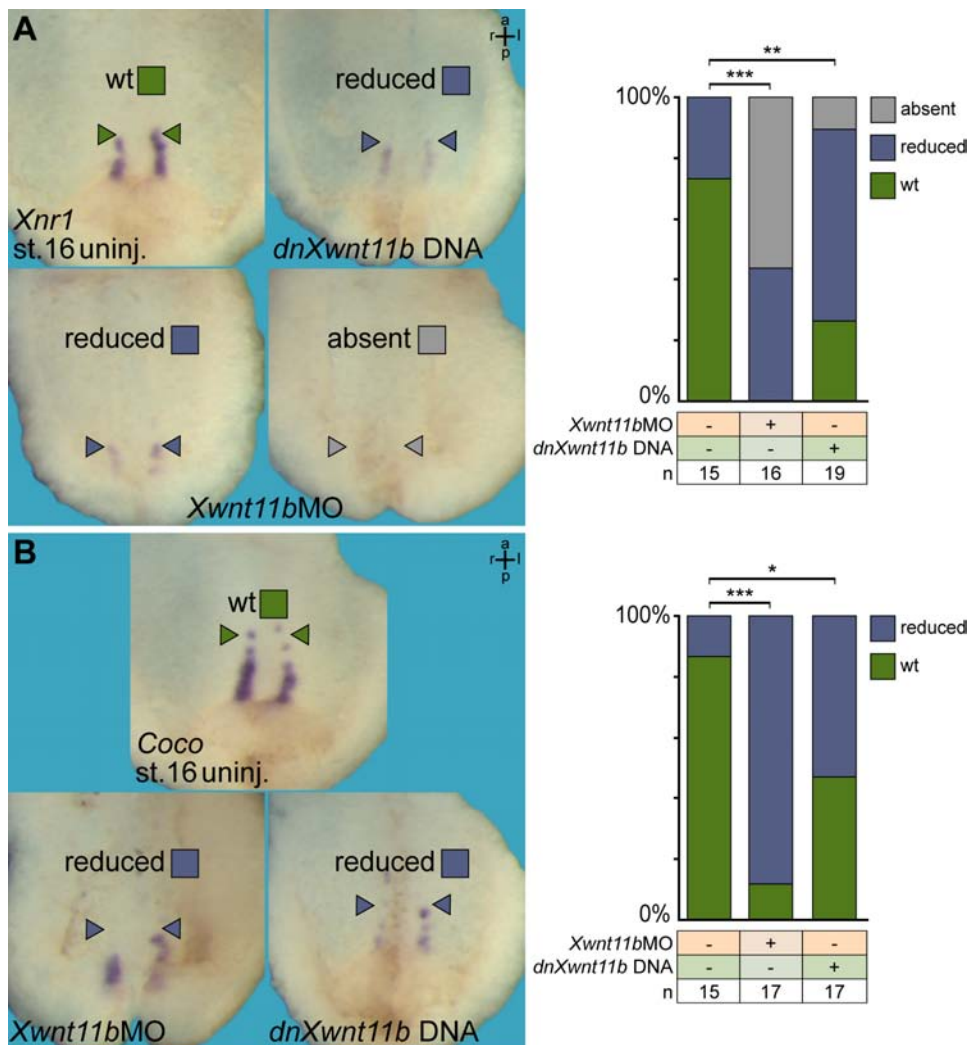
Figure 30: Post-MBT Xwnt11b-Signaling Is Required For Xnr1- And Coco-Dependent Flow Sensing

(A-B) Embryos were injected at the 4-cell stage into the DMZ, and dorsal explants were prepared at st. 16/17 (pre-flow stages). Specimens were processed for WMISH to assess GRP-*Xnr1* **(A)** and GRP-*Coco* **(B)** expression. →

(A) *Xnr1* expression in the somitic GRP was significantly reduced in *Xwnt11b*MO and *dnXwnt11b* DNA injected specimens. **(B)** *Xwnt11*MO and *dnXwnt11b* DNA injections also decreased *Coco* expression. In both cases *Xwnt11b*MO was more efficient than *dnXwnt11b* DNA, possibly indicating a role of Xwnt11b pre-MBT.

Color code: green arrowheads = wt-expression, purple arrowheads = reduced expression and gray arrowheads = absent expression. a = anterior, l = left, p = posterior and r = right. Statistical analysis: Chi²-test; ns = not significant, * = p<0.05, ** = p<0.01 and *** = p<0.001.
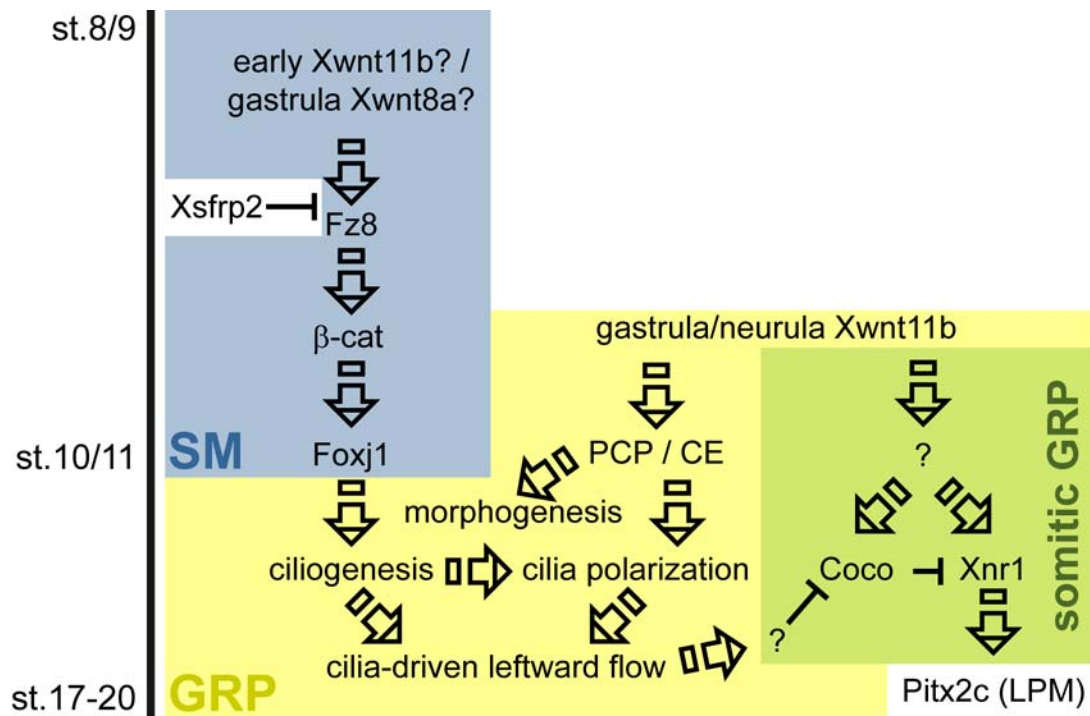
Figure 31: Graphical Summary Of Wnt-Signaling Functions In *Xenopus laevis* LR-Development

Foxj1 expression during gastrulation is possibly regulated by Xwnt8a and marginally dependent on Xwnt11b. Xsfrp2 probably restricts canonical Wnt-signaling and *Foxj1* expression to the SM (blue). Canonical Wnt-signaling via Frizzled 8 (Fz8) stimulates β-cat stabilization and *Foxj1* expression in the SM, which is required for motile ciliogenesis at the GRP (yellow). Xwnt11b is also pivotal for non-canonical Wnt/PCP-dependent convergent extention (CE) movements and cilia polarization of GRP cilia during neurulation. Both processes are required for generation of directional leftward flow and symmetry-breakage in *Xenopus laevis*. Moreover, Xwnt11b-signaling post-MBT via an unknown Wnt-branch is required for expression of *Coco* and *Xnr1* in somitic GRP portions (green), which is a prerequisite for flow sensing, induction of the nodal signaling cascade and *Pitx2c* in the left lateral plate mesoderm (LPM). st. = stage.

ATP4a And Wnt-Signaling In The Mucociliary Epithelium Of The *Xenopus* Larval Skin

ATP4a Is Required for β-cat Dependent *Foxj1* Expression And Ciliation In The *Xenopus* Larval Skin

In the epidermal ectoderm, which gives rise to the mucociliary epithelium (MCE) of the skin (Hayes et al. 2007), ATP4a protein was found at the plasma-membrane (Figure 6 A). Therefore, a potential function of ATP4a in *Foxj1*-dependent ciliogenesis was analyzed in this system as well.

IHC revealed that ATP4a was found in multiciliated cells (MCCs) and non-ciliated cells of the skin (Figure 32 C). Signal strength varied between MCCs and other cell types (indicated in Figure 32 C`), such that strong as well as very weak staining intensities were observed in neighboring non-ciliated cells. In MCCs intermediate staining intensity was observed.

*ATP4a*MO-mediated loss-of-function was performed in the skin MCE. *Foxj1* expression during neurulation (st. 15) (Figure 32 D, E) as well as cilia-driven fluid flow in tailbud stages (st. 32) (Figure 32 F-I) were examined. Embryos were unilaterally injected at the 4-cell stage, and the contra-lateral side was used as internal control. Analysis of *Foxj1* expression disclosed decrease in *Foxj1* expression after *ATP4a*MO injection (Figure 32 D, E) as compared to uninjected and CoMO-injected specimens. This finding was confirmed at the morphological level: The average number of MCCs decreased by ~30% after loss of ATP4a function (Figure 32 F-H). Moreover, SEM analysis unveiled that less individual cilia projected from the apical surface of MCCs in *ATP4a* morphants (Figure 32 F`, G`). Cilia-driven flow over the skin epithelium was analyzed (Mitchell et al. 2007; Schweickert et al. 2007; Vick et al. 2009): Stage 32 embryos were anesthetized and placed in bead solution. Movement of fluorescent beads was recorded, and ImageJ/Particle Tracker were used to quantify flow velocity in CoMO injected and *ATP4a* morphant embryos. Average flow velocity in *ATP4a*MO injected specimens was reduced to ~10μm/s (Figure 32 I), while velocity in CoMO injected specimens was ~80μm/s.
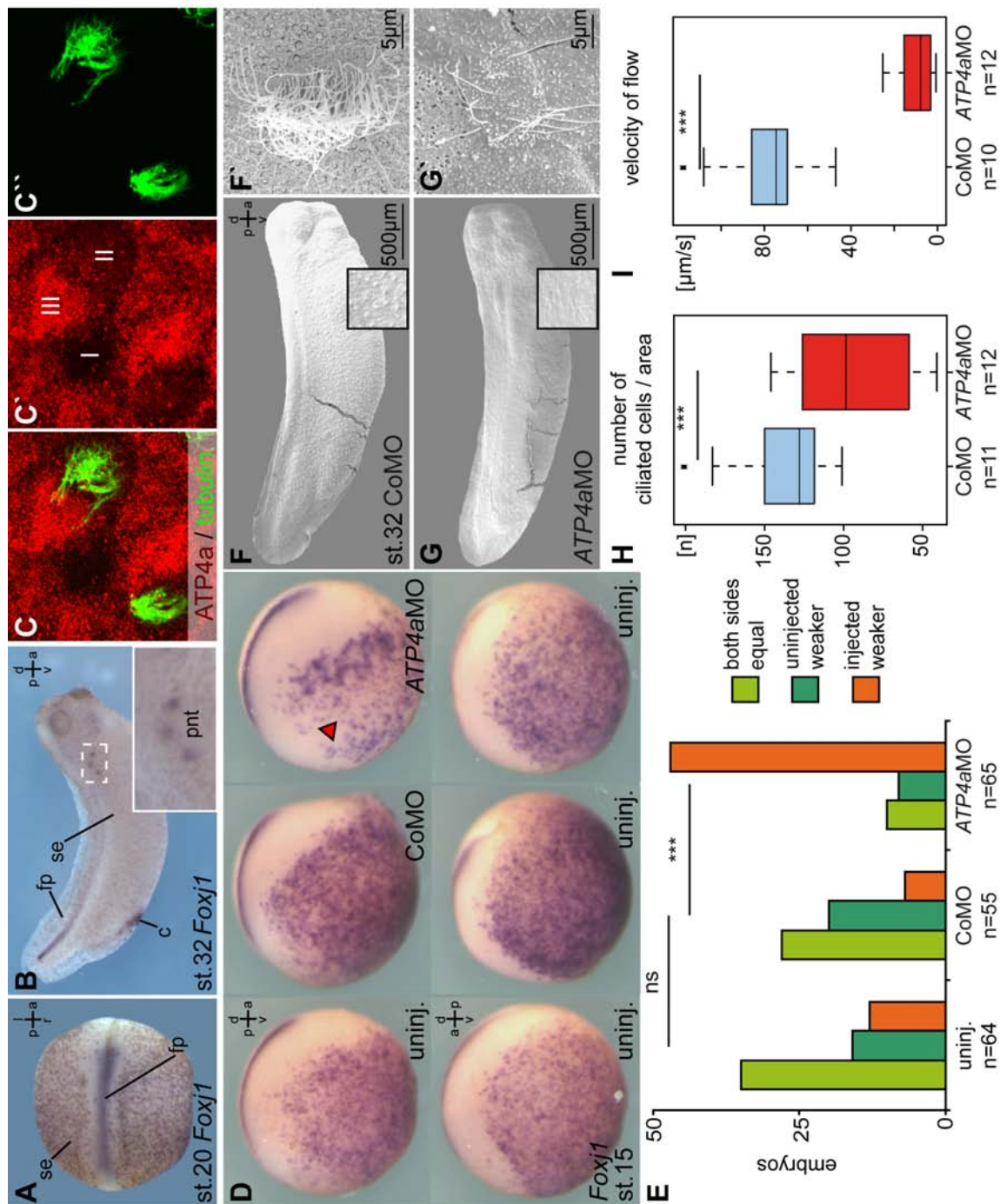
Figure 32: ATP4a Is Required For *Foxj1* Expression, Ciliation And Cilia-Driven Flow In The *Xenopus* Skin Mucociliary Epithelium

(A, B and D) WMISH for *Foxj1* expression. **(A)** *Foxj1* expression was found at the floor plate (fp) and in the skin ectoderm (se) during late neurulation (st. 29). **(B)** In tailbud stages (st. 32) *Foxj1* was expressed in the fp of the tailbud, in the se, in the cloaca (c) and in the proximal pronephric tubules (pnt, inset in **B**). **(C)** Immuno-histochemistry (IHC) for ATP4a (red) and acetylated α-tubulin (green, **C``**) revealed presence of ATP4a protein in all skin cells at st. 27 (**C, C`**). Protein amount varied in different cells (-types): low (I in **C`**), medium (II in **C`**) and high (III in **C`**). **(D-E)** Loss of *Foxj1* expression in the skin during neurulation (st. 15) after *ATP4a*MO injection (specimens were unilaterally injected to the animal pole of the ventral-right blastomere at 4-cell stage, targeting the se). **(D)** Decreased *Foxj1* expression is indicated by red arrowhead in the upper-right panel. **(E)** Quantification of results. **(F-H)** SEM analysis and quantification of ciliated skin cells in control (CoMO) and *ATP4a* morphants. **(F-G)** High-power magnification of SEM micrographs revealed a decrease in cilia number and length in ciliated cells after *ATP4a*MO **(G`)** injection, as compared to control injections **(F`)**. **(H)** Quantification of ciliated cell numbers. →

81

(I) Quantification of cilia-driven flow velocity in control and *ATP4a* morphants. Tailbud stage (st. 32) embryos were anesthetized and placed in fluorescent bead solution, movement of beads was recorded and quantified as indicated in the text and depicted in **Movie 2**.

a = anterior, d = dorsal, l = left, p = posterior, r = right, st. = stage and v = ventral. Statistical analysis: Box-plots - Wilcoxon sum of ranks (Mann-Whitney) test, Bar-graphs - Chi²-test; ns = not significant, * = p<0.05, ** = p<0.01 and *** = p<0.001.

Canonical Wnt-signaling has not been reported in the *Xenopus laevis* skin. However, loss of *Lef1* (a transcriptional co-factor of β-cat) in *Xenopus tropicalis* inhibited formation of MCCs in the skin (Semenov et al. 2007, Roël et al. 2009). Epistatic rescue experiments were performed in order to elucidate if Wnt/β-cat regulated Foxj1-mediated ciliation. Skin ciliation was analyzed by IHC for acetylated tubulin (tubulin). Upon *ATP4a*MO injection loss of ciliation (Figure 33 A, B, F, G and K) was observed. Notably, apically enriched but disorganized tubulin, which was not projecting from the apical surface, was seen in *ATP4a* morphants (Figure 33 B`, G). The number of tubulin-positive cells (i.e. ciliated cells and cells with enriched apical tubulin) did not decrease (Figure 33 K). These results suggested that the number of MCCs in the skin did not change upon *ATP4a* loss-of-function, but rather that MCCs lost their ability to form cilia. Co-injection of *ATP4a* DNA was sufficient to rescue the number of ciliated cells and the number of cilia projecting from the apical surface (Figure 33 C, H and K). Interestingly, a 2-fold average increase in tubulin-positive cells was also observed (Figure 33 K). Next, it was tested if activation of the Wnt-signaling pathway downstream of the receptor (by *β-cat* DNA) or over-expression of the target gene (by *Foxj1* DNA) was able to rescue ciliation as well. Co-injection of *β-cat* or *Foxj1* DNA together with *ATP4a*MO increased the number of ciliated cells, but not to a significant extent (p>0.05) (Figure 33 K). In contrast, the number of cilia projecting from the apical surface was significantly (p<0.01) rescued after co-injection of DNAs (Figure 33 K). Furthermore, the number of tubulin-positive cells in *ATP4a* morphants was increased after injection of *β-cat* and *Foxj1* DNAs (Figure 33 K). Analysis of cilia-driven fluid flow in uninjected, *ATP4a* morphant and rescued embryos confirmed these findings (Movie 2): Flow was lost or severely affected in *ATP4a*MO injected specimens as described above (Figure 32 I), while co-injections of *ATP4a*, *β-cat* or *Foxj1* DNAs partially restored fluid flow (representative examples are shown in Movie 2).

In conclusion, ATP4a-dependent Wnt/β-cat-signaling was required for *Foxj1* expression (Figure 33) as well as for the formation and function of motile cilia in MCCs of the skin(Figure 32).
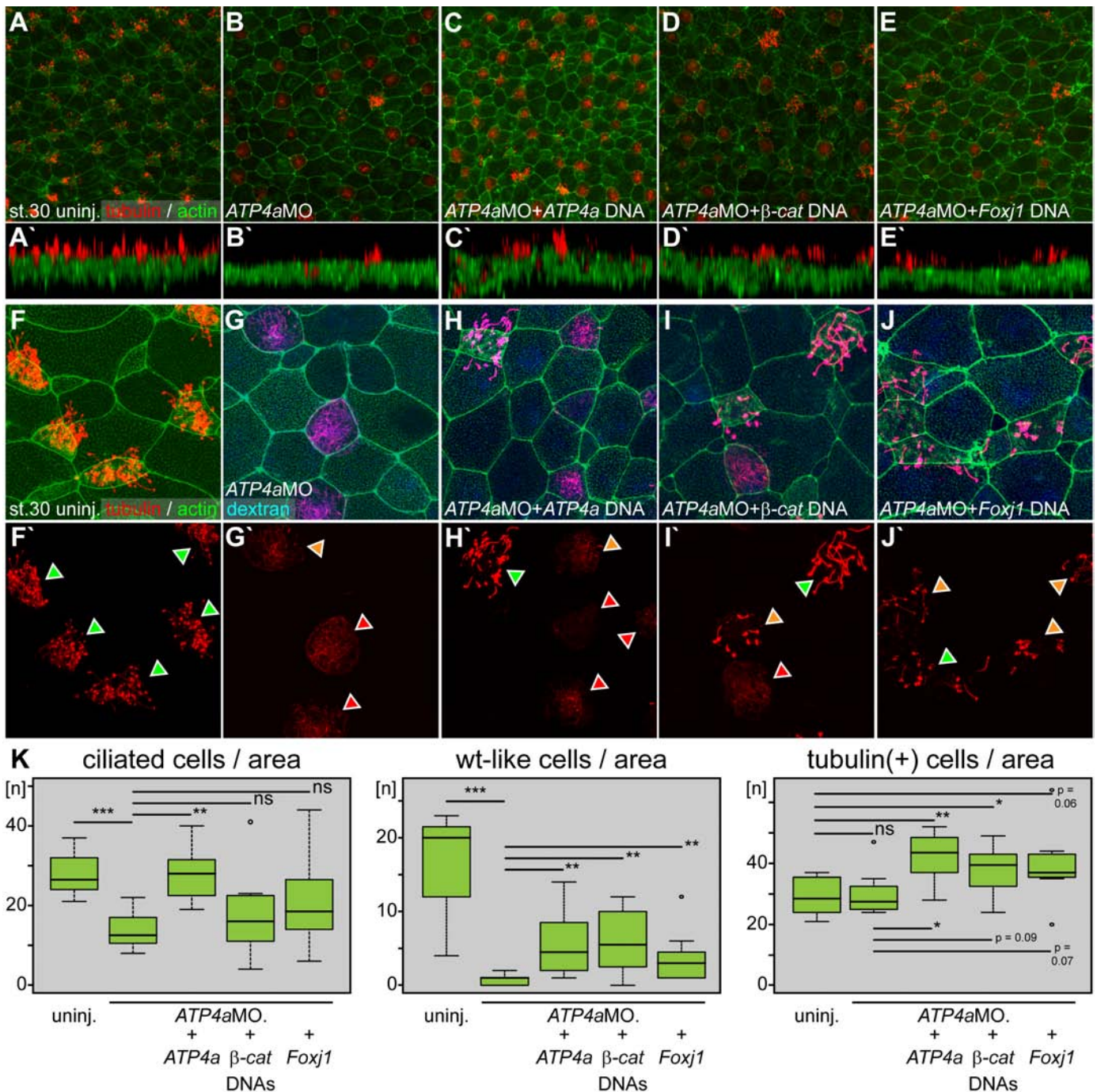
Figure 33: ATP4a Is Required For Wnt/β-cat- And Foxj1-Dependent Ciliation In The *Xenopus* Skin

(A-J) IHC for cilia (α-tubulin, red) and the actin cytoskeleton (green). Four embryos (two areas [A-E] per embryo) were analyzed per treatment. **(G-J)** Injected specimens were also analyzed for lineage tracer delivery in the blue channel (Cascade blue dextran). **(A`-E`)** Lateral projections revealed effective ciliation of the skin in control (uninj., **A**) and treated specimens. Ciliation rate was reduced in *ATP4a* morphants **(B`)**, which was in part rescued by co-injection of *ATP4a* **(C`)**, *β-cat* **(D`)** or *Foxj1* **(E`)** DNAs. **(F-J)** High-power magnification revealed long ciliary bundles (green arrowheads) in uninj. specimens **(F)**, but only apically enriched α-tubulin, which was not (red arrowhead) or only in part (orange arrowhead) projecting from the cell surface in *ATP4a* morphants **(G)**. This phenotype was rescued upon co-injection of *ATP4a* **(H)**, *β-cat* **(I)** or *Foxj1* **(J)** DNAs. **(K)** Quantification of results revealed significant rescue of ciliated cell number (marked by green and orange arrowheads in **F`-J`**) only after co-injection of *ATP4a* DNA, while the number of wt-like cells (projecting >10 cilia from the apical surface, indicated by green arrowheads in **F`-J`**) was significantly rescued in all conditions. →

83

The number of tubulin(+)-cells (indicated by green, orange and red arrowheads in **F`-J`**) was not decreased in *ATP4a* morphants, and increased in all rescue conditions, suggesting gain of Wnt/β-cat and Foxj1 signaling in *ATP4a* DNA injected specimens.

st. = stage. Statistical analysis: Wilcoxon sum of ranks (Mann-Whitney) test; ns = not significant, * = $p<0.05$, ** = $p<0.01$ and *** = $p<0.001$.

ATP4a And β-cat Are Required Downstream Of The Notch/Delta Pathway In The Skin

The MCE of the *Xenopus* skin was reported to consist of three cell types, namely MCCs, ion secreting cells (ISCs) and large goblet cells (Hayes et al. 2007; Dubaissi et al. 2011; Quigley et al. 2011). While goblet cell specification in *Xenopus* MCE has not been addressed so far, specification of MCCs and ISCs (derived from the deep layer of ectoderm) was shown to be under control of Notch/Delta-signaling (Deblandre et al. 1999; Quigley et al. 2011).

In order to evaluate the hierarchy of Wnt- and Notch/Delta-signaling events in MCC specification and *Foxj1* expression, embryos were injected with either *Dll1* (*Delta-like 1*) / *X-Su(H)-DBM* (DNA-binding mutant form of the Notch co-factor *suppressor-of-hairless*) mRNA alone or in combination with *ATP4a*MO (Figure 34). *Foxj1* expression of the injected versus the uninjected side was analyzed in neurula stage embryos (st. 19) (Figure 34 G). Inhibition of Notch-signaling via *Dll1* and *X-Su(H)-DBM* significantly ($p<0.01$) increased *Foxj1* expression on the injected side (Figure 34 B, G). When *ATP4a*MO was co-injected with either construct, *Foxj1* expression decreased below wildtype-levels (Figure 34 C, G). Therefore, ATP4a-dependent Wnt/β-cat signaling was required downstream of Notch/Delta-signaling for *Foxj1* expression in MCCs.

In order to test if Notch/Delta-signaling might be a mediator of competence during skin MCE development and maintenance, *Notch-ICD* (Notch intracellular domain) mRNA was injected and Wnt-pathway activation was manipulated by *ATP4a*MO or *β-cat* DNA co-injection (Figure 34 D-G). Upon gain of Notch-signaling *Foxj1* expression was down-regulated or lost, as compared to the contra-lateral side (Figure 34 D, G). Co-injection of *ATP4a*MO further down-regulated *Foxj1* expression, which was then virtually absent on the injected side (Figure 34 E, G). When *β-cat* DNA was co-injected with *Notch-ICD* mRNA, no rescue effect was observed (Figure 34 F, G). These findings suggested that Notch/Delta-signaling was required for the mediation of competence, upstream of Wnt-dependent *Foxj1* expression in *Xenopus* skin MCE cells.
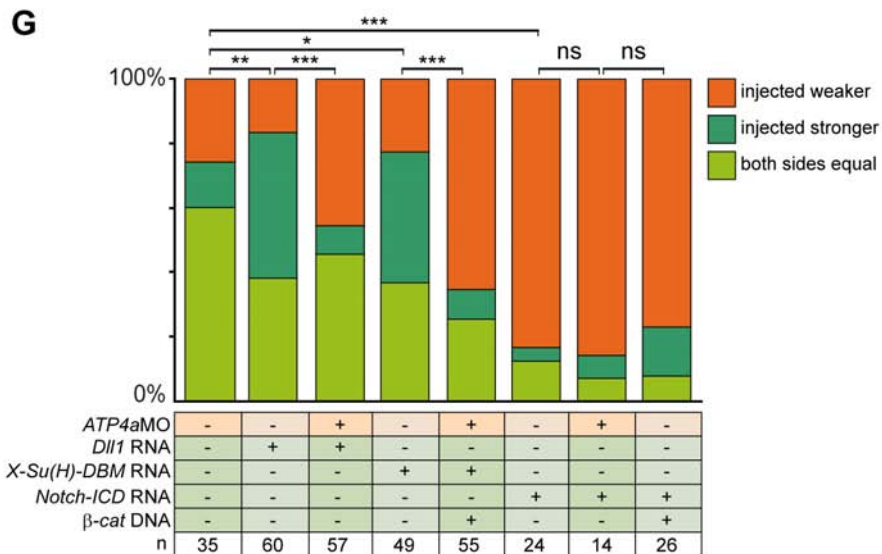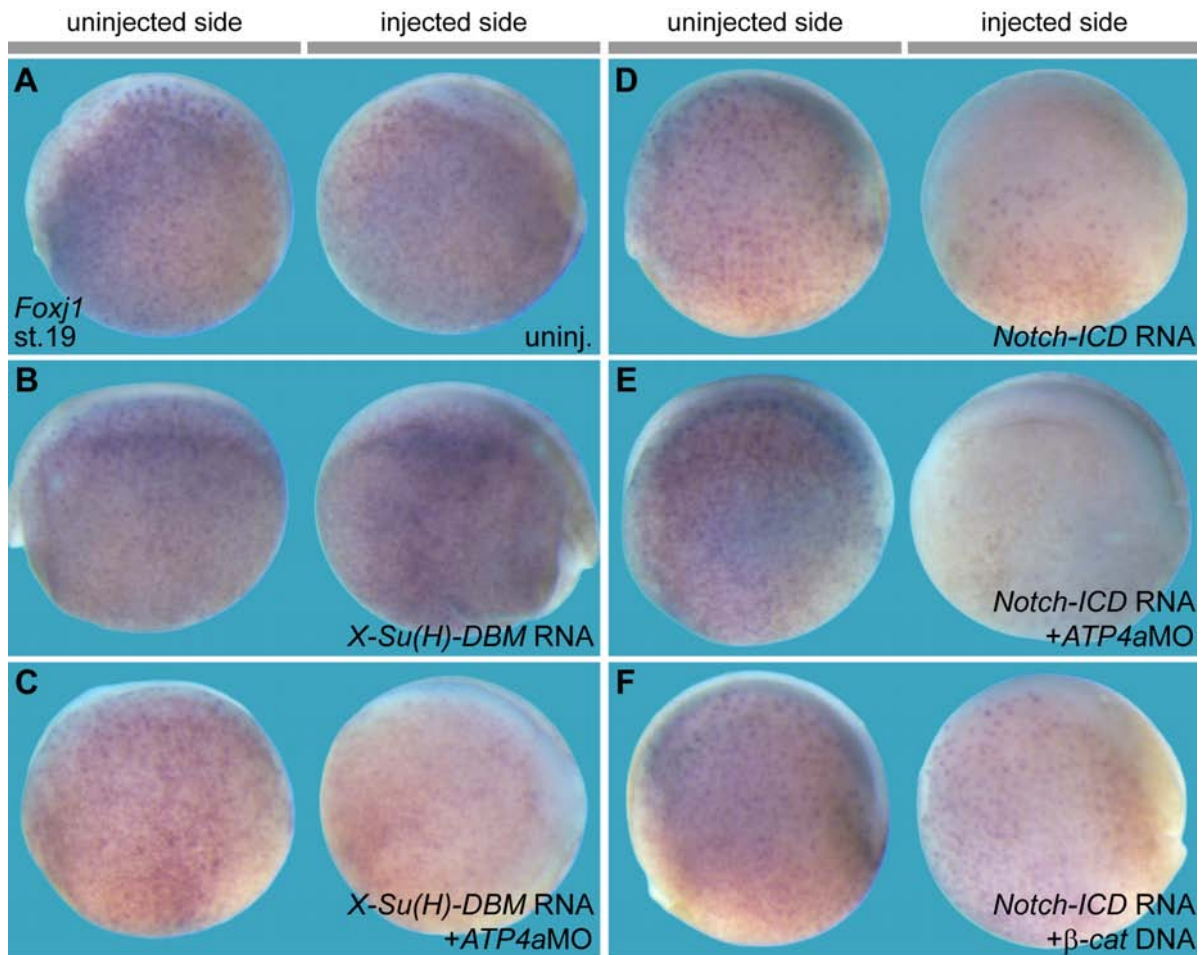
Figure 34: ATP4a And Wnt/β-cat Are Required Downstream Of Notch/Delta For *Foxj1* Expression In The Skin

(A-F) WMISH and assessment of *Foxj1* expression in the skin MCE of uninjected (uninj.) and unilaterally right injected (as indicated) neurula stage (st. 19) embryos. **(A, B and D)** Inhibition of Notch-signaling in the skin increased *Foxj1* expression **(B)**, while gain of Notch-signaling decreased *Foxj1* expression **(D)**, as compared to uninj. **(A)** controls and uninjected contra-lateral sides of respective embryos. **(C)** Inhibition of ATP4a by *ATP4a*MO co-injection prevented increase in *Foxj1* expression upon inhibition of Notch-signaling by *X-Su(H)-DBM* mRNA. **(E)** Loss of ATP4a in Notch-ICD injected specimens further decreased *Foxj1* expression. **(F)** Gain of β-cat in Notch-ICD injected embryos did not rescue *Foxj1* expression, suggesting that Delta-signaling was required during mediation of competence for *Foxj1* expression in skin cells. →

85

(G) Quantification of results.
st. = stage. Statistical analysis: Chi²-test; ns = not significant, * = p<0.05, ** = p<0.01 and *** = p<0.001.

Next, the effect of *ATP4a*MO injections on ISCs was investigated. ISCs were reported to express genes encoding the vacuolar H⁺ATPase (ATP6) and were suggested to regulate ion homeostasis. Therefore, expression of *ATP6V1E1* (E1 subunit of ATP6) was analyzed in order to elucidate if ISCs were present in *ATP4a* morphants. In contrast to *Foxj1* expression in MCCs (Figure 32 D, E), expression of *ATP6V1E1* was not affected in *ATP4a* morphants (Figure 35) (Quigley et al. 2011).

Taken together, ATP4a was required downstream of Notch/Delta-signaling (Figure 34) for *Foxj1* expression (Figure 32 D, E) and ciliation in MCCs of the skin (Figure 32 F-H and Figure 33). ATP4a was not required for specification of ISCs (Figure 35) or intercalation *per se* (Figure 33).
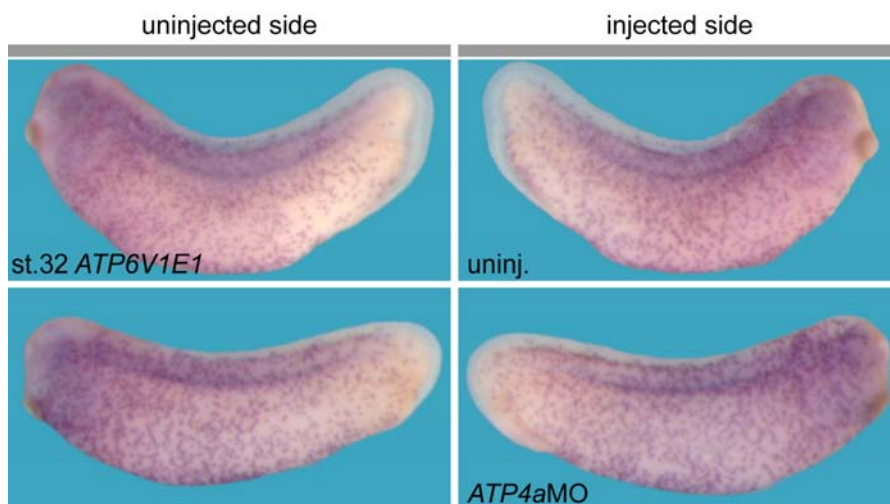
Figure 35: Specification Of Ion Secreting Cells (ISCs) And *ATP6* Expression Are Independent Of ATP4a

WMISH in tailbud stage (st. 32) embryos and assessment of *ATP6V1E1* expression, which is a marker for ISCs in the skin MCE, did not reveal decrease in expression upon loss of ATP4a function.   st. = stage.

ATP4a-Function Is Required For *Otogelin* Expression In Goblet Cells

In order to analyze effects of *ATP4a*MO injections on goblet cells, expression of the goblet cell marker *Otogelin* was analyzed by WMISH (Hayes et al. 2007). *Otogelin* expression started around stage 12 in the ventral skin ectoderm (Figure 36 A, B). Expression increased in concomitant stages (~st.15-20) (Figure 36 C) and was present until late

tailbud stages (not shown), but expression levels decreased (Figure 36 D and not shown). Next, *Otogelin* expression was analyzed in *ATP4a*MO injected specimens. *Otogelin* expression was down-regulated in *ATP4a* morphants (Figure 36 E), suggesting that ATP4-mediated Wnt-signaling could be required in this cell type as well.
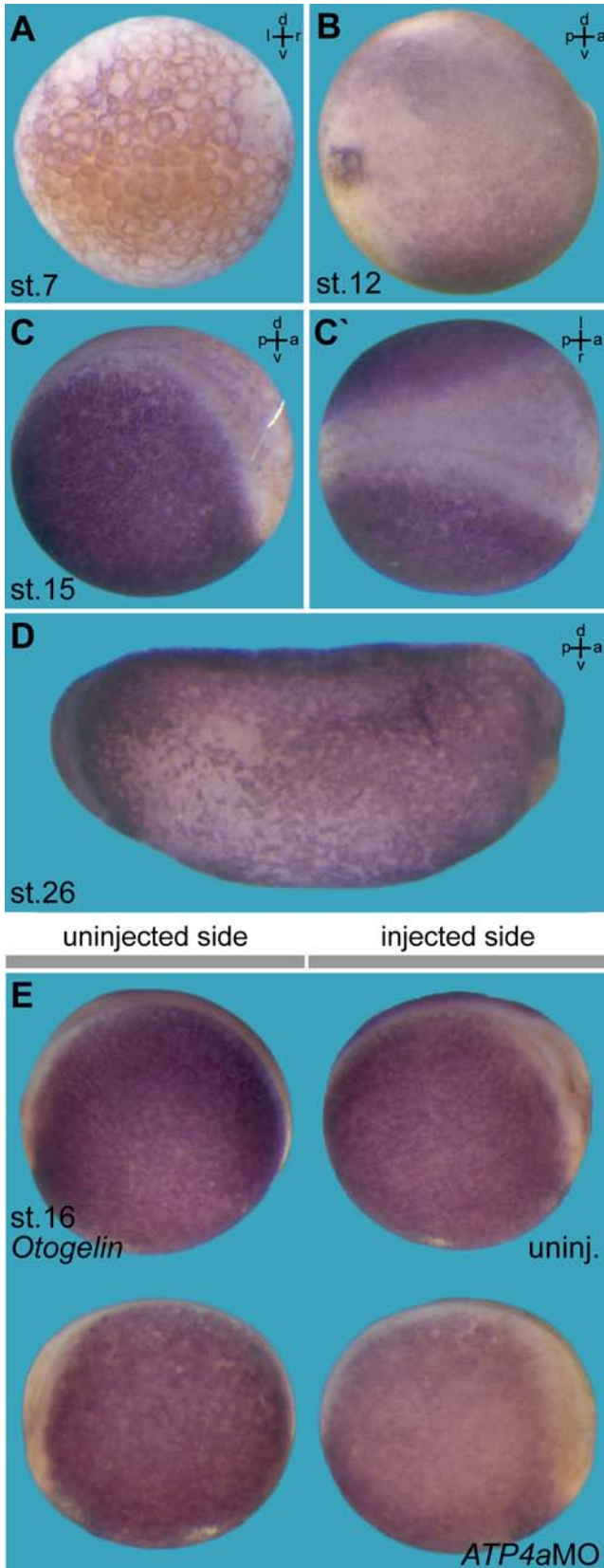
Figure 36: *Otogelin,* **A Marker Gene For Goblet Cells, Is Expressed During MCE Development In An ATP4a-Dependent Manner**

(A-D) WMISH analysis of developmental *Otogelin* expression. *Otogelin* was not expressed pre-MBT (st. 7, **A**), i.e. *Otogelin* was only expressed zygotically from st. 12 onwards **(B)**. Expression started in the ventral skin ectoderm (st. 12, **B**) and expanded towards dorsal regions during later development (st. 15, **C**), eventually covering the whole embryo, except for the neuroectoderm **(C`)**. In early tailbud stages (st. 26) expression started to decrease, and was not found at the cement gland (anterior-most structure). **(E)** *Otogelin* expression was decreased, but not lost in unilateral right injected *ATP4a* morphants, indicating requirement for ATP4a in goblet cells.

a = anterior, an = animal, d = dorsal, l = left, p = posterior, r = right, st. = stage, v = ventral and veg = vegetal.

Characterization Of A Novel Cell Type In The *Xenopus* Skin

We have recently involved serotonin (5-hydroxytryptamine; 5-HT) signaling in regulation of ciliary beat frequency (CBF) in MCCs (Thumberger 2012). Therefore, experiments were performed to test if 5-HT or the receptor HTR3 (required for CBF) regulated *Foxj1* expression as well. Loss of 5-HT signaling by means of *HTR3*MO injection or squelching of 5-HT by over-expression of a *HTR3-ligand binding-domain* (*HTR3-LBD*) mRNA (Beyer et al. 2011) were employed. Upon injection of *HTR3*MO or *HTR3-LBD* mRNA *Foxj1* expression was not down-regulation (Figure 37). Serotonin signaling was thus required for regulation of CBF, but not for *Foxj1* expression in MCCs of the *Xenopus* skin.

uninjected side   injected side
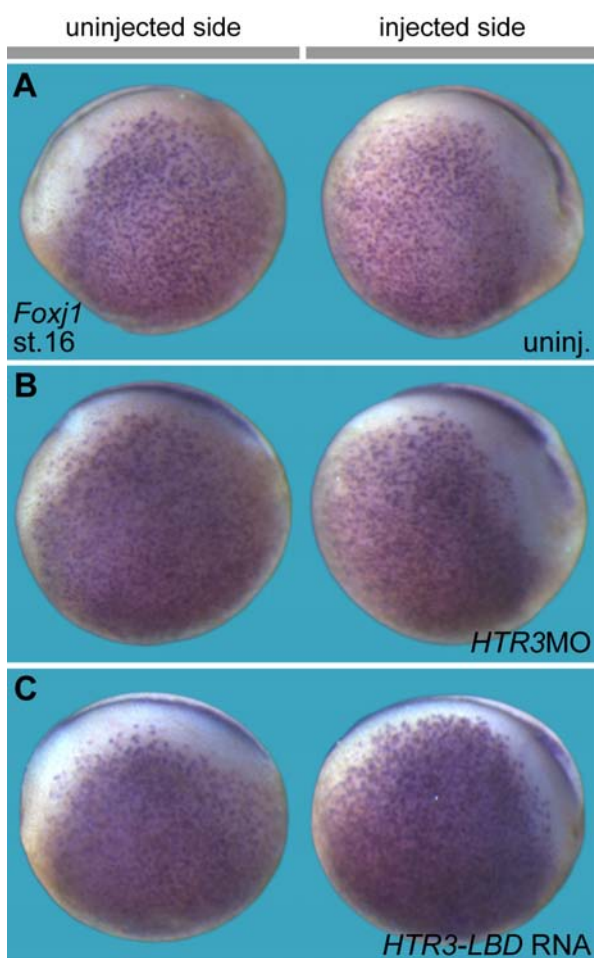
Figure 37: Serotonin (5-HT) Signaling Does Not Mediate Wnt/β-cat Signaling And *Foxj1* Expression In The Skin

(A-C) WMISH analysis of *Foxj1* expression in neurula stage (st.16) controls (uninj., **A**), unilaterally right injected *HTR3* morphants **(B)** and after unilateral right-sided *HTR3-LBD* mRNA-mediated loss of 5-HT signaling **(C)**. Note that *Foxj1* expression on the injected side was not down-regulated, and in some specimens a minor increase in staining intensity was evident **(C)**.

st. = stage.

Serotonin-positive cells were characterized by a small apical surface and presence of vesicle-like structures filled with 5-HT (Figure 38 A, B and D-E). 5-HT synthesis from tryptophan depends on tryptophan-hydroxylase (TPH) (Matthes et al. 2010). Expression of *TPH* in the MCE started around st. 25 (Figure 38 A, C). WMISH for *TPH* was combined with IHC for 5-HT and revealed co-localization of *TPH* expression and 5-HT in vesicle-like structures (Figure 38 A). Visualization of cilia (by IHC for tubulin) confirmed that *TPH-*

expressing and 5-HT containing cells were non-ciliated (Figure 38 A). Next, WMISH for the goblet cell marker *Otogelin* was combined with IHC for 5-HT. Serotonin-containing cells were not *Otogelin* positive (Figure 38 B). In order to elucidate if serotonergic cells belong to the ISC-population, Notch/Delta-signaling was manipulated (as described above), and *TPH* expression was compared with *ATP6V1E1* expression. While injection of *Notch-ICD* mRNA inhibited expression of *ATP6V1E1*, *TPH* expression was found more abundant in the skin (Figure 38 C). Conversely, when *Dll1* or *X-Su(H)-DBM* mRNAs were used, *ATP6V1E1* expression was increased, but *THP* expression was down-regulated (Figure 38 C). These findings were confirmed when 5-HT and tubulin were stained by IHC in Notch/Delta-manipulated embryos: (1) Gain of Notch-signaling by *Notch-ICD* mRNA induced increased presence of 5-HT vesicles in the skin at the expense of MCCs (Figure 38 D, E). (2) Inhibition of Notch-signaling by *Su(H)-DBM* mRNA decreased the number of 5-HT vesicles in the MCE, and the number of MCCs was increased (Figure 38 D-F). In conclusion, *TPH*-expressing and 5-HT-containing cells represented a distinct cell type in the *Xenopus* skin MCE. It is suggested to name this cell type according to its unique features features: ***T****PH*-expressing **a**nd **s**erotonin-secreting **c**ells – TASCs.

To further characterize TASCs in the skin MCE, *ATP4a* loss-of-function was performed and *TPH* expression was analyzed in unilaterally injected embryos. *TPH* expression was down-regulated in *ATP4a* morphants (Figure 39). The negative effect of *ATP4a*MO injections was partially rescued upon co-injection of *ATP4a* DNA, thereby demonstrating specificity (Figure 39). When *TPH* expression was stimulated by *Notch-ICD* mRNA injection, *β-ca*t DNA was not able to induce further increase in *TPH* expression (Figure 39). When *ATP4a*MO was co-injected with *Notch-ICD* mRNA, *TPH* expression was lost (Figure 39). Therefore, ATP4a-mediated Wnt-signaling was required downstream of the Notch/Delta-pathway, either specifically for *TPH* expression or for the induction of TASC-identity within MCE cells.
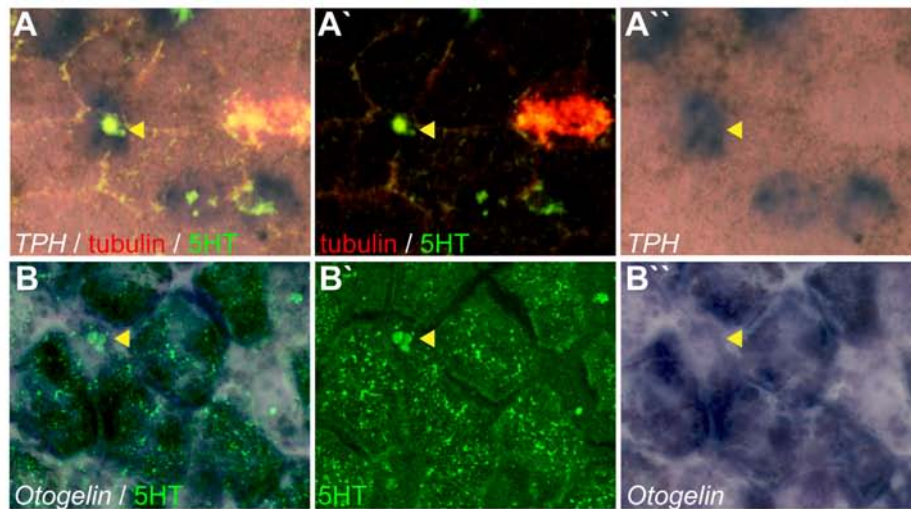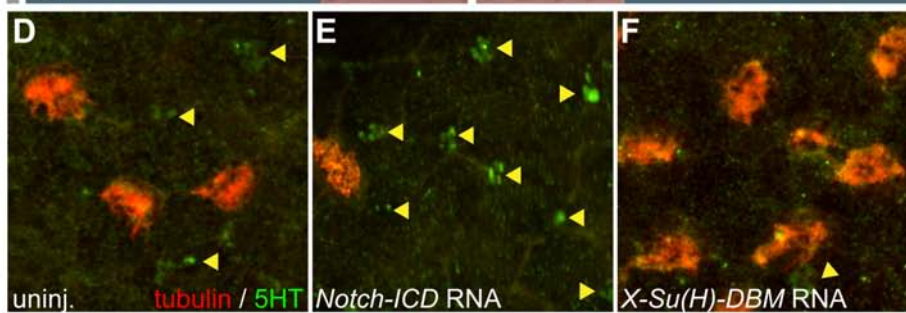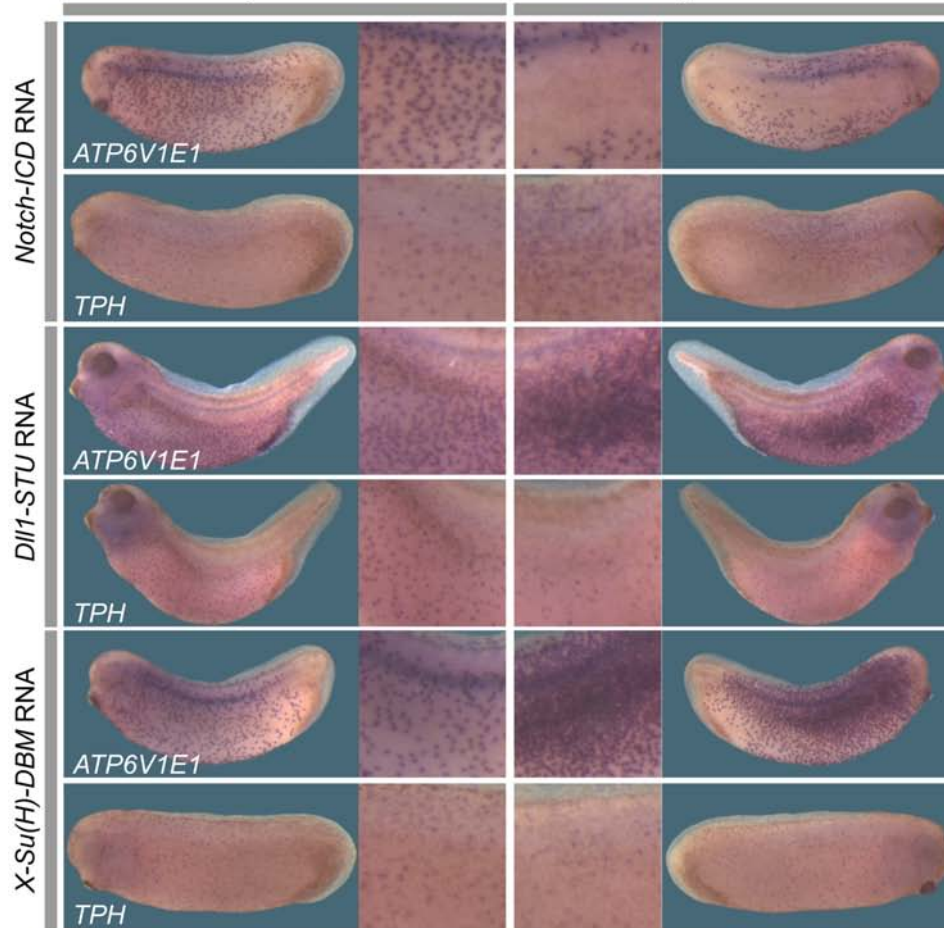
Figure 38: *Tryptophan-hydroxylase* Expressing And 5-HT Secreting Cells Represent A New Cell Type In The Skin

(A-B) Combined analysis of WMISH and IHC during tailbud stages (st. 27-35). **(A)** *TPH* expression (purple) co-localized with 5-HT vesicles (green), but not with ciliated cells (α-tubulin, red), indicating that 5-HT is actively produced and localized to vesicles in the skin. **(B)** WMISH signal (purple staining) for the goblet cell marker *Otogelin* did not co-localize with 5-HT vesicles (green) as well. **(C)** Opposite effects upon Notch/Delta-signaling manipulation in ISCs and serotonergic cells. Gain of Notch-signaling by unilaterally right injection of *Notch-ICD* mRNA prevented formation of ISCs, as judged by expression of *ATP6V1E1*, but increased expression of *TPH* in the skin (upper panel). Conversely, inhibition of Notch-signaling by injection of *Dll1-STU* or *X-Su(H)-DBM* mRNAs increased presence of ISCs, but decreased *TPH* expression (middle and lower level, respectively). **(D-F)** IHC for cilia (red) and 5-HT (green) in control (uninj.) **(D)** and manipulated specimens **(E, F)** revealed that manipulation of Notch/Delta-signaling had the same effects on ciliation (multiciliated cells, MCCs) and 5-HT, like described for ISCs and *TPH* expression **(C)**, i.e. increase in MCC abundance upon Notch-signaling inhibition, and increase of 5-HT vesicle-containing cells upon Notch-signaling stimulation.
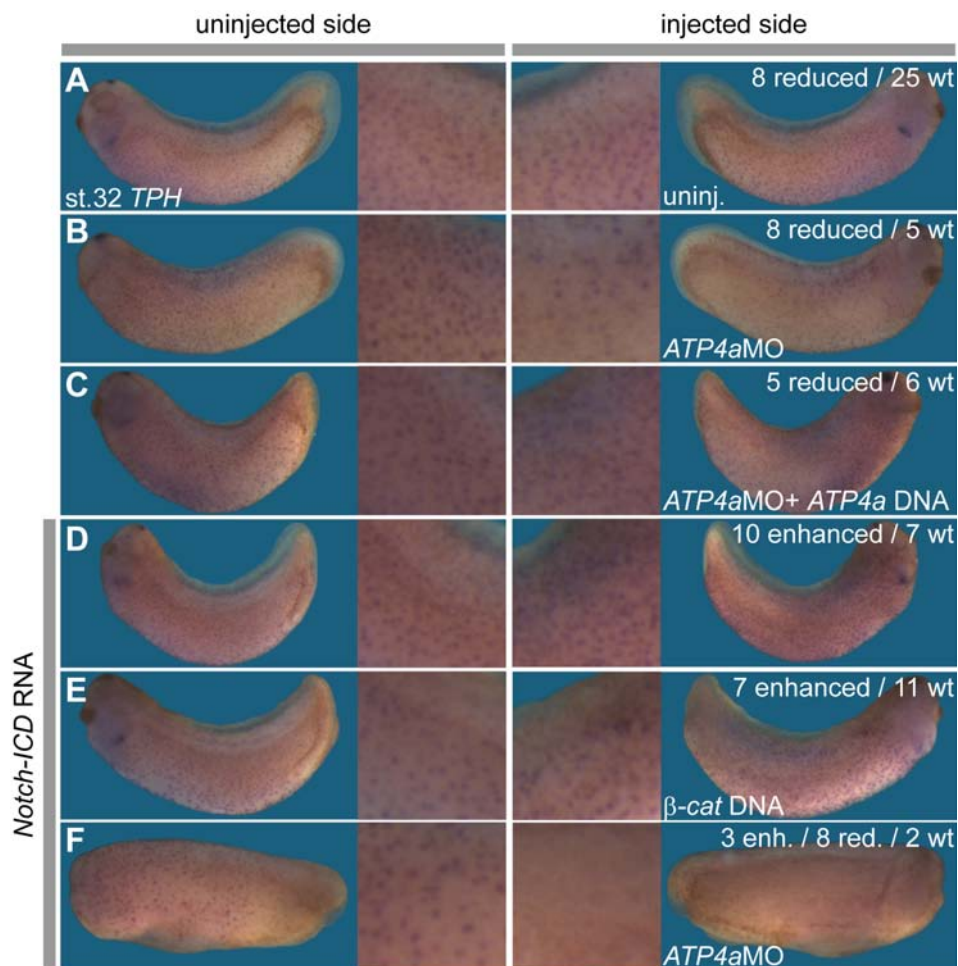
Figure 39: *TPH* Expression Requires ATP4a Mediated Wnt/β-cat Signaling Downstream Of Notch-signaling

WMISH for *TPH* in control (uninj., **A**) and manipulated embryos, which were unilaterally injected to the right-animal blastomeres at 4-cell stage. *TPH* expression was reduced in *ATP4a* morphants **(B)**, and this effect could be rescued upon co-injection of *ATP4a* DNA **(C)**. While gain of Notch-signaling (*Notch-ICD*) enhanced *TPH* expression **(D)**, co-injection of *β-cat* DNA has not further enhanced expression intensity or number of *TPH* expressing cells **(E)**. Conversely, when *ATP4a*MO was co-injected with *Notch-ICD* mRNA, *TPH* expression was reduced on the injected side **(F)**.

91

Summary

ATP4a was required downstream of Notch/Delta-signaling in MCCs for Wnt/β-cat dependent *Foxj1* expression, ciliogenesis and establishment of cilia-driven flow. It was dispensable for *ATP6V1E1* expression in ISCs. In contrast to MCCs and ISCs, TASCs did require active Notch-signaling for *TPH* expression and 5-HT localization. HTR3-mediated 5-HT-signaling in the skin was not required for *Foxj1* expression, but for regulation of CBF in MCCs (Thumberger 2011). *Otogelin* expression in goblet cells of the outer layer was down-regulated after *ATP4a* loss-of-function as well. Taken together, ATP4a-mediated Wnt-signaling was required for correct gene expression and function of the *Xenopus* skin MCE (Figure 40).
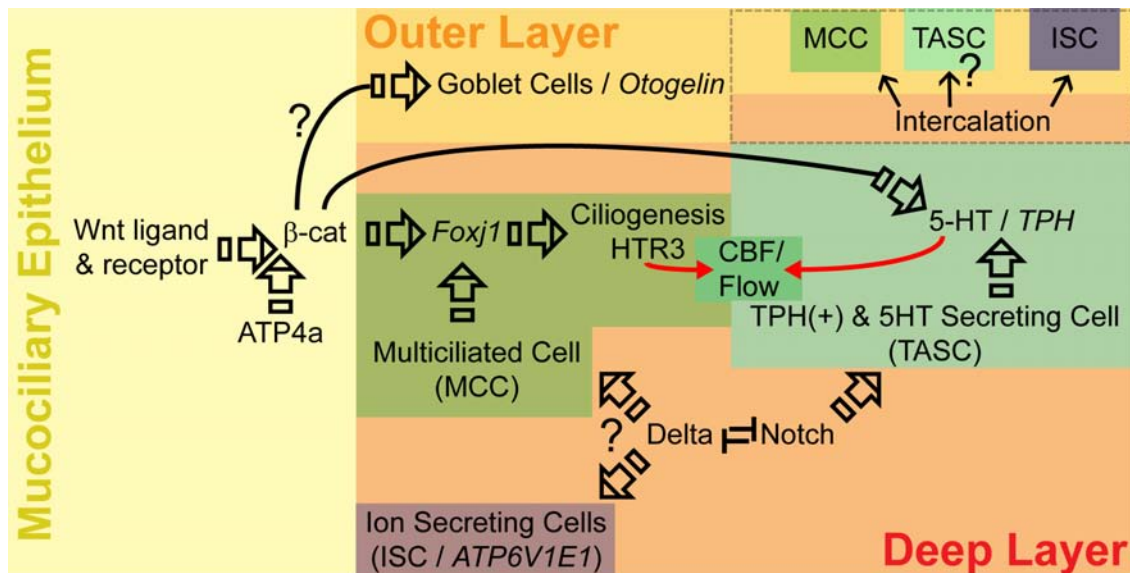
Figure 40: Graphical Summary Of ATP4a And Wnt-Signaling Functions In The *Xenopus* Skin Mucociliary Epithelium

Three out of four cell types of the skin MCE require ATP4a-mediated Wnt/β-cat signaling, i.e. goblet cells in the outer cell layer (orange), and MCCs and TASCs from the deep layer (light red). MCCs, ISCs, and probably TASCs as well, are derived from the deep layer and need to intercalate into the outer layer during MCE development (indicated by arrows in the upper-right inset). Cell fate within the deep cell layer is mainly mediated by Notch/Delta-signaling, but additional factors are required for separation between MCCs and ISCs, which are Wnt-dependent and -independent, respectively. Goblet cells express *Otogelin* and produce mucus, MCCs express *Foxj1* and project motile cilia into the mucus, ISCs express *ATP6V1E1* and regulate ion homeostasis, while TASCs express *TPH* and produce 5-HT, which they secrete to regulate ciliary beat frequency (CBF) via cilia-localized HTR3, a ligand gated Ca^{2+} receptor channel.

ATP4a, Wnt-Signaling And *Foxj1* Expression In The Neuroectoderm

ATP4a Is Required For β-cat Dependent *Foxj1* Expression In The Floor Plate Of The Neural Tube And Downstream of Hedgehog-Signaling

ATP4a-dependent Wnt/β-cat signaling was required for *Foxj1* expression and ciliation in the SM/GRP (Figure 24) as well as the MCE of the skin (Figure 40). Hence, Wnt/β-cat signaling via ATP4a could be a general regulator of motile ciliogenesis during *Xenopus* development.

Foxj1 was expressed in the floor plate (Figure 32 A and Figure 41 A) from stage 12/13 onwards (Pohl et al. 2004). Expression of *Foxj1* in the floor plate was previously reported to be under control of Sonic hedgehog (Shh) (Yu et al. 2008). Recently, a revised model proposed that Hedgehog (HH) signaling was dispensable for floor plate induction in *Xenopus* (Peyrot et al. 2011). These findings thus suggested that HH-signaling could be required for *Foxj1* expression downstream of floor plate induction. Therefore, requirement of ATP4a and Wnt-signaling for *Foxj1* expression in the floor plate and interaction of Wnt- and HH-signaling were tested.

*ATP4a*MO was injected into dorsal blastomeres at 4-cell stage. Embryos were cultured until they have reached neurula stages, and *Foxj1* expression was analyzed by WMISH. Upon MO-mediated loss of ATP4a-function, a decrease in floor plate *Foxj1* expression was observed in 15 out of 19 specimens (Figure 41 B). When *ATP4a*MO was co-injected together with *β-cat* DNA, *Foxj1* expression was at wildtype-levels in 9 of 21 manipulated embryos (Figure 41 C). This supported the idea that ATP4a-dependent Wnt/β-cat signaling was required for *Foxj1* expression in the floor plate as well. Ectopic activation of *Foxj1* was found in the anterior neural plate in *β-cat* DNA co-injected embryos (Figure 41 E), whereas it was excluded from the anterior-most portions of the neural plate in uninjected embryos (Figure 41 D). Wnt/β-cat signaling was thus necessary and sufficient for *Foxj1* expression in neural plate. In order to confirm that interference with Wnt-signaling did not affect floor plate induction or HH-signaling, floor plate-morphology and gene expression were analyzed in *ATP4a* morphants. In floor plate cells, triangular shape due to strong apical constriction was observed in uninjected and morphant embryos (Figure 41 A`, B` and C`).
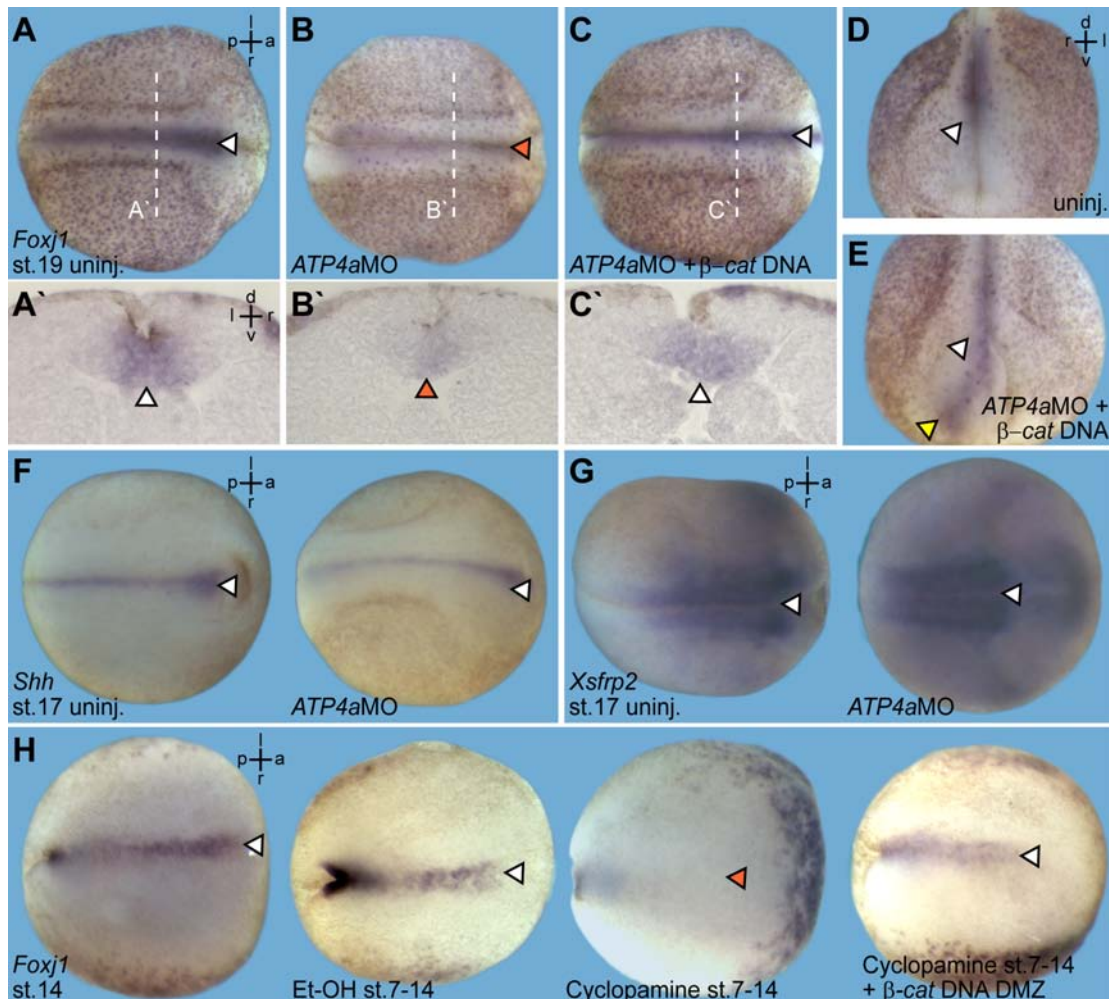
Figure 41: ATP4a And Wnt-Signaling Are Required Downstream Of Hedgehog-Signaling For *Foxj1* Expression In The Floor Plate Of The Neural Tube

WMISH in control and manipulated embryos for *Foxj1* **(A-E and H)**, *Shh* **(F)** and *Xsfrp2* **(G)** expression during neurula stages (st. 14-19). **(A-E)** *Foxj1* expression was specifically lost in the floor plate (fp), but not in the skin ectoderm upon dorsal injection of *ATP4a*MO **(B)**, and without affecting fp morphology **(A`, B`)**. **(C)** Fp-*Foxj1* was rescued upon co-injection of *β-cat* DNA in morphants. In comparison to uninjected (uninj.) controls **(D)**, *Foxj1* expression was expanded towards the anterior edge of the neural plate (yellow arrowhead in **E**), normal anterior edge of *Foxj1* expression is indicated by white arrowheads in (**D** and **E**). **(F, H)** Fp-*Shh* and neural *Xsfrp2* expression patterns were not affected in *ATP4a* morphants. **(H)** Embryos were either kept in normal medium (left panel), medium with ethanol (Et-OH) or 10µM cyclopamine, and *Foxj1* expression was assessed. Inhibition of Hedgehog (HH)-signaling by cyclopamine specifically inhibited fp-*Foxj1* expression (indicated by red arrowhead) without affecting expression in the skin ectoderm or at the blastopore. Please note that fp-*Foxj1* expression was in part restored in embryos, which were injected with *β-cat* DNA to the DMZ at the 4-cell stage before incubation.

Planes of section are indicated by dashed lines in (A-C). White arrowheads indicate wt-like expression, red arrowheads indicate reduced expression and yellow arrowhead indicates an expanded expression domain. a = anterior, d = dorsal, l = left, p = posterior, r = right, st. = stage and v = ventral.

Shh expression was not altered in *ATP4a* morphants as well (Figure 41 F). In addition, a change in *Xsfrp2* expression, which was a negative regulator of *Foxj1* expression in the SM (Figure 26 C, D), was not observed upon loss of ATP4a-function (Figure 41 G). These findings argued for normal floor plate specification in *ATP4a* morphants.

Next, interaction of the Wnt- and HH-pathway was tested. Untreated and ethanol (0.1% EtOH) treated specimens revealed strong expression of *Foxj1* in the floor plate in early neurula stages (21 of 23 in untreated; 19 of 26 EtOH-treated embryos). Inhibition of HH-signaling by 10μM cyclopamine (11-deoxojervine) inhibited floor plate *Foxj1* expression in 26 of 29 specimens (Figure 41 H). Notably, cyclopamine did not interfere with *Foxj1* expression in the skin and in the involuting SM (Figure 41 H). This suggested, that HH-signaling was required for *Foxj1* expression in the floor plate, but not for expression in other epithelia during neurulation.

Next, it was tested if Wnt/β-cat signaling was sufficient to restore *Foxj1* expression in the absence of HH-signaling. In this experiment, embryos were either incubated with 10μM cyclopamine or injected with *β-cat* DNA into dorsal blastomeres at the 4-cell stage followed by incubation. Analysis of *Foxj1* expression by WMISH revealed that *β-cat* DNA was sufficient to rescue *Foxj1* expression in 3 of 5 embryos in the presence of cyclopamine (Figure 41 H), while it was lost in 7 of 7 non-injected specimens. This preliminary finding suggested that HH-signaling was required upstream of canonical Wnt-signaling for *Foxj1* expression in the floor plate.

Taken together, *Foxj1* expression in the floor plate was also dependent on ATP4a and activation of the canonical Wnt-signaling branch (Figure 41 A-E). Furthermore, *β-cat* was sufficient to induce ectopic *Foxj1* expression in more anterior domains of the neuroectoderm (Figure 41 E). Rescue of *Foxj1* expression in absence of HH-signaling by injection of *β-cat* DNA (Figure 41 H) further demonstrated that HH-signaling was required upstream of Wnt/β-cat for *Foxj1* expression.

ATP4a Is Required For Cilia-Driven Flow In The 4th Ventricle Of The Brain

In addition to the floor plate, ciliated cells line the brain ventricles and produce flow of cerebrospinal fluid (CSF) (Kishimoto et al. 2011). Ependymal flow was previously reported to occur during late tadpole stages in *Xenopus* (Miskevich 2010). In order to elucidate the precise location of MCCs in the brain, IHC for tubulin was performed on isolated heads of stage 45 tadpoles (Figure 42 A). Following staining, the brain was prepared (Figure 42 B) and sectioned. Analysis of transversal sections (Figure 42 C-K) revealed a population of MCCs projecting from the roof of the 4th brain ventricle into the lumen (Figure 42 H`, H`` and I`, I``).

In a first approach to analyze ATP4a-function in this tissue, fluorescent bead solution was injected into the 4th brain ventricle of anesthetized stage 45 tadpoles, which were either untreated or previously injected with CoMO, *ATP4a*MO or *ATP4a*-Spl-MO. Next, movement of beads was recorded in order to visualize fluid flow. As shown in representative examples (Movie 3), ependymal flow was strong in uninjected and CoMO-injected tadpoles, but reduced in strength in *ATP4a* morphants.

Summary

Experiments revealed that ATP4a-function was also required for ciliogenesis of motile cilia in the neuroectoderm, i.e. the floor plate and the roof of the 4th brain ventricle. ATP4a mediated Wnt/β-cat signaling in the floor plate, which was necessary and sufficient for *Foxj1* expression. Epistatic experiments revealed that HH-signaling was required upstream of Wnt-signaling for *Foxj1* expression in the floor plate. Analysis of the tadpole ependyma detected MCCs in the roof of the 4th brain ventricle, which produced fluid flow in an ATP4a-dependent manner. Therefore, ATP4a and Wnt-signaling were regulators of ciliogenesis in the neuroectoderm as well.
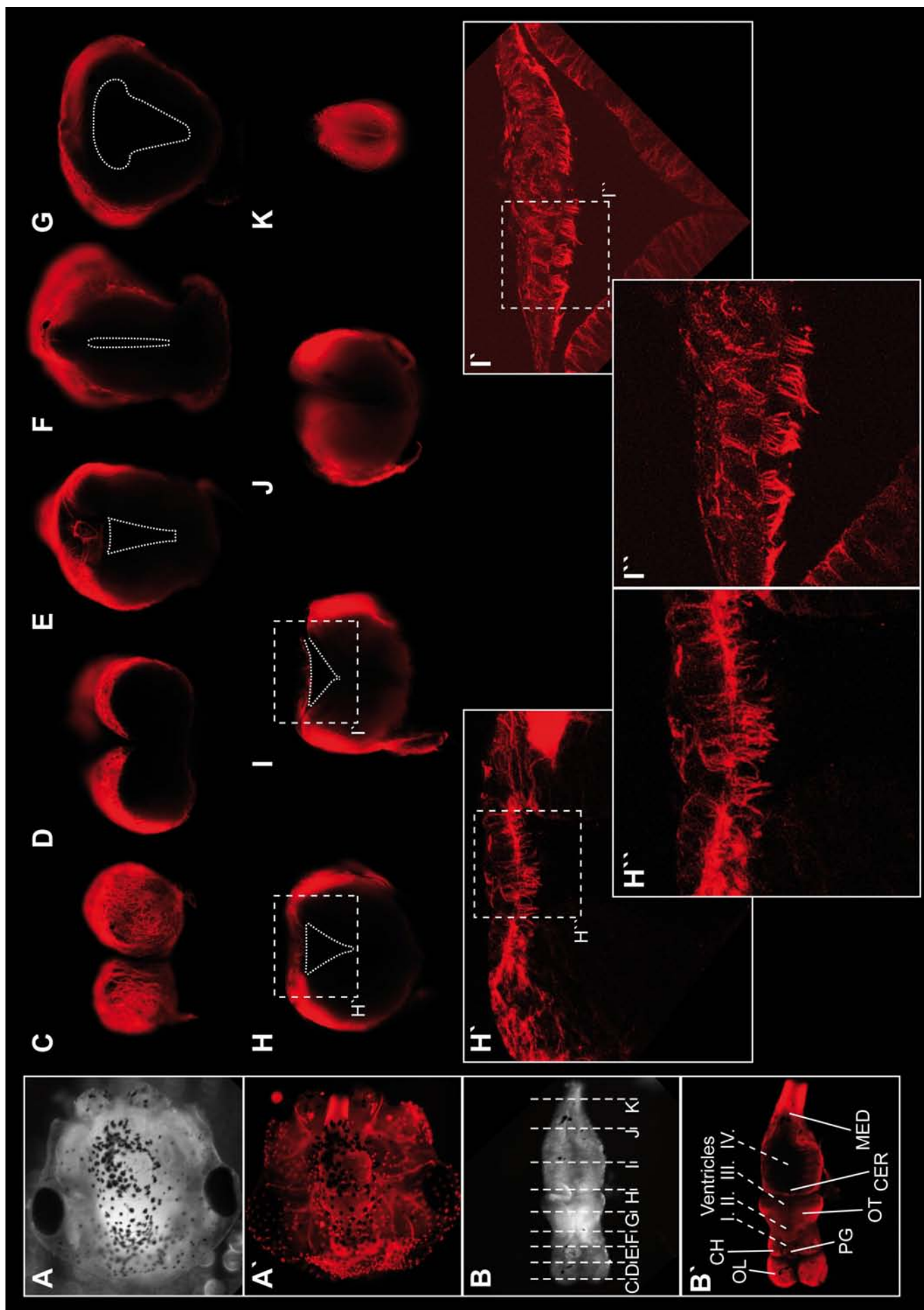
Figure 42: The Roof Of The 4ᵗʰ Ventricle Of the *Xenopus* Brain Harbors Multiciliated Cells

IHC for acetylated tubulin (red) revealed a population of MCCs in the roof of the 4ᵗʰ ventricle. **(A, A`)** IHC was performed on prepared tadpole heads – **(A)** bright field and **(A`)** fluorescent channel (red). **(B, B`)** After IHC, the brain was prepared and sectioned – **(B)** bright field channel, planes of section are indicated by dashed lines and annotated corresponding to **(C-K)**. **(B`)** Fluorescent channel (red); brain ventricles (I.-IV.) and main structures are annotated. **(C-K)** Transversal sections of the tadpole brain; ventricle lumina are outlined by dashed line in **(E-I)**. MCCs were found within the 4ᵗʰ ventricle and lined the ventricle roof **(H-H`` and I-I``)**.

Anterior to the left in (A, B). Dorsal up in (C-K). CER = cerebellum, CH – cerebral hemisphere, MED – medulla oblongata, OL – olfactory lobe, OT – tectum opticum and PG – pineal gland.

ATP4a, *Foxj1* Expression And Ciliation Of The Larval Gastrointestinal Tract

Multiciliated Cells Line The Proximal Gastrointestinal Tract Of *Xenopus*

ATP4a was required for *Foxj1* expression and/or generation of motile cilia (Figure 24, 40, 41 and Movie 3) in all analyzed epithelia. This suggested that cilia might be present in the stomach as well, i.e. the tissue where ATP4-function was well documented in vertebrates (Shin et al. 2009).

ATP4a was strongly expressed in the larval gastrointestinal tract (GIT) (Figure 43 A, B). In stage 43, expression levels were high in the gastric epithelium. Weaker expression was found more proximal extending into the oesophagus (Figure 43 A). At stage 45, staining in the stomach and oesophagus further intensified (Figure 43 C). In order to improve probe penetration during WMISH, analysis was also performed on isolated GITs (Figure 43 D). Weak expression of *ATP4a* was also found more distal to the stomach (Figure 43 C, D), i.e. at the junction of stomach and small intestine. Next, ISH for *Foxj1* was performed on whole embryos and isolated GITs. ISH revealed presence of *Foxj1* transcripts in the proximal gut as well (Figure 43 E, F). In fact, *ATP4a* and *Foxj1* were co-expressed in the oesophagus, stomach and the proximal small intestine (Figure 43 C-F). These findings revealed a new expression domain for *Foxj1* in *Xenopus*. Moreover, *Foxj1* expression indicated that ciliation extended into the stomach and small intestine.
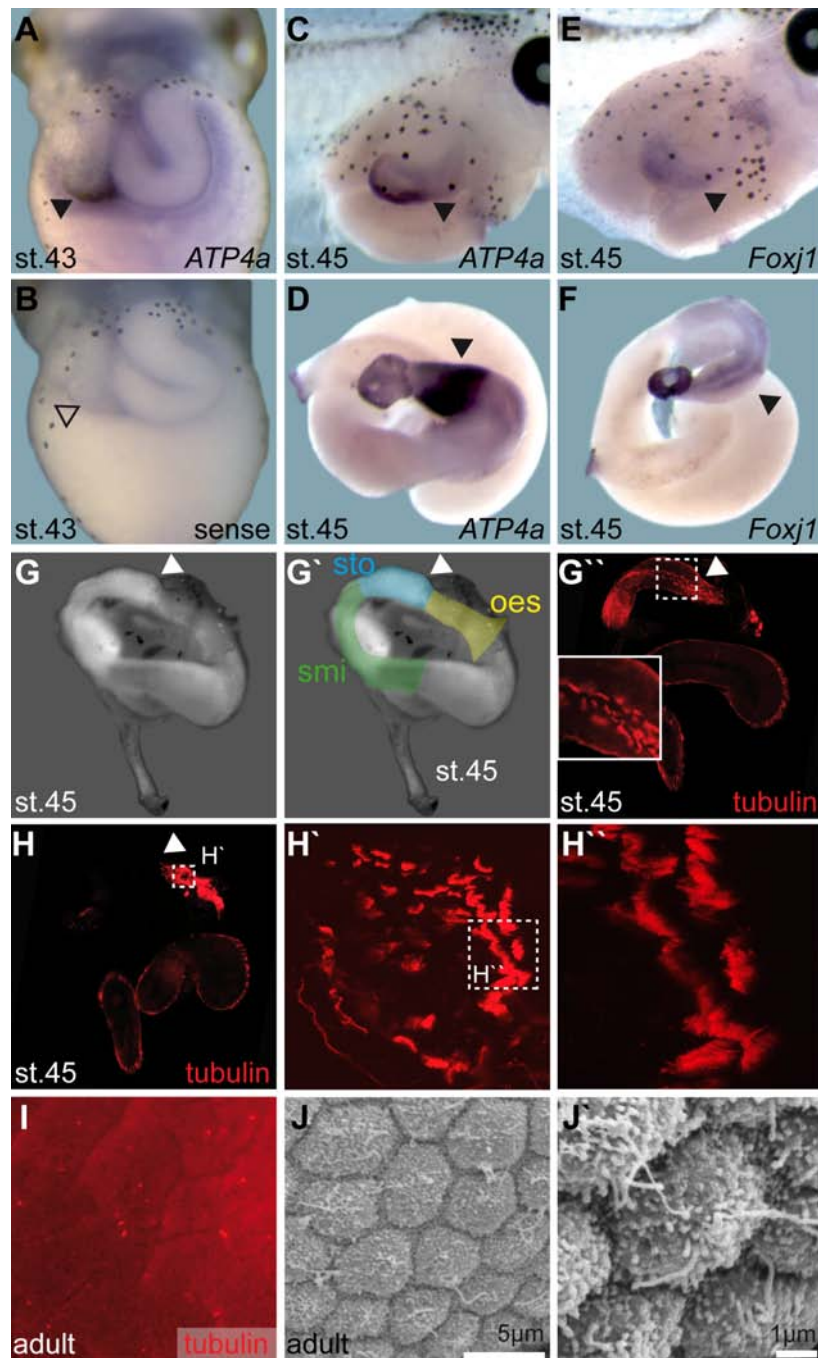
Figure 43: *ATP4a/Foxj1* Are Co-Expressed During Endoderm Development, And MCCs Are Present In The Gastrointestinal Tract

(A-F) WMISH for *ATP4a* **(A, C and D)** and *Foxj1* **(E, F)** transcripts revealed co-expression of both genes in the tadpole (st. 45) gastrointestinal tract (GIT). **(A)** Weaker, but specific staining (a sense probe did not stain the larval gut, **(B)**) was found in st. 43 **(A)**, which further intensified in st. 45 **(C, D)**. *ATP4a* and *Foxj1* expression was found in the oesophagus (oes), the stomach (sto, indicated by arrowheads in **A-F**) and the small intestine (smi) (please compare with **G`**). **(G-I)** IHC for α-tubulin (red) revealed MCCs in the proximal GIT, i.e in the oes, the sto (indicated by white arrowheads) and the smi. **(G, G`)** Bright field pictures of a prepared GIT at st. 45. The proximal GIT is annotated in **(G`)**. **(G`` and H-H``)**. Florescent channel in sectioned larval GIT revealed presence of MCCs. Inset in **(G``)** is a magnification of the area indicated by a dashed box. **(H`)** High-power magnification of stomach area indicated by dashed box in **(H)**. **(H``)** Further magnification of area indicated by dashed box in **(H`)**. **(I)** IHC for α-tubulin on adult gastric tissue revealed presence of monocilia, but not MCCs. **(J, J`)** SEM analysis of adult gastric tissue confirmed presence of monocilia on hexagonal-shaped gastric cells.

IHC for tubulin was performed on isolated GITs from stage 45 *Xenopus* tadpoles (Figure 43 G, H). After staining, samples were sectioned (Figure 42). The oesophagus, the stomach and the proximal small intestine were ciliated (Figure 43 G, H). MCCs were present within the epithelium, and cilia bundles projected from most cells (Figure 43 H`, H``). Density of MCCs decreased in the proximal small intestine (not shown) and no MCCs were found in more distal parts of the small and large intestine (Figure 43 G, H).

Next, adult gastric tissue was examined by IHC and SEM. In contrast to the larval stomach (Figure 43 G, H), adult tissue was not covered by MCCs (Figure 43 I, J). However, tubulin signals were visible in gastric cells (Figure 43 I), indicating the presence of monocilia. The adult gastric epithelium was covered by a layer of mucus, which potentially prevented penetration of the tissue by the antibody. Therefore, patches of gastric tissue were also analyzed by SEM, which did not require the use of antibodies. SEM revealed monociliated hexagonal cells in the gastric epithelium, with microvilli-like structures on the apical surface from which a cilium projected into the lumen (Figure 43 J). Hence, there were differences between the larval and adult gastric epithelium, i.e. strong ciliation and presence of MCCs in the larval stomach (Figure 43 G, H) was opposed by presence of monocilia in adult tissue (Figure I, J).

MCCs and *Foxj1* expression in the proximal larval gut further indicated that these cilia were motile (Figure 43). Therefore, an assay for gut-cilia motility was developed. For this aim, the proximal gut was isolated from an anesthetized tadpole and placed in culture medium containing anesthetic (to prevent peristaltic movements). Next, fluorescent beads were injected directly into the oesophagus. Fluorescent beads were recorded and movement was analyzed (Movie 4). The beads were translocated from the oesophagus (where they were injected) to more posterior locations, i.e. the stomach and small intestine (Movie 4). Moreover, this movement stopped in the small intestine, where fluorescent beads accumulated (Movie 4).

Summary

Analysis of gene expression and ciliation in the larval GIT of *Xenopus* located expression of *ATP4a* and *Foxj1*, and presence of MCCs in the oesophagus, stomach and small intestine. Furthermore, an assay was developed in order to functionally analyze cilia motility in this new MCE of the proximal gut.

Discussion

ATP4a And Wnt-Signaling In Vertebrate Symmetry-Breakage

The Revised Function Of ATP4a In LR-Axis Development Of *Xenopus laevis*

Previous reports (Levin et al. 2002; Aw et al. 2008) have implicated an ATP4a-function in LR-development during cleavage stages of *Xenopus*. However, the present work demonstrated that ATP4 was required during gastrula and neurula stages for the generation of a directional cilia-driven leftward flow. When ATP4a-function was lost in the dorsal-medial lineage, the nodal cascade was induced bilaterally, and single organ inversion (heterotaxia) occurred. Bilateral marker-gene expression and increased rates of heterotaxia were also observed in the initial study on ATP4 in *Xenopus* (Levin et al. 2002). This indicated that both studies have basically obtained the same results, which linked loss of ATP4a-function to ectopic gene expression in the right LPM and defects in asymmetric organ placement. Moreover, bilateral expression of left-sided genes could be linked to heterotaxia in both studies. Although gene expression patterns in the LPM were previously questioned to be of predictive nature for organ *situs* (Vandenberg 2012), they were in good agreement with organ placement in this study.

The basic finding that ATP4a was a prerequisite for correct LR-development was shared by both studies. However, several important differences were evident as well:

(1) Asymmetric expression of *ATP4a* during cleavage stages

The initial studies reported asymmetric whole mount *in situ* hybridization (WMISH) signals at and beneath the apical plasma membrane (Levin et al. 2002), although batch-dependent variability was observed (Aw et al. 2008). Symmetric signals throughout the cytoplasm of the animal hemisphere were observed in a large number of embryos from different batches in this study. The latter observation argued against early LR-asymmetries and was in line with localization patterns for many other maternal mRNAs (King et al. 2005).

It is noteworthy that in this study cleavage stage embryos were perforated at the vegetal pole before WMISH in order to increase probe penetration. In cases when the vegetal pole was not perforated, cytoplasmatic signals were reduced or absent, and precipitated dye was found outside of the cell at the plasma membranes (not shown). These specimens resembled the sub-apical mRNA-localization patterns published by Levin et al. (2002). In conclusion, the asymmetric membrane-localized mRNA pattern of *ATP4a* probably represented a staining artifact, and *ATP4a* was in fact symmetrically localized to the cytoplasm of the animal hemisphere.

In addition, asymmetric protein localization was observed as well (Aw et al. 2008), but no obvious asymmetries were observed at the protein level in this study. Asymmetric protein localization reported by Aw et al. (2008) was found predominantly within the cytoplasm. ATP4a is a transmembrane protein, and functionality requires the assembly of a tetrameric complex, consisting of two ATP4a- and two β-subunits. This assembly takes place at the membrane, and only stable β-subunit-dependent folding renders ATP4 functional. Therefore, cytoplasmatic localization of ATP4a protein is at least unusual, and these proteins are likely non-functional.

(2) Timing of ATP4-dependent events during LR-development

ATP4 was reported to act only during early stages (st. 2-~6), and that pharmacological inhibition from gastrulation onwards was ineffective in altering LR-development (Levin et al. 2002). In contrast, data from this study demonstrated that LR-defects could be obtained even when incubation started at the beginning of gastrulation (st. 10/11), but higher SCH28080 concentrations (200μM) needed to be applied. This was possibly due to the localization of GRP-forming cells before and after gastrulation: Before gastrulation, these cells were located at the outside of the embryo, but became situated within the inner cavity of the archenteron after gastrulation (Shook et al. 2004). It is conceivable that the relevant tissue thus was harder to reach by the drug from gastrulation onwards, which offered a reasonable explanation why higher concentrations had to be applied.

At the molecular level, the rescue effects of DNA-injections in *ATP4a* morphants strongly argued for a role of ATP4a from late blastula stages onwards (post-MBT; Newport et al. 1982), i.e. after the onset of zygotic transcription and much later than proposed by the "ion-flux" model.

Taken together, the previously proposed mechanism of ATP4a-function during LR-development seems highly unlikely, and a revised role of ATP4a in flow-dependent symmetry breakage is proposed (Figure Dis-1):

During specification of the LR-axis, ATP4a is required for Wnt-signaling in the SM and at the GRP. In the SM, ATP4a mediates activation of the canonical Wnt/β-cat branch, which is necessary and sufficient for mesodermal *Foxj1* expression during gastrulation. During neurulation, ciliogenesis progresses at the GRP, and Wnt/PCP-mediated posterior polarization of cilia depends on ATP4a-function. Therefore, ATP4a mediates two Wnt-dependent steps during symmetry-breakage, which take place post-MBT. These steps are both required for the generation of a directional cilia-driven leftward flow. Loss of flow directionality leads to bilateral down-regulation of *Coco* in somitic portions of the GRP, hence inducing the nodal cascade in the left and right LPM. Bilateral activation of the nodal cascade in the LPM causes heterotaxia in tadpoles after interference with ATP4-function.
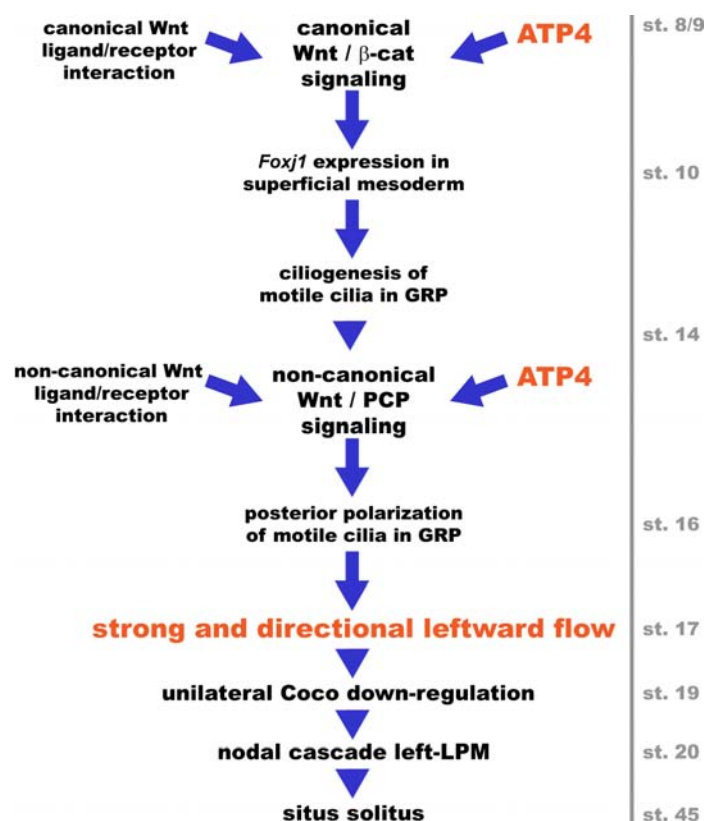
Figure Discussion-1: Timing And Role Of ATP4a-Dependent LR-Development

At the onset of MBT and gastrulation (st. 8/9), ATP4a is required for ligand-driven Wnt/β-cat signaling to induce *Foxj1* expression (st. 10) in the superficial mesoderm, from which the GRP is derived. *Foxj1* is required for motile ciliogenesis at the GRP during late gastrulation and early neurulation (st. 10-14). Furthermore, at mid neurulation (st. 14), ATP4a is required for ligand-driven Wnt/PCP signaling, which is necessary during subsequent neurulation for GRP cilia alignment to the posterior pole of cells (st. 16). Both ATP4a-dependent processes are necessary for the setup of a directional cilia-driven leftward flow (st. 17), which down-regulates Coco on the left side of the GRP (st. 19). →

103

Coco down-regulation releases repression of Xnr1, which induces the nodal cascade exclusively in the left lateral plate mesoderm (LPM), a prerequisite for correct inner organ morphogenesis, i.e. *situs solitus*.

st. = stage, GRP = gastrocoel roof plate and PCP = planar cell polarity.

Plausibility Of The "Ion-Flux" Model In *Xenopus* Without Asymmetric ATP4a-Function

The "ion-flux" model proposed that asymmetric *ATP4a* mRNA localization and function generates voltage gradients, along which 5-HT accumulates on the right side of the embryo via gap junctions (GJ) which serve as cytoplasmatic channels (Levin 2003; Levin et al. 2007). Serotonin on the right side was hypothesized to activate Mad3, which in turn inactivates *Xnr1* expression on the right side by histon deacteylase- (HDAC) dependent methylation of the *Xnr1* asymmetric enhancer region (ASE) (Carneiro et al. 2011).

The most upstream signal for asymmetric *ATP4a* mRNA localization was proposed to be the breaking of chiral symmetry of the oocyte by sperm entry, and asymmetric transport of *ATP4a* mRNA along cytoskeletal components (Aw et al. 2008, 2009). To that end, Vandenberg et al. (2010) argued that a late-induced organizer (e.g. by *Sia* mRNA injection) in UV-irradiated embryos was not able to rescue LR-development, because very early cues were missing. However, more than 70% of embryos treated this way developed *situs solitus*, which was a fairly good rescue after treatment by UV. The frequency of *situs solitus* was not different when embryos, which had the induced organizer on the same side as the endogenous organizer, were compared to embryos in which the induced organizer was in an ectopic location. These results were in conflict with predictions drawn from the "ion-flux" model (discussed in detail in Schweickert et al. 2011) (Figure Dis-2).

The lack of asymmetric ATP4a-function during LR-development also questioned the presence of any other early mechanisms implicated by the "ion-flux" model, because they were proposed to act downstream or in parallel with ATP4a. Reinvestigation of 5-HT localization and function during LR-development of *Xenopus* revealed that 5-HT did not accumulate on either side of the early embryo (Beyer et al. 2011). Interestingly, 5-HT signaling via receptor HTR3 was a prerequisite for Wnt-dependent specification of the SM, *Foxj1* expression and generation of leftward-flow, similar to ATP4a. Loss of 5-HT signaling in the early embryo had more drastic effects than loss of ATP4a (Beyer et al. 2011):

(a) *Xnr3* expression in the organizer and (b) somitic *Xnr1* expression were lost in *HTR3* morphants. In addition, (3) GRP cell size was increased. All of these aspects were unaffected in *ATP4a* morphants. This indicated overlapping but distinct functions of both players in Wnt-signaling and LR-development.

Recently, GJ communication (GJC) was also reanalyzed in *Xenopus* (Beyer et al. 2012): GJC was required in endodermal LECs post-flow, and interference with GJC inhibited the transfer of laterality cues from the midline to the LPM. This finding was confirmed by another study, which essentially proposed the same function for GJC in mouse LR-development (Viotti et al. 2012) (Figure Dis-3). Taken together, the functions of three central players of the "ion-flux" model in frog were revised and put in line with the leftward flow model of symmetry-breakage by our recent findings (Beyer et al. 2011; Beyer et al. 2012; Walentek et al. 2012).

Right-asymmetric inactivation of the *Xnr1*-enhancer via 5-HT/Mad3-dependent activation of HDAC was proposed to constitute the mechanism, by which early asymmetries are transferred to the LPM (Carneiro et al. 2011). This mechanism seems implausible in the light of recent data on 5-HT localization and function during LR-development (no LR-asymmetries in 5-HT localization were observed; Beyer et al. 2011). Moreover, 5-HT binding to Mad3 was reported to take place in the intracellular space, but earlier studies from Levin and co-workers implicated requirement for membrane-standing receptors (Fukumoto et al. 2005). This discrepancy argues against an intracellular role of 5-HT. Studies by Ohi et al. (2007) further demonstrated that the right LPM had the same potential for nodal cascade induction as the left LPM. This should not be the case when the *Xnr1* ASE-enhancer was inactivated on the right side.

Figure Discussion-2: table content:

	Nodal cascade	left	right	absent	bilateral
expected	organ situs	*situs solitus*	*situs inversus*	heterotaxia	heterotaxia
	% *situs solitus*	100	0	12.5	12.5
reported*	% *situs solitus* (n)	74 (102)	73 (168)	75 (81)	

Siamois mRNA induced axis formation in UV irradiated embryos; Vandenberg and Levin, 2010
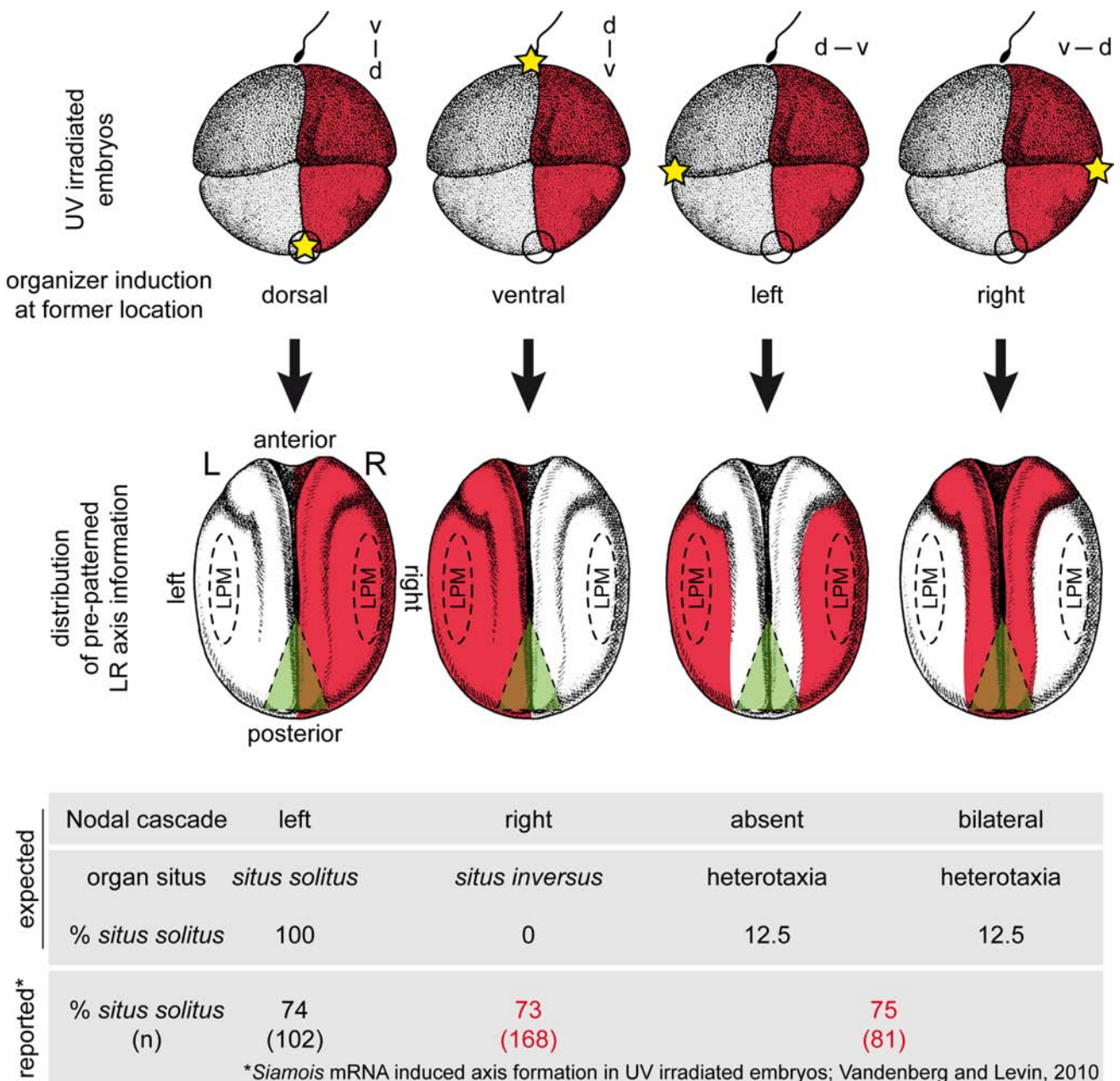
Figure Discussion-2: Spemann's Organizer Independent LR-Axis Formation

Prediction of laterality in rescued UV-irradiated embryos. 4-cell stage embryos with hypothetical predetermined LR-axis are shown (red, right; uncolored, left). Endogenous ventral and dorsal blastomeres are indicated by sperm symbols (entry site) and circles (former organizer), respectively. Following UV-irradiation and thus elimination of endogenous organizer, rescue could be targeted to four distinct positions (yellow star) relative to initial dorso-ventral (DV) and hypothetical pre-determined left-right axes. Organizer rescues could be performed at initial dorsal or ventral (sperm entry) side or at a 90° angle to initial DV axis, thus at left or right blastomeres. Induced dorso-ventral axes are indicated (d–v). Cell fates of hypothetically predetermined left and right blastomeres are superimposed on neurula specimens (red, right; uncolored, left). If the LR-axis would be prefixed, UV rescued embryos should predictably display different laterality phenotypes depending on site of rescue. Asymmetric organ placements range from wild-type (*situs solitus*), mirror image (*situs inversus*), to randomization of single organs (heterotaxia). Note the differences in the frequency of wild-type *situs solitus* between prediction of an early pre-patterned LR axis and the published experimental data by *Vandenberg and Levin (2010)*.
Reprinted from *Schweickert et al. 2011****.

In conclusion, it is unlikely that early LR-asymmetries exist in *Xenopus*. Thus the question arises how other factors implicated within the "ion-flux" hypothesis might contribute to symmetry-breakage:

(1) ATP6 (vacuolar H$^+$ATPase)

Interference with ATP6-function in *Xenopus*, chick and zebrafish embryos was linked to LR-axis defects and aberrant gene expression in the LPM (Adams et al. 2006). In *Xenopus*, ATP6 was proposed to act symmetrically (and in concert with ATP4) during cleavage stages and to control pH- and voltage-differences between the left and right side. In zebrafish, ciliogenesis in the KV was affected after pharmacological inhibition (Adams et al. 2006). ATP6 was also required for Wnt-signaling activation in *Xenopus* and human cell lines (Cruciat et al. 2010). Therefore, it is tempting to propose a function for ATP6 in LR-development, similar to that of ATP4, i.e. Wnt-dependent *Foxj1* expression and cilia polarization at the GRP. Preliminary loss-of-function experiments (Tözser 2010) further indicated that dorsal (but not ventral) loss of ATP6 was able to interfere with LR-development. A definite answer as to the role of ATP6 in LR-development might come from analysis of leftward flow, ciliation of the GRP and *Foxj1* expression in the SM after morpholino- (MO) mediated loss-of-function in future experiments. In addition, it will be interesting to elucidate if ATP4 and ATP6 have common or distinct functions during symmetry-breakage.

(2) Potassium transport

Several potassium (K$^+$) channels and transporters were shown to be required for LR-development in *Xenopus* and chick: KCNQ1, KCNE1, Kir4.1 and K-ATP, all of which were proposed to contribute K$^+$-ions to the extracellular space (Rutenberg et al. 2002; Adams et al. 2006; Aw et al. 2008; Morokuma et al. 2008). Extracellular binding of K$^+$-ions to ATP4a is a limiting step for extracellular acidification by ATP4 (Shin et al. 2009). Pharmacological inhibition of these LR-components caused heterotaxia, which was also the dominant LR-phenotype after inhibition of ATP4 (Aw et al. 2008; Morokuma et al. 2008). Therefore, loss of K$^+$-transport might have the same effect on LR-development as loss of ATP4. Loss-of-function experiments should be performed, followed by analysis of *Foxj1* expression, ciliation and leftward flow, in order to test this hypothesis.
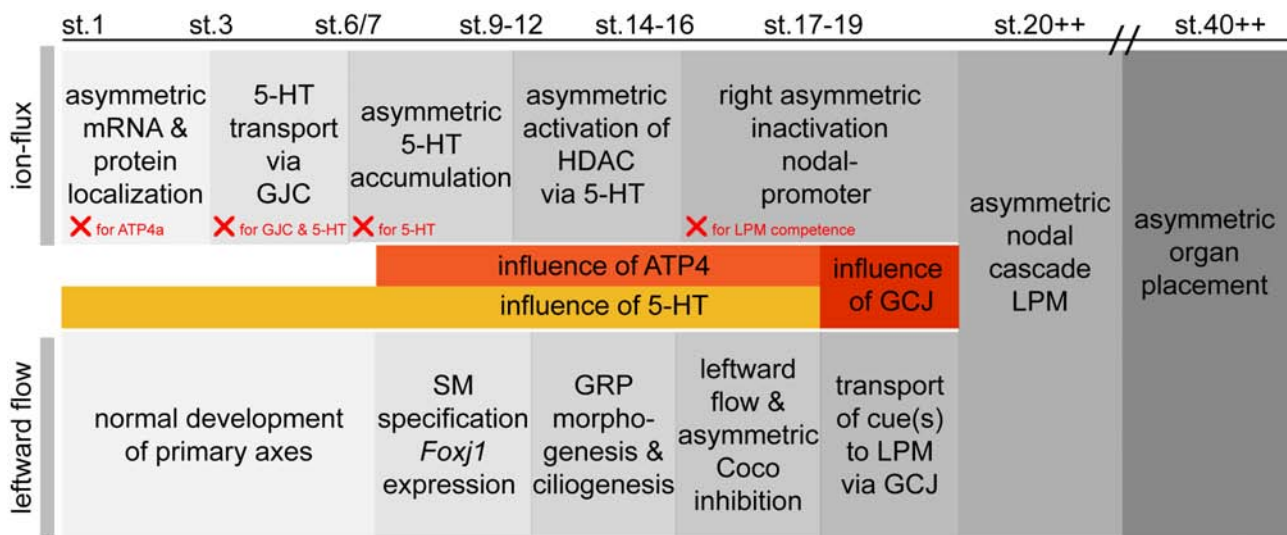
Figure Discussion-3: An Updated Comparison Of Timing and Sequence Of Events Between The "Ion-Flux" and "Leftward Flow" Models

"ion-flux": After fertilization, during early cleavage stages, mRNAs and proteins are asymmetrically distributed, which generates asymmetric membrane potentials and pH. Along electrochemical gradients, generated by asymmetric ion channels and pumps, Serotonin (5-HT) is transported via gap junction communication (GJC), and accumulates on the right side of the embryo. Asymmetric 5-HT activates the histon deacetylase (HDAC), which inhibits nodal expression on the right side of the embryo. (Mechanisms challenged by experiments from other groups are marked with a red cross and the process is indicated in red).

"leftward flow": During early development, the primary axes (anterior-posterior and dorso-ventral) are formed. When gastrulation starts, the superficial mesoderm (SM) is patterned and *Foxj1* expression is induced. After involution of the SM into the archenteron, the gastrocoel roof plate (GRP) starts to grow motile cilia, which are posteriorly localized and produce a leftward flow. Leftward flow down-regulates Coco in the left-somitic GRP, which releases repression of nodal, and laterality cues can be transported via GJC to the left lateral plate mesoderm (LPM). Asymmetric **nodal cascade** induction and **asymmetric organogenesis** are common to both models. Sensitive time-frames for loss of ATP4a (orange), 5-HT signaling (yellow) and GCJ (red) are indicated.

(3) 14-3-3 proteins

The family of dimeric 14-3-3 proteins is known to regulate sub-cellular localization and activity of target proteins (Chen et al. 2011). Inhibition of 14-3-3 proteins by the drug fusicoccin (FC) altered LR-development in *Xenopus* and was proposed to control H^+-fluxes (Bunney et al. 2003). 14-3-3 protein function was recently proposed to regulate Wnt-dependent processes as well (Takemaru et al. 2009). 14-3-3s were shown to regulate β-cat localization within cells and activation of β-cat target genes (Takemaru et al. 2009): 14-3-3ξ enhanced β-cat signaling, while 14-3-3ε and -η acted negatively on target gene expression. FC-treatment also inhibited growth in various human cancer cell-lines (de Vries-van Leeuwen et al. 2010), indicating possible inhibition of Wnt-signaling. 14-3-3β regulated Dapper 1, which promotes degradation of Dvl (Chen et al. 2011). Furthermore,

Dapper 1 and 2 were shown to play a role during development of dorsal tissues in zebrafish (Chen et al. 2011). In conclusion, a role of 14-3-3 proteins in Wnt-dependent LR-axis development seems possible. This should be addressed in future studies, using FC-treatment and MO-mediated loss-of-function. *Foxj1* expression, ciliation of the GRP and leftward flow should be analyzed in manipulated embryos, in order to gain more insight on the mechanisms of 14-3-3 proteins in LR-development.

In summary, *ATP4a* and 5-HT were not LR-asymmetric during early *Xenopus* development, and it is possible that other components of the "ion-flux" model act in Wnt- and cilia-dependent manner as well (with the exception of HDAC).

LR-relevant event	organizer / Xnr3 expression	SM Foxj1 expression	GRP / cell morphology	ciliogenesis	cilia polarization	leftward flow	somitic GRP gene expression	nodal cascade	situs
ATP4	-	+	-	+	+	+	-	bilateral	+
5-HT/ HTR3	+	+	+	+	+	+	+	absent	+
GJC	-	-	-	-	-	-	-	absent	+
Xwnt11b	-	minor	+	+	+	+	+	absent	?
PKD2	?	+	+	+	+	+	+	absent	+
xBic-C	?	?	?	+	+	+	+	absent	+

Figure Discussion-4: Comparison Of LR-Defects After Loss Of Wnt- And Ca²⁺-Signaling Components

Upper row: Processes which are relevant for normal LR-development.
Left column: Component targeted. Please see text for further details.
(+) = loss of component affected LR-relevant event, (-) = loss of component did not affect LR-relevant event, ? = effect was not determined so far, absent / bilateral = *Pitx2c* expression pattern in the LPM.

The Many Roles Of Wnt-Signaling In LR-Axis Development Of *Xenopus*

ATP4, 5-HT and Xwnt11b were all required for Wnt-signaling during LR-development, but revealed phenotypes which indicated overlapping and distinct functions of these components (Beyer et al. 2011) (Figure Dis-4).

These findings seem confusing – however, some useful hypotheses can be deduced from the presented results and previously published data (Figure Dis-5): (1) Early maternal Wnt/β-cat signaling is required for organizer induction and primary axes formation. (2) Post-MBT Wnt/β-cat is further required for *Foxj1* expression in the SM. (3) Wnt/PCP signaling aligns GRP cilia to the posterior pole of GRP cells during mid-neurula stages. (4) Wnt/Ca^{2+} (likely together with Wnt/PCP and Wnt/Ror2) is necessary for gastrulation movements and morphogenesis of prospective GRP cells during mid/late gastrulation and early neurulation. (5) Expression of genes in somitic GRP cells might be governed by Wnt/PKA in mid-neurula stages, maybe by crosstalk with the HH-pathway.

branch	Wnt/β-cat		Wnt/Ca^{2+} ?	Wnt/PCP	Wnt/PKA ?
location	early embryo	superficial mesoderm	deep dors. mesoderm	GRP	somitic GRP
target	primary axis induction	*Foxj1* & motile ciliogenesis	morpho-genesis	cilia polarization	*Xnr1*, *Coco* & *Derrierre*
Wnt compo-nents	cortical rotation & ligand driven	Xwnt8? Fz8	Xwnt11b Xwnt5a/b? Fz7?	Xwnt11b Xwnt5a/b? Fz7?	Xwnt11b Xwnt5a/b? Fz7?
process	AP-/DV-axis	flow generation	GRP morphogeneis	flow directionality	flow sensing

Figure Discussion-5: Proven And Hypothetical Influences Of Different Wnt-Signaling Processes In LR-development Of *Xenopus*

Please see text for details.
AP = anterior-posterior, DV = dorso-ventral, Fz = Frizzled, GRP = gastrocoel roof plate, PCP = planar cell polarity, PKA = protein kinase A and Xnr1 = *Xenopus* nodal related gene 1.

(1) Early effects on primary axis induction

Loss of 5-HT-signaling via HTR3 had the most severe phenotype, including loss of organizer gene expression (Vick 2009; Beyer 2011; Beyer et al. 2011). Organizer formation is a result of early maternal Wnt-signaling processes, and 5-HT/HTR3 seem to influence these processes (Heasman 2006). Serotonin-signaling probably acts prior to ATP4a-function and Xwnt11b in the SM (not including maternal-depletion of Xwnt11b; Tao et al. 2005). Notably, interference with organizer induction *per se* affects the setup of primary axes and LR-axis development. This was demonstrated by UV-irradiation of *Xenopus* embryos in which cortical rotation and organizer formation were disturbed (Danos et al. 1995). Even minor impairment of primary DV-axis induction affected formation of the dorsal mesoderm and notochordal gene expression, i.e. *Not* (called *Noto* in mouse) (von Dassow et al. 1993). *Noto* was required for PNC morphogenesis, Wnt/PCP, and *Foxj1* expression during mouse LR-development (Alten et al. 2012). A homologous mechanism in *Xenopus* seems likely, suggesting a requirement for coordinated organizer induction during *Noto*-dependent LR-development (Figure Dis-4 and Dis-5).

(2) Wnt/β-cat dependent expression of *Foxj1* in the SM

Effects on *Foxj1* expression in the SM and ciliogenesis at the GRP could be attributed to loss of post-MBT Wnt/β-cat signaling. *Foxj1* expression was least affected in *Xwnt11b* morphants, moderately affected in *ATP4a* morphants and severely affected after loss of 5-HT-signaling (Beyer et al. 2011). This process was mediated by the canonical Fz8 receptor, and restriction of *Fz8* expression to the dorsal mesoderm potentially limits the *Foxj1* expression domain towards more ventral portions of the mesodermal ring (Beyer 2011).

This conclusion is supported by the fact that the ventral mesoderm was equally competent to express *Foxj1* upon ectopic β-cat activation post-MBT. It is noteworthy that this was an essentially different finding than ventral expression of *Foxj1* after injection of Wnt-components as mRNAs (as described by Beyer 2011). mRNA injections of these signaling molecules induced a secondary organizer, therefore establishing dorsal fate in ventral cells (Sokol et al. 1991). Activation of the pathway post-MBT (by DNA injections) induced *Foxj1* expression in ventral mesoderm, without secondary organizer induction (not shown). These results indicated that ventral cell fate was not changed in this experimental setup.

A recent publication on *Foxj1* expression in the zebrafish KV has shown that *Foxj1* was a direct target of β-cat, which likely applies to *Xenopus* as well (Caron et al. 2011). Xwnt11b inhibition was insufficient for a robust loss of *Foxj1* expression in the SM, but experiments implicated that Wnt-ligands were required in this process.

Two non-canonical Wnt5-type ligands (*Wnt5a* and *Xwnt5b*) have been reported to be co-expressed with *Xwnt11b* during gastrulation (Cha et al. 2008; xenbase.org Bowes et al. 2009a, 2009b). *Foxj1* expression was equally decreased upon injection of *dnXwnt11b* DNA (not shown) as after *Xwnt11b*MO-mediated knock-down. Previous studies on the function of the *dnXwnt11b*-construct have shown that it also inhibits Wnt5-type ligands during *Xenopus* gastrulation (Smith et al. 2000; Tada et al. 2000). Therefore, a role of other non-canonical Wnt-ligands in *Foxj1* expression seems unlikely.

Wnt8a and *Wnt3a* were expressed around the KV, and loss-of-function altered LR-development in zebrafish (Caron et al. 2011). Xwnt8a is a canonical Wnt-ligand (Christian et al. 1991, 1993; Torres et al. 1996), and expression starts at the onset of gastrulation within the mesodermal ring (Christian et al. 1993). *Xwnt8a* is not expressed within the SM, however, diffusion could account for Wnt/β-cat signaling activation within the SM. *Xwnt3a* is expressed slightly later than *Xwnt8a*, and probably too late to account for *Foxj1* expression (expression profiles at xenbase.org Bowes et al. 2009a, 2009b). Hence, it is likely that *Foxj1* expression is activated by Xwnt8a via Fz8.

The *Foxj1* expression domain is potentially restricted to the SM by dorsal expression of the receptor (*Fz8*) and inhibition of signaling by secreted antagonists (e.g. Xsfrp2) towards ventral and animal aspects of the embryo (Figure Dis-4 and Dis-5).

(3) <u>Wnt/PCP dependent posterior polarization of GRP cilia</u>

In *ATP4a* morphants, Wnt/PCP dependent posterior localization of GRP cilia could be experimentally separated from Wnt/β-cat dependent induction of ciliogenesis by injection of *Foxj1* DNA. Moreover, several studies implicated that posterior localization of cilia requires the core-PCP component Vangl2 (Antic et al. 2010; Borovina et al. 2010; Song et al. 2010).

Inhibition of 5-HT signaling or Xwnt11b prevented cilia polarization as well, but these defects were accompanied by an increase in cell size. Alterations of cell size were not observed in *ATP4a* morphants or after loss of Vangl2 (Antic et al. 2010). Therefore, Wnt/PCP signaling seems to be specifically required for cilia localization, but not for cell-size regulation.

In accordance with other studies, Fz8 loss-of-function did not inhibit gastrulation movements, and polarization of remaining GRP cilia was not affected (Tada et al. 2000; Beyer 2011). These findings implicated that Fz8 mediated only canonical Wnt-signaling during LR-development. The non-canonical receptor Fz7 was reported to regulate Wnt/PCP and CE in *Xenopus*, and to interact with Xwnt11b (Djiane et al. 2000). *Fz7* is expressed in the SM during gastrulation and in the GRP during neurulation (e.g. st 14; xenbase.org Bowes et al. 2009a, 2009b). Taken together, Fz7 is a strong candidate for the receptor which regulates Wnt/PCP dependent cilia polarization in the GRP.

Gradients of non-canonical Wnt-ligands were reported to provide the initial cue for Vangl2-dependent alignment of cells in vertebrates (Gao et al. 2011). This was shown to occur via the Wnt/Ror2-pathway, but Xwnt11b did not act via this pathway during *Xenopus* gastrulation (Schambony et al. 2007; Gao et al. 2011). This suggested that the Wnt/Ror2 signaling branch is not required for cilia polarization in GRP cells.

The expression of *Xwnt11b* (and other Wnt5-type ligands) in involuting cells of the CBC (which are located posterior to the GRP) could generate such a ligand gradient and subsequent posterior localization of GRP cilia (Cha et al. 2008; expression profiles xenbase.org Bowes et al. 2009a, 2009b). This hypothesis needs to be addressed in further experiments, targeting Fz7 and Wnt5-type ligands by loss-of-function experiments, and archenteron injections of extracellular Wnt-inhibitors (e.g. Xsfrp proteins). Generation of a cilia-driven rightward-flow by an inverted gradient could be tested as well by: (a) Depletion of endogenous non-canonical Wnt-ligands (during/after involution of the SM, e.g. by caged or photoactivated MOs), and (b) application of protein-soaked beads anterior to the GRP. This inverted gradient could lead to anterior localization of GRP cilia and, consequently, a rightward flow of extracellular fluids (Figure Dis-4 and Dis-5).

(4) <u>CE, cell size regulation and expression of genes in somitic cells of the GRP</u>

In addition to Wnt/PCP, other non-canonical pathways regulate gastrulation movements and blastopore closure in *Xenopus*: Wnt/Ca^{2+}, Wnt-Ror2 and Wnt/PKA (Kühl et al. 2000; Kohna et al. 2005; Park et al. 2006; Schambony et al. 2007). While gastrulation phenotypes were rarely encountered in *ATP4a* morphants, loss of 5-HT signaling or Xwnt11b frequently impaired full blastopore closure. Xwnt11b-signaling acts in synergy with Xbra in CE of the dorsal mesoderm (Tada et al. 2000). Andre (2009) has demonstrated that loss of Xbra perturbs morphogenesis of the GRP and *Xnr1* expression in somitic cells of the GRP.

Xwnt11b was shown to be only required for non-canonical Wnt-signaling during gastrulation (Smith et al. 2000; Tao et al. 2005). Wnt11-type ligands can act via Wnt/PCP, Wnt/Ca^{2+} and Wnt/PKA, suggesting that 5-HT/Xwnt11b-signaling could be required for activation of additional signaling branches, beyond Wnt/β-cat and Wnt/PCP (Uysal-Onganer et al. 2012).

Interference with Xwnt11b- or 5-HT-signaling also increased cell size in the GRP and reduced expression of genes in lateral cells of GRP, i.e. *Xnr1* and *Coco*. In conclusion, these effects could potentially be ascribed to non-canonical Wnt-signaling defects, apart from Wnt/PCP.

The following model tries to integrate Ca^{2+}-, Wnt- and Wnt/Ca^{2+}-signaling in the regulation of gastrulation movements/GRP formation, cell size regulation and gene expression in somitic cells of the GRP (Figure Dis-5):

During early stages, 5-HT/HTR3-signaling might regulate general Ca^{2+}-homeostasis. This is required for canonical Wnt/β-cat signaling and organizer induction. *Xenopus* Bicaudal C (xBicC) and PKD2-dependent Ca^{2+}-waves could activate *Xzic3* expression in the dorsal mesoderm of the gastrula. Xzic3 is required for inhibition of β-cat and possibly de-repression of non-canonical Wnt-signaling. Mesodermal Xwnt11b activates non-canonical Wnt-signaling of various branches. Wnt/PCP is Dvl-/ATP4-dependent and required in the GRP to mediate posterior localization of cilia. Xwnt11b-activated Wnt/Ca^{2+} signaling is potentially required for sustained inhibition of Wnt/β-cat signaling in the SM/GRP, therefore promoting gastrulation movements and blastopore closure. Both processes require Dvl-

function as well. Wnt-dependent regulation of intracellular Ca^{2+}-levels might regulate cell size in GRP cells. In somitic cells of the GRP, higher *xBicC* levels inhibit Dvl-mediated signaling, i.e Wnt/PCP dependent posterior localization of cilia and Wnt/Ca^{2+} signaling could be prevented. Inhibition of Dvl-dependent signaling in somitic cells might increase activation of the Wnt/PKA-branch. Gli3 is not activated by HH-signaling in these cells, and activated PKA could cleave Gli3, turning it into a repressor (Gli3R). Gli3R could regulate target gene repression in these cells with the help of Xzic3. Down-regulation of HH-target genes could facilitate gene-expression in the somitic cells required for flow sensing, i.e. *Xnr1*, *Coco* and *Derierre* .

Several lines of evidence support such a model:

(4. A) Ca^{2+} and *Xenopus* LR-development

Cell size control in epithelial cells was implicated to depend on regulation of intracellular Ca^{2+}-levels (Schreiber 2005; Mongin et al. 2011). Increased cell size was also reported after loss of Wnt11-function in the zebrafish KV (Oteiza et al. 2010). HTR3 is an atypical 5-HT receptor, which was previously shown to mediate Ca^{2+}-influx in epithelial cells (Doran 2004).

Increase in cell size and loss of *Xnr1*/*Coco* expression were also observed after interference with the Ca^{2+}-channel PKD2 during gastrulation in *Xenopus* (Vick 2009), and LR-defects were reported in the zebrafish (Bisgrove et al. 2005). Depletion of endoplasmatic Ca^{2+}-stores by application of thapsigargin during gastrulation or neurulation caused LR-defects as well (Schneider et al. 2008; Tingler 2011).

Ca^{2+}-waves were observed in *Xenopus* embryos during gastrulation, and experiments indicated that they were required for cell polarity and CE movements (Wallingford et al. 2001; Kohna et al. 2005; Kreiling et al. 2008).

In conclusion, Ca^{2+}-homeostasis and Ca^{2+}-dependent processes are a prerequisite for gastrulation and LR-development.

(4. B) <u>Functions for Ca^{2+}-signaling in SM-patterning and GRP-morphogenesis</u>

Ca^{2+}-release from intracellular stores during late blastula/early gastrula stages was required for induction of *Xzic3* expression (Leclerc et al. 2003). *Xzic3* was expressed in the deep dorsal mesoderm, and was a regulator of LR-development in vertebrates (Ware et al. 2006; Cast et al. 2012). *Xzic3* expression was also under control of Xbra in *Xenopus* (Kitaguchi et al. 2002). *Xzic3* could block β-cat to activate target gene expression, and *Xzic3* expression was necessary for CE (Fujimi et al. 2011; Cast et al. 2012).

It is thought that canonical and non-canonical Wnt-signaling branches can inhibit each other, although a parallel activation of Wnt/β-cat and Wnt/PCP was shown in certain tissues (Torres et al. 1996; Li et al. 2008). Expression of *Xzic3* in a Ca^{2+}-dependent manner could thus be required to release β-cat dependent inhibition of non-canonical branches in the dorsal mesoderm. Furthermore, manipulation of Wnt-signaling affected Ca^{2+}-wave frequency, also indicating interaction between Wnt- and Ca^{2+}-signaling during gastrulation (Kohna et al. 2005). Hence, *Xzic3* expression should be analyzed by WMISH after thapsigargin treatment or MO-mediated loss of PKD2/HTR3 function.

(4. C) <u>Xzic3 and the regulation of gene expression in somitic GRP cells</u>

The somitic expression *nodal* in the mouse was regulated by *Zic3* as well, and gain of *Xzic3* in frog enhanced expression of *Xnr1* (Ware et al. 2006; Maurus et al. 2009). Although this regulation was mediated by the 2.7 kb *nodal* enhancer region, the nature of the regulatory process remained obscure. Zic3 belongs to the superfamily of Gli transcriptional regulators and is known to enhance target gene activation by physical interaction with Gli3 (Zhu et al. 2008). However, a Gli3-binding site was not found within the 2.7 kb *nodal* enhancer region (Ware et al. 2006).

Hedgehog (HH) signaling, which is the main regulator of Gli3-mediated transcriptional control, was dispensable for early LR-development. It was required in the mouse for the competence of the LPM to respond to nodal cascade activation (Tsiairis et al. 2009). Therefore, is seems unlikely that Zic3 and Gli3 depend on HH-signaling in the GRP. This could be tested by analysis of gene-expression and morphology at the GRP after application of cyclopamine during gastrulation/neurulation.

(4. D) <u>xBicC/Gli3/PKA and the regulation of somitic gene expression</u>

Xenopus Bicaudal C (xBicC) was required for inhibition of Dvl-dependent canonical Wnt-signaling (Maisonneuve et al. 2009). Loss of xBicC caused cilia mispolarization, flow-defects and loss of gene expression at the somitic GRP (Maisonneuve et al. 2009; Montino 2011). xBicC was further implicated in post-transcriptional regulation of PKD2 via micro RNA (miR) 17 (Tran et al. 2010). In this scenario, xBicC repressed the miR-17 dependent translational inhibition and degradation of *PKD2* mRNA.

xBicC mediates inhibition of Dvl-dependent Wnt-signaling and might thus prevent posterior localization of cilia in lateral domains of the GRP (where it was stronger expressed than in the medial GRP) (Blum et al. 2007; Schweickert et al. 2007; Maisonneuve et al. 2009; Vick 2009).

Gli3 was also proposed to be dependent on miR-17 post-transcriptional regulation (Tran et al. 2010). Hence, one could imagine that a miR-17 regulating process involving xBicC acts in the dorsal mesoderm and controls the presence of Gli3 and PKD2 proteins. Gli3-mediated events can occur in two flavors: Gli3 can act as transcriptional activator or inhibitor of target genes (Jiang et al. 2008). These functional differences of Gli3 were mediated at the basal body of cilia by PKA-dependent modification of the protein (Chen et al. 2007).

Wnt1- and Wnt7a-mediated regulation of PKA-activity controlled the myogenic program via transcriptional regulation of CREB and other factors in the paraxial mesoderm of the mouse (Chen et al. 2005). Ca^{2+}-signaling was required for correct paraxial mesoderm development in *Xenopus* as well (Ferrari et al. 1999; Kohna et al. 2005). Therefore, the transcriptional repressor version of Gli3 (enhanced by Xzic3) could act on target genes in somitic (paraxial) GRP cells. This in turn could mediate competence for *Xnr1*, *Coco* and *Derierre* expression, which did not require HH-signaling activation (Tsiairis et al. 2009). If this idea is applicable, MO-mediated knock-down of Gli3 or pharmacological inhibition of PKA-activity should reduce expression of *Xnr1*, *Coco* and *Derierre*.

Taken together, one can distinguish between (at least) five phases and modes of Wnt-signaling during GRP formation, generation of leftward flow and mediation of laterality cues from the midline to the LPM (Figure Dis-5).

The Inductive Potential Of A Weak Cilia-Driven Flow Argues In Favor Of The Two-Cilia Model

In addition to the setup of the GRP and leftward flow, the interpretation of flow-generated signals is a prerequisite for LR-development. Inhibition of cilia-driven fluid flow by knock-down of ciliary motor-proteins or increase of fluid viscosity prevented expression of asymmetric genes in the LPM (Schweickert et al. 2007; Vick et al. 2009). In *ATP4a* morphants, a weak and turbulent flow was sufficient to induce the nodal cascade bilaterally, in the absence of midline-barrier defects (Cheng et al. 2000). Moreover, a recent report claimed that only two rotating cilia were required to induce the nodal cascade in mouse embryos (Shinohara et al. 2012). Both findings indicate that sensing of leftward flow might be much more sensitive than previously estimated. Four conclusions can be drawn:

(1) Cilia-dependent symmetry breakage is a very robust process, which can cope with dramatic loss of ciliation and still account for correct LR-development.

(2) Bilateral expression does not always indicate midline-barrier defects, therefore, it might be worth to (re-)investigate ciliation and flow-patterns in experimental conditions when bilateral nodal cascade induction is/was predominant.

(3) Vertebrate symmetry-breakage does not require a large ciliated epithelium during development, as only two rotating cilia were the minimum requirement for nodal cascade induction in the mouse (Shinohara et al. 2012).

(4) Even small changes in flow patterns and velocity might be potentially sensed in systems like the kidney or the ependyma, where fluid flows regulate functions in adult tissue, and dysfunction was associated with human disease (Sawamoto et al. 2006; Wessely et al. 2008).

Despite the very sensitive flow-detection mechanism, it was surprising to see that turbulent flow on the left side enhanced induction of the nodal cascade on the right side of the GRP. The nature of cilia-driven flows is that of low Reynolds numbers (Freund et al. 2012). The Reynolds number characterizes the influence of inertia and viscosity on fluid dynamics. When the Reynolds number is small, viscosity is the dominating factor. Hence, a particle

stops when it is not actively moved by a cilium. The results from epistatic experiments in this study and the results obtained by Shinohara et al. (2012) therefore argue against a morphogen-based model of symmetry breakage and favor the two-cilia model (Figure Dis-6).

The two-cilia model proposes that sensory cilia at the lateral edges of the flow-generating structure (GRP, node/PNC, KV) detect fluid flow by deflection (McGrath et al. 2003; Norris et al. 2005; Hirokawa et al. 2006, 2009; Hamada 2008; Vick et al. 2009; Field et al. 2011; Kamura et al. 2011; Hirokawa et al. 2012). As Shinohara et al. (2012) pointed out in their discussion, mechanical motion of fluid (a "wave") can be transmitted fast and at distance, even when Reynolds numbers are low. In conclusion, flow on the contra-lateral side of the GRP can be relevant for symmetry breakage within the two-cilia model. Thus, only when flow is completely ablated (e.g. loss of ciliary motion by*Dnah9*MO), induction does not take place (Vick et al. 2009).

Experiments by Vick et al. (2009) revealed that nodal cascade induction was inhibited upon loss of cilia-driven flow on the left side of the GRP. This was somewhat contradictory to the findings discussed above. A possible explanation for the lack of nodal cascade induction in unilaterally injected *Dnah9* morphants could be the presence of immobilized motile cilia on the left side of the GRP. These cilia might act like "wave breakers" and interfere with the fluid motion generated by rotating cilia on the right side, thereby preventing deflection of sensory cilia on the left side. This idea could be tested in experiments which specifically target the formation of motile cilia on the left side of the GRP, without affecting sensory cilia. However, such an experimental separation will be hard to achieve with techniques available to date.
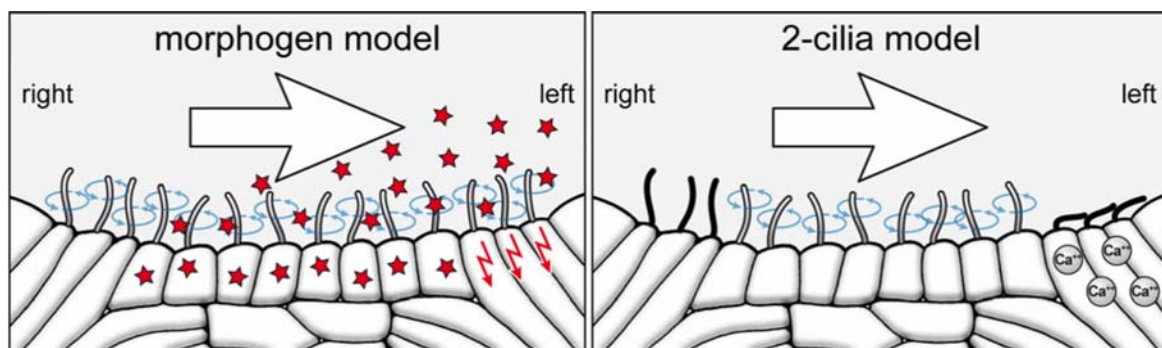
Figure Discussion-6: Two Models Of Flow Sensing In LR-Development

Morphogen model (left panel). In this illustration the molecules (red stars) are secreted from the ciliated epithelium. **2-cilia model** (right panel) with motile cilia at the center and immotile sensory cilia at the margin of the ciliated epithelium. These would initiate a Ca^{2+}-signal.
Please see text for further details. Illustration and text taken from: *Vick 2009[###]*.

Evolution Of Symmetry-Breakage And LR-Axis Development

LR-axis asymmetries and asymmetric nodal cascade expression was found in protostomes as well as deuterostomes (Levin et al. 1995; Blum et al. 2009; Schweickert et al. 2011; Hirokawa et al. 2012). This indicated that asymmetric nodal expression and LR-axis development were features of the urbilateria, about 600 million years ago (Robertis et al. 1996).

(1) Symmetry-breakage in deuterostomes

In this study, I have shown that the proton pump ATP4a was required for Wnt-dependent ciliation and ciliary function in the frog *Xenopus*. The fact that inhibition of ATP4 caused LR-defects throughout the deuterostomes strongly suggested that ATP4-dependent Wnt-signaling events were highly conserved in this lineage (Levin et al. 2002; Hibino et al. 2006; Shimeld et al. 2006; Gros et al. 2009). Therefore, this connection probably emerged with the evolution of ATP1-like ATPases into proton pumps (ATP4 and ATP12). It was proposed that this event took place after separation from the protostomes (Axelsen et al. 1998; Okamura et al. 2003).

Flow-mediated symmetry-breakage was so far confirmed for the mouse, rabbit, frog, axolotl and two fish species (Nonaka et al. 1998; Essner et al. 2002, 2005; Okeda et al. 2005; Feistel et al. 2006; Blum et al. 2009; Schweickert et al. 2011). In contrast, cilia-independent mechanisms were proposed for the pig, chick, urochordates and echinoderms (Levin 2003; Tabin 2006; Levin et al. 2007; Aw et al. 2009; Gros et al. 2009; Vandenberg et al. 2009; Vandenberg 2012; Thompson et al. 2012).

(1. A) Symmetry breakage in vertebrates and the "chick problem"

In the pig and in birds, morphological asymmetries of the node (the equivalent of Spemann's organizer) were reported to initiate asymmetric gene expression (Blum et al. 2009; Gros et al. 2009). At least in birds, this node-asymmetry was generated by ATP4-dependent cell migration (Gros et al. 2009). Asymmetric cell migration of node cells was proposed to follow the asymmetric function of ATP4, but no asymmetries in expression patterns were reported, and a mechanism which could account for these functional asymmetries was not elucidated so far. (Levin et al. 2002).

Serotonin-signaling, ATP6- and K$^+$-channel-function, and GJC were also shown to be necessary for correct LR-development in the chick (Levin et al. 2002; Gros et al. 2009; Vandenberg et al. 2009; Zhang et al. 2009). They were proposed to act in an "ion-flux" mechanism of symmetry breakage. In contrast to *Xenopus*, where these factors were suggested to act very early in development, the function in LR-asymmetry of the chick was attributed to gastrula/neurula stages (Levin et al. 2002, 2007). This is the time-frame in which our group has found connections of these factors to cilia-dependent symmetry breaking events in *Xenopus*, i.e. generation of flow and transfer of asymmetric cues from the midline to the LPM (Beyer et al. 2011; Beyer et al. 2012; Walentek et al. 2012).

Preliminary data revealed presence of *Foxj1* expression in the chick prior to asymmetric cell migration (Geyer 2010). A large ciliated epithelium was not detected, however, some cilia were present before and during asymmetric migration of node cells (Geyer 2010). Experiments in frog and mouse embryos demonstrated that a weak flow and as few as two cilia were sufficient to break symmetry (Shinohara et al. 2012). This argued against the requirement for a large ciliated epithelium in symmetry breakage of the chick as well.

Studies on Talpid3 (ta3) in chick, which was required for cilia assembly, argued against a ciliary mechanism for symmetry-breakage in birds: The ta3 mutant developed normally in terms of LR-axis formation, but cilia-dependent HH-signaling in the limb and other organs was compromised (Ede et al. 1964; Davey et al. 2006; Tabin 2006).

Recently, experiments on ta3 in zebrafish revealed that zygotic depletion did not significantly perturb LR-development, but late developmental events were affected (e.g. pronephros development). When maternally derived transcripts were targeted as well, ciliogenesis in the KV and LR-development were compromised (Bangs et al. 2011; Ben et al. 2011). This suggested that a separation of maternal and zygotic effects of ta3 in the chick could be possible as well.

HH-signaling around the chick node was required for asymmetric gene expression in the LPM and correct laterality (Levin et al. 1995). The fact that ta3-mutant chick embryos developed a normal LR-axis argued against a loss of ciliation during early stages: Primary cilia seemed to be present and capable of HH-signaling transduction – hence, probably maternally contributed ta3 mRNA or protein might compensate for loss of zygotic *ta3* during early development and symmetry-breakage of the chick.

Taken together, it is tempting to speculate that ATP4-dependent *Foxj1* expression, motile ciliogenesis and cilia polarization act upstream of node asymmetry in birds. This is supported by experiments of Zhang et al. (2009), which demonstrated involvement of Vangl2 in chick symmetry-breakage. The authors presented an "ion-flux" related explanation: Blastoderm cells located on the left and right side already know about their left or right "identity" from earlier cues and Vangl2 mediates imprinting. A direct link between Wnt/PCP and direction of cell migration might be envisaged to account for asymmetric morphology of the node and gene expression, but would still require a LR-biasing mechanism (Aw et al. 2009; Wan et al. 2011). It could thus not account for generation of *de novo* asymmetry, which was required for LR-development in the chick as well (Levin et al. 1997).

As discussed above, Vangl2 was required for alignment of cells along a gradient of non-canonical Wnt-ligands in mammalian cells (Gao et al. 2011). Beyond that, Wnt/PCP and Vangl2 governed posterior localization of cilia within the GRP/PNC (Antic et al. 2010; Borovina et al. 2010; Song et al. 2010). Non-canonical Wnt-ligands are expressed around the primitive streak of the chick and were required for gastrulation movements, like in *Xenopus* and the mouse (Hardy et al. 2008). Therefore, I would like to propose that Vangl2 localization within blastoderm cells of the chick was correlated with gastrulation movements towards the streak. Hence, loss of Vangl2-function in the chick might have prevented correct gastrulation and cilia polarization, which in consequence could have affected LR-development (Harrisson 1989; Tada et al. 2000; Hardy et al. 2008; Zhang et al. 2009; Antic et al. 2010; Song et al. 2010).

Therefore, loss of Foxj1-function, cilia motility or bathing the embryo in methyl-cellulose should all prevent asymmetric node-cell migration and asymmetric gene expression in chick as well. This will be tested in future experiments in order to resolve conservation of symmetry-breakage in vertebrates.

(1. B) Symmetry breakage in urochordates and echinoderms

ATP4-dependent LR-asymmetries were reported in urochordates and echinoderms (Hibino et al. 2006; Shimeld et al. 2006):

In urochordates, head/brain structures were asymmetric, i.e. right-asymmetric sensory cells, and the tail of the larva bended towards the left side within the vitelline membrane (Nishide et al. 2012). Moreover, nodal cascade activation occured asymmetrically on the left side, like in vertebrates (Blum et al. 2009). In *Ciona intestinalis*, inhibition of ATP4 during gastrula and neurula stages caused aberrant *Pitx* expression (Shimeld et al. 2006). Interestingly, bilateral expression was found in up to 40% of treated embryos, suggesting a similar function of ATP4 in urochordate LR-development, as seen in *Xenopus* (Levin et al. 2002; Shimeld et al. 2006).

Two recent publications readdressed LR-development in urochordates (Nishide et al. 2012; Thompson et al. 2012). In *C. intestinalis* and *Halocynthia roretzi*, posterior localized cilia were found in the ectoderm during neurulation and before the onset of asymmetric gene expression. While one study, judged by morphological analysis of cilia, claimed that these were not motile (Thompson et al. 2012), the other study has linked motility of cilia to LR-development: Nishide et al. (2012) demonstrated that different species of urochordates (including *C. intestinalis*) rotated within the vitelline membrane. Rotation in *H. roretzi* stopped when the left side of the embryo started to express *nodal* (Nishide et al. 2012). These experiments revealed an unexpected but tempting mechanism for cilia-driven symmetry-breakage in urochordates, which could unify symmetry-breakage in vertebrates and urochordates.

In radial-symmetric adult echinoderms (sea urchins, starfish, etc.), the bilateral symmetric body-plan was lost during evolution (Duboc et al. 2005; Hibino et al. 2006; Amemiya 2007; Smith et al. 2008). However, the echinoderm pluteus larva is bilaterally symmetrical, and the adult develops from only one of the paired coelomic sacs (Hibino et al. 2006). During this developmental process, asymmetric nodal cascade expression within the coelomic sacs decided from which of the paired anlage the adult animal emerged (Hibino et al. 2006).

Like in urochordates and in *Xenopus*, inhibition of ATP4 in sea urchins affected the expression of asymmetric genes and asymmetric development, i.e. formation of the adult rudiment in only one of the coelomic sacs (Hibino et al. 2006). During gastrulation, motile cilia were present and a rotational movement of the larva could be observed during these stages of development, which probably preceded asymmetric gene expression (Soliman 1983, 1984; Duboc et al. 2005; and Schweickert unpublished observation). In the light of the experiments presented in this study and data on urochordate symmetry-breakage, it is attractive to propose that cilia-driven rotational movement of the gastrula might break symmetry in echinoderms as well. This possibility should be addressed in future experiments, e.g. by manipulation of swimming and analysis of ciliation after pharmacological inhibition of ATP4.

In summary, it seems possible that ATP4- and cilia-dependent events control LR-axis patterning throughout the deuterostomes.

(2) Symmetry breakage in protostomes

Asymmetries in the cleavage pattern were ascribed to be instructive for asymmetric *nodal*/*Pitx* expression and morphogenesis in snails (Grande et al. 2009; Kuroda et al. 2009; Oliverio et al. 2010). Asymmetric gene expression was shown to start during trochophora stages (Grande et al. 2009). Timing of expression implicated that symmetry-breakage and nodal cascade activation slightly preceded these stages in snails (Schweickert et al. 2011). This seems to be a comparable developmental stage to gastrulation/neurulation stages, when symmetry is broken in (most) deuterostomes (Blum et al. 2009). Furthermore, a rotational movement of pre-trochophora and early trochophora larvae was reported (Kuang et al. 2002; Byrne et al. 2009; Shartau et al. 2010). In conclusion, cilia-driven rotational movements of the embryo seems to be a suitable mechanism for symmetry-breakage in snails (like in urochordates and echinoderms).

It is possible that maternal cues (like in *Xenopus*) establish DV-axis by asymmetric cleavages one and two in spiralian embryos, and that this DV-information is in turn instructive for micromere positioning in respect to macromeres, e.g. by affecting the plane of cleavage (Grande 2010). Micromere positioning (and the angle in respect to macromeres) could determine cilia-dependent swimming direction (Vladar et al. 2009; Grande 2010). Cleavage-plane determination involved actin-dependent processes, which

also mediated cilia polarization in vertebrates (Azoury et al. 2009; Vladar et al. 2009; Song et al. 2010). Hence, actin-dependent determination of the cleavage-plane in comparison to swimming behavior could be attractive targets for future experiments. This could be investigated by incubation of snail embryos in methyl-cellulose or actin inhibitors, followed by analysis of micromere arrangement, asymmetric gene-expression and ciliation.

Thus, I would like to speculate about a conserved organizer- and cilia-dependent mechanism, which breaks symmetry in proto- and deuterostomes (Figure Dis-7):

Fluid motions are generated either by rotational movement of larvae or by generation of a leftward-flow. These fluid motions are sensed by deflection of cilia and concomitant Ca^{2+}-influx. This would mean that during evolution, motile cilia on the embryonic surface would have been incorporated into the primitive gut, which might also offer an explanation why symmetry-breakage is still developmentally connected to the gastric proton pump ATP4 (Figure Dis-7).

Figure Discussion-7: Hypothetical Evolution Of Cilia-Driven Symmetry-Breakage

(A) Schematic representation for symmetry-breakage by larval rotation within the vitelline membrane.
(B) Schematic representation for symmetry-breakage by leftward flow at the GRP.
(C) Schematic representation of the hypothetical evolution of cilia-driven symmetry-breakage from the urbilateria (last common ancestor of protostomes and deuterostomes) to modern protostomes (e.g. snails) and deuterostomes (e.g. sea urchins, ascidians, modern fish, amphibians, birds and mammals). Evolutionary events are indicated in red and mode of symmetry-breakage is indicated in blue. Please see text for further details.
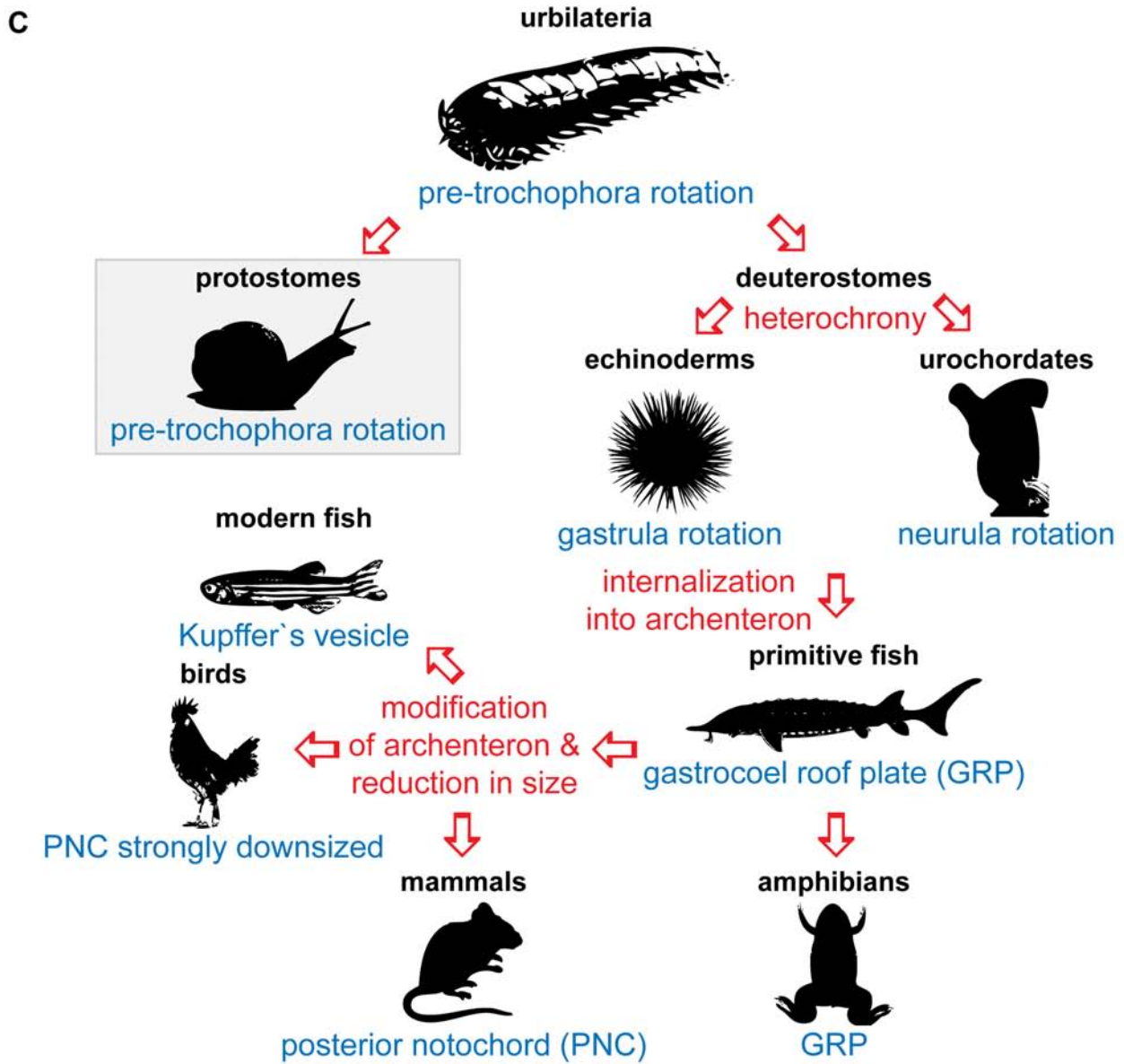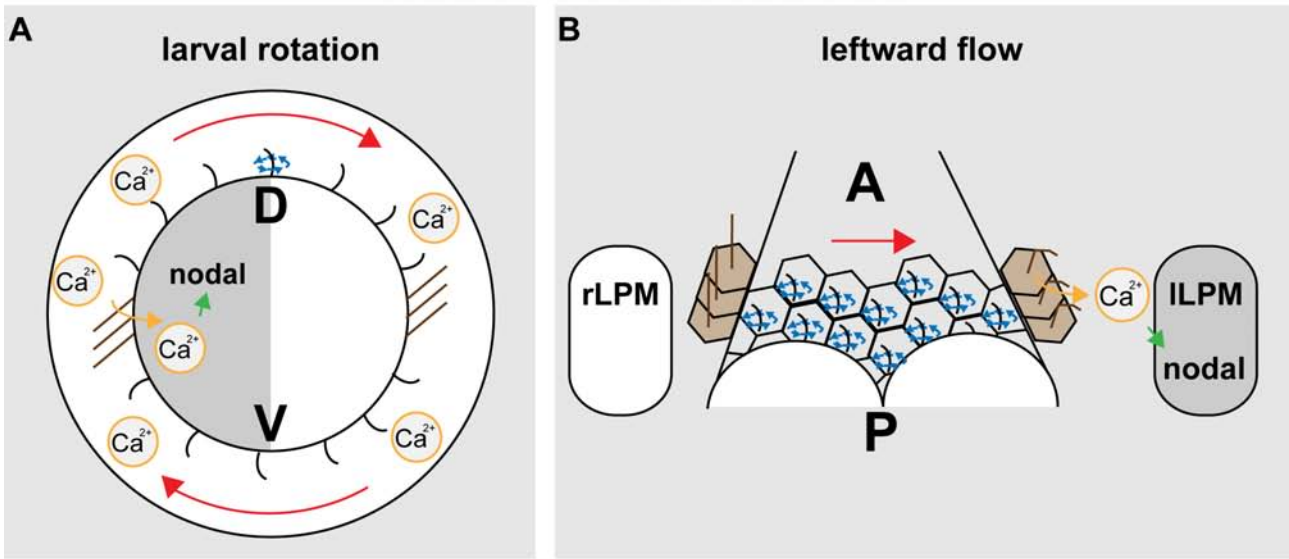
ATP4a And The Regulation Of *Foxj1* Expression In Ciliated Epithelia During *Xenopus* Development

ATP4a And Wnt-Signaling In The Mucociliary Epithelium Of The Skin

The ciliated *Xenopus* skin epithelium was proposed to serve as a model for the investigation of conserved mechanisms in mucociliary epithelia (MCE) development and function (Look et al. 2001; Hayes et al. 2007; Dubaissi et al. 2011). MCEs are broadly found in animals and humans, e.g. MCEs are lining the airways, the oviduct and the ependyma (Norris et al. 2012). The *Xenopus* skin MCE consists of mucus secreting goblet cells from the outer cell layer and cell types derived from the deep ectodermal layer, i.e. multiciliated cells (MCCs) and ion secreting cells (ISCs) (Stubbs et al. 2008; Quigley et al. 2011; Dubaissi et al. 2011; Stubbs et al. 2012).

Tryptophan-hydroxylase- (TPH) expressing and 5-HT-secreting cells (TASCs) constituted a novel cell type of the skin, which regulated ciliary beat frequency (CBF) in MCCs (Thumberger 2011). The small apical surface (in comparison to goblet cells) and sensitivity to Notch/Delta-signaling manipulation were common features of TASCs, MCCs and ISCs (Deblandre et al. 1999; Quigley et al. 2011). Thus TASCs are likely derived from the deep ectodermal layer as well. However, direct experimental evidence still needs to be provided by transplantation of cells from the outer epithelium of a wildtype embryo on deep ectodermal cells of a fluorescent host (Stubbs et al. 2012). When TASCs also intercalate from the deep layer, 5-HT vesicles should be found in fluorescent cells from the host embryo.

While goblet cells, MCCs and ISCs have been also described in human MCEs, TASCs have not been described in human tissue so far (Mucenski et al. 2005; Ross et al. 2007). However, functional studies established a link between 5-HT and coordinated Ca^{2+}-elevation via HTRs in human airway epithelia (Bayer et al. 2007). Serotonin was also able to regulate CBF in the mouse, and Ca^{2+} was an important regulator of CBF in many other tissues (Doran 2004; Katow et al. 2007; König et al. 2009; Schmid et al. 2011). Hence, Ca^{2+}-influx by activated cilia-localized HTR3 receptor-channels (Thumberger 2011) could be a possible mechanism how 5-HT from TASCs regulates CBF in *Xenopus*. The 5-HT/Ca^{2+}/CBF-regulatory module was also present in lower deuterostomes and

protostomes (Kuang et al. 2002; Doran 2004; Katow et al. 2007). Therefore, the regulation of CBF seems to be a conserved and ancient mechanism in MCEs from various animals and humans.

This study revealed that ATP4a-mediated Wnt/β-cat signaling was not only required for *Foxj1* expression in the SM, but also in the skin MCE. When DNA expression vectors encoding ATP4a, Foxj1 or Wnt/β-cat were co-injected in *ATP4a* morphants, cilia-driven flow and ciliation were rescued. These experiments suggested that the skin MCE and the SM underlie a common mechanism of transcriptional control for the generation of motile cilia.

In the *Xenopus* skin, Notch-signaling activation inhibited MCC- and ISC-formation, while inhibition promoted specification of these cell types (Deblandre et al. 1999; Ross et al. 2007). In contrast to MCCs and ISCs, TASCs required Notch-signaling activation and appeared later in development (Deblandre et al. 1999; Quigley et al. 2011). This could constitute a functional backup, which guarantees robust mucus flow over the skin ectoderm: When less MCCs are specified during early MCE-development, more TASCs can appear at later stages, which in turn stimulate higher CBF. This idea could be tested by quantitative analysis of fluid flow velocity and cell type abundance after mild manipulations of Notch/Delta-signaling in tadpoles.

MCCs and ISCs had in common that they needed to intercalate into the outer epithelium after specification (Quigley et al. 2011). In *ATP4a* morphants, cells with apically enriched but disorganized tubulin were found within the outer epithelium. ISCs were unaffected. This suggested that in MCCs and ISCs cell-fate specification took place and that both cell types could intercalate. Beyond the role of *Foxj1* in transcriptional activation of the ciliogenesis program, earlier studies proposed that actin-dependent basal-body docking to the apical membrane was deficient after loss of *Foxj1* in MCCs (Huang et al. 2003; Pan et al. 2007). This was in good agreement with the subcellular phenotype in *ATP4a* morphants. Interestingly, when *β-cat* or *Foxj1* DNAs were over-expressed in *ATP4a* morphants, more tubulin-positive cells were observed in the MCE. This could indicate that in addition to MCCs ISCs were forced to start the ciliary program, but failed to form cilia. RhoA GTPase activity was required for apical docking of basal-bodies and cilia outgrowth in MCCs, downstream of Foxj1 (Pan et al. 2007). RhoA-activity was regulated by Wnt/PCP and acted downstream of ATP4a (and independent of Wnt/β-cat) in CE. *Foxj1* was

sufficient to rescue ciliation rate at the GRP, but not Wnt/PCP dependent posterior localization of cilia. Therefore, it is tempting to speculate that ATP4a not only controls Wnt/β-cat dependent expression of *Foxj1*, but also Wnt/PCP and RhoA dependent docking of basal bodies in the skin. Wnt/PCP was also shown to align cilia beating in the *Xenopus* skin and, thereby, to control the directionality of cilia-driven flow (Mitchell et al. 2007, 2009). Whereas cilia-driven flow was virtually absent in *ATP4a* morphants, rescue by *β-cat* and *Foxj1* DNAs could restore fluid flow. However, directionality was not re-established, suggesting a similar separation of Wnt/β-cat and Wnt/PCP defects, as demonstrated for GRP cilia.
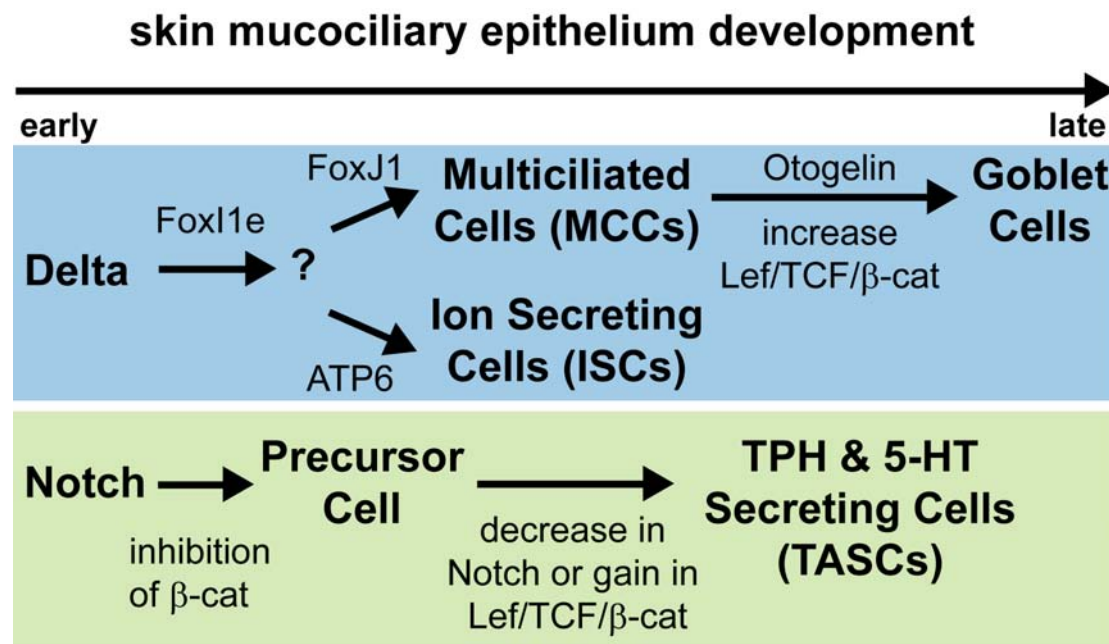
Figure Discussion-8: Model Of Skin Mucociliary Epithelial Development In *Xenopus*

Relative developmental time is indicated by arrow (upper-most).
Delta-signaling dependent development of MCCs and ISCs (incl. additional factors) is represented in the light blue box. Please note that this model suggests a Wnt-dependent transformation of MCCs into goblet cells during later development (not further discussed in the text). Notch-signaling dependent development of precursor cells and TASCs is depicted in the green box. Please see text for further details.

Such a separation of Wnt-dependent events during MCE-development can be tested by analysis of basal-body docking (using γ-tubulin staining) in *ATP4a*MO injected specimens. Alignment of basal-bodies in *ATP4a* morphants and morphants rescued by *Foxj1* can be analyzed as well (by Mig12-GFP; Hayes et al. 2007). Rescue of *ATP4a* morphants with *ATP4a* DNA was more efficient in restoring ciliation than rescue with *Foxj1* or *β-cat* DNAs, supporting this notion. Furthermore, increased numbers of tubulin-positive cells were observed, implicating that gain of *ATP4a* could result in a gain of Wnt/β-cat signaling and *Foxj1* expression in the MCE.

Experiments suggested that expression of *TPH* and possibly *Otogelin* were regulated by ATP4a-dependent Wnt/β-cat in TASCs and goblet cells, respectively. In MCCs and TASCs, Wnt-signaling was downstream of Notch/Delta-signaling and probably accounted for cell-type maturation. Presence of Wnt-signaling is also a shared feature of MCEs from *Xenopus*, mouse and humans (Mucenski et al. 2005; Park et al. 2006; Ross et al. 2007). Wnt-signaling thus needs to be incorporated into the conserved tool-box of signaling pathways during MCE-development, in addition to Notch/Delta-signaling (Figure-Dis-8).

ATP4a And Canonical Wnt-Signaling In The Floor Plate

Foxj1 expression in the floor plate was attributed to Shh-dependent activation of the HH-pathway in the zebrafish (Yu et al. 2008). In *Xenopus*, gain of *β-cat* in the floor plate lineage restored *Foxj1* expression in *ATP4a* morphants and after inhibition of the HH-pathway by application of cyclopamine. Thus, ATP4a-dependent Wnt/β-cat signaling acted downstream of HH-signaling in the floor plate, and activation of both pathways was required for *Foxj1* expression. These findings were in agreement with a revised model for dorsal cell fate specification in *Xenopus*, which proposed that HH-signaling plays only a minor role during induction of floor plate identity (Peyrot et al. 2011).

In the mouse neural tube, HH-signaling regulates the expression of the secreted Wnt-inhibitor *sFRP2* (Lei et al. 2006). Upon inhibition of HH-signaling, *sFRP2* expression was extended towards ventral portions of the neural tube and Wnt-dependent gene expression was down-regulated (Lei et al. 2006). Similar to *sFRP2* in the mouse, *Xsfrp2* was expressed in the *Xenopus* neural tube (Pera et al. 2000). Therefore, it is possible that HH-dependent *Foxj1* expression in the frog is regulated by a similar mechanism. This could be experimentally addressed by analysis of *Xsfrp2* expression in cyclopamine-incubated embryos.

Motile Cilia And Wnt-Signaling

Preliminary experiments from the brain ependyma and the gastrointestinal tract indicated a link between ATP4a, Wnt-signaling, *Foxj1* expression and ciliation in these tissues as well. Hence, the data suggested that formation of motile cilia was regulated by Wnt/β-cat signaling throughout *Xenopus* development. *Foxj1* expression in zebrafish was also regulated by Wnt/β-cat (Caron et al. 2011), which argues for conservation of mechanisms in vertebrates. This in turn reveals a new interaction between Wnt-signaling and motile cilia, in addition to the established role for Wnt/PCP signaling (Pan et al. 2007; Mitchell et al. 2009; Zeng et al. 2010; Wallingford et al. 2011; Yasunaga et al. 2011).

Figure Discussion-9: Hypothetical Mechanism Of ATP4a- And pH-Dependent Wnt-Signaling Activation

Upper row left: Before ligand binding, components are present in the membrane of the signal-receiving cell.
Upper row right: Upon binding of the Wnt-ligand to the Fz-receptor, Dvl is recruited to the intracellular part of Fz and gets activated. Moreover, Fz-bound ligands recruit membrane-standing LRP6 co-receptors to the complex. Activated Dvl-molecules polymerize and recruit more ligand-receptor/co-receptor complexes. ATP4 is bound to this complex by an unknown adaptor protein.
Middle row right: Dvl-polymerization induces formation of the Wnt-signalosome by endocytosis.
Middle row left: After signalosome endocytosis, ATP4-mediated proton pumping acidifies the signalosome lumen.
Lower row left: Signalosome acidification permits a conformational change of the LRP6 intracellular tail and subsequent phosphorylation by CK1 and GSK3β.
Lower row right: Recruitment of GSK3β to the signalosome prevents stabilization of APC/β–cat/GSK3β complexes, which ultimately stabilizes cytoplasmatic β-cat and stimulates Lef/TCF-dependent target gene expression.
Please see text for further details.

ATP4a And pH-Dependent Wnt-Signaling
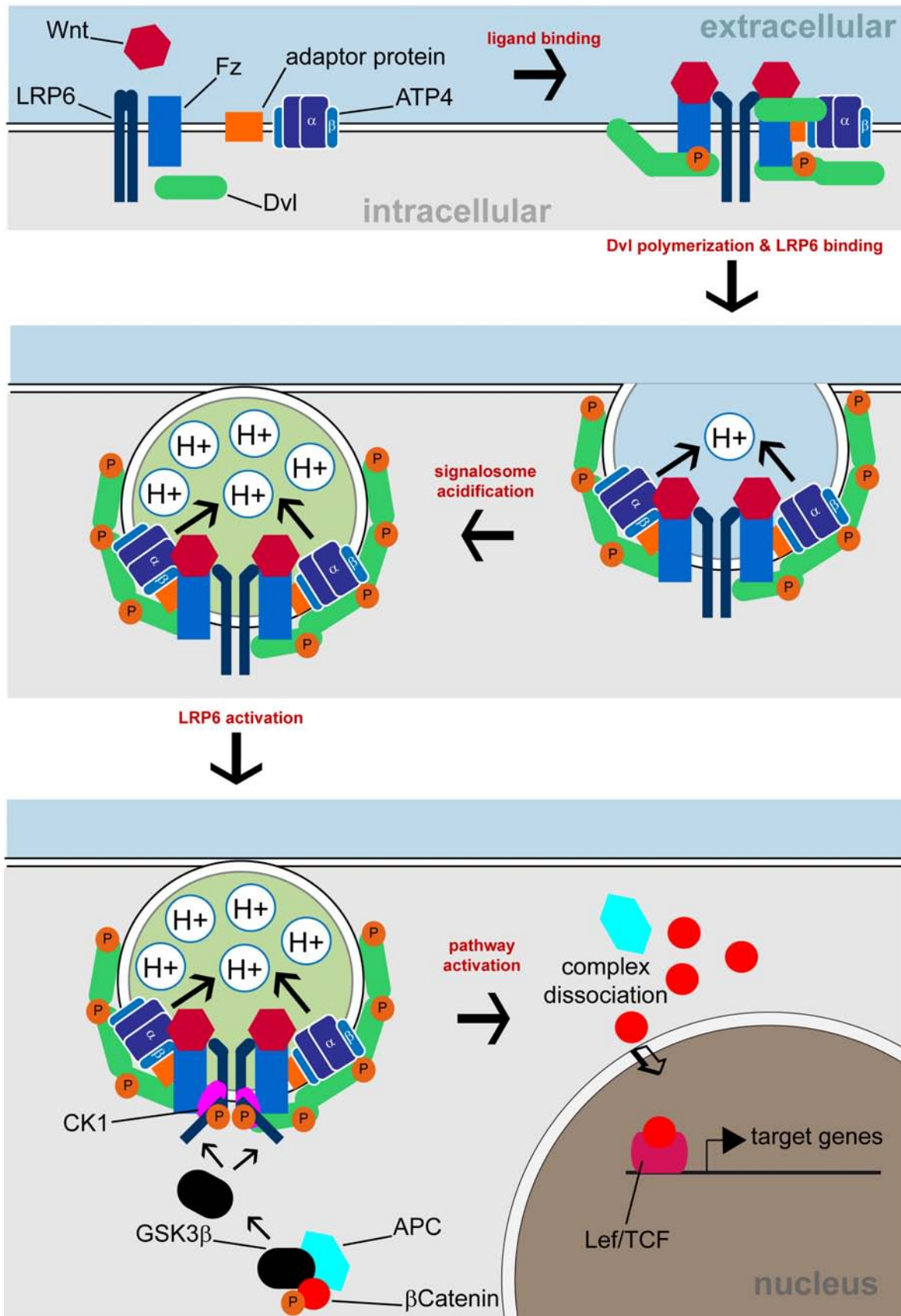
Functional experiments and subcellular ATP4a localization suggested interaction with Wnt-signaling at the level of membrane-associated pathway components (ligand, receptor and Dvl) (Borchers et al. 2000; Wallingford et al. 2001; Tao et al. 2005; Tran et al. 2007; Niehrs et al. 2010). ATP6 and ATP4 were required for Wnt/β-cat and Wnt/PCP signaling (Bilic et al. 2007; Buechling et al. 2010; Cruciat et al. 2010). ATP6 was proposed to account for Wnt-signalosome formation and acidification, which was a prerequisite for activation of LRP6 (Cruciat et al. 2010). ATP4a was found in vesicle-like structures near the apical membrane, which suggested that ATP4 might be required for acidification of signalosomes as well.

Down-regulation of non-canonical Wnt/PCP, Wnt/Ca^{2+}, Wnt/Ror2 or Wnt-PKA signaling can affect gastrulation and blastopore closure in *Xenopus* (Kohna et al. 2005; Park et al. 2006; Schambony et al. 2007). This was also observed upon loss of Xwnt11b function. In contrast, gastrulation movements and blastopore closure were not considerably affected in *ATP4a* morphants. As ATP4 and ATP6 were both expressed in the dorsal mesoderm (Cruciat et al. 2010), lack of gastrulation defects upon inhibition of one proton pump might have indicated redundant functions. Nevertheless, inhibition of a single ATPase reliably down-regulated β-cat dependent gene expression and Wnt/PCP mediated processes (Cruciat et al. 2010). Interestingly, these Wnt-branches required LRP6 for correct signaling (Tahinci et al. 2007). Thus, ATP4- and ATP6-dependent signalosome acidification possibly regulates only the transduction of signals via LRP6, without affecting other non-canonical signaling branches.

In theory, pH-change within the signalosome could trigger a conformational change of the LRP6 extracellular domain, which was shown to repress activation of LRP6 dimers (Liu et al. 2003). This change in the extracellular conformation could consequently change the conformation of the intracellular tail of LRP6 and promote downstream events as previously suggested by Liu et al. (2003). Taken together, the following model of ATP4/Wnt-interaction is envisaged (Figure-Dis-9):

After Wnt-binding to Fz, the receptor gets activated and recruits Dvl to the membrane. In addition, ligands of the canonical and Wnt/PCP branch recruit LRP6 to this complex by binding to the extracellular domains. Fz-bound Dvl polymerizes with other Dvl molecules, thereby promoting signalosome formation and internalization (Niehrs et al. 2010). The

signalosome constitutes an enclosed compartment, which can be acidified by proton pumps (Buechling et al. 2010; Cruciat et al. 2010). pH-shift induces a conformational change within the extracellular domain of LRP6, which is accompanied by a conformational change of the intracellular part of the protein (Liu et al. 2003). Such a mechanism could explain the requirement of proton pump-mediated acidification of signalosomes in Wnt-signaling activation. This model will be tested by sequence-modification of LRP6 extracellular domains and functional experiments on pH-dependency of manipulated proteins.

Concluding Remarks

The data provided in this thesis work uncovered a new role for ATP4 in ciliogenesis and LR-development of *Xenopus laevis* and potentially beyond. Furthermore, ATP4-function was required for activation and regulation of Wnt-signaling in diverse tissues, contributing a new player to this important signaling pathway. Taken together, these findings argue for conservation of symmetry-breakage among vertebrates and multiple roles for Wnt-signaling within this process.

Materials & Methods

In vitro fertilization

X. laevis can be kept in tanks filled with 18-22 °C cold water. For experiments, *X. laevis* females were stimulated for ovulation by injection of human chorion gonadotropin (β-HCG, Sigma; 400-500µl) into the dorsal lymph sac. About 12 hours after injection females started to spawn and kept laying eggs for throughout the following day. Eggs have been obtained by massaging and were collected in culture dishes (water was removed). For sperm extraction the testicles of males were removed and stored in 1 x MBSH at 4°C for up to 2 weeks. For fertilization a small peace of a testicle was dissected and added to freshly obtained eggs. After gently mixing movement of sperms was induced by decreasing the salt concentration of the 1 x MBSH using water. ~40 min after fertilization the fertilization jelly was removed by incubation in 2% cystein @ pH8 for up to 7 min. Isolated eggs have been washed 4-5x in 0.1xMBSH and transferred into 1 x MBSH for microinjection.

Fixation

Embryos were cultivated to the stage of interest and then transferred into 5 ml of freshly prepared 1 x MEMFA (WMISH), 1-5 ml of 4% PFA (IHC) or 2% PFA / 2.5% GA (SEM) for fixation. After incubation for 1-2h at room temperature or overnight at 4°C embryos were washed in buffer and either stored in ethanol at -20 °C or further prepared for IHC or post-fixed in a second step for SEM.

Incubation

SCH28080

For whole mount incubation experiments, SCH28080, which was dissolved in DMSO, was applied directly into the culture medium and vortexed for ~15sec. A stock solution of SCH28080 in DMSO was stored for up to two months at -20°C. As control, DMSO without SCH28080 was used. 200MM concentrations were used if not specified otherwise in the figure legend.

Cyclopamine

For whole mount incubation experiments, cyclopamine, which was dissolved in Ethanol, was applied directly into the culture medium and vortexed for ~15sec. A stock solution of cyclopamine in Ethanol was stored for up to two years at -20°C. As control, Ethanol without cyclopamine was used. Application started at st. 8. 10µM concentrations were used.

Microinjections

For the injections embryos were transferred to 2% Ficoll in 1 x MBSH solution in a Petri dish coated with 1% agarose. Embryos were injected at the 2-8-cell stage using a Harvard

Apparatus setup with a thin glass-needle (5-10µm diameter). Drop size was calibrated to about 7-8 nl per injection. In all experiments only embryos with a clear dorso-ventral segregation of pigment were used for injections (Danilchik et al. 1988; Klein 1987) and only correctly targeted specimens were processed for further analysis. The targeting was controlled by co-injection of either lineage tracer mRNAs (eGFP, mGFP, mRFP; diluted to a concentration of about 50-100ng/µl) or Dextranes (25mg/ml stock was diluted 1:10-1:40) as indicated.

Morpholino Oligonucleotides (MOs)

Specific MOs were provided by GeneTools.

Morpholino concentrations of **ATP4aMO** (5`-GTCATATTGTTCCTTTTTCCCCATC-3`) or CoMO (random control oligo; Gene Tools) used in cases not specified in the figure legends:
1x 0.5 pmol: Figure 18 C.
2x 0.5 pmol: Figure 10, Figure 11, Figure 14 A-D, Figure 15 B-C, Figure 16, Figure 17, Figure 18 A-C and E, Figure 21 A-B and H, Figure 22, Figure 23, Figure 32 D-E and G-I, Figure 33, Figure 34, Figure 35, Figure 36 E, Figure 39, Figure 41 A-E, Movie 1, Movie 2, Movie 3.
4x 0.5 pmol: Figure 20 D.
1x 1 pmol: Figure 19 G, Figure 20 A and E-F.
2x 1 pmol: Figure 19 A-B, Figure 20 B.

Morpholino concentrations of **ATP4a-Spl-MO** (5`-CCCCCCCCCCCCATTTCTTACAATGT-3`) are specified in the figure legends and **2x 0.5 pmol** was used in Movie 3.

Morpholino concentrations of **ATP4bMO** (5`-TCATTGAAAGTTGCCATTTCTCTCC-3`) are specified in the figure legends.

dnah9MO (dnah9-SB-MO in Vick et al. 2009) was used at concentrations of **1 pmol** per injection.

Xnr1MO (Schweickert et al. 2010) was used at concentrations of **0.5 pmol** per injection.

Foxj1MO (ATG-MO in Stubbs et al. 2008) concentrations are specified in the figure legends.

Fz8MO (Beyer 2011) was used at concentrations of **1 pmol** per injection.

Xwnt11bMO (5`-TAACCCAGTGACGGGTCGGAGCCAT-3`) was used at concentrations of **1 pmol** per injection.

HTR3MO (HTR3MO-A in Beyer et al. 2011) was used at concentrations of **2x 1 pmol**.

mRNA and DNA injections

mRNAs were prepared using the Ambion message machine kit and diluted to the following concentrations:

30 ng/ml RhoA CA **and RhoA DN** (Paterson et al., 1990)
60 - 80 ng/ml **ATP4a-MT** (60ng/µl in Figure 20 B; 80ng/µl in Figure 9 B and Figure 20 A)
80 ng/ml **Dvl2** (Sokol, 1996)
100 ng/ml **Xwnt8a** (Sokol et al., 1991)
100ng/µl **β-cat:GFP** (Miller and Moon, 1997)
150ng/µl **Notch-ICD** (Deblandre et al. 1999)
150ng/µl **Dll1-STU** (Deblandre et al. 1999)
150ng/µl **X-Su(H)-DBM** (Deblandre et al. 1999)

DNAs were purified using the PureYield Plasmid Midiprep kit (Promega) and diluted to the following concentrations:

0.5 ng/µl **HTR3-LBD** (Beyer et al. 2011)
0.5 ng/µl **Foxj1-CS2+** (Stubbs et al. 2008)
1 ng/µl **ATP4a-CS2+MT**
1 ng/µl **ATP4b-CS2+**
1 ng/µl **β-cat-GFP-CS2+** (Miller and Moon, 1997)
1 ng/µl **CS2+** (empty vector)
1 ng/µl **Xsfrp2-CS2+** (VON STEINBEISSER)
1 ng/µl **dnXwnt11b-CS2+** (Tada et al. 2000)

Whole-mount in situ hybridization (WMISH)

Was performed as described in detail by (Greenan and Metzinger 2008). This protocol was developed by the De Robertis laboratory, following basic procedures described in (Harland 1991), and can be obtained following this link:
 http://www.hhmi.ucla.edu/derobertis/protocol_page.
AP-conjugated anti-Fab-fragments antibody (Roche) was used @ 6µl / 50ml Blocking.

Immuno-histochemistry (IHC)

Embryos were fixed as described above (or processed for WMISH) and washed 3x in PBS @ RT for 5`.
Membranes were permeabilized by PBS with 0.01% Triton-X100 (3x 20 min @ RT) before each blocking step. CAS-blocking was used at a dilution of 1:10 in PBS with Triton-X100. Blocking took place for 2h @ RT or over night @ 4°C before application of Antibodies. Antibodies were diluted in 100% CAS as indicated below and incubated over night @ 4°C. Actin (phalloidin) and Nucleus (Hoechst) staining was performed as last step (at least 1h incubation @ RT) after antibody incubation and reagents were diluted as indicated below in PBS with Triton-X100.

Anti-ATP4a (rabbit, 1:500) (Chen et al., 1998)
Anti-Tubulin Acetylated (mouse, 1:700; Sigma)

137

Anti-rabbit Alexa 555 (goat, 1:250; Invitrogen)
Anti-mouse DyLight 488 (rabbit, 1:250; Jackson Immuno Research)
Anti-mouse Cy3 (sheep, 1:250; Sigma)
Alexa488-conjugated phalloidin (Invitrogen, 1:40)
Hoechst 33342 (Molecular Probes, 1:15.000 or below)

Combined WMISH and IHC

WMISH was performed as described above and washed 3 times for 30min at RT. Than IHC was performed as described above.

Scanning electron microscopy (SEM)

Embryos were freshly dissected (to uncover the GRP) in 0.1xMBSH and fixed in a mixture of 2% paraformaldehyde (PFA) and 2.5% glutaraldehyde (GA) for 1hr at room temperature or overnight at 4°C. The specimens were washed three times for 10min in 0.1M phosphate buffer (PB, pH7.5) and were then postfixed for 1-2hrs in 1% OsO4/0.1M PB at 4°C. After extensive washing embryos were gradually dehydrated in an ethanol series and stored in 100% ETOH at -20°C until submitted to the drying procedure. Critical point drying was performed using CO2 as drying agent. Embryos were sputter with gold and viewed under a LEO DSM 940A.
[Please note that all SEM preparations and microscopy was performed by T. Beyer or I. Schneider and details should be obtained from Beyer 2011].

Quantitative GRP-analysis

SEM or IHC was performed on dorsal explants as described above. For quantification the customized software tool "Cell Gridder" was used, which was developed by T. Thumberger and which is described in Thumberger (2011).

Quantification of MCC-phenotypes in the *Xenopus* skin

From each embryo two confocal image z-stacks were taken, which were non-overlapping. The z-stacks were processed for maximum intensity z-project in ImageJ and tubulin-stained cells and phenotypes were scored as described in the respective figure legend.

Flow analysis

For analysis of leftward flow at the GRP, a semi-automated tool was used. For visualization of extracellular particle movement driven by ciliary motility, fluorescent beads were added to the GRP and their motion was documented by taking time-lapse movies in a time window of 25 sec. Only the central region of the GRP was analyzed what was achieved by applying a mask of a defined size. Particle movement was analyzed using the ImageJ plug-in ParticleTracker, measurements and statistics were calculated. Slow and random movements which most likely displayed Brownian motion were excluded using the Rayleigh's test of uniformity on each trajectory. Particles movements which reach a mean resultant length (rho) of 0.6 were count as being directed. The resulting data were summarized and significances have been calculated by analyzing the mean resultant

length towards the left side against the mean length of all trajectories excluding random movement. Significances were calculated by Mann-Whitney-U test (Bonferroni corrected) in statistical-R. This analysis was developed by Thomas Thumberger (formerly Weber) and is described in detail in Vick et al. (2009) and Thumberger 2011.

Skin flow was analyzed in anesthetized tadpole embryos, placed in fluorescent bead solution. Velocity of flow was determined using Particle Tracker.

Animal cap assay

Embryos were injected four times into the animal pole at the four-cell stage and cultivated until late blastula stages (st. 8/9). Injection efficiency was controlled by analysis of fluorescent lineage tracer analysis. The animal cap was prepared and treated with activin following standard procedures (Green and Smith 1990). Recombinant human Activin A (R&D Systems) was added immediately after dissection, and embryos were cultured until control specimens reached stage 22–30.

Clearing of embryo tissue

For clearing embryos were transferred into increasing concentrations of Methanol (25, 50, 75 and 100%) and methy-salicylate or a 1:2 mixture of benzyl alcohol and benzyl benzoate.

Cloning

Total RNA isolation

Total RNA was isolated using a standardized protocol. Embryos were transferred into Trifast (PEQGold) and macerated. After incubation at room temperature (at least 10 min) 200µl chloroform have been added and vortexed for 15 sec, incubated @ RT for 5 min and centrifuged. The aqueous phase was transferred into a new reaction tube, 500µl isopropanol were added. After vortexing 10min incubation @ RT, the sample have been centrifuged for 15 min @ 4°C and 14000rpm. Supernatant was discarded, RNA pellet was washed using 75% ethanol. Discarding the supernatant and drying was followed by re-suspension in 30 µl autoclaved water. The final RNA concentration was measured and the RNA was stored at -80°C.

Reverse transcriptase (RT) reaction, cDNA synthesis

Up to 1µg total RNA was used for preparation of cDNA. RNA and 0,5µl random hexamers (Promega) were diluted in water to a final volume of 14µl. After 5min @ 70°C and snap cooling on ice the following components were added:

5 µl M-MLV RT Buffer (5x)
1.25 µl dNTPs (10mM)
3.75µl H_2O dest.
1µl M-MLV Reverse transcriptase with volume of 25µl.

After 10min @ RT and 60min at 50°C the reaction was stopped by 15 min at 70°C. The cDNA was stored at -20°C.

Standard PCR

Each reaction contained:

1-5µl cDNA
5µl Taq Buffer (5x)
2.5µl dNTPs (2mM)
1µl forward primer
1µl reverse primer
0.2µl Taq polymerase
add water to obtain a total volume of 20µl.

The standard PCR protocol included the following steps:

(1) Denaturation step, 5min @ 95°C
(2) Denaturation step, 30sec @ 95°C
(3) Primer annealing, 45sec @ variable temperature.
(4) Elongation, 1min/1kb @ 72°C
(5) Stop of reaction, 8°C for ever

Steps (2)-(4) were repeated. For subsequent ligation into pGEM-TEasy vector, an extra step was programmed (10min at 70°C), in which an adenosine was added at each 3'-terminus by the Taq-polymerase.

Primers used in this study:

Full-length ATP4a:
forward 5`-ATGGGGAAAAAGGAACAATATG-3`
reverse 5`-TTAATAATACATCTCCTTGTCGAAC-3`

Cloning of ATP4a Intron2 sequence:
HKaEx2-for 5`-GCATGAAAAAATGGAC-3
HKaEx3-rev 5`-CTGTTCTAGCCGACAG-3

Verification of ATP4a Intron2 sequence in Figure 12:
HKaEx2-for 5`-GCATGAAAAAATGGAC-3
HKaInt2-rev 5`-TCCTGTCTGCCAATAAACCC-3

Elongation factor 1α:
forward 5`-CAGATTGGTGCTGGATATGC-3`
reverse 5`-ACTGCCTTGATGACTCCTAG-3`

Actin cytoskeletal type-8:
forward 5`-AGGGTGTAATGGTTGGTATGG-3`
reverse 5`-ACCTTCTACAATGAACTTCGTG-3`

PCR-products were cloned into the pGem TEasy vector.
All sequences have been verified by sequencing.

Ligation

PCR products have been ligated into the PGEM-T-Easy vector. Each reaction contained:
2.5µl Rapid Ligation buffer (2x)
0.5µl PGEM-T Easy Vector
0.5µl T4 DNA Ligase
0.5µl H2O
1µl PCR product
After gently mixing the reaction incubated at 4°C over night followed by transformation of competent *E. coli* (XL1-blue) using the heat shock method. The bacteria solution was plated onto LB-agar plates (100µg/ml Ampicillin, 0.5mM IPTG, 80µg/ml X-Gal) and incubated over night at 37°C. Blue staining indicated no insertion of a DNA fragment into the multiple cloning site of the vector whereas white colonies were further analyzed.

Mini preparation

Plasmid DNA from *E. coli* cultures was isolated using a modified alkaline lysis protocol. All centrifugation steps were done at 4°C. 3ml of selective LB medium (100µg/ml Ampicillin) were inoculated with a single bacteria colony from a selective plate and grown overnight @ 37°C. 1.5 ml of the culture were poured into a microcentrifuge tube and bacteria were pelleted in a microcentrifuge at 6000g for 15min. The supernatant was discarded and the pellet re-suspended by vortexing in 100µl P1 buffer. When the bacteria suspension appeared uniform, 200µl of P2 buffer were added and the tube was flicked several times to thoroughly mix the reagents.
Alkaline lysis was allowed to proceed for 5min and was then stopped by neutralizing with 150µl of P3 and mixed gently. After 20 min of incubation on ice, the lysate was cleared by centrifugation in a microcentrifuge at 14.000rpm for 10min. 400µl of the clear supernatant were transferred to a fresh tube and mixed with 1ml of 100% Ethanol to precipitate the plasmid DNA. After precipitation for 30min at -20°C the plasmid DNA was pelleted by centrifuging at 14.000rpm for 10min. The pellet was washed in 70% ethanol, dried and re-suspended in 50µl sterile water.

Restriction enzyme digests of DNA (20µl)

To check for insertion of the correct PCR-product after mini-prep, inserts were released from the plasmids by digestion with a restriction enzyme cutting on both sides of the multiple cloning site (e.g. EcoR1). 5µl of plasmid-DNA, 2µl 10x buffer, 0.2 µl BSA and 0.5µl enzyme were added, and 12.3µl sterile water to a final volume of 20µl. Incubation took place at 37°C for 2h and after digestion the reaction was analyzed on an agarose gel. The products of each reaction were checked on a standard 1% agarose gel supplemented with an end concentration 0.4µg/ml ethidium bromide solution.

DNA amplification (midi preparation)

100ml of selective LB medium (100µg/ml Ampicillin) were inoculated with 1ml of a positively tested bacteria culture and grown overnight shaking at 37°C. Bacteria were harvested by centrifugation, lysed and DNA was purified following the Promega "PureYield Plasmid Midiprep System" using the vacuum method. The concentration of nucleic acids in

aqueous solutions was determined via spectrophotometry. The ratio of absorption (A) at 260nm and 280nm wavelength indicated the purity of the solution (pure nucleic acid solution: 1.8 for DNA, 2.0 for RNA). The content of either DNA or RNA was inferred from the A260 value with 1 unit corresponding to 50µg/µl DNA and 40µg/µl RNA. For sub-cloning into other vectors (i.e. Cs2+ or CS2+MT) the insert and the desired vector were digested by restriction enzymes, the insert was purified from a 1% agarose gel using DNA-Purification-Kit (Biozym) and re-ligated into the new vector.

mRNA synthesis

Restriction enzyme digests of DNA (50µl)

For linearization of plasmids 20µg of plasmid DNA was used in a 50µl reaction. 2µl of restriction enzyme were used and the digestion was incubated overnight at 37°C. Approximately 600ng of the digestion were controlled on a 1% agarose gel. Efficiency of linearization was tested on a 1% agarose gel by comparison with the unlinearized plasmid.

Synthesis of capped RNA

For capped RNA synthesis the Ambion kit mMESSAGE mMACHINE (High yield capped RNA Transcription kit) was used, following the suggested standard protocol. Concentration of the mRNA was then determined by spectrophotometry and the quality by running on an agarose gel.

Histological analysis of embryos after WMISH

After re-hydration embryos were equilibrated in a small volume of embedding medium (~1ml, gelatin-albumin mix). 2ml of embedding medium were mixed shortly but vigorously with 140µl of glutaraldehyde and poured into a square mold formed of two glass brackets. The mixture was allowed to harden and the equilibrated embryo was transferred upon the surface of the block, excess of embedding medium was carefully removed. Another 2ml of embedding medium mixed with glutaraldehyde were poured into the mold so that the embryo was sandwiched between two layers of embedding mix. The hardened block was trimmed with a razor blade and attached onto a plate. The plate was mounted into the holder of the vibratome and 30-80µm thick sections were prepared. The sections were arranged onto glass slides, embedded with Mowiol and protected with glass cover slips.

Photo documentation

Documentation of living or fixed embryos was performed after re-hydration in PBS- with a Zeiss dissecting microscope STEREO Discovery.V12, a LEICA MZFLIII with a digital camera (AxioCam HRc, Zeiss) or a Zeiss microscope Axioskop 2 with a digital camera (AxioCam Hrc, Zeiss). Confocal imaging was performed on a Zeiss LSM700 or LSM 5 Pascal. Fluorescent images were processed using ImageJ and TIFF-files were generated. Further manipulations (replacement of background, brightness, contrast, color, etc.) of all images was performed using Adobe Photoshop. Figures were designed in Adobe Illustrator. Hereby I confirm that in no case original data was manipulated in an inappropriate way, i.e. the content of a picture was not changed in a way, which would qualitatively change the information contained.

Buffers, Solutions and Media

WMISH/IHC

<u>10x Phosphate Buffered Saline (PBS, 1l)</u>
80g NaCl
2g KCl
14.4g Na_2HPO_4
2.4g KH_2PO_4
800ml DDW
adjust pH to 7.4, add DDW to 1L, autoclave
1x PBSw (500ml)
50ml PBS- (10x)
500µl Tween20
add DDW to 500ml

WMISH

<u>1x Alkaline Phosphatase Buffer (AP1, 1l)</u>
100ml TRIS (pH 9.5, 1M)
20ml NaCl (5M)
50ml $MgCl_2$ (1M)
adjust pH to 9.5, add DDW to 1l

<u>1x Maleic Acid Buffer (MAB, 1l)</u>
11.61g Maleic Acid (100mM)
30ml NaCl (5M)
800ml DDW
adjust pH to 7.5, add DDW to 1l, autoclave

<u>20x Sodium Citrate Buffer (SSC, 1l)</u>
175.3g NaCl
88.2g Sodium citrate
800ml DDW
adjust pH to 7, add DDW to 1l, autoclave

<u>Hybridization solution (1l)</u>
10g Boehringer Block
500ml Formamide
250ml SSC (20x)
Heat to 65°C for 1 hour
120ml DDW
100ml Torula RNA (10mg/ml in DDW, dissolved at 65°C; filtered)
2ml Heparin (50mg/ml in 1xSSC pH 7)
5ml Tween20 (20%)
10ml CHAPS (10%)
10ml EDTA (0.5M)
filter (5µm)

143

Antibody Blocking Buffer (1l)
10g Boehringer Block
dissolve in 800ml PBS- at 70°C, vortex frequently,
100ml Goat Serum (30min at 56°C heat inactivated)
add PBS- to 1l, filter (0.45µm)
1ml Tween-20

Frog experiments

5x MBSH (1l)
25.7g NaCl
0.375g KCl
1g NaHCO3
1g MgSO4*7H2O
0.39g (CaNO3)2*4H2O
0.3g CaCl2*2H2O
11.9g Hepes
5 ml Penicillin/Streptomycin
add DDW to 1l, adjust pH of 7.4, filter (0.45µm)
10xMEMFA (1ml)
500ml MOPS (0.1M, pH 7.4)
200ml EGTA (2mM)
10ml MgSO4 (1M)
add DDW to 1l, autoclave

1x MEMFA (100ml)
10ml MEMFA (10x)
10ml Formaldehyde (37%)
80ml H2O

Gurdon's buffer
88mMNaCl
15mM HEPES
1mM KCl
15mMTris-HCl, pH 7.6

Ficoll
2% Ficoll diluted in 1xMBSH

Cystein
2% Cystein diluted in DDW, adjust pH to 7.99

Bacteria culture

Super Optimal Catabolite repression medium (S.O.C., 500ml)
2.5g Yeast extract
10g Tryptone
1ml NaCl (1M)
1.25ml KCl (1M)
5ml MgCl2 (1M)
5ml MgSO4 (1M)
1.8g Glucose
autoclave

Lysogeny Broth (LB) medium (1l)
10g Tryptone
10g NaCl
5g Yeast extract
add DDW to 1l, adjust pH to 7 (for LB agar add 15g/l agar) autoclave

DNA preparation

P1 (Re-suspension buffer)
50mM TRIS-HCl
10mM EDTA (pH8)
add RNaseA (DNase free) to a final concentration of 100µg/ml

P2 (Lysis buffer)
0,2M NaOH
1% SDS

P3 (Neutralization buffer)
3M Potassium acetate, pH 5.5

Other applications

Embedding medium for vibratome sections
2.2g Gelatine
135g Bovine Serum Albumin
90g Sucrose
dissolve in 450ml PBS.

Mowiol (Mounting medium)
96g Mowiol 488
24g Glycerol
24ml DDW
stir for 2h, then add
48ml TRIS 0.2M pH 8.5
stir for 20min at 50°C
centrifuge for 15min at 5000rpm, keep supernatant
and store at -20°C.

<u>50x Tris Acetate EDTA Electrophoresis Buffer (TAE, 1l)</u>
15.1g Tris base
57.1ml Glacial acetic acid

<u>100ml EDTA (0.5M, pH8)</u>
add DDW to 1l, adjust pH to 8.5

<u>Sörensen phosphate buffer</u>
Stock solution A: 0.2M NaH2PO4 *H2O
Stock solution B: 0.2M Na2HPO4
for 200ml 0.1M, pH 7.4: 19ml A + 81ml B + 100ml H2O
for 200ml 0.1M, pH 7.0: 39ml A + 61ml B + 100ml H2O

Sources of supply

Chemicals and lab-ware

Acetic acid AppliChem, Darmstadt
Agarose Roth, Karlsruhe
Albumin fraction V AppliChem, Darmstadt
Ampicillin AppliChem, Darmstadt
Anti-Digoxigenin-AP Roche, Mannheim
BM Purple Roche, Mannheim
Boehringer Block Roche, Mannheim
Bovine serum albumin AppliChem, Darmstadt
BSA AppliChem, Darmstadt
CAS-Block Invitrogen, Karlsruhe
CHAPS Sigma, Schnelldorf
Chloroform Merck, Darmstadt
Cyclopamine Biomol, Hamburg
Cystein Roth, Karlsruhe
Desoxynucleosidtriphosphate (dNTPs) Promega, Mannheim
DIG RNA Labeling Mix Roche, Mannheim
Dimethylsulfoxid (DMSO) Roth, Karlsruhe or AppliChem, Darmstadt
Disodium hydrogen phosphate AppliChem, Darmstadt
Dithioreitol (DTT) Promega, Mannheim
DMSO Roth, Karlsruhe
EDTA Roth, Karlsruhe
Ethanol Roth, Karlsruhe
Ethidium Bromide Roth, Karlsruhe
Ethyl-p-Aminobenzoat (Benzocain) Sigma, Schnelldorf
Ethylenediamine tetraacetic acid EDTA Roth, Karlsruhe
Ethyleneglycol tetraacetic acid EGTA Roth, Karlsruhe
Ficoll AppliChem, Darmstadt
FluoSphere Fluorescent beads 500nm Invitrogen, (Molecular Probes), Karlsruhe
Formaldehyd AppliChem, Darmstadt
Forceps (#3, #5) Fine Science Tools, Heidelberg
Formamide Roth, Karlsruhe
Gelatine Roth, Karlsruhe
Glass coverslips Roth, Karlsruhe

Glass slides Roth, Karlsruhe
Glucose AppliChem, Darmstadt
Glutaraldehyde AppliChem, Darmstadt
Glycerol Roth, Karlsruhe
Glycin AppliChem, Darmstadt
Goat serum Sigma, Schnelldorf
HCG (human chorionic gonadotropin) Sigma, Schnelldorf
HCl (37%) Merck, Darmstadt
Hepes AppliChem, Darmstadt
Heparin Sigma, Schnelldorf
Injection-needle Sterican (0,4x20 mm) B. Braun, Melsungen
Injection syringe F1, 1ml B. Braun, Melsungen
Lambda-DNA Promega, Mannheim
Ligase (T4-Ligase) Promega, Mannheim
Lithium chloride Serva, Heidelberg
Loading Buffer AppliChem, Darmstadt
Magnesium chloride Roth, Karlsruhe
Magnesium sulfate AppliChem, Darmstadt
Maleic acid Roth, Karlsruhe
Methanol Roth, Karlsruhe
Methyl salicylate AppliChem, Darmstadt
Micro centrifuge tubes Sarstedt, Nümbrecht
Morpholino Oligonucleotides Gene Tools, Philomath
Objective slides Roth, Karlsruhe
Oligonucleotides Operon, Cologne
Osmium tetroxide Plano, Wetzlar
Parafilm Roth, Karlsruhe
Paraformaldehyde AppliChem, Darmstadt
PBS+ (10x) Gibco (Invitrogen) Karlsruhe
Penicillin/Streptomycin Gibco (Invitrogen) Karlsruhe
pGEM-T-Easy-Vektor Promega, Mannheim
Phenol/chloroform (Rotiphenol) Roth, Karlsruhe
Plastic pipettes Sarstedt, Nümbrecht
2-Propanol Roth, Karlsruhe
Proteinase K Roth, Karlsruhe
Rhodamine-B-dextran Molecular Probes (Invitrogen), Karlsruhe
RNAse A Roth, Karlsruhe
RNAsin Promega, Mannheim
Saccharose Applichem, Darmstadt
SCH28080, Sigma, Schnelldorf
Sodium acetate Roth, Karlsruhe
Sodium chloride Roth, Karlsruhe
Sodium citrate Roth, Karlsruhe
Sodium dihydrogen phosphate AppliChem, Darmstadt
Sodium hydroxide AppliChem, Darmstadt
Sp6-RNA-Polymerase Promega, Mannheim
Sucrose AppliChem, Darmstadt
Syringe filters Whatman, Dassel
T7-RNA-Polymerase Promega, Mannheim
Taq-DNA-Polymerase (Go-Taq) Promega, Mannheim
Torula RNA Sigma, Schnelldorf
TRIS base AppliChem, Darmstadt

TRIS HCl AppliChem, Darmstadt
Triton-X100 Serva, Heidelberg
Tryptone AppliChem, Darmstadt
Tween-20 AppliChem, Darmstadt

Kits
DNA-Purification-Kit (Easy-Pure) Biozym, Hessisch Oldendorf
mMESSAGE mMACHINE SP6 Ambion, Darmstadt
pGEM-T Easy Vector System Promega, Mannheim
PureYield Plasmid Midiprep System Promega, Mannheim
PeqGOLD TriFast Peqlab, Erlangen

Proteins and Antibodies
Restriction enzymes and buffers Promega, Mannheim or New England Biolabs, Ipswich
Modifying enzymes and buffers Promega, Mannheim
Anti-digoxigenin-AP Roche, Mannheim

IHC-antibodies (cf. Immono-histochemistry)

Special Hardware

Peltier Thermal Cycler PTC-200 Biozym, Hessisch Oldendorf
Vibratome Leica, Bensheim
Stereo microscope Zeiss, Oberkochen
Zeiss DSM 940A Zeiss, Oberkochen
LSM 5 Pascal Zeiss, Oberkochen
LSM 700 Zeiss, Oberkochen
Axioplan 2 Zeiss, Oberkochen
Critical point dryer CPD 030 Balzers, Austria
Sputter coater SCD 050 Balzers, Austria
LEO DSM 940A Zeiss, Oberkochen

Animals

Adult African clawed frogs (*Xenopus laevis*) were obtained from Guy Pluck, Xenopus express, Ancienne Ecole de Vernassal, Le Bourg 43270, Vernassal, Haute-Loire, France. They were kept species-appropriate at a 12h light-cycle in the animal facility of the Institute of Zoology, University of Hohenheim.

Materials and Methods sections adapted and modified/extended from Beyer (2011).

Information On Reprinted Figures

<u>Blum et al. 2009b##</u>

Reprinted from Developmental Dynamics 238, Blum, M., Beyer, T., Weber, T., Vick, P., Andre, P., Bitzer, E., Schweickert, A., "Xenopus, an ideal model system to study vertebrate left-right asymmetry" / Experimental manipulations of GRP and flow, Page 1221, Copyright (2009), with permission from Wiley-Liss, Inc.

<u>Vick et al. 2009###</u>

* Reprinted from Vick design by T. Thumberger, P., "Functional dissection of leftward flow." / Pkd2 and the two-cilia model, Page 22, Copyright (2009), with permission from P. Vick.

References

Aartsma-Rus, A. (Ed.) (2012) Exon Skipping. Methods and Protocols Series: Methods in Molecular Biology, Vol. 867. Humana Press.

Abu-Issa, R., and Kirby, M. L. (2007). Heart field: from mesoderm to heart tube. Annual review of cell and developmental biology 23, 45-68.

Adams, D. S., Robinson, K. R., Fukumoto, T., Yuan, S., Albertson, R. C., Yelick, P., Kuo, L., McSweeney, M., and Levin, M. (2006). Early, H+-V-ATPase-dependent proton flux is necessary for consistent left-right patterning of non-mammalian vertebrates. Development (Cambridge, England) 133, 1657-71.

Afzelius, B. A. (1976). A human syndrome caused by immotile cilia. Science (New York, N.Y.) 193, 317-9.

Afzelius, B. A. (1999). Asymmetry of cilia and of mice and men. The International journal of developmental biology 43, 283-6.

Alberts, B., Johnson, A., Lewis, J., Raff, M., Roberts, K., and Walter, P. (2008a) Chapter 15: Mechanisms of Cell Communication. Molecular biology of the cell. 5th edition. Garland Science.

Alten, L., Schuster-Gossler, K., Beckers, A., Groos, S., Ulmer, B., Hegermann, J., Ochs, M., and Gossler, A. (2012). Differential regulation of node formation, nodal ciliogenesis and cilia positioning by Noto and Foxj1. Development (Cambridge, England) 1284, 1276-1284.

Amato, M. A., Boy, S., and Perron, M. (2004). Hedgehog signaling in vertebrate eye development: a growing puzzle. Cellular and molecular life sciences : CMLS 61, 899-910.

Amemiya, S. (2007). Micromere-Derived Signal Regulates Larval Left-Right Polarity During Sea Urchin Development. J. Exp. Zool. 262, 249-262.

Andersson, E. R., Sandberg, R., and Lendahl, U. (2011). Notch signaling: simplicity in design, versatility in function. Development 138, 3593-3612.

Antic, D., Stubbs, J. L., Suyama, K., Kintner, C., Scott, M. P., and Axelrod, J. D. (2010). Planar cell polarity enables posterior localization of nodal cilia and left-right axis determination during mouse and Xenopus embryogenesis. PloS one 5, e8999.

Aoki, K., and Taketo, M. M. (2007). Adenomatous polyposis coli (APC): a multi-functional tumor suppressor gene. Journal of cell science 120, 3327-35.

Asashima, M., Ito, Y., Chan, T., Michiue, T., Nakanishi, M., Suzuki, K., Hitachi, K., Okabayashi, K., Kondow, A., and Ariizumi, T. (2009). In vitro organogenesis from undifferentiated cells in Xenopus. Developmental dynamics : an official publication of the American Association of Anatomists 238, 1309-20.

Avasthi, P., and Marshall, W. F. (2011). Stages of ciliogenesis and regulation of ciliary length. Differentiation; research in biological diversity, 1-13.

Aw, S., Adams, D. S., Qiu, D., and Levin, M. (2008). H,K-ATPase protein localization and Kir4.1 function reveal concordance of three axes during early determination of left-right asymmetry. Mechanisms of development 125, 353-72.

Aw, S., and Levin, M. (2009). Is left-right asymmetry a form of planar cell polarity?

Development (Cambridge, England) 136, 355-66.

Axelsen, K. B., and Palmgren, M. G. (1998). Evolution of substrate specificities in the P-type ATPase superfamily. Journal of molecular evolution 46, 84-101.

Bangs, F., Antonio, N., Thongnuek, P., Welten, M., Davey, M. G., Briscoe, J., and Tickle, C. (2011). Generation of mice with functional inactivation of talpid3, a gene first identified in chicken. Development (Cambridge, England) 138, 3261-72.

Basu, B., and Brueckner, M. (2008). Cilia multifunctional organelles at the center of vertebrate left-right asymmetry. 1st ed. (Elesvier Inc.).

Bayer, H., Müller, T., Myrtek, D., Sorichter, S., Ziegenhagen, M., Norgauer, J., Zissel, G., and Idzko, M. (2007). Serotoninergic receptors on human airway epithelial cells. American journal of respiratory cell and molecular biology 36, 85-93.

Bayramov, A. V., Eroshkin, F. M., Martynova, N. Y., Ermakova, G. V., Solovieva, E. A., and Zaraisky, A. G. (2011). Novel functions of Noggin proteins: inhibition of Activin/Nodal and Wnt signaling. Development (Cambridge, England) 5356, 5345-5356.

Beggah, A. T., Béguin, P., Bamberg, K., Sachs, G, and Geering, K. (1999). Beta-subunit assembly is essential for the correct packing and the stable membrane insertion of the H,K-ATPase alpha-subunit. The Journal of biological chemistry 274, 8217-23.

Belo, J. A. et al. (2009). Generating asymmetries in the early vertebrate embryo: the role of the Cerberus-like family. The International journal of developmental biology 53, 1399-407.

Ben, J., Elworthy, S., N., A. S. M., Eeden, F. van, and Ingham, P. W. (2011). Targeted mutation of the talpid3 gene in zebrafish reveals its conserved requirement for ciliogenesis and Hedgehog signalling across the vertebrates. Development 138, 4969-4978.

Berbari, N. F., O'Connor, A. K., Haycraft, C. J., and Yoder, B. K. (2009). The primary cilium as a complex signaling center. Current biology : CB 19, R526-35.

Berdon, W. E., McManus, C., and Afzelius, B. (2004). More on Kartagener's syndrome and the contributions of Afzelius and A.K. Siewert. Pediatric radiology 34, 585-6.

Beyer, T. et al. (2011). Serotonin Signaling Is Required for Wnt-Dependent GRP Specification and Leftward Flow in Xenopus. Current Biology, 1-7.

Beyer, T., Thumberger, T., Schweickert, A., and Blum, M. (2012). Connexin26-mediated transfer of laterality cues in Xenopus. Biology Open.

Bilic, J., Huang, Y.-L., Davidson, G., Zimmermann, T., Cruciat, C.-M., Bienz, M., and Niehrs, C. (2007). Wnt induces LRP6 signalosomes and promotes dishevelled-dependent LRP6 phosphorylation. Science (New York, N.Y.) 316, 1619-22.

Bisgrove, B. W., Snarr, B. S., Emrazian, A., and Yost, H. J. (2005). Polaris and Polycystin-2 in dorsal forerunner cells and Kupffer's vesicle are required for specification of the zebrafish left-right axis. Developmental biology 287, 274-88.

Bisgrove, B. W., and Yost, H. J. (2006). The roles of cilia in developmental disorders and disease. Development (Cambridge, England) 133, 4131-43.

Blum, M., Beyer, T., Weber, T., Vick, P., Andre, P., Bitzer, E., and Schweickert, A. (2009b). Xenopus, an ideal model system to study vertebrate left-right asymmetry. Developmental dynamics : an official publication of the American Association of Anatomists 238, 1215-25.

Blum, M. et al. (2007). Ciliation and gene expression distinguish between node and

posterior notochord in the mammalian embryo. Differentiation; research in biological diversity 75, 133-46.

Blum, M., Gaunt, S. J., Cho, K. W., Steinbeisser, H., Blumberg, B., Bittner, D., and Robertis, E. M. De (1992). Gastrulation in the mouse: the role of the homeobox gene goosecoid. Cell 69, 1097-106.

Blum, M., Weber, T., Beyer, T., and Vick, P. (2009). Evolution of leftward flow. Seminars in cell & developmental biology 20, 464-71.

Borchers, A., Epperlein, H. H., and Wedlich, D. (2000). An assay system to study migratory behavior of cranial neural crest cells in Xenopus. Development genes and evolution 210, 217-22.

Borovina, A., Superina, S., Voskas, D., and Ciruna, B. (2010). Vangl2 directs the posterior tilting and asymmetric localization of motile primary cilia. Nature cell biology 12, 407-12.

Bourhis, E., Tam, C., Franke, Y., Bazan, J. F., Ernst, J., Hwang, J., Costa, M., Cochran, A. G., and Hannoush, R. N. (2010). Reconstitution of a frizzled8 Wnt3a LRP6 signaling complex reveals multiple Wnt and Dkk1 binding sites on LRP6. The Journal of biological chemistry 285, 9172-9.

Brent, A. E., and Tabin, C. J. (2002). Developmental regulation of somite derivatives: muscle, cartilage and tendon. Current opinion in genetics & development 12, 548-57.

Brown, N. A., and Wolpert, L. (1990). The development of handedness in left/right asymmetry. Development (Cambridge, England) 109, 1-9.

Buechling, T., Bartscherer, K., Ohkawara, B., Chaudhary, V., Spirohn, K., Niehrs, C., and Boutros, M. (2010). Wnt/Frizzled signaling requires dPRR, the Drosophila homolog of the prorenin receptor. Current Biology 20, 1263-8.

Bunney, T. D., Boer, A. H. De, and Levin, M. (2003). Fusicoccin signaling reveals 14-3-3 protein function as a novel step in left-right patterning during amphibian embryogenesis. Development (Cambridge, England) 130, 4847-58.

Byrne, R. A., Rundle, S. D., Smirthwaite, J. J., and Spicer, J. I. (2009). Embryonic rotational behaviour in the pond snail Lymnaea stagnalis: influences of environmental oxygen and development stage. Zoology (Jena, Germany) 112, 471-7.

Cadigan, K. M., and Liu, Y. I. (2006). Wnt signaling: complexity at the surface. Journal of cell science 119, 395-402.

Carneiro, K., Donnet, C., Rejtar, T., Karger, B. L., Barisone, G. a, Díaz, E., Kortagere, S., Lemire, J. M., and Levin, M. (2011). Histone deacetylase activity is necessary for left-right patterning during vertebrate development. BMC developmental biology 11, 29.

Caron, A., Xu, X., and Lin, X. (2011). Wnt/β-catenin signaling directly regulates Foxj1 expression and ciliogenesis in zebrafish Kupffer's vesicle. Development (Cambridge, England) 524, 514-524.

Cast, A. E., Gao, C., Amack, J. D., and Ware, S. M. (2012). An essential and highly conserved role for Zic3 in left-right patterning, gastrulation and convergent extension morphogenesis. Developmental biology, 1-10.

Cha, S.-W., Tadjuidje, E., Tao, Q., Wylie, C., and Heasman, J. (2008). Wnt5a and Wnt11 interact in a maternal Dkk1-regulated fashion to activate both canonical and non-canonical signaling in Xenopus axis formation. Development (Cambridge, England) 135, 3719-29.

Cha, Y. R., Takahashi, S., and Wright, C. V. E. (2006). Cooperative non-cell and cell autonomous regulation of Nodal gene expression and signaling by Lefty/Antivin and Brachyury in Xenopus. Developmental biology 290, 246-64.

Campbell, N. A. (1997) Kapitel 37. Ernährung der Tiere. Biologie 4/e. Spektrum Akademischer Verlag.

Chan, H. et al. (2010). The p-type ATPase superfamily. Journal of molecular microbiology and biotechnology 19, 5-104.

Chang, D. T., López, a, Kessler, D. P. von, Chiang, C, Simandl, B. K., Zhao, R., Seldin, M. F., Fallon, J. F., and Beachy, P. A. (1994). Products, genetic linkage and limb patterning activity of a murine hedgehog gene. Development (Cambridge, England) 120, 3339-53.

Carneiro, K., Donnet, C., Rejtar, T., Karger, B. L., Barisone, G. A., Díaz, E., Kortagere, S., Lemire, J. M., and Levin, M. (2011). Histone deacetylase activity is necessary for left-right patterning during vertebrate development. BMC developmental biology 11, 29.

Chen, R. H., Ding, W. V., and McCormick, F. (2000). Wnt signaling to beta-catenin involves two interactive components. Glycogen synthase kinase-3beta inhibition and activation of protein kinase C. The Journal of biological chemistry 275, 17894-9.

Chen, A. E., Ginty, D. D., and Fan, C.-M. (2005). Protein kinase A signalling via CREB controls myogenesis induced by Wnt proteins. Nature 433, 317-22.

Chen, H., Liu, L., Ma, B., Ma, T. M., Hou, J.-J., Xie, G.-M., Wu, W., Yang, F.-Q., and Chen, Y.-G. (2011). Protein kinase A-mediated 14-3-3 association impedes human Dapper1 to promote dishevelled degradation. The Journal of biological chemistry 286, 14870-80.

Chen, P.-X., Mathews, P. M., Good, P. J., and Rossier, B. C. (1998). Unusual degradation of alpha -beta complexes in Xenopus oocytes by beta -subunits of Xenopus gastric H-K-ATPase. Am J Physiol Cell Physiol, 139-145.

Chen, J. K., Taipale, J., Cooper, M. K., and Beachy, P. A. (2002). Inhibition of Hedgehog signaling by direct binding of cyclopamine to Smoothened. Genes & development 16, 2743-8.

Chen, M.-H., Wilson, C. W., Li, Y.-J., Law, K. K. L., Lu, C.-S., Gacayan, R., Zhang, X., Hui, C.-chung, and Chuang, P.-T. (2009). Cilium-independent regulation of Gli protein function by Sufu in Hedgehog signaling is evolutionarily conserved. Genes & development 23, 1910-28.

Chen, M.-H., Wilson, C. W., and Chuang, P.-T. (2007). SnapShot: hedgehog signaling pathway. Cell 130, 386.

Cheng, A. M., Thisse, B., Thisse, C., and Wright, C. V. (2000). The lefty-related factor Xatv acts as a feedback inhibitor of nodal signaling in mesoderm induction and L-R axis development in xenopus. Development (Cambridge, England) 127, 1049-61.

Chiang, C., Litingtung, Y., Lee, E., Young, K., Corden, J., Westphal, H., and Beachy, P. (1996). Cyclopia and defective axial patterning in mice lacking SHH gene function. Nature 383, 407-413.

Cohen, M. M. (2003). The hedgehog signaling network. American journal of medical genetics. Part A 123A, 5-28.

Cole, D. G., and Snell, W. J. (2009). SnapShot: Intraflagellar transport. Cell 137, 784-784.e1.

Copp, A. J., and Greene, N. D. E. (2010). Genetics and development of neural tube defects. Journal of Pathology, The, 217-230.

Couso, J. P. (2009). Segmentation, metamerism and the Cambrian explosion. The International journal of developmental biology 53, 1305-16.

Christian, J. L., McMahon, J. A., McMahon, A. P., and Moon, R. T. (1991). Xwnt-8, a Xenopus Wnt-1/int-1-related gene responsive to mesoderm-inducing growth factors, may play a role in ventral mesodermal patterning during embryogenesis. Development (Cambridge, England) 111, 1045-55.

Christian, J. L., and Moon, R T (1993). Interactions between Xwnt-8 and Spemann organizer signaling pathways generate dorsoventral pattern in the embryonic mesoderm of Xenopus. Genes & Development 7, 13-28.

Cruciat, C.-M., Ohkawara, B., Acebron, S. P., Karaulanov, E., Reinhard, C., Ingelfinger, D., Boutros, M., and Niehrs, C. (2010). Requirement of prorenin receptor and vacuolar H+-ATPase-mediated acidification for Wnt signaling. Supplement. Science (New York, N.Y.) 327, 459-63.

Cuykendall, T. N., and Houston, D. W. (2009). Vegetally localized Xenopus trim36 regulates cortical rotation and dorsal axis formation. Development (Cambridge, England) 136, 3057-65.

Danos, M. C., and Yost, H. J. (1995). Linkage of cardiac left-right asymmetry and dorsal-anterior development in Xenopus. Development (Cambridge, England) 121, 1467-74.

Dassow, G. von, Schmidt, J. E., and Kimelman, D. (1993). Induction of the Xenopus organizer: expression and regulation of Xnot, a novel FGF and activin-regulated homeo box gene. Genes & Development 7, 355-366.

Davenport, J. R., and Yoder, B. K. (2005). An incredible decade for the primary cilium: a look at a once-forgotten organelle. American journal of physiology. Renal physiology 289, F1159-69.

Davey, M. G. et al. (2006). The chicken talpid3 gene encodes a novel protein essential for Hedgehog signaling. Genes & development 20, 1365-77.

Deblandre, G., Wettstein, D., Koyano-Nakagawa, N., and Kintner, C (1999). A two-step mechanism generates the spacing pattern of the ciliated cells in the skin of Xenopus embryos. Development (Cambridge, England) 126, 4715-28.

Delmas, P. (2008). SnapShot: ion channels and pain. Cell 134, 366-366.e1.

Djiane, A., Riou, J., Umbhauer, M., Boucaut, J., and Shi, D. (2000). Role of frizzled 7 in the regulation of convergent extension movements during gastrulation in Xenopus laevis. Development (Cambridge, England) 127, 3091-100.

Donoughe, S., and DiNardo, S. (2011). Dachsous and frizzled contribute separately to planar polarity in the Drosophila ventral epidermis. Development (Cambridge, England) 138, 2751-9.

Doran, S. A. (2004). Effect of serotonin on ciliary beating and intracellular calcium concentration in identified populations of embryonic ciliary cells. Journal of Experimental Biology 207, 1415-1429.

Dubaissi, E., and Papalopulu, N. (2011). Embryonic frog epidermis: a model for the study of cell-cell interactions in the development of mucociliary disease. Disease models & mechanisms 4, 179-92.

Duboc, V., Röttinger, E., Lapraz, F., Besnardeau, L., and Lepage, T. (2005). Left-right

asymmetry in the sea urchin embryo is regulated by nodal signaling on the right side. Developmental cell 9, 147-58.

DuBose, T. D. J., Gitomer, J., and Codina, J. (1999). H+ ,K+ -ATPase. Curr Opin Nephrol Hypertens 8, 1-15.

Dutko, J. a, and Mullins, M. C. (2011). SnapShot: BMP signaling in development. Cell 145, 636, 636.e1-2.

Ede, D. A., and Kelly, W. A. (1964). Developmental Abnormalities in the Trunk and Limbs of the Talpid3 Mutant of the Fowl. Journal of embryology and experimental morphology 12, 339-56.

Eggenschwiler, J. T., and Anderson, K. V. (2007). Cilia and developmental signaling. Annual review of cell and developmental biology 23, 345-73.

Elinson, R. P., and Pasceri, P. (1989). Two UV-sensitive targets in dorsoanterior specification of frog embryos. Development (Cambridge, England) 106, 511-8.

Eisen, J. S., and Smith, J. C. (2008). Controlling morpholino experiments: don't stop making antisense. Development 135, 1735-1743.

Epperlein, H. H., Löfberg, J., and Olsson, L. (1996). Neural crest cell migration and pigment pattern formation in urodele amphibians. The International journal of developmental biology 40, 229-38.

Essner, J. J., Amack, J. D., Nyholm, M. K., Harris, E. B., and Yost, H. J. (2005). Kupffer's vesicle is a ciliated organ of asymmetry in the zebrafish embryo that initiates left-right development of the brain, heart and gut. Development (Cambridge, England) 132, 1247-60.

Essner, J. J., Vogan, K. J., Wagner, M. K., Tabin, C. J., Yost, H. J., and Brueckner, M. (2002). Conserved function for embryonic nodal cilia. Nature 418, 37-8.

Fakhro, K. A., Choi, M., Ware, S. M., Belmont, J. W., Towbin, J. a, Lifton, R. P., Khokha, M. K., and Brueckner, M. (2011). Rare copy number variations in congenital heart disease patients identify unique genes in left-right patterning. Proceedings of the National Academy of Sciences of the United States of America.

Feistel, K., and Blum, M. (2006). Three Types of Cilia Including a Novel 9 4 Axoneme on the Notochordal Plate of the Rabbit Embryo. Developmental dynamics : an official publication of the American Association of Anatomists 235, 3348 -3358.

Ferrari, M. B., and Spitzer, N. C. (1999). Calcium signaling in the developing Xenopus myotome. Developmental biology 213, 269-82.

Field, S. et al. (2011). Pkd1l1 establishes left-right asymmetry and physically interacts with Pkd2. Development (Cambridge, England) 1142, 1131-1142.

Fliegauf, M., Benzing, T., and Omran, H. (2007). When cilia go bad: cilia defects and ciliopathies. Nature Reviews Molecular Cell Biology 8, 880-893.

Fohl, A. L., and Regal, R. E. (2011). Proton pump inhibitor-associated pneumonia: Not a breath of fresh air after all? World journal of gastrointestinal pharmacology and therapeutics 2, 17-26.

Forte, J. G., and Zhu, L. (2010). Apical recycling of the gastric parietal cell H,K-ATPase. Annual review of physiology 72, 273-96.

Freund, J. B., Goetz, J. G., Hill, K. L., and Vermot, J. (2012). Fluid flows and forces in development: functions, features and biophysical principles. Development

(Cambridge, England) 139, 1229-45.

Fujimi, T. J., Hatayama, M., and Aruga, J. (2011). Xenopus Zic3 controls notochord and organizer development through suppression of Wnt/beta-catenin signaling pathway. Developmental biology.

Fukumoto, T., Blakely, R., and Levin, M. (2005b). Serotonin transporter function is an early step in left-right patterning in chick and frog embryos. Developmental neuroscience 27, 349-63.

Fukumoto, T., Kema, I. P., and Levin, M. (2005a). Serotonin signaling is a very early step in patterning of the left-right axis in chick and frog embryos. Current biology : CB 15, 794-803.

Gallet, A. (2011). Hedgehog morphogen: from secretion to reception. Trends in cell biology 21, 238-46.

Gao, B. et al. (2011). Wnt Signaling Gradients Establish Planar Cell Polarity by Inducing Vangl2 Phosphorylation through Ror2. Developmental cell 20, 163-76.

Gao, C., and Chen, Y.-G. (2010). Dishevelled: The hub of Wnt signaling. Cellular signalling 22, 717-27.

Geering, K. (2001). The functional role of beta subunits in oligomeric P-type ATPases. Journal of bioenergetics and biomembranes 33, 425-38.

Gilbert, S. F. (2003a) "Chapter 10: Early development and axis formation in amphibians." Developmental Biology, Seventh Edition. Sinauer.

Gilbert, S. F. (2003b) "Chapter 12: The emergence of the ectoderm: The central nervous system and the epidermis." Developmental Biology, Seventh Edition. Sinauer.

Gilbert, S. F. (2003c) "Chapter 14: Paraxial and intermediate mesoderm." Developmental Biology, Seventh Edition. Sinauer.

Gilbert, S. F. (2003d) "Chapter 15: Lateral plate mesoderm and endoderm." Developmental Biology, Seventh Edition. Sinauer.

Glinka, A., Delius, H., Blumenstock, C., and Niehrs, C.(1996). Combinatorial signalling by Xwnt-ll and Xnr3 in the organizer epithelium. Mechanisms of Development 60, 221-231.

Gomperts, B. N., Gong-Cooper, X., and Hackett, B. P. (2004). Foxj1 regulates basal body anchoring to the cytoskeleton of ciliated pulmonary epithelial cells. Journal of cell science 117, 1329-37.

Grande, C. (2010). Left-right asymmetries in Spiralia. Integrative and comparative biology 50, 744-55.

Grande, C., and Patel, N. H. (2009). Nodal signalling is involved in left-right asymmetry in snails. Nature 457, 1007-11.

Green, J.B., and Smith, J.C. (1990). Graded changes in dose of a Xenopus activin A homologue elicit stepwise transitions in embryonic cell fate. Nature 347, 391–394.

Gros, J., Feistel, K., Viebahn, C., Blum, M., and Tabin, C. J. (2009). Cell movements at Hensen's node establish left/right asymmetric gene expression in the chick. Science (New York, N.Y.) 324, 941-4.

Gurdon, J. B., and Hopwood, N. (2000). The introduction of Xenopus laevis into developmental biology: of empire, pregnancy testing and ribosomal genes. The International journal of developmental biology 44, 43-50.

Hamada, H. (2008). Breakthroughs and future challenges in left-right patterning. Development, growth & differentiation 50 Suppl 1, S71-8.

Harder, J. L., and Margolis, B. (2008). SnapShot: tight and adherens junction signaling. Cell 133, 1118, 1118.e1-2.

Hardy, K. M., Garriock, R. J., Yatskievych, T. a, D'Agostino, S. L., Antin, P. B., and Krieg, P. A. (2008). Non-canonical Wnt signaling through Wnt5a/b and a novel Wnt11 gene, Wnt11b, regulates cell migration during avian gastrulation. Developmental biology 320, 391-401.

Harland, R. M., and Grainger, R. M. (2011). Xenopus research: metamorphosed by genetics and genomics. Trends in genetics : TIG 27, 507-515.

Harrisson, F. (1989). The extracellular matrix and cell surface, mediators of cell interactions in chicken gastrulation. The International journal of developmental biology 33, 417-38.

Hashimoto, M., and Hamada, H. (2010). Translation of anterior-posterior polarity into left-right polarity in the mouse embryo. Current opinion in genetics & development 20, 433-7.

Hashimoto, H., Rebagliati, M., Ahmad, N., Muraoka, O., Kurokawa, T., Hibi, M., and Suzuki, T. (2004). The Cerberus/Dan-family protein Charon is a negative regulator of Nodal signaling during left-right patterning in zebrafish. Development (Cambridge, England) 131, 1741-53.

Hayes, J. M., Kim, S. K., Abitua, P. B., Park, T. J., Herrington, E. R., Kitayama, A., Grow, M. W., Ueno, N., and Wallingford, J. B. (2007). Identification of novel ciliogenesis factors using a new in vivo model for mucociliary epithelial development. Developmental biology 312, 115-30.

Heasman, J. (1997). Patterning the Xenopus blastula. Development (Cambridge, England) 124, 4179-91.

Heasman, Janet (2006). Maternal determinants of embryonic cell fate. Seminars in cell & developmental biology 17, 93-8.

Heitzmann, D., and Warth, R. (2008). Physiology and pathophysiology of potassium channels in gastrointestinal epithelia. Physiological reviews 88, 1119-82.

Hendrickx, M., and Leyns, L. (2008). Non-conventional Frizzled ligands and Wnt receptors. Develop. Growth Differ. 50, 229-243.

Hermle, T., Saltukoglu, D., Grünewald, J., Walz, G., Simons, M., Gru, J., and Division, R. (2010). Regulation of Frizzled-dependent planar polarity signaling by a V-ATPase subunit. Current biology : CB 20, 1269-76.

Herrmann, M., Selige, J., Raffael, S., Sachs, G., Brambilla, A., and Klein, T. (2007). Systematic expression profiling of the gastric H+/K+ ATPase in human tissue. Scandinavian journal of gastroenterology 42, 1275-88.

Hibino, T., Ishii, Y., Levin, M., and Nishino, A. (2006). Ion flow regulates left-right asymmetry in sea urchin development. Development genes and evolution 216, 265-76.

Hilfinger, A., and Jülicher, F. (2008). The chirality of ciliary beats. Physical biology 5, 016003.

Hirokawa, N., and Noda, Y. (2008). Intracellular transport and kinesin superfamily proteins, KIFs: structure, function, and dynamics. Physiological reviews 88, 1089-118.

Hirokawa, N., Tanaka, Y., Okada, Y., and Takeda, S. (2006). Nodal flow and the generation of left-right asymmetry. Cell 125, 33-45.

Hirokawa, N., Tanaka, Y., and Okada, Y. (2012). Cilia, KIF3 molecular motor and nodal flow. Current Opinion in Cell Biology 24, 31-39.

Hirokawa, N., Tanaka, Y., and Okada, Y. (2009). Left-right determination: involvement of molecular motor KIF3, cilia, and nodal flow. Cold Spring Harbor perspectives in biology 1, a000802.

Huang, T. et al. (2003). Foxj1 is required for apical localization of ezrin in airway epithelial cells. Journal of cell science 116, 4935-45.

Ikuzawa, M. , Yasumasu, S., Kobayashi, K.-I., Inokuchi, T. and Iuchi, I. (2004). Stomach remodeling-associated changes of H+/K+-ATPase b subunit expression in Xenopus laevis and H+/K+-ATPase-dependent acid secretion in tadpole stomach. Journal of Experimental Zoology 301A:992-1002.

Ilagan, M. X. G., and Kopan, R. (2007). SnapShot: notch signaling pathway. Cell 128, 1246.

In der Rieden, P. M. J., Vilaspasa, F. L., and Durston, A. J. (2010). Xwnt8 directly initiates expression of labial Hox genes. Developmental dynamics : an official publication of the American Association of Anatomists 239, 126-39.

Ishiuchi, T., Misaki, K., Yonemura, S., Takeichi, M., and Tanoue, T. (2009). Mammalian Fat and Dachsous cadherins regulate apical membrane organization in the embryonic cerebral cortex. The Journal of cell biology 185, 959-67.

Ja, H., J,, Y., J., T., Visan, I., and C., G. (2003). Developmental Biology : Frontiers for Clinical Genetics Notch signaling in development and disease. Clinical Genetics 1, 461-472.

Jackson, P. K. (2011). Do cilia put brakes on the cell cycle ? Nature cell biology 13, 340-342.

Jiang, J., and Hui, C.-C. (2008). Hedgehog signaling in development and cancer. Developmental cell 15, 801-12.

Kamura, K., Kobayashi, D., Uehara, Y., Koshida, S., Iijima, N., Kudo, A., Yokoyama, T., and Takeda, H. (2011). Pkd1l1 complexes with Pkd2 on motile cilia and functions to establish the left-right axis. Development (Cambridge, England) 138, 1121-9.

Karcher, C., Fischer, A., Schweickert, A., Bitzer, E., Horie, S., Witzgall, R., and Blum, Martin (2005). Lack of a laterality phenotype in Pkd1 knock-out embryos correlates with absence of polycystin-1 in nodal cilia. Differentiation; research in biological diversity 73, 425-32.

Katow, H., Yaguchi, S., and Kyozuka, K. (2007). Serotonin stimulates [Ca2+]i elevation in ciliary ectodermal cells of echinoplutei through a serotonin receptor cell network in the blastocoel. The Journal of experimental biology 210, 403-12.

Kawano, Y., and Kypta, R. (2003). Secreted antagonists of the Wnt signalling pathway. Journal of cell science 116, 2627-34.

Keller, R., Davidson, L. A., and Shook, D. R. (2003). How we are shaped: the biomechanics of gastrulation. Differentiation; research in biological diversity 71, 171-205.

Keller, R., Shook, D., and Skoglund, P. (2008). The forces that shape embryos: physical

aspects of convergent extension by cell intercalation. Physical biology 5, 015007.

Kitaguchi, T., Mizugishi, K., Hatayama, M., Aruga, J., and Mikoshiba, K. (2002). Xenopus Brachyury regulates mesodermal expression of Zic3, a gene controlling left-right asymmetry. Development, growth & differentiation 44, 55-61.

King, M. L., Messitt, T. J., and Mowry, K. L. (2005). Putting RNAs in the right place at the right time: RNA localization in the frog oocyte. Biology of the cell / under the auspices of the European Cell Biology Organization 97, 19-33.

Klein, S. L. (1987). The first cleavage furrow demarcates the dorsal-ventral axis in Xenopus embryos. Developmental biology 120, 299-304.

Kishimoto, N., and Sawamoto, K. (2011). Planar polarity of ependymal cilia. Differentiation; research in biological diversity, 1-5.

Kitaguchi, T., Mizugishi, K., Hatayama, M., Aruga, J., and Mikoshiba, K. (2002). Xenopus Brachyury regulates mesodermal expression of Zic3, a gene controlling left-right asymmetry. Development, growth & differentiation 44, 55-61.

Knecht, A. K., and Harland, R. M. (1997). Mechanisms of dorsal-ventral patterning in noggin-induced neural tissue. Development (Cambridge, England) 124, 2477-88.

Kofron, M., Birsoy, B., Houston, D., Tao, Q., Wylie, C., and Heasman, J. (2007). Wnt11/beta-catenin signaling in both oocytes and early embryos acts through LRP6-mediated regulation of axin. Development (Cambridge, England) 134, 503-13.

Kohna, A. D., and Moon, R. T. (2005). Wnt and calcium signaling: b-Catenin-independent pathways. cell calcium 38, 439-446.

König, P., Krain, B., Krasteva, G., and Kummer, W. (2009). Serotonin increases cilia-driven particle transport via an acetylcholine-independent pathway in the mouse trachea. PloS one 4, e4938.

Kopan, R., and Ilagan, M. X. G. (2009). The canonical Notch signaling pathway: unfolding the activation mechanism. Cell 137, 216-33.

Kreiling, J. A., Balantac, Z. L., Crawford, A. R., Ren, Y., Toure, J., Zchut, S., Kochilas, L., and Creton, R. (2008). Suppression of the endoplasmic reticulum calcium pump during zebrafish gastrulation affects left-right asymmetry of the heart and brain. Mechanisms of development 125, 396-410.

Krieger, J., and Breer, H. (1999). Olfactory Reception in Invertebrates. Science 286, 720-723.

Kuang, S., Doran, S. A., Wilson, R. J. A., Goss, G. G., and Goldberg, J. I. (2002). Serotonergic sensory-motor neurons mediate a behavioral response to hypoxia in pond snail embryos. Journal of neurobiology 52, 73-83.

Kühl, M., Sheldahl, L. C., Malbon, C. C., and Moon, R T (2000). Ca(2+)/calmodulin-dependent protein kinase II is stimulated by Wnt and Frizzled homologs and promotes ventral cell fates in Xenopus. The Journal of biological chemistry 275, 12701-11.

Kuroda, R., Endo, B., Abe, M., and Shimizu, M. (2009). Chiral blastomere arrangement dictates zygotic left-right asymmetry pathway in snails. Nature 462, 790-4.

Leclerc, C., Lee, M., Webb, S. E., Moreau, M., and Miller, A. L. (2003). Calcium transients triggered by planar signals induce the expression of ZIC3 gene during neural induction in Xenopus. Developmental Biology 261, 381-390.

Lecuit, T., and Goff, L. Le (2007). Orchestrating size and shape during morphogenesis. Nature 450, 189-92.

Lei, Q., Jeong, Y., Misra, K., Li, S., Zelman, A. K., Epstein, D. J., and Matise, M. P. (2006). Wnt signaling inhibitors regulate the transcriptional response to morphogenetic Shh-Gli signaling in the neural tube. Developmental cell 11, 325-37.

Levin, M., Johnson, R. L., Stern, C. D., Kuehn, M., and Tabin, C. (1995). Determining Left-Right Asymmetry in Chick Embryogenesis. Cell 82, 803-814.

Levin, M, Pagan, S., Roberts, D. J., Cooke, J., Kuehn, M. R., and Tabin, C. J. (1997). Left/right patterning signals and the independent regulation of different aspects of situs in the chick embryo. Developmental biology 189, 57-67.

Levin, M., and Mercola, M. (1998). Gap junctions are involved in the early generation of left-right asymmetry. Developmental biology 203, 90-105.

Levin, M, and Mercola, M (1999). Gap junction-mediated transfer of left-right patterning signals in the early chick blastoderm is upstream of Shh asymmetry in the node. Development (Cambridge, England) 126, 4703-14.

Levin, M., Thorlin, T., Robinson, K. R., Nogi, T., and Mercola, M. (2002). Asymmetries in H+/K+-ATPase and cell membrane potentials comprise a very early step in left-right patterning. Cell 111, 77-89.

Levin, M. (2003). Motor protein control of ion flux is an early step in embryonic left-right asymmetry. BioEssays : news and reviews in molecular, cellular and developmental biology 25, 1002-10.

Levin, Michael, and Palmer, R. A. (2007). Left-right patterning from the inside out: widespread evidence for intracellular control. BioEssays : news and reviews in molecular, cellular and developmental biology 29, 271-87.

Linask, K. K., and Vanauker, M. (2007). A role for the cytoskeleton in heart looping. TheScientificWorldJournal 7, 280-98.

Liu, G., Bafico, A., Harris, V. K., and Aaronson, S. A. (2003). A Novel Mechanism for Wnt Activation of Canonical Signaling through the LRP6 Receptor. Society 23, 5825-5835.

Lohr, J. L., Danos, M. C., and Yost, H. J. (1997). Left-right asymmetry of a nodal-related gene is regulated by dorsoanterior midline structures during Xenopus development. Development (Cambridge, England) 124, 1465-72.

Lohr, J. L., Danos, M. C., Groth, T. W., and Yost, H. J. (1998). Maintenance of asymmetric nodal expression in Xenopus laevis. Developmental genetics 23, 194-202.

Look, D. C., Walter, M. J., Williamson, M. R., Pang, L., You, Y, Sreshta, J. N., Johnson, J. E., Zander, D. S., and Brody, S. L .(2001). Effects of paramyxoviral infection on airway epithelial cell Foxj1 expression, ciliogenesis, and mucociliary function. The American journal of pathology 159, 2055-69.

Lucero, O. M., Dawson, D. W., Moon, R. T., and Chien, A. J. (2010). A re-evaluation of the "oncogenic" nature of Wnt/beta-catenin signaling in melanoma and other cancers. Current oncology reports 12, 314-8.

Lyu, R. M., and Farley, R. A. (1997). Amino acids Val115-Ile126 of rat gastric H(+)-K(+)-ATPase confer high affinity for Sch-28080 to Na(+)-K(+)-ATPase. The American journal of physiology 272, C1717-25.

MacDonald, B. T., Tamai, K., and He, X. (2009). Wnt/beta-catenin signaling: components, mechanisms, and diseases. Developmental cell 17, 9-26.

MacDonald, B. T., Semenov, M. V., and He, X. (2007). SnapShot Wnt β-Catenin Signaling. Cell 131, 1204.

Maisonneuve, C., Guilleret, I., Vick, P., Weber, T., Andre, P., Beyer, T., Blum, M., and Constam, D. B. (2009). Bicaudal C, a novel regulator of Dvl signaling abutting RNA-processing bodies, controls cilia orientation and leftward flow. Development (Cambridge, England) 136, 3019-30.

Marques, S., Borges, A. C., Silva, A. C., Freitas, S., Cordenonsi, M., and Belo, J. A. (2004). The activity of the Nodal antagonist Cerl-2 in the mouse node is required for correct L/R body axis. Genes & development 18, 2342-7.

Marshall, W F, and Rosenbaum, J. L. (2001). Intraflagellar transport balances continuous turnover of outer doublet microtubules: implications for flagellar length control. The Journal of cell biology 155, 405-14.

Matthes, S., Mosienko, V., Bashammakh, S., Alenina, N., and Bader, M. (2010). Tryptophan hydroxylase as novel target for the treatment of depressive disorders. Pharmacology 85, 95-109.

Matthews, H. K., Broders-Bondon, F., Thiery, J. P., and Mayor, R. (2008). Wnt11r is required for cranial neural crest migration. Developmental dynamics : an official publication of the American Association of Anatomists 237, 3404-9.

Maurus, D., and Harris, W. A. (2009). Zic-associated holoprosencephaly: zebrafish Zic1 controls midline formation and forebrain patterning by regulating Nodal, Hedgehog, and retinoic acid signaling. Genes & development 23, 1461-73.

Mayor, R., and Aybar, M. (2001). Induction and development of neural crest in Xenopus laevis. Cell and Tissue Research 305, 203-209.

McGrath, J., Somlo, S., Makova, S., Tian, X., and Brueckner, M. (2003). Two populations of node monocilia initiate left-right asymmetry in the mouse. Cell 114, 61-73.

McGrew, L. L., Takemaru, K., Bates, R., and Moon, R. T. (1999). Direct regulation of the Xenopus engrailed-2 promoter by the Wnt signaling pathway, and a molecular screen for Wnt-responsive genes, confirm a role for Wnt signaling during neural patterning in Xenopus. Mechanisms of development 87, 21-32.

Mii, Y., and Taira, M. (2009). Secreted Frizzled-related proteins enhance the diffusion of Wnt ligands and expand their signalling range. Development (Cambridge, England) 136, 4083-8.

Mimoto M. S., Christian J. L. Manipulation of Gene Function in Xenopus laevis. Methods Mol Biol. 2011;770:55-75.

Miskevich, F. (2010). Imaging fluid flow and cilia beating pattern in Xenopus brain ventricles. Journal of neuroscience methods 189, 1-4.

Mitchell, B., Jacobs, R., Li, J., Chien, S., and Kintner, C. (2007). A positive feedback mechanism governs the polarity and motion of motile cilia. Nature 447, 97-101.

Mitchell, B., Stubbs, Jennifer L, Huisman, F., Taborek, P., Yu, C., and Kintner, Chris (2009). The PCP pathway instructs the planar orientation of ciliated cells in the Xenopus larval skin. Current biology : CB 19, 924-9.

Molla-Herman, A. et al. (2010). The ciliary pocket: an endocytic membrane domain at the base of primary and motile cilia. Journal of cell science 123, 1785-95.

Mongin, A. A., and Orlov, S. N. (2011). Mechanisms Of Cell Volume Regulation. Physiology and maintenance I.

Morokuma, J., Blackiston, D., and Levin, M. (2008). KCNQ1 and KCNE1 K + Channel Components are Involved in Early Left-Right Patterning in Xenopus laevis Embryos.

Cellular Physiology and Biochemistry, 357-372.

Morth, J. P., Pedersen, B. P., Buch-Pedersen, M. J., Andersen, J. P., Vilsen, B., Palmgren, Michael G, and Nissen, P. (2011). A structural overview of the plasma membrane Na+,K+-ATPase and H+-ATPase ion pumps. Nature reviews. Molecular cell biology 12, 60-70.

Mucenski, M. L. et al. (2005). Beta-catenin regulates differentiation of respiratory epithelial cells in vivo. American journal of physiology. Lung cellular and molecular physiology 289, L971-9.

Munson, K., Law, R. J., and Sachs, G. (2007). Analysis of the gastric H,K ATPase for ion pathways and inhibitor binding sites. Biochemistry 46, 5398-417.

Nagai, K., Ishida, T., Hashimoto, T., Harada, Y., Ueno, S., Ueda, Y., Kubo, H., and Iwao, Y. (2009). The Sperm-surface glycoprotein, SGP, is necessary for fertilization in the frog, Xenopus laevis. Development, growth & differentiation 51, 499-510.

Newport, J., and Kirschner, M. (1982). A major developmental transition in early Xenopus embryos: I. characterization and timing of cellular changes at the midblastula stage. Cell 30, 675-86.

Niehrs, C. (2001). The Spemann organizer and embryonic head induction. The EMBO journal 20, 631-7.

Niehrs, C. (2010). On growth and form: a Cartesian coordinate system of Wnt and BMP signaling specifies bilaterian body axes. Development (Cambridge, England) 137, 845-57.

Niehrs, C., and Boutros, M. (2010). Trafficking, acidification, and growth factor signaling. Science signaling 3, pe26.

Nieuwkoop and Faber (1994) Normal Table of Xenopus laevis (Daudin). Garland Publishing Inc.

Nishide, K., Mugitani, M., Kumano, G., and Nishida, H. (2012). Neurula rotation determines left-right asymmetry in ascidian tadpole larvae. Development (Cambridge, England) 1475, 1467-1475.

Nishita, M., Enomoto, M., Yamagata, K., and Minami, Y. (2010). Cell/tissue-tropic functions of Wnt5a signaling in normal and cancer cells. Trends in cell biology 20, 346-54.

Nonaka, S., Tanaka, Y., Okada, Y., Takeda, S., Harada, A., Kanai, Y., Kido, M., and Hirokawa, N (1998). Randomization of left-right asymmetry due to loss of nodal cilia generating leftward flow of extraembryonic fluid in mice lacking KIF3B motor protein. Cell 95, 829-37.

Nonaka, S., Shiratori, H., Saijoh, Y., and Hamada, H. (2002). Determination of left – right patterning of the mouse embryo by artificial nodal flow. Nature 418, 96-99.

Norris, D. (2005). Breaking the left-right axis: do nodal parcels pass a signal to the left? BioEssays : news and reviews in molecular, cellular and developmental biology 27, 991-4.

Norris, D. P., and Grimes, D. T. (2012). Mouse models of ciliopathies: the state of the art. Disease Models & Mechanisms 5, 299-312.

Nusse, R., and Varmus, H. E. (1982). Many tumors induced by the mouse mammary tumor virus contain a provirus integrated in the same region of the host genome. Cell 31, 99-109.

Oh, E. C., and Katsanis, N. (2012). Cilia in vertebrate development and disease. Development 139, 443-448.

Ohi, Y., and Wright, C. V. E. (2007). Anteriorward shifting of asymmetric Xnr1 expression and contralateral communication in left-right specification in Xenopus. Developmental biology 301, 447-63.

Ohkawara, B., Glinka, A., and Niehrs, C. (2011). Rspo3 Binds Syndecan 4 and Induces Wnt/PCP Signaling via Clathrin-Mediated Endocytosis to Promote Morphogenesis. Developmental cell 20, 303-14.

Okamura, H., Yasuhara, J. C., Fambrough, D. M., and Takeyasu, K. (2003). P-type ATPases in Caenorhabditis and Drosophila: implications for evolution of the P-type ATPase subunit families with special reference to the Na,K-ATPase and H,K-ATPase subgroup. The Journal of membrane biology 191, 13-24.

Okeda, Y., Takeda, S., Tanaka, Y., Izpisúa Belmonte, J. C., and Hirokawa, N. (2005). Mechanism of nodal flow: a conserved symmetry breaking event in left-right axis determination. Cell 121, 633-44.

Oliverio, M., Digilio, M. C., Versacci, P., Dallapiccola, B., and Marino, B. (2010). Shells and heart: are human laterality and chirality of snails controlled by the same maternal genes? American journal of medical genetics. Part A 152A, 2419-25.

Oteiza, P. et al. (2010). Planar cell polarity signalling regulates cell adhesion properties in progenitors of the zebrafish laterality organ. Development (Cambridge, England) 137, 3459-68.

Pan, J., You, Yingjian, Huang, T., and Brody, S. L. (2007). RhoA-mediated apical actin enrichment is required for ciliogenesis and promoted by Foxj1. Journal of cell science 120, 1868-76.

Park, E., Kim, G.-H., Choi, S.-C., and Han, J.-K. (2006). Role of PKA as a negative regulator of PCP signaling pathway during Xenopus gastrulation movements. Developmental biology 292, 344-57.

Paterson, H. F., Self, A. J., Garrett, M. D., Just, I., Aktories, K., and Hall, A. (1990). Microinjection of recombinant p21rho induces rapid changes in cell morphology. The Journal of cell biology 111, 1001-7.

Pearce, J. J., Penny, G., and Rossant, J. (1999). A mouse cerberus/Dan-related gene family. Developmental biology 209, 98-110.

Pera, E. M., and Robertis, E. M. D. (2000). A direct screen for secreted proteins in Xenopus embryos identifes distinct activities for the Wnt antagonists Crescent and Frzb-1. Mechanisms of development 96, 183-195.

Pennekamp, P., Karcher, C., Fischer, A., Schweickert, A., Skryabin, B., Horst, J., Blum, M., and Dworniczak, B. (2002). The ion channel polycystin-2 is required for left-right axis determination in mice. Current biology : CB 12, 938-43.

Perrimon, N., and Mahowald, A. P. (1987). Multiple functions of segment polarity genes in Drosophila. Developmental biology 119, 587-600.

Peyrot, S. M., Wallingford, J. B., and Harland, R. M. (2011). A revised model of Xenopus dorsal midline development: differential and separable requirements for Notch and Shh signaling. Developmental biology 352, 254-66.

Pohl, B. S., and Knöchel, W. (2004). Isolation and developmental expression of Xenopus FoxJ1 and FoxK1. Development genes and evolution 214, 200-5.

Quigley, I. K., Stubbs, J. L., and Kintner, C. (2011). Specification of ion transport cells in the Xenopus larval skin. Development (Cambridge, England) 138, 705-14.

Rabon, E. C., and Reuben, M. A. (1990). The mechanism and structure of the gastric H,K-ATPase. Annual review of physiology 52, 321-44.

Reuben, M. A., Lasatero, L. S., Chowl, D. C., and Forte, J. G. (1991). The H,K-ATPase beta-Subunit Can Act as a Surrogate for the beta-Subunit of Na,K-pumps. October 41, 19131-19134.

Riedel-Kruse, I. H., Hilfinger, A., Howard, J., and Jülicher, F. (2007). How molecular motors shape the flagellar beat. HFSP journal 1, 192-208.

Robertis, E. D., and Sasai, Y. (1996). A common plan for dorsoventral patterning in Bilateria. Nature 380, 37-40.

Roël, G., Gent, Y. Y. J., Peterson-Maduro, J., Verbeek, F. J., and Destrée, O. (2009). Lef1 plays a role in patterning the mesoderm and ectoderm in Xenopus tropicalis. International Journal 89, 81-89.

Rogers, C. D., Archer, T. C., Cunningham, D. D., Grammer, T. C., and Casey, E. M. S. (2008). Sox3 expression is maintained by FGF signaling and restricted to the neural plate by Vent proteins in the Xenopus embryo. Developmental biology 313, 307-19.

Rohatgi, R., Milenkovic, L., and Scott, M. P. (2007). Patched1 regulates hedgehog signaling at the primary cilium. Science (New York, N.Y.) 317, 372-6.

Ross, A. J., Dailey, L. A. (2007) Differentiation in human airway epithelial cells. American journal of respiratory cell and molecular biology 37, 169-85.

Ruel, L., and Thérond, P. P. (2009). Variations in Hedgehog signaling: divergence and perpetuation in Sufu regulation of Gli. Genes & development 23, 1843-8.

Rutenberg, J., Cheng, S.-M., and Levin, M. (2002). Early embryonic expression of ion channels and pumps in chick and Xenopus development. Developmental dynamics : an official publication of the American Association of Anatomists 225, 469-84.

Satir, P. (1980). Structural basis of ciliary movement. Environmental health perspectives 35, 77-82.

Satir, P., and Christensen, S. T. (2007). Overview of structure and function of mammalian cilia. Annual review of physiology 69, 377-400.

Sawaguchi, A., McDonald, K. L., and Forte, J. G. (2004). High-pressure Freezing of Isolated Gastric Glands Provides New Insight into the Fine Structure and Subcellular Localization of H+/K+-ATPase in Gastric Parietal Cells. Journal of Histochemistry & Cytochemistry 52, 77-86.

Sawamoto, K. et al. (2006). New neurons follow the flow of cerebrospinal fluid in the adult brain. Science (New York, N.Y.) 311, 629-32.

Schambony, A., and Wedlich, D. (2007). Wnt-5A/Ror2 regulate expression of XPAPC through an alternative noncanonical signaling pathway. Developmental cell 12, 779-92.

Scharf, S. R., and Gerhart, J. C. (1980). Determination of the dorsal-ventral axis in eggs of Xenopus laevis: complete rescue of uv-impaired eggs by oblique orientation before first cleavage. Developmental biology 79, 181-98.

Schmid, A., and Salathe, M. (2011). Ciliary beat co-ordination by calcium. Biology of the cell / under the auspices of the European Cell Biology Organization 103, 159-69.

Schneider, I., Houston, D. W., Rebagliati, M. R., and Slusarski, D. C. (2008). Calcium fluxes in dorsal forerunner cells antagonize beta-catenin and alter left-right patterning. Development (Cambridge, England) 135, 75-84.

Schreiber, R. (2005). Ca2+ signaling, intracellular pH and cell volume in cell proliferation. The Journal of membrane biology 205, 129-37.

Schweickert, A., Steinbeisser, H., and Blum, M. (2001). Differential gene expression of Xenopus Pitx1, Pitx2b and Pitx2c during cement gland, stomodeum and pituitary development. Mechanisms of development 107, 191-4.

Schweickert, A., Vick, P., Getwan, M., Weber, T., Schneider, I., Eberhardt, M., Beyer, T., Pachur, A., and Blum, Martin (2010). The Nodal Inhibitor Coco Is a Critical Target of Leftward Flow in Xenopus. Current Biology 20, 738-743.

Schweickert, A., Walentek, P., Thumberger, T., and Danilchik, M. (2011). Linking early determinants and cilia-driven leftward flow in left-right axis specification of Xenopus laevis: A theoretical approach. Differentiation; research in biological diversity, 1-11.

Schweickert, A., Weber, T., Beyer, T., Vick, P., Bogusch, S., Feistel, K., and Blum, M. (2007). Cilia-driven leftward flow determines laterality in Xenopus. Current biology : CB 17, 60-6.

Semenov, M. V., Habas, R., Macdonald, B. T., and He, X. (2007). SnapShot: Noncanonical Wnt Signaling Pathways. Cell 131, 1378.

Shartau, R. B., Harris, S., Boychuk, E. C., and Goldberg, J. I. (2010). Rotational behaviour of encapsulated pond snail embryos in diverse natural environments. The Journal of experimental biology 213, 2086-93.

Shimeld, S. M., and Levin, M. (2006). Evidence for the regulation of left-right asymmetry in Ciona intestinalis by ion flux. Developmental dynamics : an official publication of the American Association of Anatomists 235, 1543-53.

Shin, J.-B., Adams, D., Paukert, M., Siba, M., Sidi, S., Levin, M., Gillespie, P. G., and Gründer, S. (2005). Xenopus TRPN1 (NOMPC) localizes to microtubule-based cilia in epithelial cells, including inner-ear hair cells. Proceedings of the National Academy of Sciences of the United States of America 102, 12572-7.

Shin, J. M., Munson, K., Vagin, O., and Sachs, G. (2009). The gastric HK-ATPase: structure, function, and inhibition. Pflügers Archiv : European journal of physiology 457, 609-22.

Shin, J. M., and Sachs, G. (2006). Gastric H,K-ATPase as a drug target. Digestive diseases and sciences 51, 823-33.

Shiratori, H. et al. (2001). Two-step regulation of left-right asymmetric expression of Pitx2: initiation by nodal signaling and maintenance by Nkx2. Molecular cell 7, 137-49.

Shinohara, K. et al. (2012). Two rotating cilia in the node cavity are sufficient to break left-right symmetry in the mouse embryo. Nature communications 3, 622.

Shook, D. R., Majer, C., and Keller, R. (2004). Pattern and morphogenesis of presumptive superficial mesoderm in two closely related species, Xenopus laevis and Xenopus tropicalis. Developmental biology 270, 163-85.

Sive, H. L., Grainger, R. M., Harland, R. M. (2000). Early Development of Xenopus Laevis: A Laboratory Manual. Cold Spring Harbor Press.

Skirkanich, J., Luxardi, G., Yang, J., Kodjabachian, L. and Klein, P. S. (2011). An essential role for transcription before the MBT in Xenopus laevis. Developmental biology 357,

478-91.

Skoglund, P., Rolo, A., Chen, X., Gumbiner, B. M., and Keller, R. (2008). Convergence and extension at gastrulation require a myosin IIB-dependent cortical actin network. Development (Cambridge, England) 135, 2435-44.

Smith, J. C., Conlon, F. L., Saka, Y., and Tada, M. (2000). Xwnt11 and the regulation of gastrulation in Xenopus. Philosophical transactions of the Royal Society of London. Series B, Biological sciences 355, 923-30.

Smith, M. S., Turner, F. R., and Raff, R. A. (2008). Nodal expression and heterochrony in the evolution of dorsal-ventral and left-right axes formation in the direct-developing sea urchin Heliocidaris erythrogramma. Journal of experimental zoology. Part B, Molecular and developmental evolution 310, 609-22.

Sokol, S., Christian, J. L., Moon, R. T., and Melton, D. A. (1991). Injected Wnt RNA induces a complete body axis in Xenopus embryos. Cell 67, 741-52.

Soliman, S. (1983). Pharmacological control of ciliary activity in the young sea urchin larva. Effects of cholinergic anticholinergic agents. 74, 397-407.

Soliman, S. (1984). Pharmacological control of ciliary activity in the young sea urchin larva. Studies on the role of Ca2+ and cyclic nucleotides. Comparative biochemistry and physiology. C, Comparative pharmacology and toxicology 78, 183-91.

Song, H., Hu, J., Chen, W., Elliott, G., Andre, P., Gao, B., and Yang, Y. (2010). Planar cell polarity breaks bilateral symmetry by controlling ciliary positioning. Nature 466, 378-82.

Spemann, H., Mangold, H. (1924). Über Induktion von Embryonalanlagen durch Implantation artfremder Organisatoren. Development Genes and Evolution Volume 100, Numbers 3-4, 599-638.

Steinbeisser, H., Fainsod, A., Niehrs, C, Sasai, Y., and Robertis, E. M. De (1995). The role of gsc and BMP-4 in dorsal-ventral patterning of the marginal zone in Xenopus: a loss-of-function study using antisense RNA. The EMBO journal 14, 5230-43.

Stubbs, J. L., Oishi, I., Izpisúa Belmonte, J. C., and Kintner, C. (2008). The forkhead protein Foxj1 specifies node-like cilia in Xenopus and zebrafish embryos. Nature Genetics 40, 1-7.

Stubbs, J. L., Vladar, E. K., Axelrod, J. D., and Kintner, C. (2012). Multicilin promotes centriole assembly and ciliogenesis during multiciliate cell differentiation. Nature Cell Biology 14, 1-10.

Tabin, C. J. (2006). The key to left-right asymmetry. Cell 127, 27-32.

Tada, M., and Smith, J. C. (2000). Xwnt11 is a target of Xenopus Brachyury: regulation of gastrulation movements via Dishevelled, but not through the canonical Wnt pathway. Development (Cambridge, England) 127, 2227-38.

Tadjuidje, E., Cha, S.-W., Louza, M., Wylie, C., and Heasman, J. (2011). The functions of maternal Dishevelled 2 and 3 in the early Xenopus embryo. Developmental dynamics : an official publication of the American Association of Anatomists 240, 1727-36.

Tahinci, E., Thorne, C. A., Franklin, J. L., Salic, A., Christian, K. M., Lee, L. A., Coffey, R. J., and Lee, E. (2007). Lrp6 is required for convergent extension during Xenopus gastrulation. Development (Cambridge, England) 134, 4095-106.

Takeda, S., Yonekawa, Y., Tanaka, Y., Okada, Y., Nonaka, S., and Hirokawa, N. (1999).

New Insights in Determination of Laterality and Mesoderm Induction by kif3A-/- Mice Analysis. The Journal of cell biology 145, 825-836.

Takemaru, K.-I., Fischer, V., and Li, F.-Q. (2009). Fine-tuning of nuclear-catenin by chibby and 14-3-3. Cell Cycle 8, 210-213.

Talora, C., Campese, A. F., Bellavia, D., Felli, M. P., Vacca, A., Gulino, A., and Screpanti, I. (2008). Notch signaling and diseases: an evolutionary journey from a simple beginning to complex outcomes. Biochimica et biophysica acta 1782, 489-97.

Tanaka, Y., Okada, Y., and Hirokawa, N. (2005). FGF-induced vesicular release of Sonic hedgehog and retinoic acid in leftward nodal flow is critical for left-right determination. Nature 12;435: 172-7.

Tanaka, C., Sakuma, R., Nakamura, T., Hamada, H., and Saijoh, Y. (2007). Long-range action of Nodal requires interaction with GDF1. Genes & development 21, 3272-82.

Tao, Q. et al. (2005). Maternal wnt11 activates the canonical wnt signaling pathway required for axis formation in Xenopus embryos. Cell 120, 857-71.

Tran, U., Pickney, L. M., Ozpolat, B. D., and Wessely, O. (2007). Xenopus Bicaudal-C is required for the differentiation of the amphibian pronephros. Developmental biology 307, 152-64.

Taschner, M., Bhogaraju, S., and Lorentzen, E. (2011). Architecture and function of IFT complex proteins in ciliogenesis. Differentiation; research in biological diversity, 1-11.

Tételin, S., and Jones, E. A. (2010). Xenopus Wnt11b is identified as a potential pronephric inducer. Developmental dynamics : an official publication of the American Association of Anatomists 239, 148-59.

Thompson, H., Shaw, M., and Dawe, H. (2012). The formation and positioning of cilia in Ciona intestinalis embryos in relation to the generation and evolution of chordate left-right asymmetry. Developmental Biology, 214-223.

Tian, J., Gong, H., Thomsen, G. H., and Lennarz, W. J. (1997a). Gamete interactions in Xenopus laevis: identification of sperm binding glycoproteins in the egg vitelline envelope. The Journal of cell biology 136, 1099-108.

Tian, J., Gong, H., Thomsen, G. H., and Lennarz, W. J. (1997b). Xenopus laevis sperm-egg adhesion is regulated by modifications in the sperm receptor and the egg vitelline envelope. Developmental biology 187, 143-53.

Torres, M. A., Yang-Snyder, J. A., Purcell, S. M., DeMarais, A. A., McGrew, L. L., and Moon, R. T. (1996). Activities of the Wnt-1 class of secreted signaling factors are antagonized by the Wnt-5A class and by a dominant negative cadherin in early Xenopus development. The Journal of cell biology 133, 1123-37.

Toyoizumi, R., Ogasawara, T., Takeuchi, S., and Mogi, K. (2005). Xenopus nodal related-1 is indispensable only for left-right axis determination. The International journal of developmental biology 49, 923-38.

Tran, U., Zakin, L., Schweickert, A., Agrawal, R., Döger, R., Blum, M., Robertis, E. M. De, and Wessely, O. (2010). The RNA-binding protein bicaudal C regulates polycystin 2 in the kidney by antagonizing miR-17 activity. Development (Cambridge, England) 137, 1107-16.

Tsiairis, C. D., and McMahon, A. P. (2009). An Hh-dependent pathway in lateral plate mesoderm enables the generation of left/right asymmetry. Current biology : CB 19, 1912-7.

Tuson, M., He, M., and Anderson, K. V. (2011). Protein kinase A acts at the basal body of the primary cilium to prevent Gli2 activation and ventralization of the mouse neural tube. Development (Cambridge, England) 4930, 4921-4930.

Ueno, N., and Greene, N. D. E. (2003). Planar cell polarity genes and neural tube closure. Birth defects research. Part C, Embryo today : reviews 69, 318-24.

Uysal-Onganer, P., and Kypta, R. M. (2012). Wnt11 in 2011 - the regulation and function of a non-canonical Wnt. Acta physiologica (Oxford, England) 204, 52-64.

Vandenberg, L. N. (2012). Laterality defects are influenced by timing of treatments and animal model. Differentiation; research in biological diversity 83, 26-37.

Vandenberg, L. N., and Levin, M. (2009). Perspectives and open problems in the early phases of left-right patterning. Seminars in cell & developmental biology 20, 456-63.

Vandenberg, L. N., and Levin, M. (2010). Consistent left-right asymmetry cannot be established by late organizers in Xenopus unless the late organizer is a conjoined twin. Development (Cambridge, England) 137, 1095-105.

Vick, P., Schweickert, A., Weber, T., Eberhardt, M., Mencl, S., Shcherbakov, D., Beyer, T., and Blum, M. (2009). Flow on the right side of the gastrocoel roof plate is dispensable for symmetry breakage in the frog Xenopus laevis. Developmental biology 331, 281-91.

Viotti, M., Niu, L., Shi, S.-H., and Hadjantonakis, A.-K. (2012). Role of the gut endoderm in relaying left-right patterning in mice. PLoS biology 10, e1001276.

Vladar, E. K., Antic, D., and Axelrod, J. D. (2009). Planar cell polarity signaling: the developing cell's compass. Cold Spring Harbor perspectives in biology 1, a002964.

Vladar, E. K., and Axelrod, J. D. (2008). Dishevelled links basal body docking and orientation in ciliated epithelial cells. Trends in cell biology 18, 517-20.

Vonica, A., and Brivanlou, A. H. (2007). The left-right axis is regulated by the interplay of Coco, Xnr1 and derrière in Xenopus embryos. Developmental biology 303, 281-94.

Vries-van Leeuwen, I. J. de, Kortekaas-Thijssen, C., Nzigou Mandouckou, J. A., Kas, S., Evidente, A., and Boer, A. H. de (2010). Fusicoccin-A selectively induces apoptosis in tumor cells after interferon-alpha priming. Cancer letters 293, 198-206.

Walentek, P., Beyer, T., Thumberger, T., Schweickert, A., and Blum, M. (2012). ATP4a Is Required for Wnt-Dependent Foxj1 Expression and Leftward Flow in Xenopus Left-Right Development. CellReports. 1 516–527.

Wallingford, J. B., Ewald, A. J., Harland, R. M., and Fraser, S. E. (2001). Calcium signaling during convergent extension in Xenopus. Current biology : CB 11, 652-61.

Wallingford, J. B., and Harland, R. M. (2001). Xenopus Dishevelled signaling regulates both neural and mesodermal convergent extension: parallel forces elongating the body axis. Development (Cambridge, England) 128, 2581-92.

Wallingford, J. B., Fraser, S. E., and Harland, R. M. (2002). Convergent extension: the molecular control of polarized cell movement during embryonic development. Developmental cell 2, 695-706.

Wallingford, J. B. (2006). Planar cell polarity, ciliogenesis and neural tube defects. Human molecular genetics 15 Spec No, R227-34.

Wallingford, J. B. et al. (2009). Xenopus Community White Paper 2009 Xenopus - a crucial model organism for biomedical research : NIH Investment in Xenopus : Xenopus as a

Model System and Human Disease : English Journal, 1-74.

Wallingford, J. B., and Mitchell, B. (2011). Strange as it may seem: the many links between Wnt signaling, planar cell polarity, and cilia. Genes & development 25, 201-13.

Wallingford, J B, Vogeli, K. M., and Harland, R. M. (2001). Regulation of convergent extension in Xenopus by Wnt5a and Frizzled-8 is independent of the canonical Wnt pathway. The International journal of developmental biology 45, 225-7.

Wallis, D. E., and Muenke, M. (1999). Molecular mechanisms of holoprosencephaly. Molecular genetics and metabolism 68, 126-38.

Wan, L. Q., Ronaldson, K., Park, M., Taylor, G., Zhang, Yue, Gimble, J. M., and Vunjak-Novakovic, G. (2011). Micropatterned mammalian cells exhibit phenotype-specific left-right asymmetry. Proceedings of the National Academy of Sciences of the United States of America, 1-6.

Wang, Y., McMahon, A. P., and Allen, B. L. (2007). Shifting paradigms in Hedgehog signaling. Current opinion in cell biology 19, 159-65.

Ware, S. M., Harutyunyan, K. G., and Belmont, J. W. (2006). Heart defects in X-linked heterotaxy: evidence for a genetic interaction of Zic3 with the nodal signaling pathway. Developmental dynamics : an official publication of the American Association of Anatomists 235, 1631-7.

Watanabe, H., Fujisawa, T., and Holstein, T. W. (2009). Cnidarians and the evolutionary origin of the nervous system. Development, growth & differentiation 51, 167-83.

Wend, P., Holland, J. D., Ziebold, U., and Birchmeier, W. (2010). Wnt signaling in stem and cancer stem cells. Seminars in cell & developmental biology 21, 855-863.

Wessely, O., and Obara, T. (2008). Fish and frogs: models for vertebrate cilia signaling. Frontiers in Bioscience 13, 1866-1880.

Wessely, O., and Tran, U. (2011). Xenopus pronephros development-past, present, and future. Pediatric nephrology (Berlin, Germany).

Xu, Q., Amore, P. A. D., and Sokol, S. Y. (1998). Functional and biochemical interactions of Wnts with FrzA , a secreted Wnt antagonist. Genescreen 4776, 4767-4776.

Yamada, T., and Modak, S. P. (1998). Genetic evidence for posterior specification by convergent extenstion in the Xenopus embryo. Development growth and differentiation 40, 125-132.

Yamamoto, H., Sakane, H., Michiue, T., and Kikuchi, A. (2008). Wnt3a and Dkk1 regulate distinct internalization pathways of LRP6 to tune the activation of beta-catenin signaling. Developmental cell 15, 37-48.

Yasunaga, T., Itoh, K., and Sokol, S. Y. (2011). Regulation of basal body and ciliary functions by Diversin. Mechanisms of development 128, 1-11.

Yokota, C. (2003). A novel role for a nodal-related protein; Xnr3 regulates convergent extension movements via the FGF receptor. Development 130, 2199-2212.

Yu, X., Ng, C. P., Habacher, H., and Roy, S. (2008). Foxj1 transcription factors are master regulators of the motile ciliogenic program. Nature genetics 40, 1445-53.

Zavros, Y., Orr, M. A., Xiao, C., and Malinowska, D. H. (2008). Sonic hedgehog is associated with H+-K+-ATPase-containing membranes in gastric parietal cells and secreted with histamine stimulation. American journal of physiology. Gastrointestinal and liver physiology 295, G99-G111.

Zeng, H., Hoover, A. N., and Liu, A. (2010). PCP effector gene Inturned is an important regulator of cilia formation and embryonic development in mammals. Developmental biology 339, 418-28.

Zhang, Y., and Levin, M. (2009). Left-right asymmetry in the chick embryo requires core planar cell polarity protein Vangl2. Genesis (New York, N.Y. : 2000) 47, 719-28.

Zhu, L., Marvin, M. J., Gardiner, A., Lassar, A. B., Mercola, M., Stern, C. D., and Levin, M. (1999). Cerberus regulates left-right asymmetry of the embryonic head and heart. Current biology : CB 9, 931-8.

Zhu, L., Zhou, G., Poole, S., and Belmont, J. W. (2008). Characterization of the Interactions of Human ZIC3 Mutants With GLI3. Human Mutation 29, 99-105.

Acknowledgements / Danksagung

First, I want to thank Prof. Dr. Martin Blum for the suggestion and the opportunity to work on this project, as well as the freedom he granted me throughout the time of this work. I am also deeply thankful for introducing me to the wonderful world of developmental biology.

I also want to thank Priv. Doz. Dr. Axel Schweickert for all his help throughout the years. His advise and teaching has fundamentally and constantly improved my experiments and my theoretical approaches towards understanding the embryo. Thank you for being a great and patient teacher!

Tina Beyer and Isabelle Schneider have contributed the SEM micrographs to this study. I thank you very much for all the hours of work. Thomas Thumberger has contributed customized software for analysis of phenotypes.

The expert technical help of Susanne Bogusch, Verena Andre, Anna Schäfer and Anna Iwanska is greatly acknowledged – thank you all for running the lab, fighting the chaos and all the support. Without you not a single experiment would have been possible.

I thank Dr. Silke Schmalholz for the handling of my (countless) contracts. Without you I would not have been able to pay my rent a couple of times.

I thank all former and current members of the Institute of Zoology for their help, the great discussions, the advice and the friendship they offered. You made the last 10 years a wonderful time for me!

Especially the members of the Blum-laboratory were a constant source of ideas, support and encouragement – during good and suboptimal phases – I will miss you: Cathrin Hagenlocher, Eva Bitzer, Kerstin Feistel, Maike Getwan, Matthias Tisler, Philipp Vick, Phillip Andre, Tina Beyer and Thomas Thumberger. My very special "thanks" is dedicated to Bärbel Ulmer and Isabelle Schneider, who became very good friends during the time we shared.

I very much thank the following people for providing constructs, valuable discussions and critical comments during this project:

Drs. Abraham Fainsod, Brian Mitchell, Christina Sirrenberg-Cruciat, Christof Niehrs, Christoph Viebahn, Christopher Kintner, Christopher Wright, Edgar Pera, Guojun Sheng, Herbert Steinbeisser, Jan Christian, John Wallingford, Käthi Geering, Michael Danichik, Michael Levin, Nikoloz Tsikolia, Oliver Wessely, Peter Vize, Randall Moon, Ray Keller, Richard Harland, Takuya Nakayama, and Thomas Hollemann.

In especially I have to thank the Xenopus community and the organizers, teachers and participants of the Cold Spring Harbor course "Cell And Developmental Biology Of Xenopus 2010" for the great course and a lot of fun.

I also thank all students who worked with me on various projects, in especially Simone Geyer.

I thank Jan Votteler for his unlimited support, especially during editing and correction of manuscripts, proposals and this thesis work.

Ich möchte mich auch herzlich bei meiner Familie bedanken, die meinen wissenschaftlichen Werdegang immer moralisch und finanziell unterstützt hat. Besonderer Dank gilt hierbei meinen Eltern für die Ermöglichung meines Studiums und dieser Dissertation.

Meinen Freunden danke ich für ihr Verständnis, auch wenn ich selten Zeit hatte: Ihr seid immer da gewesen wenn man Euch gebraucht hat – zum Feiern, zum Reden oder einfach nur zur Ablenkung.

Curriculum Vitae

Peter Walentek

Reinsburgstr 109a
70197 Stuttgart
Germany
Tel: 0049-176-24386890
Email: walentek@uni-hohenheim.de

DATE OF BIRTH IN	12/25/1980 Chorzow / Poland
EMIGRATION TO GERMANY	1987
EDUCATION	1988–1992 Herbert Hoover Primary School / Stuttgart
	1992–2001 Eschbach Gymnasium (High School) / Stuttgart (Abitur with Degree: 2.1)
	2001–2002 Alternative Civilian Service at AWO / Stuttgart
	2002–2007 Academic Studies in Biology and Graduation (Diploma/M.Sc. with Degree: 1.1) at the University of Hohenheim / Germany Thesis Work Title: "The Role of the H^+/K^+ATPase in *Xenopus laevis* Left–Right Axis Development" Blum Laboratory
	2006 Research Project on "Ions and Gap Junctions in Planarian Regeneration" at Levin Laboratory / Forsyth Inst./Harvard School of Dental Medicine / Boston, USA
	Dec. 2007 – June 2012 Doctoral Student in Molecular Developmental Biology at the University of Hohenheim Project Title: "Ion Homeostasis in *X. laevis* Left–Right Axis Development" Blum Laboratory

PUBLICATIONS	2009	*Oviedo, Morokuma, Walentek, Kema, Gu, Ahn, Hwang, Gojobori and Levin* "Long-range neural and gap junction protein-mediated cues control polarity during planarian regeneration" *Developmental Biology 339:188f*
	2011	*Schweickert, Walentek, Thumberger and Danilchik* "Linking early determinants and cilia-driven leftward flow in left-right axis specification of Xenopus laevis: a theoretical approach." *Differentiation 83(2):67f*
	2011	*Beyer, Danilchik, Thumberger, Vick, Tisler, Schneider, Bogusch, Ander, Ulmer, Walentek, Niesler, Blum and Schweickert* "Serotonin signaling is required for Wnt-dependent GRP specification and leftward flow in Xenopus*" Current Biology 22(1):33f*
	2012	*Walentek, Beyer, Thumberger, Schweickert, Blum* "ATP4a is required for Wnt-dependent Foxj1 expression and leftward flow in Xenopus left-right development ."*Cell Reports 1(5)*

MEETING PARTICIPITATION / COURSES	2008	12th International Xenopus Conference Leiwen, Germany / Poster
	2008	7th GFE School Meeting Günzburg, Germany / Talk
	2009	4th German–Italian Xenopus Meeting Loveno, Italy / Poster
	2009	18th GFE Meeting Hannover, Germany / Poster
	2010	Cell & Developmental Biology of Xenopus Cold Spring Harbor, USA / Course
	2010	SFB592 International Meeting Freiburg, Germany / Poster
	2011	19th International Joined Meeting of GFE & JSDB Dresden, Germany / Poster
	2011	70th Society for Developmental Biology Meeting Chicago, USA / Poster
ACADEMIC WORK EXPERIENCE (AT THE UNIVERSITY OF HOHENHEIM)	2003–2004	Creation of Lecture Notes (Biochemical Pathways) for Prof. M. Küppers / Inst. of Botany
	2003–2004	Tutorial in Basic Zoology / Inst. of Zoology
	2003–2006	Dendrochronological Measuring of Subfossil Woods and Computer Network Supervision / Work Group Dendrochronology (Botany)
	2004	Support of Basic Anatomical and Histological Course / Inst. of Zoology
	2004	Keeping of Laboratory Animals (Vertebrates and Insects) / Inst. of Zoology

2005	Support of Basic Taxonomic Classification Course Inst. of Zoology
2007	Computer-Aided Measurement of Leave Surface Areas / Inst. of Botany

LANGUAGES German, Polish, English, French

COMPUTER SKILLS Word, Power Point, Excel, Photoshop, Ilustrator, AxioVision, Dreamweaver MX, Fireworks MX, QuarkXPress, Network and Hardware Supervision